The Paroo Fault and the Mount Isa copper orebodies; a revised structural and evolutionary model, Mt Isa, Queensland, Australia

Thesis submitted by

Ryan David Long MSc Camborne School of Mines

BSc (Hons) Cardiff University

September 2010

for the degree of Doctor of Philosophy

in the School of Earth and Environmental Sciences at

James Cook University of North Queensland

Statement of Access

I, the undersigned, author of this work, understand that James Cook University will make this thesis available for use within the University Library and, via the Australian Digital Theses network, for use elsewhere.

All users consulting this thesis will have to sign the following statement:

“In consulting this thesis I agree not to copy or closely paraphrase it in whole Or in part without the written consent of the author; and to make proper public written acknowledgment for any assistance that I have obtained from it.”

I understand that, as an unpublished work, a thesis has significant protection under the Copyright Act and;

.... 9/9/10 ....

Signature Date

Statement of Sources

Declaration

I declare that this thesis is my own work and has not been submitted in any form for another degree or diploma at any university or other institution of tertiary education. Information derived from the published or unpublished work of others has been acknowledged in the text and a list of references is given.

9/9/10

Signature   Date

Statement of Contributions

General contributions towards this study have included:

- Xstrata Community Partnership Program, North Queensland
- ARC linkage project, “From exploration to mining: new geological strategies for sustaining high levels of copper production from the Mount Isa district”

Contributions to the manuscripts within this thesis have come from:

- Section A – Associate Professor Thomas Blenkinsop and Professor Nick Oliver are thanked for editorial support as co-authors of this paper.
- Section B – Professor Nick Oliver, Associate Professor Thomas Blenkinsop and Dr Brian Rusk and are thanked for editorial support as co-authors of this paper.
- Section C – Associate Professor Thomas Blenkinsop and Professor Nick Oliver are thanked for editorial support as co-authors of this paper.
- Section D – Professor Nick Oliver, Dr Poul Emsbo, Dr Brian Rusk and Associate Professor Thomas Blenkinsop and are thanked for editorial support as co-authors of this paper.

Normal supervisory contributions throughout the term of this PhD project by Associate Professor Thomas Blenkinsop, Professor Nick Oliver and Dr Brian Rusk are also acknowledged.

Acknowledgements

First I would like thank Daniela without your unwavering support this thesis would have been merely an illusive dream. You have been there constantly for me over the past two and a half years supporting, consoling and caring, thank you Daniela I will always be grateful.

Mum, Dad, Jnr, Christina, Trevor and Steven your love and support from the other side of the world has made the distance between us bearable. Your visits were the highlight of our time here and we look forward to spending more time with you when we return.

Tom, Nick and Brian thank you for you enthusiastic supervision, support and productive discussions. I have learned so much about geology and life during the course of this PhD and I thank you all for all you have done.

I greatly appreciate all the help and support given to me by the geologists and other staff from Xstrata copper and Xstrata copper exploration. Thanks in particular to Richard Lilly, Nathan Bullock, Trevor Shaw, Brad Miller, Chloe Conway, Dan Woolmer, Jed Williams, Kim Head, Eamon Dare, Tim Raggat, Chloe McDonald, Simon West, Helen Coackley, Vanessa Di Florio, Tom Lucas, James West and David Assidi. Without your knowledge of good outcrops and support during field work this project would have gone nowhere.

John thanks for your company at lunch it brightened my day. Gustav, Cathy, Rich, Carsten, Iris, Berit, Dexian, Sally, Paul, Joao, Rob, Mark, Stephan and Johannes thank you for keeping me sane with many great times. Judy, Ann, Kiri and all the ladies upstairs in the office thank you for all the help and support you provided. Thanks also to everyone else in the department over the course of my PhD.

Special thanks to Xstrata Copper for providing logistical support partly funded through the Xstrata Community Partnership Program, North Queensland, and the ARC through its Linkage Projects scheme.

Abstract

Numerous studies on the Mount Isa copper orebodies have assumed the role of the Paroo Fault, which has juxtaposed the Mount Isa Group against the Eastern Creek Volcanics, and forms a footwall to the copper and lead-zinc-silver orebodies. The copper orebodies have largely been considered to have formed during east northeast-west southwest shortening, late during the 1590-1500 Ma Isan Orogeny. This thesis examines the Paroo Fault from the km-scales to the sub mm-scales in order to understand its development and role in the mineralisation of the copper orebodies. Recent techniques such as Gaussian Curvature analysis, fold profile analysis, dilation and slip tendency analysis, spanned length analysis as well as established techniques such as thickness analysis and geological mapping have been used to examine the km-scales geometry of the Paroo Fault. This has lead to a new proposed timing for initial reactivation of the Paroo Fault during the final stages of deposition of the Mount Isa group, followed by folding during east-west shortening and refolding during east northeast-west southwest shortening. Detailed geological mapping of the Paroo Fault Zone at 10s of m-scales supports the conclusions drawn from the macro-scale observations and suggests a new interpretation of the timing for the formation of the copper orebodies, before or early in the east-west shortening event, at Mount Isa. Re-examination of the mapping database collected by mine geologists (MIM and Xstrata Copper) has demonstrated that at the hunreds of metres scale, folds formed during the east northeast-west southwest shortening bend around the copper orebodies, indicating that the copper orebodies formed earlier than this event, consistent with conclusions drawn from the mapping of the Paroo

Fault at the tens of m scale. Previously unrecognised east-west orientated folds which have no relationship to the copper orebodies and appear to predate them have also been recognised, indicating a phase of north-south shortening prior to ore genesis and prior to the east-west shortening. Halogen systematics on fluid inclusions from the copper orebodies, Paroo Fault Zone filling, silica-dolomite halo and basement rocks demonstrate that the ore system penetrated into the footwall, thus predating the sealing of the Paroo Fault Zones quartz-rich infill. The copper orebodies have a bittern brine source for halogens, which in the previous model for late metamorphic ore genesis, posed some problems because of the high Br/Cr ratios requiring an exotic (unknown) basin to have been placed above the Mount Isa Group during ore genesis. In the revised model here, such basinal brines are inferred to be residual evolved diagenetic brines within the Mount Isa Group or broader sedimentary package, which mixed with metamorphic fluids (with lower Br/Cl) during ore genesis, early in the inversion and shortening history.

Table of contents

List of figure

List of tables

Introduction and aims of this thesis

The Mount Isa Inlier located in NW Queenland contains three tectonic units (Fig. 1a); the Western Fold Belt, the Kalkadoon-Leichhardt Belt, and the Eastern Fold Belt (Blake et al., 1990). The world class Mount Isa copper orebodies lie within the Proterozoic Western Fold Belt which consists of a series of three stacked Paleoproterozoic to Mesoproterozoic Superbasins above the ~ 1900 to 1800 Ma Kalkadoon Leichhardt Block (Jackson et al., 2000; Scott et al., 2000; Southgate et al., 2000).

The oldest of these Superbasins is the Leichhardt Superbasin, which contains the Quilalar Formation, Myally Subgroup, Eastern Creek Volcanics and the Mount Guide Quartzite. The Eastern Creek Volcanics forms the immediate footwall to the Mount Isa copper orebodies. The Leichhardt Superbasin units are a succession of metabasaltic lava flows, volcanoclastics with minor quartzite, immature sandstones and suboridinate amounts of poorly sorted siltstones and redbeds (Derrick, 1982; Jackson et al., 2000). These rocks were deposited between 1780 and 1750 Ma into NNW-trending half-graben basins (Gibson, 2006) by fluvial and lacustrine processes (Jackson et al., 2000). The equivalent units in the Eastern Fold Belt are the carbonate facies sediments of the Corella Formation.

The younger Superbasins are the Isa and the Calvert, which contain the Lower MacNamara Group, Mount Isa Group (hosting the copper orebodies), Surprise Creek Formation, Fiery Creek Volcanics and Bigie Formation. Deposition of sediment into the Calvert Superbasin occurred during the start of rifting. Coarse sandstones and conglomerates were deposited into fault controlled basins by fluvial processes. Magmatic rocks from the Carters Bore Rhyolite are found within the sediments of the Calvert Superbasin and give an age of 1678 Ma (U-Pb; Page and Sweet, 1998). Sedimentation was terminated by felsic volcanism from the emplacement of the Fiery Creek Volcanics and the Weberra Granite (1710 Ma; Gibson, 2006). Sedimentation continued after the felsic volcanism forming the Prize Supersequence, in a deltaic to shallow marine environment (O'Dea et al., 1997; Gibson, 2006). The sedimentation in Calvert Superbasin was followed by increased magmatic activity in both the Mt Isa Eastern and Western Fold Belts.

Deposition of the Isa Superbasin sequences occurred between 1670 Ma and 1645 Ma (U-Pb; Neumann et al, 2006). The Isa Superbasin sequences host the majority of copper and lead-zinc orebodies in the Western and Eastern Fold Belts. In the Western Fold Belt the lower McNamara Group, in the Leichhardt River Fault Trough, and the lower Mt Isa Group are dominantly siliciclastic. These units grade into the carbonate-rich, upper McNamara and Mt Isa Groups. The Eastern Fold Belt equivalents, the Soldiers Cap Group, are turbiditic carbonaceous sediments from deep water depositional environments (Neumann et al, 2006).

The last phase of basin-forming extension was terminated by the onset of the Isan Orogeny (~1590-1500 Ma; Betts and Lister, 2002) during which time complex folding and faulting has affected the rocks of the Isa Superbasin.

The world class Mount Isa copper orebodies are contained within the X41 and Enterprise Mines, and have been exploited continuously since the 1940's. The orebodies have produced over 200 million tonnes at approximately 2 % Cu and still have a remaining measured resources of 48 Mt at 2.1 % Cu from the X41 Mine and 49 Mt at 3.2% Cu from the Enterprise Mine (Xstrata Copper ore reserves and resources, 2009). The copper orebodies have an epigenetic texture (Robertson, 1982; Perkins, 1984) with chalcopyrite forming the matrix to breccias and vein networks. A long-standing controversy relates to the astonishing spatial association of these world class copper orebodies with lead-zinc-silver orebodies, which have a syngenetic texture (Stanton, 1963; Finlow-Bates and Stumpfl, 1979), and are also world class.

The Paroo Fault lies immediately below the copper and lead-zinc-silver orebodies. It has juxtaposed the footwall "basement" Eastern Creek Volcanics (1710 ± 25 Ma; Gulson et al., 1983) against the overlying Mount Isa Group (c. 1655 ± 4 Ma; Page et al., 2000). The timing of this juxtaposition has not been previously clearly defined. The Paroo Fault has an unusual sigmoidal geometry that appears to have developed by folding (Perkins, 1984). The Paroo Fault's prominent position relative to the copper and lead-zinc-silver orebodies has lead to numerous authors suggesting that it had a role as a conduit in the mineralisation processes (Robertson, 1982; Perkins, 1984; Andrew et al., 1989; Heinrich et al., 1989; 1993; 1995; Gessner et al., 2006; Kendrick et al., 2006; Kühn and Gessner, 2006; 2009; Kühn et al., 2006). No direct evidence of the Paroo Fault's role as a conduit has been provided, however, and its role has been largely assumed.

This thesis uses recently developed techniques and the mine database, which has expanded considerably since work by previous researchers, to resolve the controversy that still exists for the formation of the Mount Isa copper orebodies. This thesis aims to use km-scale to sub mm-scale observations from the Paroo Fault and Urquhart Shale to understand;

- When and how the Eastern Creek Volcanics (1710 ± 25 Ma; Gulson et al., 1983) became juxtaposed against the Mount Isa Group (c. 1655 ± 4 Ma; Page et al., 2000)? (Paper 1)
- What was the sequence of deformation events that affected the host rocks and Paroo Fault? (Papers 1, 2 and 3)
- When and how did the Paroo Fault Zone form with alternations of quartz and graphite (± dolomite and sulphides)? (Papers1 and 2)

- When and how did the copper orebodies and associated alteration form and what deformation events have affected them? (Papers 1, 2, 3 and 4)

Structure of the thesis

This thesis is presented as four manuscripts, for peer review publication in international journals, which will be submitted in the coming months. Each manuscript is independent but links with the subsequent manuscripts (explained in preamble between each paper), which together redefine the geological history of the Mount Isa deposits. An outline of the methods and aims of each paper is provided below:

Paper 1 - Analysis of the m- to km-scale geometry and history of the refolded and reactivated Paroo Fault, Mount Isa, NW Queensland

This paper applies techniques such as Gaussian curvature, spanned length roughness, slip and dilation tendency, and thickness analysis of the fault zone filling to the meso- to macroscale to (m-km) geometry of the Paroo Fault and Mount Isa Group. The aim is to understand the formation of the Paroo fault and the deformation events that have subsequently affected it.

Paper 2 - The formation and development of the Paroo Fault and its relationship to the Mount Isa copper orebodies, NW Queensland

This paper uses micro- to mesoscale (μm-m) observations, including underground mapping and scanning electron microscope cathodoluminescence, to understand the formation of the Paroo Fault Zone filling, the deformation events that have subsequently affected it at these scales, and the timing of the copper mineralisation relative to these features.

Paper 3 - The formation of the Mount Isa copper orebodies, NW Queensland – a new paragenesis based on macroscopic structural elements

This paper uses mostly macroscale (10s of m-km) observations from the geological mapping database to understand the deformation events that have affected the Urquhart Shale and the timing of copper formation.

Paper 4 - The Mount Isa Copper orebodies, insights from fluid inclusion halogens

This paper uses fluid inclusion halogen systematics of sulphides and quartz as well as halogens systematics collected by previous authors to understand the formation of the copper orebodies in light of the new deformation sequence presented here.

Paper 1 - Analysis of the m- to km-scale geometry and history of the refolded and reactivated Paroo Fault, Mount Isa, NW Queensland Queensland

Ryan D. Long, Thomas G. Blenkinsop and Nicholas H. S. Oliver

1. Abstract

This study investigates how fault surfaces behave during multiple deformation events. It describes the detailed km to m scale geometry of a reactivated, refolded fault using recently developed techniques such as Gaussian curvature analysis, spanned length analysis and dilation and slip tendency analysis, as well as thickness analysis, on the exceptionally detailed dataset that exists for the Paroo Fault in the Mount Isa Inlier, Australia. A new timing and mechanism for the formation/reactivation of the Paroo Fault (and the genesis of the Mount Isa copper deposit) is proposed. Detailed observations of the fault's 3D geometry and its relationship to the hangingwall and footwall strata have lead to a new, simpler explanation for the formation and development of the fault. The fault formed or was reactivated by normal movement during compaction of the hangingwall sediments, and was deformed into a sigmoidal shape by two subsequent episodes of folding. The Paroo Fault was folded on the km scale in the first event, and a quartz-graphite fault zone filling developed. Copper mineralisation and a surrounding silica-dolomite

alteration halo was formed early in this event. The second fold event caused smaller (200 m wavelength) north northwest-south southeast trending folds. These folds deform the Paroo Fault around the non-stratiform copper orebodies. During its polyphase history, the fault was folded, refolded and reactivated as a shear zone that created dilation, yet enough indications of its early history were preserved to interpret the sequence of events.

Keywords: Mount Isa copper deposit, Dilation and slip tendency, Spanned length, Gaussian curvature analysis, Paroo Fault, reactivation.

2. Introduction

The geometry of fault surfaces is important for understanding earthquake mechanics (Sibson, 1995; Talwani, 1999; Kondo et al., 2005), sedimentation (White et al., 1986; Childs et al., 2003), fault kinematics (Jackson and McKenzie, 1999; Rowland and Sibson, 2001), fault zone processes (Power et al., 1988; Power, 1995; Caine et al., 1996; Childs et al., 2009), and tectonic history (Walsh and Watterson, 1989). Fault surfaces used in such studies are analysed from maps, surface outcrops or seismic data in sedimentary basins, and most studies have been restricted to faults with a relatively simple deformation history. On the other hand, the role of faults as long lived structures subject to reactivation is well recognised (Holdsworth et al., 2001; Ghisetti and Sibson, 2006; Mazzoli, 2006; Andrés et al., 2009). The geometry of reactivated fault surfaces has been studied in much less detail (Kelly et al., 1999; Gray and Gregory, 2003). In many cases of reactivation, the fault surface remains planar, and acts as a zone of persistent weakness. However it has been suggested that fault dips can change during inversion (Hayward and Graham, 1989), and the faults may become substantially deformed (Butler, 1989).

The primary aims of this study are to describe the detailed geometry and history of a fault (the Paroo Fault) that has been subject to several phases of brittle and ductile deformation, and thus to gain some insights into what fault features may be preserved through multiple deformation events, whether faults reactivate as planar features or deform passively, and why. The study takes advantage of a rare data set from a fault with a complex history that is captured in exceptional detail on a regional scale. The Paroo Fault has been mapped to an accuracy of 1 m in most places over a strike length of 6.5 km and a down dip extent of 3 km, from underground development and drill-holes of the Mount Isa copper and lead-zinc-silver deposits (Figs. 1 and 2). Movies of the deposit model (Movie 1) and the results presented here (Movie 2) should be viewed using windows media player. The movies can be accessed from the CD with this thesis to improve comprehension of the geology.

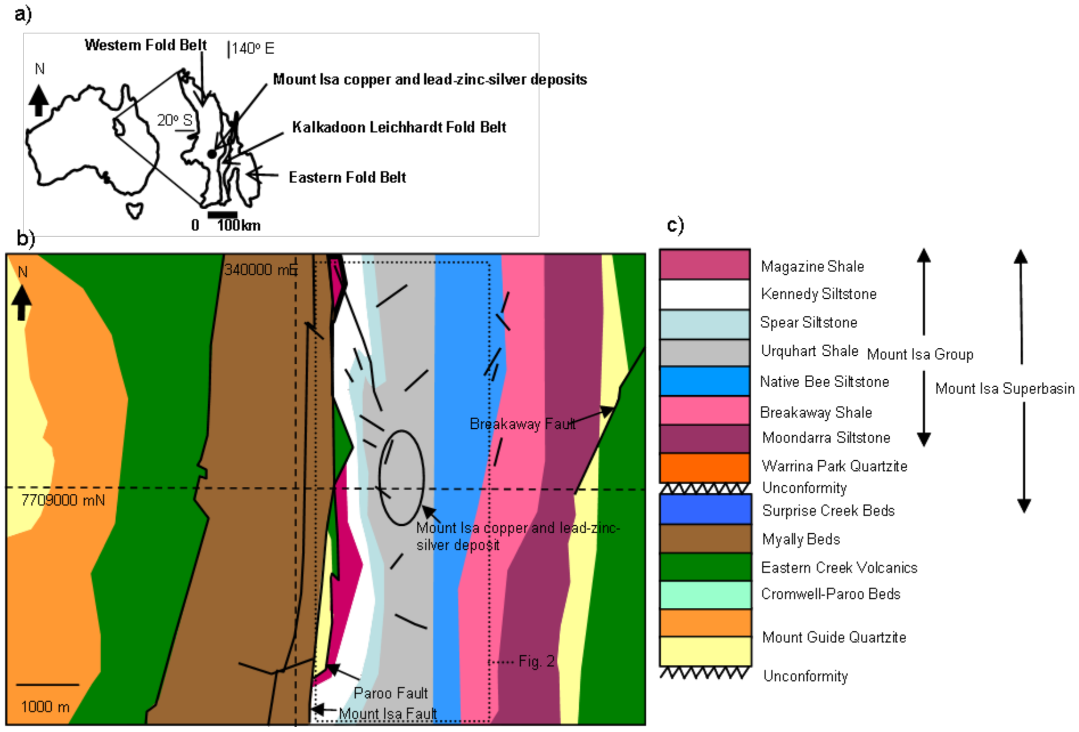

Fig. 1. The regional geology of the Mount Isa Copper deposit; a) Simplified tectonic map of the Mount Isa Inlier showing the Mount Isa copper and lead-zinc-silver deposit; b) Schematic map of the regional geology in the vicinity of the Mount Isa copper and lead-zinc-silver deposit (after BMR 1978), dotted box shows surface outcrop of Fig. 2; c) Schematic stratigraphic column of the rock types in the Mount Isa area (after BMR 1978).

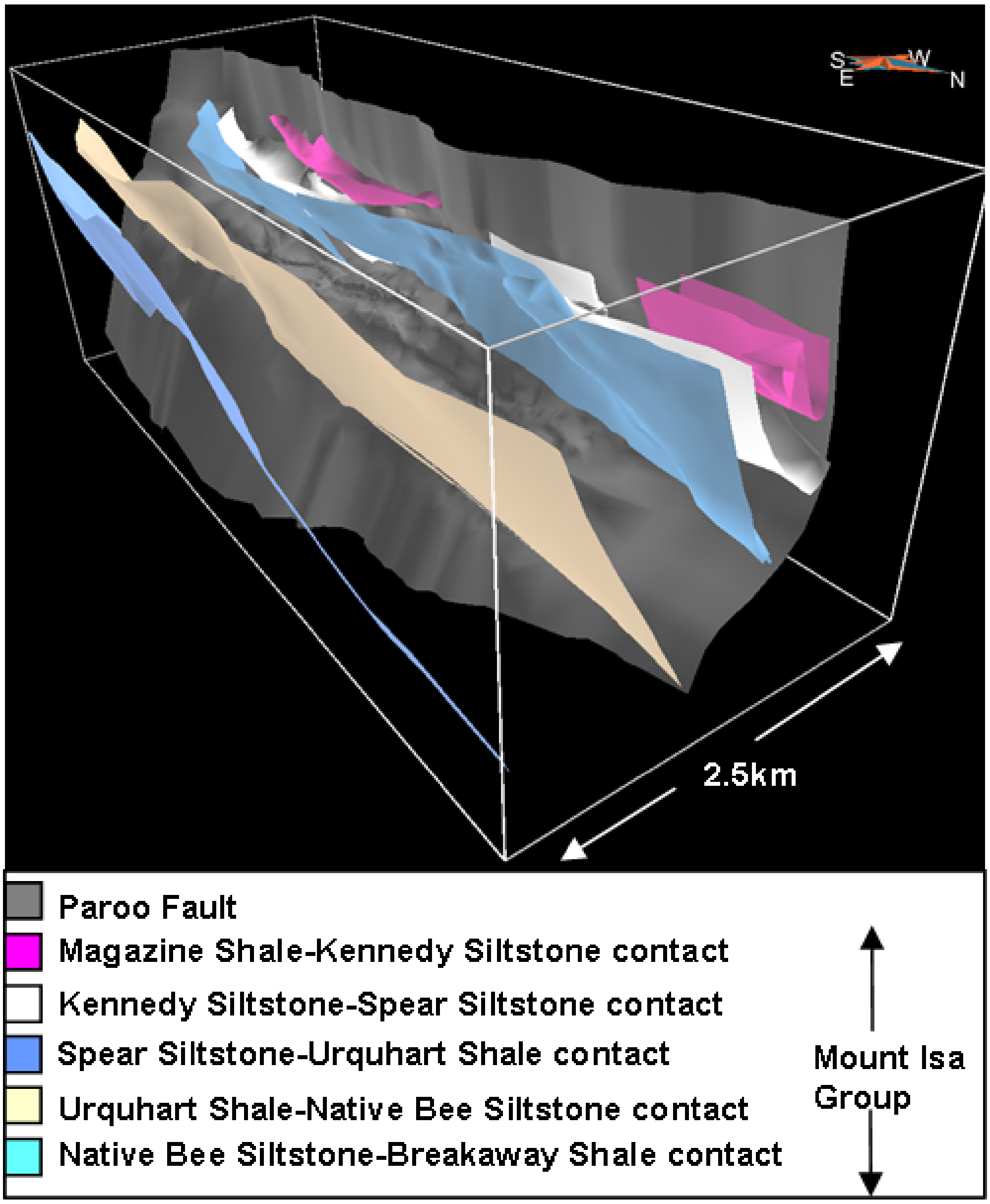

Fig. 2. The Paroo Fault and the Mount Isa Group, dominantly dipping to the west apart from the Kennedy Siltstone and Magazine Shale which are folded, the folds are open in the southern section and closed in the northern section

The Paroo Fault forms the footwall to the world class Mount Isa copper orebodies and associated silica-dolomite alteration, and lies in close proximity to the Mount Isa lead-zinc-silver orebodies, which also constitute a world class resource (Figs. 3 and 4; Movie 1; Perkins, 1984). The position of the fault adjacent to the copper orebodies makes it an obvious candidate for a feeder structure to the mineralising and alteration fluid that formed the copper orebodies, silica-dolomite alteration and lead-zinc-silver orebodies (Robertson, 1982). In current ore genesis models, the role of the fault has largely been assumed and not directly studied (Gulson et al., 1983; Swager, 1983; 1985; Perkins, 1984; 1990; 1997; 1998; Swager et al., 1987; Andrew et al., 1989; Heinrich and Cousens, 1989; Heinrich et al., 1989; McGoldrick and Keays, 1990; Hannan et al., 1993; Heinrich et al., 1993; 1995; Waring et al., 1998; Painter et al., 1999; Perkins et al., 1999; Davis, 2004; Gessner et al., 2006; Kendrick et al., 2006; Kühn and Gessner, 2006; 2009; Kühn et al., 2006; Wilde et al., 2006; Gessner, 2009), though it is clear that the fault has been reactivated and deformed in several events (e.g. Betts et al., 2003). An additional motivation for this study is therefore to examine the role of the fault in affecting fluid flow and mineralisation.

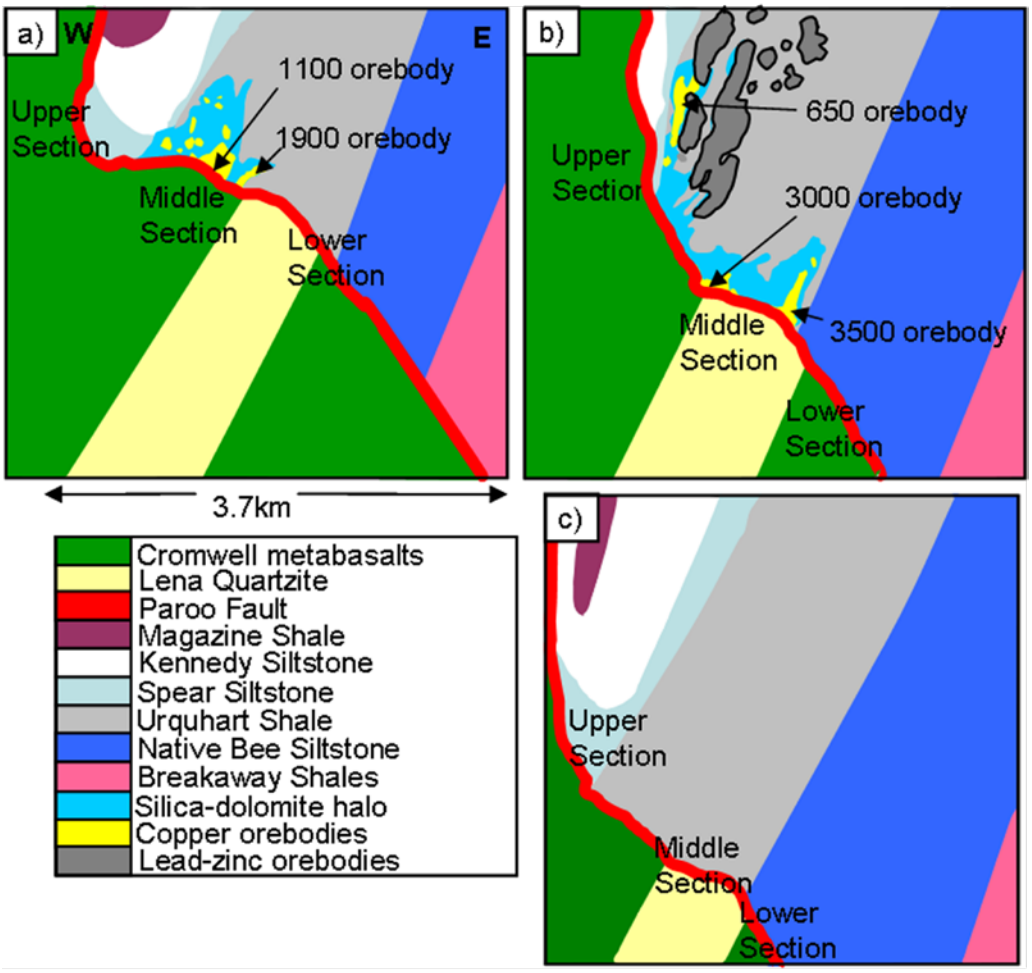

Fig. 3. Simplified ture scale cross sections of the Mount Isa copper orebodies showing the Upper, Middle and Lower sections of the Paroo Fault; a) has a northing of 5300 m and displays the 1100 orebody; b) has a northing of 6800 m and displays the lead-zinc-silver mineralisation, the perched 650 orebody and the 3000 and 3500 orebodies; c) has a northing of 8300 m and is north of the copper mineralisation. See Fig. 6 for cross section locations.

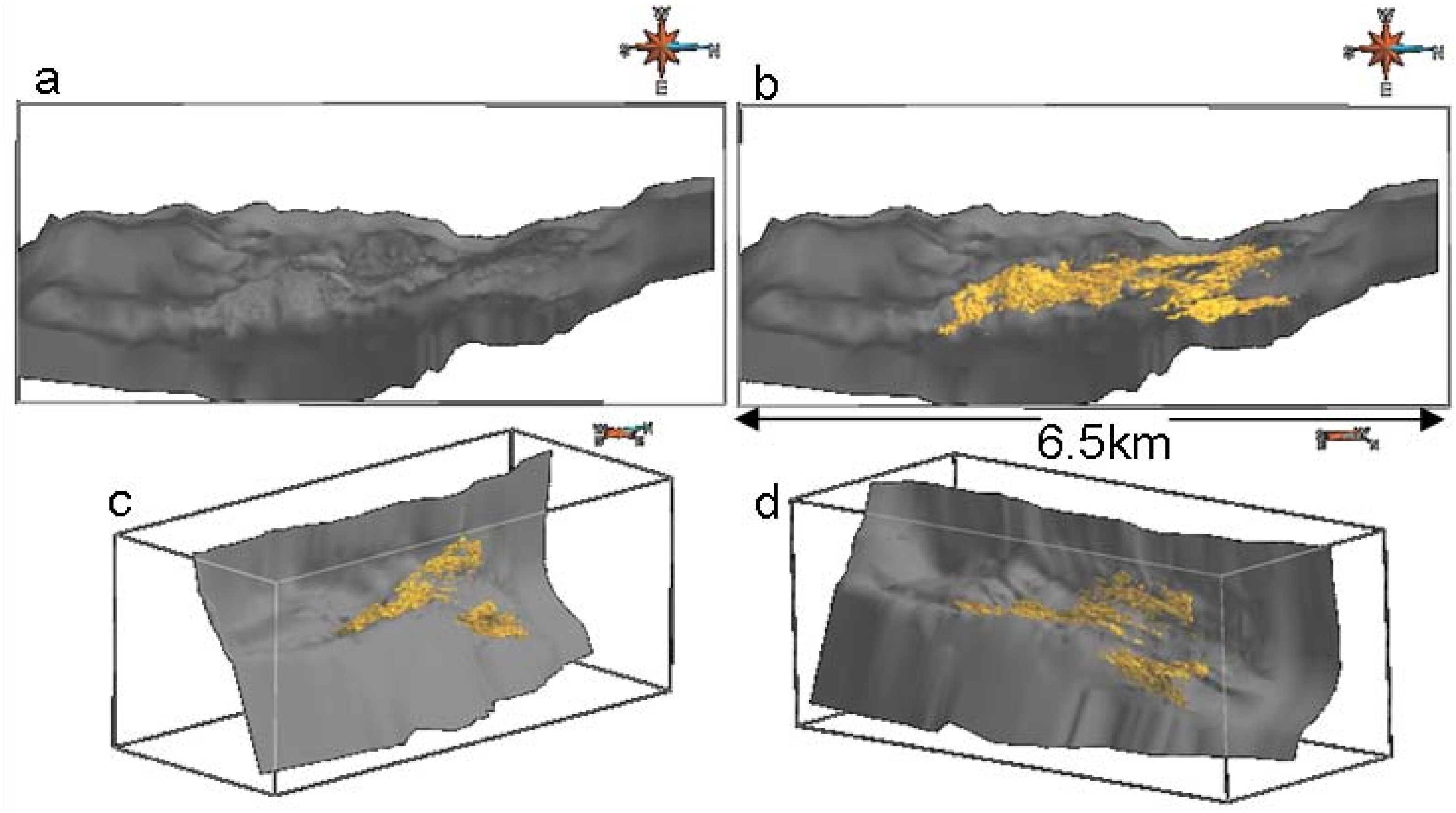

Fig. 4. Images of the Paroo Fault (grey surface) copper orebodies in yellow. a) View from above; b) View from above with the copper orebodies; c) View looking northwest; d) View looking southwest.

3. Background Geology

The rocks of the Western Fold Belt consist of a series of three stacked superbasins; the Leichhardt Superbasin, the Calvert Superbasin and the Isa Superbasin (Jackson et al., 2000; Scott et al., 2000; Southgate et al., 2000). The Calvert Superbasin and the Isa Superbasin were formed during the Isa Rift Event (Lister et al., 1999). The Mount Isa Group, which hosts the orebodies, was deposited during the formation of the Isa Superbasin, which was terminated by the onset of the Isan Orogeny (~1590 Ma; Southgate et al., 2000).

The 23 km long Paroo Fault juxtaposes the Mount Isa Group (age of the Urquhart Shale Formation is 1655 ± 4 Ma, Page et al., 2000) against the Eastern Creek Volcanics (1710 ± 25 Ma, Gulson et al., 1983; Figs. 2 and 3; Movie 1). The footwall to the Paroo Fault is of the Cromwell Metabasalt and the Lena Quartzite of the Eastern Creek Volcanics which generally dip steeply to the west, and can be regarded as “basement” (BMR, 1978). The Mount Isa Group in the hangingwall to the fault also generally dips to the west at steep to moderate angles (on average 60^{o}), apart from the Kennedy Siltstone and Magazine Shale, which dip both east and west in the core of a synform (Fig. 2; Movie 1). The copper and the lead-zinc-silver mineralisation are stratabound within the Urquhart Shale Formation of the Mount Isa Group (Solomon, 1965; McDonald, 1970). Surrounding the copper mineralisation to a distance of 400 m, but not the lead-zinc-silver mineralisation, is a halo of silica-dolomite (Finlow-Bates and Stumpfl, 1979). This has a core of more siliceous material that is commonly brecciated, grading into more dolomitic rocks which can also be brecciated.

3.1. Previous work on the Paroo Fault

The Mount Isa Group was described as forming during penecontemporaneous faulting by Smith (1969), because of thickness variations in the Moondarra Siltstone in the region of the Lagoon Creek Fault and Moondarra Fault, 8 km northeast of the Mount Isa copper deposit. Fifteen km north of the deposit, the Breakaway Shale, Native Bee Siltstone and Urquhart Shale of the Mount Isa Group to the north of the Transmitter Fault are about half the thickness of the same units to the south of the fault, demonstrating that this fault in addition to others was active at the time of deposition (Smith, 1969). These faults do not have the same orientation as the Paroo Fault, and the Paroo Fault does not have Mount Isa Group rocks in the footwall, so a direct comparison between these faults and the Paroo Fault cannot be made. Further evidence of penecontemporaneous faulting during the deposition of the Mount Isa Group comes from a sedimentary breccia within the Kennedy Siltstone and Spear Siltstone (Mathias and Clark, 1975) that could be due to movement on the Paroo Fault during the compaction/sedimentation.

Increased outcrops due to mine development allowed Mathias and Clark (1975) to recognise three separate faults interpreted to represent different episodes of faulting. An upper steep east dipping fault was termed the Western Block contact and a flatter fault that dips to the west the Plateau type contact. A lower, steeply west dipping fault was termed the Scarp type contact. The Paroo Fault was first recognised as a single structure rather than three separate faults by Dunnet (1976), who proposed that it formed by the linkage of earlier structures. Four regional deformation events are described by Dunnet (1976), starting with early normal faulting that strikes west northwest and was active during deposition of the Myally Beds, which overly the Eastern Creek Volcanics (Fig. 1b). This was followed by local slumping and soft sediment deformation, folding of the lead-zinc-silver ore and Urquhart Shale. Normal faults such as the Paroo Fault then became merged into a 'spoon fault' by late flat normal faults cutting and rotating the earlier normal faults, causing north-south extension. The 'spoon fault' was shortened causing an increase in the initial curvature of the fault and producing D_2 folds adjacent to the Mount Isa Fault (Dunnet, 1976).

An alternative concept for the formation for the fault was put forward by Bell (1983) who described the Paroo Fault initiating as a thrust in a duplex during a north-south orientated contractional event (D_1) and subsequently rotated during an east-west shortening event (D_2) in to its present orientation. A final phase of east northeast-west southwest shortening (D_3) caused the development of the copper orebodies by dilation on the pre-existing D_2 fold (Swager, 1983; 1985; Perkins, 1984; Bell et al., 1988; Davis, 2004; Miller, 2007). A fourth deformation event that had two parts, east-west shortening (D_{4a}; Bell et al., 1988; Miller, 2007) and north northwest-south southeast shortening (D_{4b}), has been suggested based on late faults which overprint the copper breccias (Miller, 2007).

Bell et al. (1988) argue against the 'spoon fault' model (Dunnet, 1976) and syn-sedimentary fault model (Smith, 1969) on the basis that the sigmoidal shape of the Paroo Fault could not be formed by these models without later complex interfering folds. Bell et al. (1988) also suggested that there is no evidence of syn-faulting deposition of the Mount Isa Group sediments, and that on the surface and underground, the Paroo Fault shows evidence of folding during D_3.

The thrust duplex model put forward by Bell (1983) for explaining the juxtaposition of the Eastern Creek Volcanics against the Mount Isa Group has been challenged by many authors (Connors et al., 1992; Nijman et al., 1992a; b; Stewart, 1992; Lister, 1993; O'Dea et al., 1996; 1997a; Betts et al., 1998; 2003; Betts, 1999; Betts and Lister, 2002; Gibson and Henson, 2005). Stewart (1992) examined locations of importance for the thrusting model and found no evidence of the roof thrusts and demonstrated that the thrust imbricates are actually normal fault blocks. Many of the east-west thrust faults termed D_1 by Bell (1983) have been demonstrated to cross-cut D_2 folds and are therefore younger (Stewart, 1992). Further some of the D_1 thrust faults dip towards the south not the north (Dunnet, 1976; Derrick, 1982; Nijman et al., 1992a; b; Stewart, 1992; O'Dea and Lister, 1995; O'Dea et al., 1997a) as required if the thrusts were part of a duplex.

Perkins (1984) demonstrated that the Paroo Fault had a sigmoidal shape in cross section, and provided the first three-dimensional image of the Paroo Fault. He noted the consistent orientation of the shales relative to the fault, as well as the location of a copper orebody (the 1100 orebody) within a local synform in the fault (Movie 1).

A fourth formation model for the formation of the Paroo Fault was introduced based on regional studies (Betts and Lister, 2002; Betts et al., 2003). According to these authors the Mount Isa Group was deposited during the sag phase of the Mount Isa Rift Event. In this interpretation the structures called thrust imbricates by Bell (1983) are normal faults. Betts and Lister (2002) and Betts et al. (2003) suggest that the Paroo Fault formed as a normal fault bounding a half graben (the Leichhardt Rift), and was reactivated during the Mount Isa Rift Event. The sigmoidal shape of the fault was caused by later folding and shearing associated with uplift of the Sybella Batholith which acted as a buttress during D_2 shortening (Betts and Lister, 2002). Work by various authors supports an extensional regime during the deposition of the Mount Isa Group (Connors et al., 1992; Nijman et al., 1992a; b; Stewart, 1992; Lister, 1993; O'Dea et al., 1996; 1997a; Betts et al., 1998; 2003; Betts, 1999; Betts and Lister, 2002; Gibson and Henson, 2005).

Mapping to the south of the Mount Isa copper deposit (MacCready, 2006) was used to propose a fifth model for the formation of the Paroo Fault. This model is based on structural observations from the Native Bee Fault. This fault was formed prior to the D_1-D_3 sequence of Bell (1983) during north-south stretching. The Satellite-Biotite Fault and the Clone Fault crosscut and displace the Native Bee Fault. The faults were originally steep, but rotation during D_2 regional folding changed their geometry to gently dipping, juxtaposing the Eastern Creek Volcanic and the Mount Isa Group, with a similar sigmoidal geometry to the Paroo Fault.

The duplex theory of Bell (1983) is now widely dismissed but Bell's sequence of deformation events is still relevant as north-south shortening and thrusting has been demonstrated to occur within the Western Fold Belt, after north-south extension (e.g. Gibson et al., 2005). This modified deformation sequence has been widely recognised throughout the Western Fold Belt (Loosveld and Schreurs, 1987; Connors, 1992; Stewart, 1992; Connors and Lister, 1995; O'Dea et al., 1997b; Adshead-Bell, 1998; MacCready, 2006) and will be used here.

4. Data and methods

The macroscale observations presented here are based on data collected by the mine geologists (MIM and Xstrata Copper) since the 1930's. Such a large data set on the Mount Isa copper deposit has not been previously available. This has allowed analysis of the macroscale geometry of the Paroo Fault using new techniques. The figures and data presented in this paper come from a three-dimensional model of the Paroo Fault and the Mount Isa copper and lead-zinc-silver deposits.

4.1. The Paroo fault model

The three-dimensional model of the Paroo Fault was created by mine geologists (Xstrata Copper) in the mining software Minesight using over 20,000 drill-holes and geological mapping acquired over 85 years. Due to the variation between drill-hole orientations and the drill-hole traces in the digital mine model, which would result in small scale inaccuracies (<1 m) in the three-dimensional model of the Paroo Fault, interpretations of variations in geometry of the fault if less than 1 m amplitude are not made.

The Paroo Fault Zone is over 25 m wide in places and the fault zone is filled by sub-parallel alternations of graphite and quartz. There has been shearing along the graphitic layers, and extensive deformation microstructures exist within the quartz. The fault has an upper and lower contact with the adjacent wall rocks; the lower contact separates the fault zone filling from the underlying Lena Quartzite and Cromwell Meta-basalt, and the upper contact separates the fault zone filling from the Urquhart Shale. There was sufficient similarity in the shapes of the two contacts that only the results from the lower fault contact are presented here, except for the thickness analysis which used both the upper and lower contacts.

The original Minesight model was imported into GoCAD and Vulcan Envisage. The lower contact of the Paroo Fault triangulation consists of over 7175 points and 12,579 triangles. It represents a section of the Paroo Fault, (which has a total strike length of 23 km), with a length of 6.5 km, a width of 2.5 km, extending to a depth of 3 km. The Paroo Fault merges with the Mount Isa Fault north of the deposit (Movie 1).

4.2. Analysis of the shapes of profiles of folded surfaces

The sigmoidal shape of the Paroo Fault suggests that fold shape analysis techniques may be useful to understand folds that may have affected the Paroo Fault. Fold shape analysis was undertaken on three cross sections along the Paroo Fault (Fig. 5) using the software Fold Profiler (Lisle et al., 2006) to gain an understanding of how the shape of the Paroo Fault changes at a variety of scales. The code works by comparing the shape of the observed fold with mathematical functions. The cubic Bezier curve method was used for simplicity, as the shape result depends only on two variables; the aspect ratio and the shape parameter.

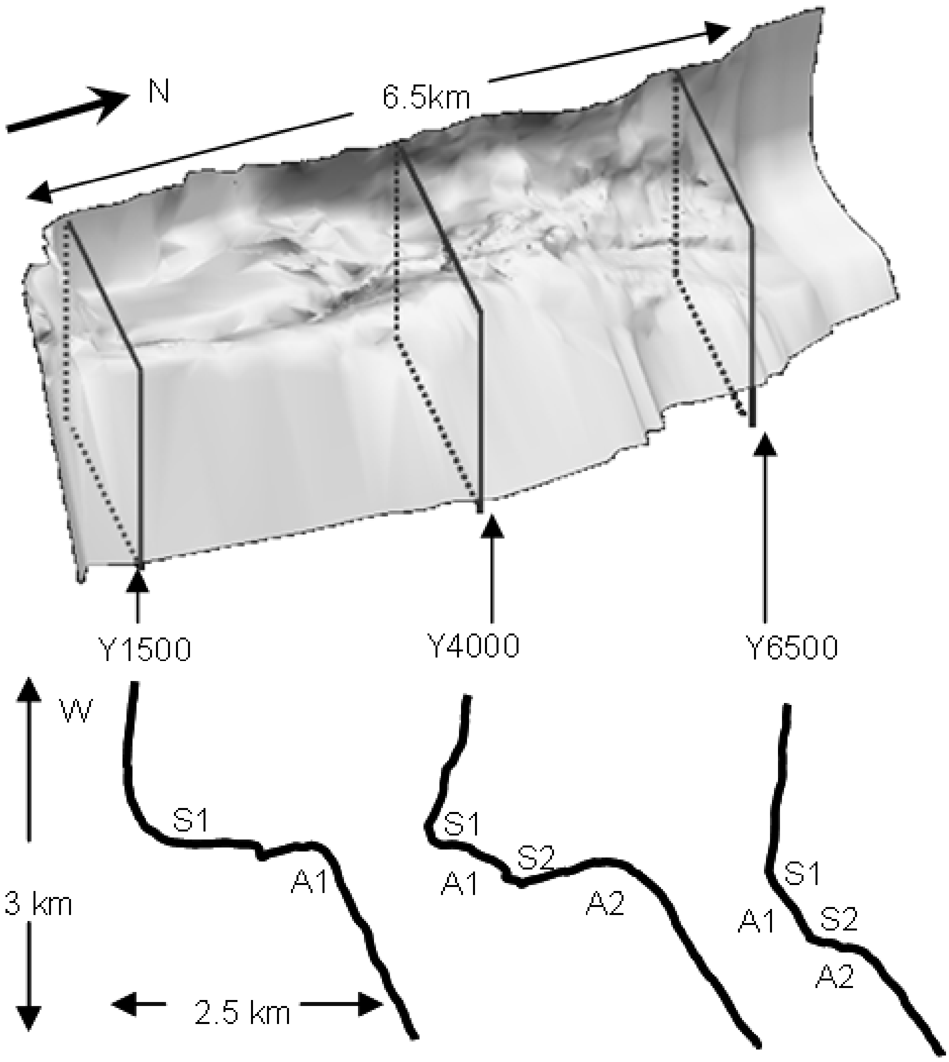

Fig. 5. The Paroo Fault showing the three vertical cross sections (1500 m, 4000 m and 6500 m) and the synforms (S) and antiforms (A) used in these cross sections for fold shape analysis.

4.3. Gaussian Curvature analysis

The Gaussian curvature (k_G) was calculated using the MATLAB code created by Mynatt et al. (2007), which quantifies the shape and orientation of points on a folded surface. This was undertaken to understand what aspects of the curvature relate to the surrounding geology and copper orebodies, and to recognize the effects of deformation events that have affected the Paroo Fault. A curvature threshold value can be applied to the data to allow the assessment of the fold shape at different scales. The results from this analysis were converted into a format suitable for input into GoCAD. This allowed quality control by comparison with the existing model of the Paroo Fault, and analysis of the relationship between the Paroo Fault and the copper orebodies. The curvature analysis is colour coded in GoCAD to differentiate between the synformal and antiformal structures.

4.4. Spanned length method of roughness analysis

Roughness analysis is conventionally applied to understand slip vectors and growth histories of planar faults (Aviles and Scholz, 1987; Power and Tullis, 1991). Here it has been used to indicate the intensity of folding/deformation that has affected the Paroo Fault. The spanned length method is used in this paper to calculate the fractal dimension (D) which gives the fault roughness. The method relies on the way the spanned or chord length L of a curve scales with the total curve length X (Suteanu, 2009):

$$L \sim X^{-1/D}$$

A straight line has a D value of 1 and D increases with roughness. This method eliminated the “stepping effect” seen in the results of a similar but more widely used technique known as the divider method.

Unlike previous three-dimensional fractal studies of fault surfaces which were limited to a much smaller scale (m^2; e.g. Power and Tullis, 1992; Power and Durham, 1997; Giaccio et al., 2003; Sagy et al., 2007; Candela et al., 2009), this study deals with the Paroo Fault over a strike length of 6500 m and an area of ~ 26,000,000 m^2. The three dimensional model of the Paroo Fault was sliced into three vertical sections, two horizontal sections and one long section across the flat portion of the fault (Fig. 6), to gain an understanding of the variation in roughness of the fault in all directions. Each of the three vertical sections were then split into three domains; 1) a steep dominantly west dipping upper portion, 2) a flat middle portion and 3) a steep east dipping lower portion. The flat portion of the fault was also split in to three domains; south, central and north.

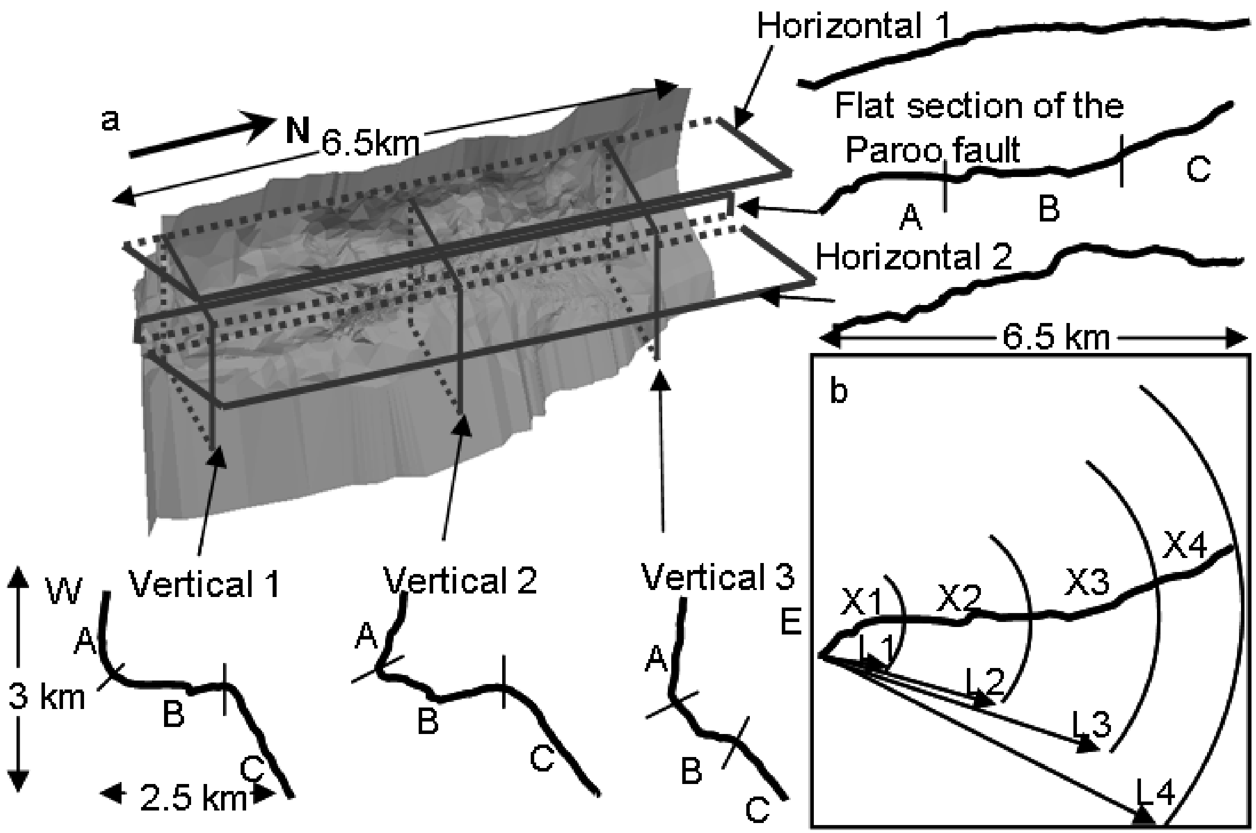

Fig. 6. The method and sections along which the spanned length analysis was done a) Image of the Paroo Fault showing the three vertical, two horizontal sections, and one section at 90° to the flat part of the fault along which the roughness of the Paroo Fault was measured using the spanned length method; b) A diagram showing how the spanned length method works by the way the span length of curve (L) scales with the total length of the curve (X): L ~ X-1/D.

4.5. Thickness analysis

In semi-planar faults thickness variations are commonly related to fault dilation e.g. thicker fault zone filling is typically considered a response to movement on dilated fault bends. Folding can modify thickness of a faulted layer; therefore thickness analysis of the Paroo Fault was undertaken. The thickness of the Paroo Fault Zone filling was calculated using the upper and lower contact of the fault from the mine model in Vulcan Version 7.5. The program creates a distance vector from each point on the first triangulation to the closest point on the second triangulation.

4.6. Slip Tendency

Slip tendency is normally applied to faults that are semi-planar. Here it is applied to a folded surface to examine if movement on the folded surface has affected the thickness of the fault zone filling, the position of the copper orebodies or the roughness on the Paroo Fault. Slip tendency evaluates the potential of a fault to slip based on a set of stress states (Morris et al., 1996). Slip tendency is defined by the ratio resolved shear stress (τ) to the normal stress (σ_n; Morris et al., 1996). The normalised slip tendency (T_s; Lisle and Srivastava, 2004) includes the coefficient of friction

(μ) to give a range of T_s between 0 (no resolved shear stress) and 1 (slipping);

$$T_s = \tau/\mu\sigma_n$$

The normal stress and shear stress of a fault are defined by the orientation and magnitude of the three principal stresses σ_1, σ_2 and σ_3 (Morris et al., 1996). Compression is taken as positive. If these variables are unknown then it has been demonstrated (Ferrill et al., 1999; Lisle and Srivastava, 2004), that this technique can be modified and applied to paleostress analysis by using the orientation of the principal stress axis and the ratio of the principal stress difference (Φ) which can be defined as;

$$\Phi = (\sigma_2 - \sigma_3)/(\sigma_1 - \sigma_3)$$

A variety of orientations and magnitudes of σ_1, σ_2 and σ_3 can be tested to determine the most likely conditions that would cause slip on a fault.

Slip tendency analysis was undertaken on the Paroo Fault using two possible D_3 stress orientations (Table 1). Several phi values (0.1, 0.5 and 0.9) were used for each model because the orientations of σ_1, σ_2 and σ_3 are known but not their proportions. As demonstrated below, D_3 was the deformation event responsible for forming the current geometry of the Paroo Fault and it is therefore possible to use the stress tensors to predict where areas of slip would have occurred provided the local stress state did not vary significantly from the regional stress.

Event	σ_1		σ_2		σ_3	
	Trend	Plunge	Trend	Plunge	Trend	Plunge
D_3	60	0	158	0	60	90
D_3	60	0	60	90	158	0

Table 1. The most favourable stress tensors used to represent D3 in the dilation and slip tendency analysis.

Using known X, Y and Z coordinates of 7155 points from the GoCAD model of the Paroo Fault, the strike and dip of each point was calculated using the GenLab software (Fernández-Martínez and Lisle, 2009). The slip tendency for each point was then calculated using two orientations and three relative magnitudes of σ_1, σ_2 and σ_3.

4.7. Dilation Tendency

Dilation tendency analysis was undertaken on the Paroo Fault to observe where dilation during D_3 would occur on the fault because this is when some authors have suggested the copper orebodies formed. The dilation tendency (T_d) evaluates the potential for a fault to dilate from the difference between the maximum principal stress σ_1 and the normal stess on the fault, normalised using the differential stress (Ferrill, 1999; Nemcok et al., 2004; Moeck et al., 2009);

$T_d = (\sigma_1 - \sigma_n)/(\sigma_1 - \sigma_3)$

Dilation tendency varies between 0 for a fault perpendicular to σ_1 to 1 for a fault that has the greatest potential to dilate. The dilation tendency has been measured using the same method and stress vectors outlined for the slip tendency results.

5. Results

5.1. The shapes of profiles of the folded Paroo Fault surfaces

The sigmoidal cross-section of the north-south striking Paroo Fault varies from north to south. There are three main domains within the fault (Fig. 3; Movie 1). The upper portion generally dips steeply towards the west, changing to dominantly gently east dipping (but locally variable) middle portion with depth. The lower portion of the Paroo Fault dips steeply to the east. These domains can be seen in a stereonet of poles to the fault surface which uses the dips and strikes of 7155 points obtained from the three-dimensional GoCAD model (Fig. 7).

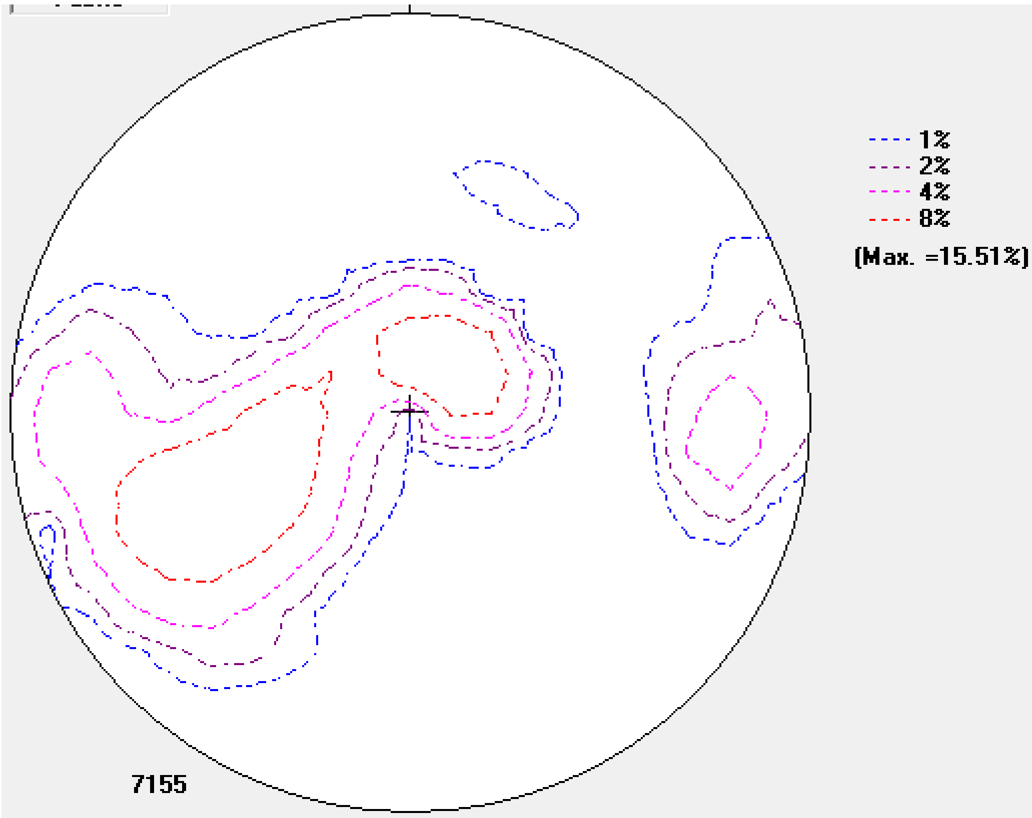

Fig. 7. An equal area lower hemisphere stereoplot with 7155 poles to the Paroo Fault. Three main groups of orientation correspond to the steep west dipping upper section of the fault, the middle section of the fault that has a shallow dip with a variable orientation, and the third group is the lower section of the fault which dips steeply to the east.

5.1.1 Upper portion

At the southern end of the mine (northing of 1500 m) the upper portion of the fault dips steeply west to a depth of 787 m below the surface where a north-south orientated close synformal cosine fold changes its orientation (Figs. 5 and 8). The upper portion of the fault in the central section (northing of 4000 m) dips towards the west like the northern end of the system. In the northern end of the mine (northing of 6500 m) the Paroo

Fault dips steeply towards the east to a depth of 1457 m below the surface.

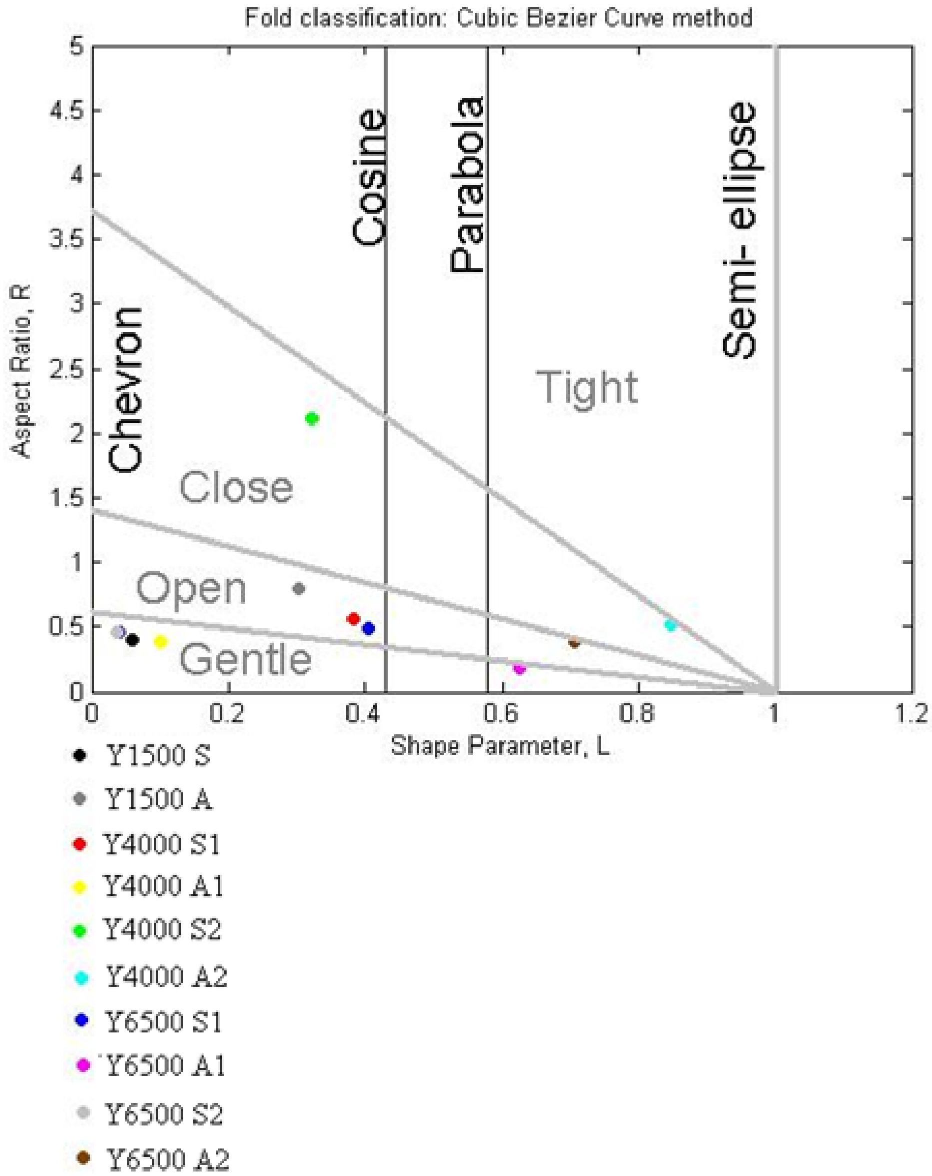

Fig. 8. The variation in fold shape using the cubic Bezier curve method. Folds vary from gentle to close and are dominantly cosine and chevron with some parabolas and rare semi-ellipses. Produced by Fold Profiler (Lisle et al., 2006).

5.1.2 Middle portion

Towards the southern end of the mine from 787 m depth, the fault becomes gently eastward dipping and locally west dipping to a depth of 1458 m below the surface (Figs. 5 and 8). The Paroo Fault is cross-cut by an inferred west southwest dipping fault that possibly caused the rotation of part of the Paroo Fault into a very shallow west dipping orientation up to a depth of 1345 m below the surface.

In the central section of the mine at a depth of 1140 m below the surface, there is a north-south orientated open synformal cosine fold and gentle antiformal chevron fold (Figs. 5 and 8). The dip is low towards the east, similar to the southern end. At 1378 m depth below the surface there is a north northwest-south southeast close synformal cosine fold (Figs. 5 and 8) in the fault below this depth the fault moderately dips towards the east.

In the northern section at a depth of 1457 m below the surface the dip changes from steeply west to steeply east to a depth of 1890 m, due to a north-south orientated synformal open cosine fold and gentle antiformal parabola fold (Figs. 5 and 8), till a depth of 1890 m below the surface where a gentle synformal chevron fold (Figs. 5 and 8) causes it to become slightly shallower. There is no shallow east dipping middle portion.

5.1.3 Lower portion

Towards the south at a depth of 1519 m below the surface the Paroo Fault is folded by a north-south close semi-elliptical antiform dipping to the west (Figs. 5 and 8). In the central section 1458 m below the surface there is a north-south gentle antiformal chevron fold (Figs. 5 and 8) where the dip of the fault changes to steeply east. The extent to which this continues with depth is shown by Betts and Lister (2002) in a cross section of the Mount Isa deposit. In the northern section at a depth of 2058 m below the surface the dip steepens at a north-south open antiformal parabola fold (Figs. 5 and 8).

5.2. Curvature analysis

The curvature analysis reveals two main sets of structures in the Paroo Fault (Fig. 9; Movie 2). The first set are two pairs of north-south orientated synforms and antiforms, that have amplitudes of 200-300 m; one set is located near to the eastern large scale synformal bend in the Paroo Fault and the other set is situated near the antiform of the large bend in the Paroo Fault. These folds have been disrupted by two pairs of north northwest-south southeast orientated synforms and antiforms in the Paroo Fault, which have amplitudes of 100-300 m, also recognised by Miller (2007). The non-stratiform copper orebodies are located above the NNW trending synforms.

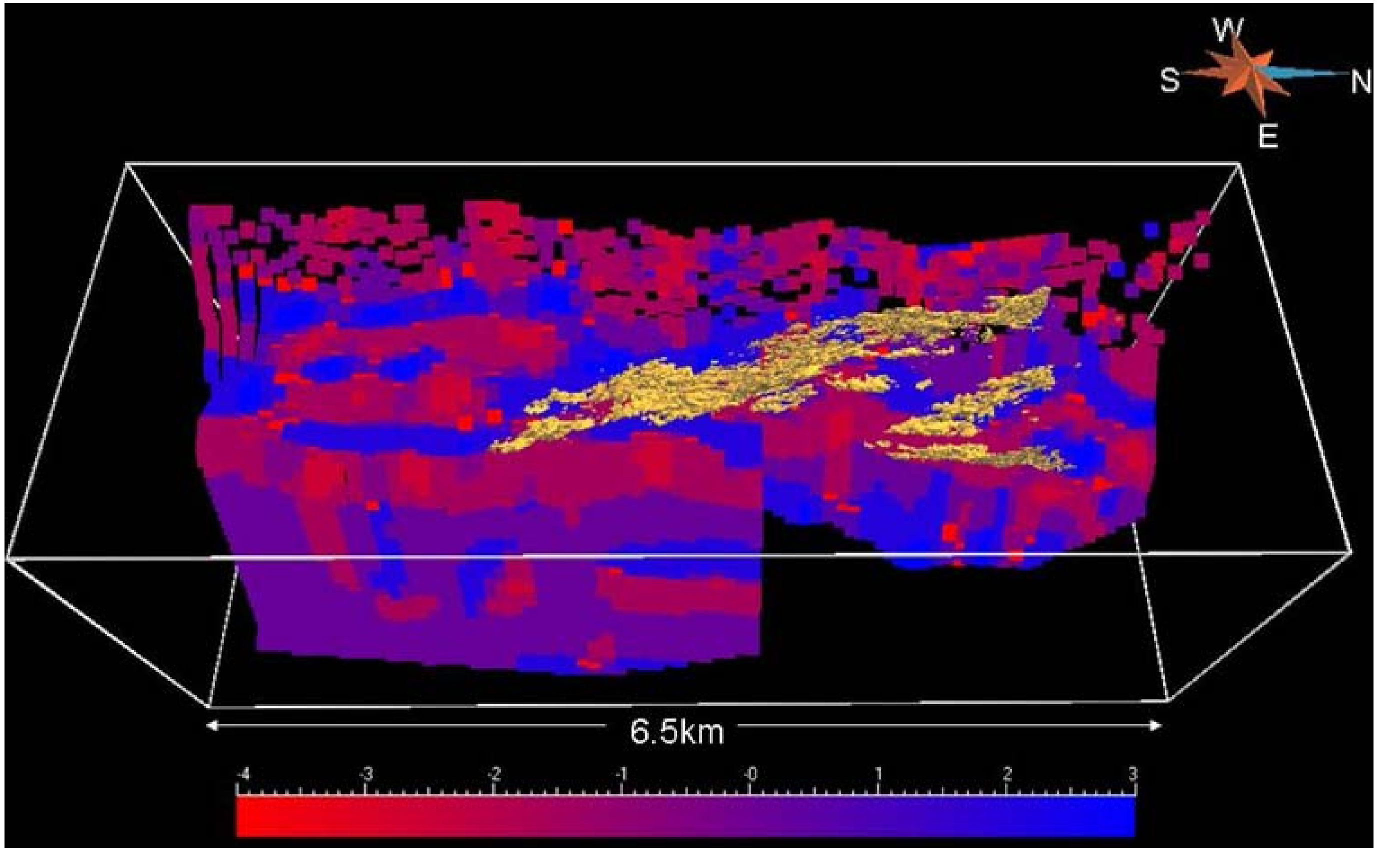

Fig. 9. The curvature of the Paroo Fault with the copper orebodies shown in yellow. Synforms have a Gaussian curvature value 1< K_G ≤3, shown in blue, the antiforms (-4< k_G <-1) shown in red and planar areas (-1 < K_G <1) shown in purple. Two dominant orientations of paired synforms and antiforms can be seen; north-south and north northwest-south southeast.

5.3. Spanned Length

The spanned length results (Table 2 and Fig. 10) show that in general the central portions (B) of the vertical sections are rougher than the upper and lower portions (A and C) and that the central portions of middle vertical section (2) is rougher than the central portions of the outer vertical sections (1 and 3). The flat section of the Paroo Fault has a higher roughness than the horizontal sections. Within the flat section of the Paroo Fault portion A is the roughest and the roughness decreases towards portion B and C.

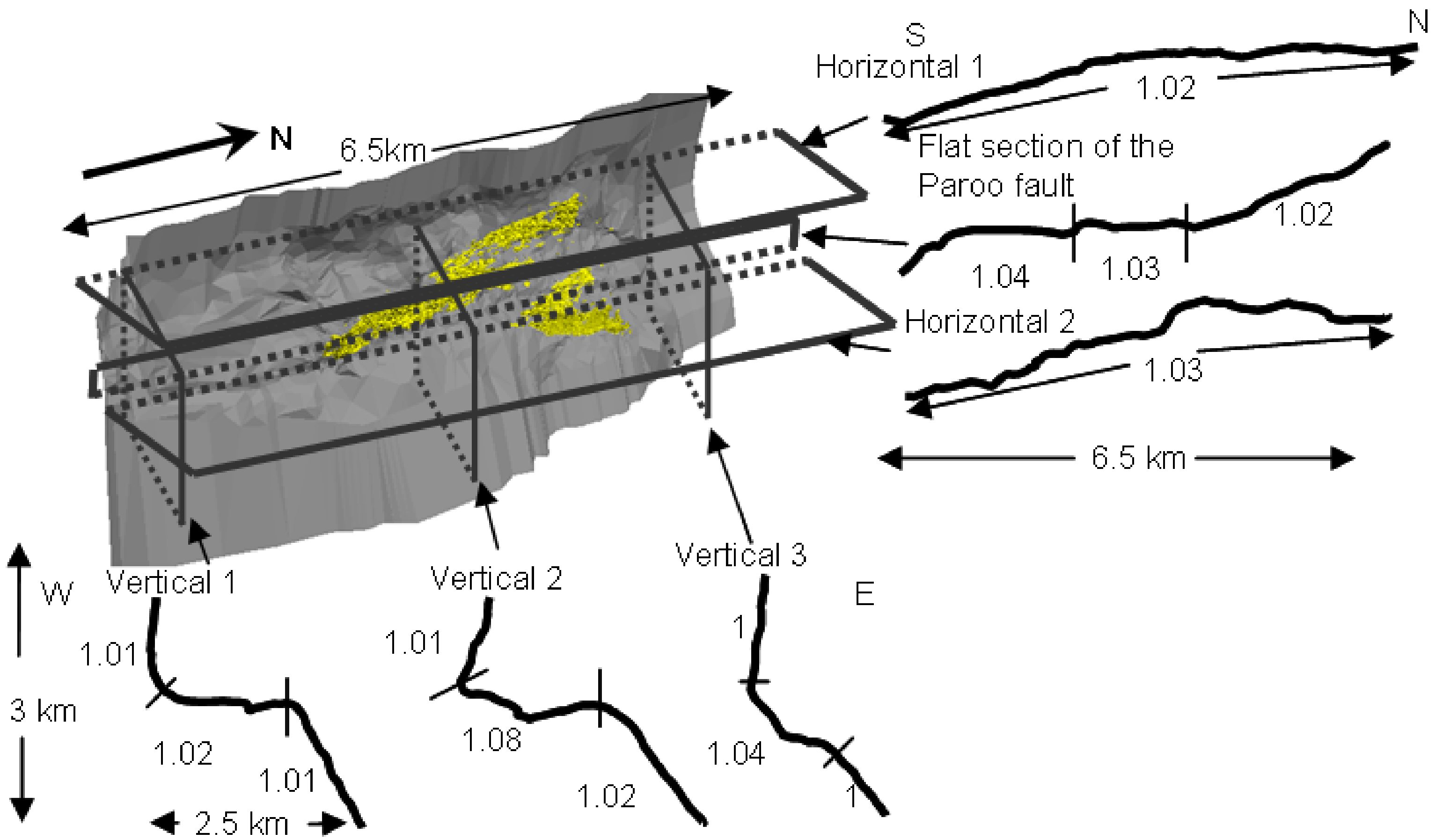

Fig. 10. Results of the roughness analysis from the spanned length method (numbers) demonstrating that the shallowly dipping middle portion is rougher than the steep upper and lower portions of the fault.

Spanned length			
Section	Slope (D)	Standard error	Correlation coefficient (R2)
Vertical 1A	1.01	0	1
Vertical 1B	1.02	0	1
Vertical 1C	1.01	0.01	1
Vertical 2A	1.01	0	1
Vertical 2B	1.08	0.01	1
Vertical 2C	1.02	0.01	1
Vertical 3A	1	0	1
Vertical 3B	1.04	0.01	1
Vertical 3C	1	0	1
Horizontal 1	1.02	0	1
Horizontal 2	1.02	0	1
Flat section of the fault A	1.04	0	1
Flat section of the fault B	1.03	0	1
Flat section of the fault C	1.02	0	1

Table 2. Results of the roughness analysis using the spanned length method. Roughness (D) is higher in the central portion of the fault than the upper and lower section.

5.4. Thickness

In general the shallow east dipping central section of the fault is thicker than the steeply dipping sections. The thicker parts of the Paroo Fault Zone filling in the central section are not located in the hinge of the large antiformal bend, but just to the west between the antiform and the copper orebodies (Fig. 11; Movie 2). The area of thickest fault zone filling is located to the east of the 1100 orebody; the fault zone filling here is over 25 m thick. The thick fault zone filling forms a band about 2 km long and 25 m wide that thins out in all directions. In between the 3000 and 3500 orebodies and to the east of the 3500 orebody there is another area of thicker fault zone filling (5-15 m). The thinner parts of the Paroo Fault Zone filling are more widely distributed and include the fault zone filling below the north-south orientated folds and the north northwest-south southeast orientated folds that underlie the copper mineralisation.

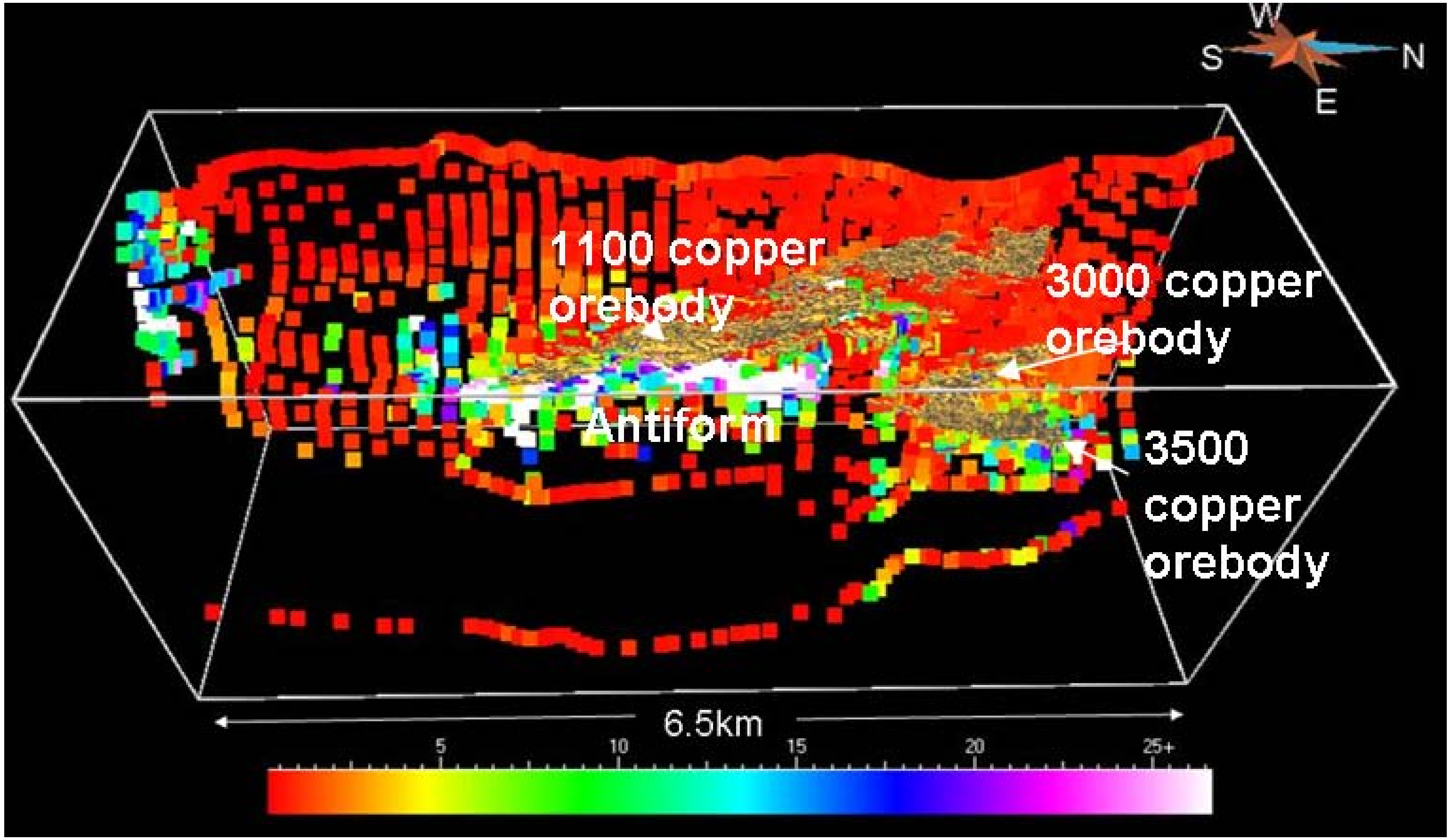

Fig. 11. Thickness of the Paroo Fault with the copper orebodies shown in yellow. The thickest areas of fault zone filling (white) lies on the western side of the large D_2 antiform in the Paroo Fault.

5.5. Slip tendency

The slip tendency work based on the Paroo Fault's current orientation demonstrates that it is possible to create the areas of high slip on the Paroo Fault for a variety of stress vectors and phi values. σ_1 in an east northeast-south southwest orientation (D_3) with a low phi value (0.1) and a vertical σ_3 produces an area of high slip on the western edge of the discordant cooper orebodies that are located on the Paroo Fault (Fig. 12; Movie 2). This correlates with the areas on the Paroo Fault in which the copper orebodies are situated, and also the areas of larger thicknesses of fault zone filling on the eastern side of the Paroo Fault.

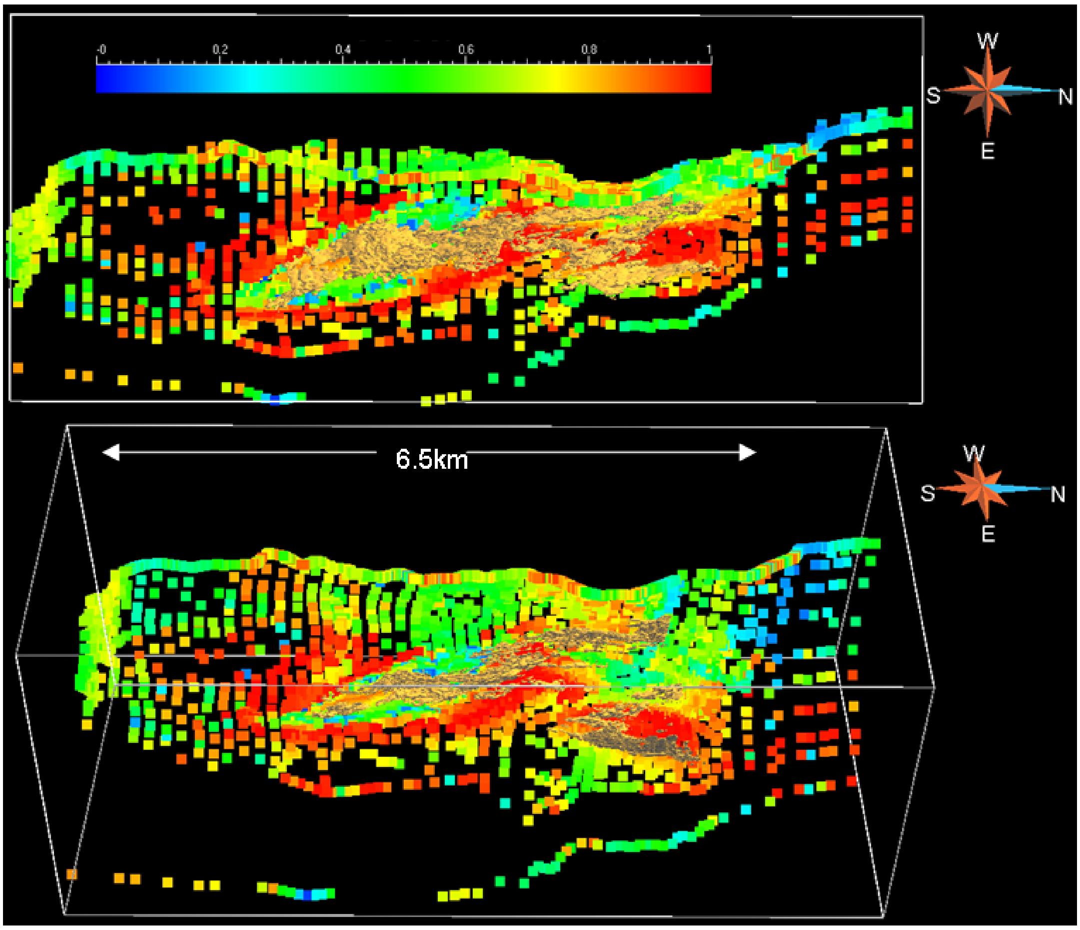

Fig. 12. Slip tendency of the Paroo Fault using an east northeast-west southwest orientation for σ_1 and a phi value of 0.1. The copper orebodies are shown in yellow. There is a correlation between high slip tendency and the flanks of folds where they bend around the orebodies. This indicates the possibility of reactivation of the fault by shearing, during folding of the fault around the orebodies.The upper figure is a plan view of the results while the lower is a three-dimensional view.

5.6. Dilation tendency

Dilation tendency analysis shows that areas of high dilation tendency on the Paroo Fault can be created in the vicinity of the copper orebodies (Fig. 13; Movie 2). Stress tensors which have a strong correlation with the position of the copper orebodies had a vertical σ_3 and low phi value (0.1). The other phi values (0.5 and 0.9) used also produced a good, but less strong correlation. Models which used a vertical σ_2 did not have a good correlation with the copper orebodies. Therefore the relative values of $\sigma_{1,}$ σ_2 and σ_3 are not the important control on dilation tendency, but σ_3 being vertical is critical. Only the model with the highest correlation to the copper orebodies is presented.

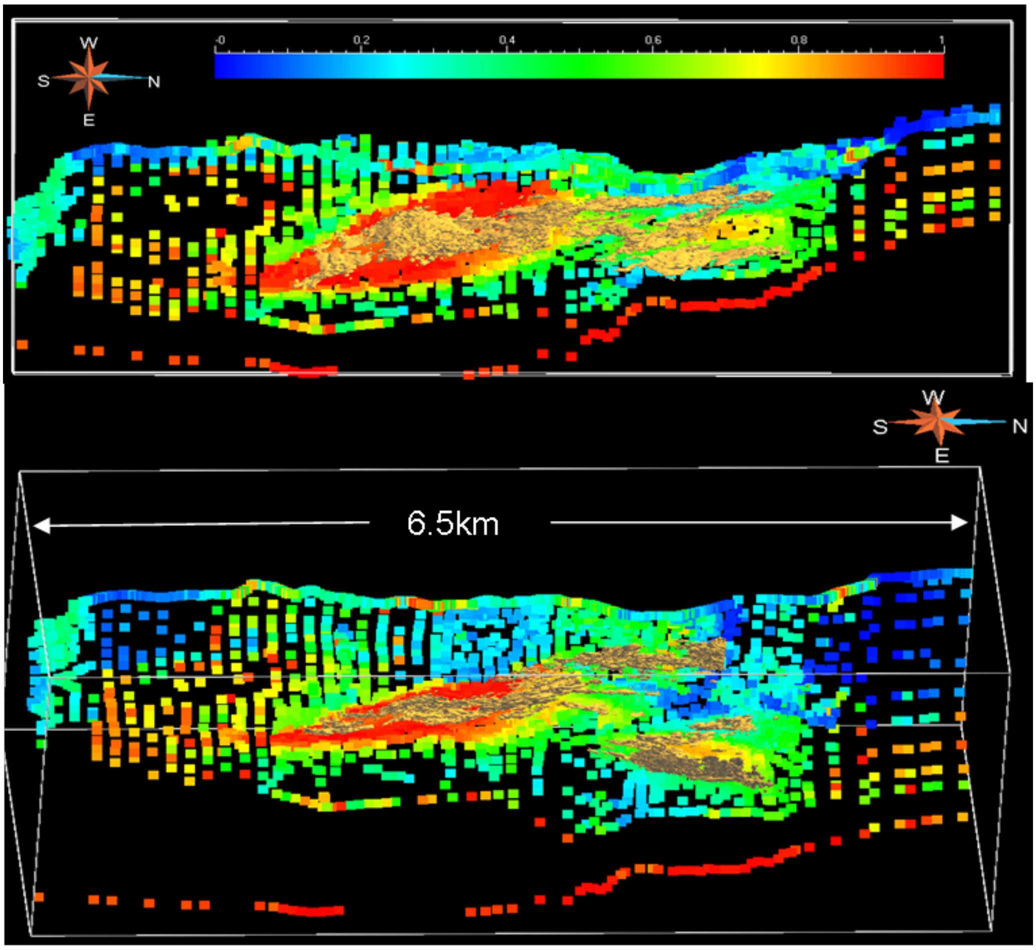

Fig. 13. Dilation tendency of the Paroo Fault using D_3 stress tensors (vertical σ_3 and a phi value of 0.1). The copper orebodies are shown in yellow. For these stress vectors there is clear correlation between the position of the orebodies and areas of high dilation tendency (red and yellow), indicating remobilising of pre-existing copper could occur in D_3. The upper figure is a plan view of the results while the lower is a three-dimensional view.

6. Discussion

There is little direct evidence at the Mount Isa copper and lead-zinc-silver mines to support the idea that the Paroo Fault was active during the deposition of the Mount Isa Group. Folding within the lead-zinc-silver orebody that Dunnet (1976) suggested was due to syn-faulting slumping may have formed during later deformation (McDonald, 1970). Bell (1983) argues against the idea that the Paroo Fault formed during sedimentation of the Mount Isa Group (Smith, 1969; Mathias and Clark, 1975) on the basis that the sigmoidal shape of the Paroo Fault was not active at this stage because there were no later complex interfering folds, which were not recognised. However, the new view of the detail geometry of the Paroo Fault shown in this study (Figs. 5, 8; Movie 2) reveals that it was affected by two sets of overprinting folds, opening up the possibility that the fault formed before folding, and during sedimentation of the Mount Isa Group.

Bell et al. (1988) also suggested out that there is no evidence of syn-faulting deposition of the Mount Isa Group sediments. Earlier work however, had demonstrated that there is indeed evidence for penecontemporaneous faulting during the deposition of the Mount Isa Group within the vicinity of the deposits (Smith, 1969; Mathias and Clark, 1975). The Kennedy Siltstone and Magazine Shale dip both east and west in the core of a synform (Fig. 2; Movie 1). These members represent the last stages of deposition of the Mount Isa Group, and may have developed a hangingwall synform due to compaction during normal movement on the Paroo Fault. There is no evidence of large scale folds in the footwall of the fault, suggesting that the synform is related to the fault development. Several extension related synforms within the Mount Isa Group occur within the hangingwalls of fault blocks throughout the Western Fold Belt (O'Dea et al., 1996; 1997a). Synsedimentary faulting of the Mount Isa Group has also been firmly established east and northeast (Nijman et al., 1992a; b; Betts, 1999) and to the south and southwest of the Mount Isa deposits (Connors et al., 1992; Stewart, 1992). These extension related synforms and syn-sedimentary faults formed due to movement on rift blocks during the sag phase of the Isa Superbasin (O'Dea et al., 1996; 1997a; Betts et al., 1998; Betts and Lister, 2002).

The evidence presented here is in agreement with Betts and Lister's (2002) suggestion that the Paroo Fault represents a basin bounding normal fault formed during the Leichhardt Rift Event, which was subsequently reactivated during the sag phase of the Isa Superbasin development. Evidence for reactivation during the deposition of the Kennedy Siltstone and Magazine Shale is present at Mount Isa mines. The majority of the Mount Isa Group was deposited during the sag phase of the Mount Isa Rift Event, and there is evidence of tectonic driven subsidence, uplift and fault activity during this time (Betts and Lister, 2001). The orientation of extension during the deposition of the Mount Isa Group is northwest-southeast (O'Dea et al., 1997a; Betts et al., 1998; 1999; 2006; Betts, 2001; Betts and Lister, 2001), and caused the reactivation north-south faults, such as the Paroo Fault, and east-west cross faults, as growth faults (Betts et al., 1998; 2003; Betts and Lister, 2001).

The model of MacCready (2006) generates a sigmoidal shape similar to the shape Paroo Fault using two steeply dipping faults and a shallower dipping fault. The major problem with this model is that it requires three faults which would have a similar orientation to the Satellite-Biotite Fault, Native Bee Fault and the Clone Fault. The Mount Isa deposit shows no evidence of three such structures, and the three-dimensional model of the geometry of the Paroo Fault is based on over 20,000 drill-holes, none of which show evidence of a sub-vertical fault within the Eastern Creek Volcanics to the west of the copper orebodies, or a sub-vertical fault to the east of the copper orebodies within the Mount Isa Group.

6.1. A new model for the Paroo Fault

A model for the formation and timing of the Paroo Fault and the development of the copper orebodies is presented here (Fig. 14) based on Betts and Lister's (2002) concept that the Paroo Fault originally represented a basin bounding fault. The Paroo Fault could have formed prior to sedimentation of the Mount Isa Group, and reactivated during sedimentation/ compaction of the Kennedy Siltstone and Magazine Shale to form a hangingwall syncline. This initial fold may have been tightened during D_2 and D_3 creating the observed fold geometry.

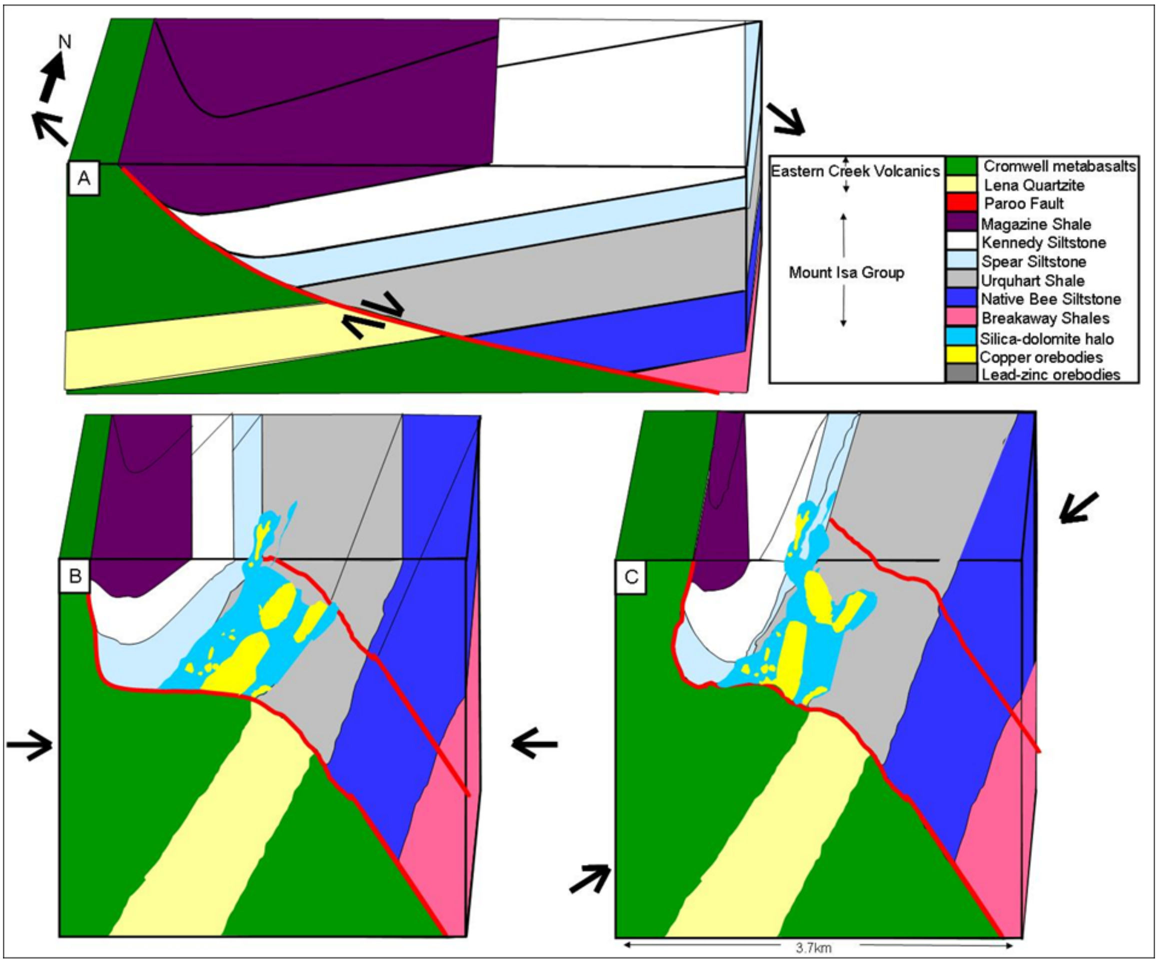

Fig. 14. Cartoon showing the deformation history of the Paroo Fault and the formation of the Mount Isa copper deposit; a) normal faulting on a listric fault during the sedimentation of the Kennedy Siltstone and Magazine Shale; b) East-west shortening causing folding of the Paroo Fault, Kennedy Siltstone and Magazine Shale as well as the formation of the copper orebodies and Paroo Fault fill; c) East northeast-west southwest shortening causing the folding of the Paroo Fault and Urquhart Shale around the copper orebodies. The Paroo Fault fill becomes sheared into its present position.

The normal movement provides a timing constraint for the formation or major reactivation of the Paroo Fault. Page and Sweet (1998) obtained a 207Pb/206Pb age of 1652 ± 7 Ma using U-Pb SHRIMP methods on zircons from a tuff in the Urquhart Shale near the Mount Isa copper deposit. This provides the best constraint on the maximum age for the development or initial reactivation of the fault currently available.

Several elements of the deformation sequence of Bell (1983) are consistent with the observations given above. North-south orientated fold hinges within the Paroo Fault indicated by the Gaussian curvature analysis (Fig. 10; Movie 2) are compatible with the D_2 event described regionally (Swager, 1983). The north-south folds in the Paroo Fault (D_2) are disrupted by subsequent north northwest-south southeast orientated folds (D_3). The location of the Lena Quartzite in the basement may have had a key role in the localization of the D_2 north-south orientated folds on the Paroo Fault (Figs. 3b and c; Movie 1).

It seems likely that the later deformation event (D_3) and the presence of the copper orebodies has caused the variation in fold shape (Figs. 5 and 8). In Fig. 15 and Movie 1 the Paroo Fault is observed to bend around the non-stratiform copper orebodies in D_3 folds. This suggests that the orebodies may have formed prior to this deformation event. Further support for the D3 folds in the Paroo Fault forming after at least some of the chalcopyrite mineralisation comes from the spanned length analysis (Fig. 9). This has shown that central portions (B) of the vertical sections are rougher than the upper and lower portions (A and C). This could be due to the Paroo Fault being folded irregularly around the copper orebodies, increasing the roughness in the central portions.

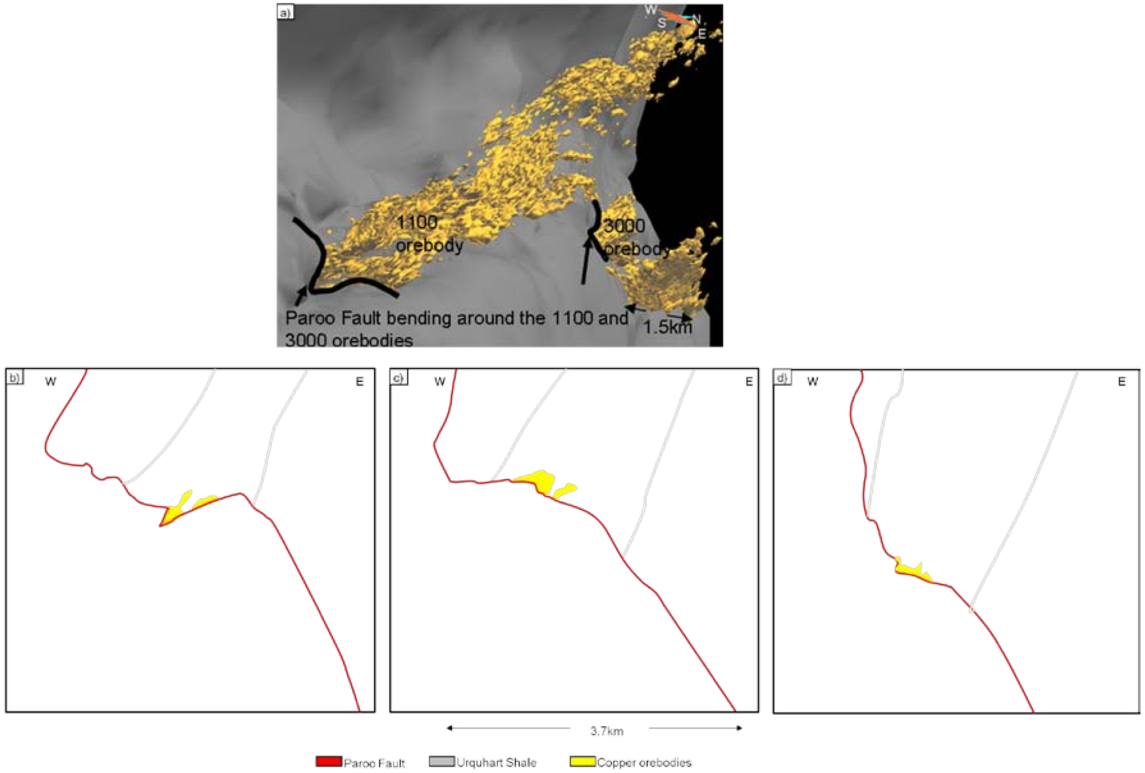

Fig. 15. a) Image of the three-dimensional GoCAD model of the Paroo Fault (Grey) buttressing and bending around the 1100 and 3000 copper orebodies (Yellow) in D_3 folds, indicating the copper orebodies may have formed prior to D_3; b) cross-section of the Paroo Fault bending around the southern end of the 1100 orebody; c) cross-section of the Paroo Fault bending around the northern end of the 1100 orebody; d) cross-section of the Paroo Fault bending around the 3000 copper orebody.

The dilation tendency results (Fig. 13; Movie 2) suggest that D_3 dilation could have occurred above parts of the Paroo Fault. D_3 dilation may have remobilised the non-stratiform orebodies creating the D_3 characteristics described by Swager (1983; 1985); Perkins (1984); Bell et al. (1988); Davis (2004); Miller, (2006). This dilation may also be responsible for the development of late quartz veins within the Lena Quartzite, Paroo Fault zone filling and silica-dolomite halo.

Within the vicinity of the Mount Isa deposits the majority of folds have been demonstrated to be parallel folds (Winsor, 1983; Perkins, 1984; 1997) which would form by normal folding mechanisms such as buckling/tangential longitudinal strain and flexural slip flow. These folding mechanisms are unlikely to create a situation where a fold is thinnest in its hinge. Some of the thinnest parts of the Paroo Fault zone filling, however, are located in the hinge of the large D_2 antiformal bend (Fig. 11; Movie 2). If the fault zone filling developed during this deformation event, the hinges should not be the thinnest areas of fault zone filling. Similarly it would be expected that if the fault zone filling had developed during D_3 folding, these hinges would not be the thinnest areas of fault zone filling. However, the filling below the D_3 north northwest-south southeast orientated synforms that are associated with the copper mineralisation are some of the thinnest areas of fault zone filling (Fig.11).

The Paroo Fault Zone filling therefore either formed post D_3, forming around the copper orebodies (unlikely because of the thickness variations described above), or the fault zone filling was formed before or early during D_2 deformation, and was sheared out from under the orebodies and the hinges of the D_2 folds in the fault during D_3 folding. Slip tendency analysis for a D_3 stress tensor indicates areas of high slip likelihood to west and east of the copper orebodies, which could have caused the Paroo Fault Zone filling to become sheared from these areas into its current position during D_3. The Paroo Fault zone filling consists of alternations of graphite and quartz which likely formed before or early in D_2 and would provide multiple slip surfaces for the fault to reactivate during D_2. The Paroo Fault however did not simply reactivate under brittle conditions during D_2, but underwent significant continuous deformation. The Lena Quartzite as a high competency layer within the Cromwell Metabasalt may have caused stress perturbations around the fault causing it to fold and not reactivate. The precipitation of quartz may have also augmented fault cohesion so that folding occurred rather than just shear reactivation.

West dipping faults within the deposit have been suggested to have a D_{4a} age as they offset the copper orebodies which have been assumed to form during D3 (Miller, 2007). Since the copper orebodies are now interpreted to have formed in early D_2 (papers 2 and 3), the west dipping faults which offset the copper mineralisation could have developed during late D_2. The D_{4a} faults are crosscut by northwest and northeast trending faults termed D_{4b} by Miller (2007). Another implication of the copper mineralisation forming during early D_2 is the D_{4b} conjugate faults could have formed during D_3 deformation.

7. Conclusions

The Paroo Fault data set examined in this study provided the opportunity to analyse the history of a fault throughout a complex history at scales from meters to kilometres. The fault was formed or reactivated during the deposition of the Mount Isa Group as a basin-bounding normal fault (Fig. 15). The fault was subsequently folded during east-west contraction (D_2) forming the north-south trending folds. A subsequent event (D_3) formed north northwest-south southeast folds within the Paroo Fault, which wrap around pre-existing copper orebodies and overprint the D_2 folds. Curvature and roughness analysis suggest that the orebodies formed during D_2, and D_3 caused the folded fault to wrap around the orebodies.

Stress perturbations caused by the presence of the silica-dolomite halo and Lena Quartzite caused the fault to bend rather than simply reactivate during shortening. The Paroo Fault deformed partly by folding during D_2 and D_3 events, and it was sheared and dilated; its behaviour involved both folding and reactivation. The complex geometry of the Paroo Fault surface shows that fault surfaces can preserve a remarkable record of the sequence of multiple deformation events. Fault surfaces can be clearly recognised after folding by more than one generation of folds, as well as being reactivated in shear and dilation in subsequent events. Even syn-sedimentary features can be preserved in the vicinity of faults that have been multiply deformed.

8. Acknowledgements

Thanks to Xstrata Copper for providing logistical support partly funded through the Xstrata Community Partnership Program, North Queensland. We thank the entire mine and exploration geology staff for all their help. Granddad and Uncle Ian thank you for your love and support you will always be missed.

9. References:

Adshead-Bell, N. S. 1998. Evolution of the Starra and Selwyn high-strain zones, Eastern fold belt, Mount Isa Inlier; implications for Au-Cu mineralization. Economic Geology 93, 1450-1462.

Andrés, M., Tatiana, G., Jonas, K., Diana, M., Mauricio, P., Luis Ignacio, Q., German, R. & Manfred, R. S. 2009. The role of inherited extensional fault segmentation and linkage in contractional orogenesis: a reconstruction of Lower Cretaceous inverted rift basins in the Eastern Cordillera of Colombia. Basin Research 21, 111-137.

Andrew, A. S., Heinrich, C. A., Wilkins, R. W. T. & Patterson, D. J. 1989. Sulfur isotope systematics of copper ore formation at Mount Isa, Australia. Economic Geology and the Bulletin of the Society of Economic Geologists 84, 1614-1626.

Aviles, C. A., and Scholz, C. H., 1987. Fractal Analysis Applied to Characteristic Segments of the San Andreas Fault. Journal of Geophysical Research 92, 331-344.

Bell, T. H. 1983. Thrusting and duplex formation at Mount Isa. Nature 304, 493-497.

Bell, T. H. & Hickey, K. A. 1998. Multiple Deformations with Successive Subvertical and Subhorizontal Axial Planes in the Mount Isa Region: Their Impact on Geometric Development and Significance for Mineralization and Exploration. Economic Geology 93, 1369-1389.

Bell, T. H., Perkins, W. G. & Swager, C. P. 1988. Structural controls on development and localization of syntectonic copper mineralization at Mount Isa, Queensland. Economic Geology and the Bulletin of the Society of Economic Geologists 83, 69-85.

Betts, P. G., 2001, Three-dimensional structure along the inverted Palaeoproterozoic Fiery Creek fault system, Mount Isa Terrane, Australia. Journal of Structural Geology 23, 1953-1969.

Betts, P. G. 1999. Palaeoproterozoic mid-basin inversion in the northern Mt. Isa terrane, Queensland. Australian Journal of Earth Sciences 46, 735-748.

Betts, P. G., Giles, D. & Lister, G. S. 2003. Tectonic environment of shale-hosted massive sulfide Pb-Zn-Ag deposits of Proterozoic northeastern Australia. Economic Geology and the Bulletin of the Society of Economic Geologists 98, 557-576.

Betts, P. G., Giles, D., Mark, G., Lister, G. S., Goleby, B. R., and Aillères, L., 2006, Synthesis of the proterozoic evolution of the Mt Isa Inlier. Australian Journal of Earth Sciences 53, 187-211.

Betts, P. G., and Lister, G. S., 2001, Comparison of the 'strike-slip' versus the 'episodic rift -sag' models for the origin of the Isa Superbasin. Australian Journal of Earth Sciences 48, 265-280.

Betts, P. G. & Lister, G. S. 2002. Geodynamically indicated targetting strategy for shale-hosted massive sulfide Pb-Zn-Ag mineralisation in the Western Fold Belt, Mt Isa terrane. Australian Journal of Earth Sciences 49, 985-1010.

Betts, P. G., Lister, G. S. & O'Dea, M. G. 1998. Asymmetric extension of the middle Proterozoic lithosphere, Mount Isa Terrane, Queensland, Australia. Tectonophysics 296, 293-316.

Betts, P. G., Lister, G. S., and Pound, K. S., 1999, Architecture of a Palaeoproterozoic rift system; evidence from the Fiery Creek Dome region, Mt. Isa Terrane. Australian Journal of Earth Sciences 46, 533-554.

BMR. 1978. Mount Isa 1:100 000 Geological Series, Sheet 6756 (edited by Australia, G.).

Butler, R. W. H. 1989. The influence of pre-existing basin structure on thrust system evolution in the Western Alps. Geological Society of London, Special Publications 44, 105-122.

Caine, J. P., Evans, J. P. & Forster, C. B. 1996. Fault zone architecture and permeability structure. Geology 24, 1025-1028.

Candela, T., Renard, F., Bouchon, M., Brouste, A., Marsan, D., Schmittbuhl, J. & Voisin, C. 2009. Characterization of Fault Roughness at Various Scales: Implications of Three-Dimensional

High Resolution Topography Measurements. Pure and Applied Geophysics 166, 1817-1851.

Childs, C., Manzocchi, T., Walsh, J. J., Bonson, C. G., Nicol, A. & Schöpfer, M. P. J. 2009. A geometric model of fault zone and fault rock thickness variations. Journal of Structural Geology 31, 117-127.

Childs, C., Nicol, A., Walsh, J. J. & Watterson, J. 2003. The growth and propagation of synsedimentary faults. Journal of Structural Geology 25, 633-648.

Connors, K. 1992. Hunter Resources Limited EPM 8315: Structural Controls on MIneralization in the Gunpowder Area. Etheridge & Henley Geoscience Consultants, 37.

Connors, K. A. & Lister, G. S. 1995. Polyphase deformation in the western Mount Isa Inlier, Australia; episodic or continuous deformation? Journal of Structural Geology 17, 305-328.

Connors, K. A., Proffett, J. M., Lister, G. S., Scott, R. J., Oliver, N. H. S. & Young, D. J. 1992. Geology of the Mount Novit Ranges, southwest of Mt Isa mine. In: Detailed Studies of the Mt Isa Inlier (edited by Stewart, A. J. & Blake, D. H.) 243. Australian Geological Survey Organisation, Canberra, 137-160.

Davis, T. P. 2004. Mine-scale structural controls on the Mount Isa Zn-Pb-Ag and Cu orebodies. Economic Geology and the Bulletin of the Society of Economic Geologists 99, 543-559.

Derrick, G. M. 1982. A Proterozoic rift zone at Mount Isa, Queensland, and implications for mineralisation. BMR Journal of Australian Geology and Geophysics 7, 81-92.

Dunnet, D. 1976. Mt Isa; reconstruction of a faulted ore body. Philosophical Transactions of the Royal Society of London, Series A: Mathematical and Physical Sciences 283, 333-344.

Farquharson, R. B. & Richards, J. R. 1974. U-Th-Pb isotope systematics related to igneous rocks and ore Pb, Mount Isa, Queensland. Mineralium Deposita 9, 339-356.

Fernández-Martínez, J. L. & Lisle, R. J. 2009. GenLab: A MATLAB®-based program for structural analysis of folds mapped by GPS or seismic methods. Computers & Geosciences 35, 317-326.

Ferrill, D. A., Winterle, J., Wittmeyer, G., Sims, D., Colton, S., Armstrong, A., and Morris, A.P. 1999. Stressed Rock strains groundwater at yucca Mountain, Nevada. GSA Today 9, 1-8.

Finlow-Bates, T. & Stumpfl, E. F. 1979. The copper and lead-zinc-silver orebodies of Mt. Isa Mine, Queensland; products of one hydrothermal system. Annales de la Societe Geologique de Belgique 102, 497-517.

Gessner, K. 2009. Coupled Models of Brittle-plastic Deformation and Fluid Flow: Approaches, Methods, and Application to Mesoproterozoic Mineralisation at Mount Isa, Australia. Surveys in Geophysics 30, 211-232.

Gessner, K., Jones, P. A., Wilde, A. R. & Kühn, M.2006. Significance of strain localization and fracturing in relation to hydrothermal mineralization at Mount Isa, Australia. Journal of Geochemical Exploration 89, 129-132.

Ghisetti, F. C. & Sibson, R. H. 2006. Accommodation of shorteningal inversion in north-western South Island (New Zealand): Old faults versus new? Journal of Structural Geology 28, 1994-2010.

Giaccio, B., Galadini, F., Sposato, A., Messina, P., Moro, M., Zreda, M., Cittadini, A., Salvi, S. & Todero, A. 2003. Image processing and roughness analysis of exposed bedrock fault planes as a tool for paleoseismological analysis: results from the Campo Felice fault (central Apennines, Italy). Geomorphology 49, 281-301.

Gibson, G. M. & Henson, P. A. 2005. Chapter 6: Post-depositional deformation in the Western Succession. In: Project I1: 3D Basin Architecture & Mineral Systems in the Mt Isa Western Succession (edited by Gibson, G. M. & Hitchman, A. P.). Predictive Mineral Discovery Cooperative Research Centre, Canberra, 147-176.

Gray, D. R. & Gregory, R. T. 2003. Fault geometry as evidence for inversion of a former rift basin in the Eastern Lachlan Orogen. Australian Journal of Earth Sciences: An International Geoscience Journal of the Geological Society of Australia 50, 513 - 523.

Gulson, B. L., Perkins, W. G. & Mizon, K. J. 1983. Lead isotope studies bearing on the genesis of copper orebodies at Mount Isa, Queensland. Economic Geology and the Bulletin of the Society of Economic Geologists 78, 1466-1504.

Hannan, K. W., Golding, S. D., Herbert, H. K. & Krouse, H. R. 1993. Contrasting alteration assemblages in metabasites from Mount Isa, Queensland; implications for copper ore genesis. Economic Geology and the Bulletin of the Society of Economic Geologists 88, 1135-1175.

Hayward, A. B. & Graham, R. H. 1989. Some geometrical characteristics of inversion. Geological Society London, Special Publications 44, 17-39.

Heinrich, C. A., Andrew, A. S., Wilkins, R. W. T. & Patterson, D. J. 1989. A fluid inclusion and stable isotope study of synmetamorphic copper ore formation at Mount Isa, Australia. Economic Geology and the Bulletin of the Society of Economic Geologists 84, 529-550.

Heinrich, C. A., Bain, J. H. C., Mernagh, T. P., Wyborn, L. A. I., Andrew, A. S., and Waring, C. L., 1995, Fluid and mass transfer during metabasalt alteration and copper mineralization at Mount Isa, Australia. Economic Geology and the Bulletin of the Society of Economic Geologists 90, 705-730.

Heinrich, C. A., Bain, J. H. C., Fardy, J. J. & Waring, C. L. 1993. Br/Cl geochemistry of hydrothermal brines associated with Proterozoic metasediment-hosted copper mineralization at Mount Isa, northern Australia. Geochimica et Cosmochimica Acta 57, 2991-3000.

Heinrich, C. A. & Cousens, D. R. 1989. Semi-quantitative electron microprobe analysis of fluid inclusion salts from the Mount Isa copper deposit (Queensland, Australia). Geochimica et Cosmochimica Acta 53, 21-28.

Holdsworth, R. E., Stewart, M., Imber, J. & Strachan, R. A. 2001. The structure and rheological evolution of reactivated continental fault zones: a review and case study. Geological Society of London, Special Publications 184, 115-137.

Jackson, J. & McKenzie, D. 1999. A hectare of fresh striations on the Arkitsa Fault, central Greece. Journal of Structural Geology 21, 1-6.

Jackson M.J., Scott D.L. & Rawlings D.J. 2000. Stratigraphic framework for the Leichhardt and Calvert Superbasins: review and correlations of the pre-1700 Ma successions between Mt Isa and McArthur River. Australian Journal of Earth Sciences 47, 381-403.

Kelly, P. G., Peacock, D. C. P., Sanderson, D. J. & McGurk, A. C. 1999. Selective reverse-reactivation of normal faults, and deformation around reverse-reactivated faults in the Mesozoic of the Somerset coast. Journal of Structural Geology 21, 493-509.

Kendrick, M. A., Duncan, R. & Phillips, D. 2006. Noble gas and halogen constraints on mineralizing fluids of metamorphic versus surficial origin: Mt Isa, Australia. Chemical Geology 235, 325-351.

Keys, D. (2009) Mechanical localization of copper deposits in the Mt Isa Inlier, North Queensland , Ph.D. thesis, James Cook Univ.

Kondo, H., Awata, Y., Emre, O., Dogan, A., Ozalp, S., Tokay, F., Yildirim, C., Yoshioka, T. & Okumura, K. 2005. Slip Distribution, Fault Geometry, and Fault Segmentation of the 1944 Bolu-Gerede Earthquake Rupture, North Anatolian Fault, Turkey. Bulletin of the Seismological Society of America 95, 1234-1249.

Kühn, M., Dobert, F. & Gessner, K. 2006. Numerical investigation of the effect of heterogeneous permeability distributions on free convection in the hydrothermal system at Mount Isa, Australia. Earth and Planetary Science Letters 244, 655-671.

Kühn, M. & Gessner, K. 2006. Reactive transport model of silicification at the Mount Isa copper deposit, Australia. Journal of Geochemical Exploration 89, 195-198.

Kühn, M. & Gessner, K. 2009. Testing Hypotheses for the Mount Isa Copper Mineralisation with Numerical Simulations. Surveys in Geophysics 30, 253-268.

Lisle, R. J., Fernandez Martinez, J. L., Bobillo-Ares, N., Menendez, O., Aller, J. & Bastida, F. 2006. FOLD PROFILER: A MATLAB—based program for fold shape classification. Computers & Geosciences 32, 102–108.

Lisle, R. J. & Srivastava, D. C. 2004. Test of the frictional reactivation theory for faults and validity of fault-slip analysis. Geology 32, 569-572.

Lister, G. S. 1993. The role of thrusting in the structural development of the Mount Isa Mine and its relevance to exploration in the surrounding region; discussion. Economic Geology and the Bulletin of the Society of Economic Geologists 88, 479.

Lister G.S., O'Dea M.G. & Somaia I. 1999. A tale of two synclines: rifting, inversion and

transpressional popouts at Lake Julius, northwestern Mt Isa terrane, Queensland. Australian Journal of Earth Sciences 46, 233-250.

Loosveld, R. & Schreurs, G. 1987. Discovery of thrust klippen, northwest of Mary Kathleen, Mt. Isa Inlier, Australia. Australian Journal of Earth Sciences 34, 387-402.

MacCready, T. 2006. Structural evolution of the southern Mt Isa Valley. Australian Journal of Earth Sciences 53, 27-40.

Mathias, B. V. & Clark, G. J. 1975. Mount Isa copper and silver-lead-zinc orebodies; Isa and Hilton mines. Monograph Series - Australasian Institute of Mining and Metallurgy no. 5, 351-371.

Mazzoli, R. W. H. B. a. S. 2006. Styles of continental contraction: A review and introduction. Geological Society of America Special Papers 414, 1-10.

McDonald, J. A. 1970. Some effects of deformation on sulfide-rich layers in lead-zinc ore bodies, Mount Isa, Queensland. Economic Geology and the Bulletin of the Society of Economic Geologists 65, 273-298.

McGoldrick, P. J. & Keays, R. R. 1990. Mount Isa copper and lead-zinc-silver ores; coincidence or cogenesis? Economic Geology and the Bulletin of the Society of Economic Geologists 85, 641-650.

Miller, J. M. 2007. Structural controls on the Mt Isa Copper deposit, QLD. In: Project I7. Predictive Mineral Discovery CoOperative Research Centre, 70.

Moeck, I., Kwiatek, G. & Zimmermann, G. 2009. Slip tendency analysis, fault reactivation potential and induced seismicity in a deep geothermal reservoir. Journal of Structural Geology 31, 1174-1182.

Morris, A., Ferrill, D. A. & Henderson, D. B. 1996. Slip-tendency analysis and fault reactivation. Geology 24, 275-278.

Mynatt, I., Bergbauer, S. & Pollard, D. D. 2007. Using diffrential geometry to describe 3-D folds. Journal of Structural Geology 29, 1256-1266.

Nemcok, M., Moore, J. N., Allis, R. & McCulloch, J. 2004. Fracture development within a stratovolcano: the Karaha-Telaga Bodas geothermal field, Java volcanic arc. Geological Society of London, Special Publications 231, 223-242.

Nijman, W., Mijnlieff, H. F. & Schalkwijk, G. 1992a. The Hero Fan Delta (Lower Mount Isa Group) and its structural control: deformation in the Hero/Western Fault Zone and Paroo Range compared, Proterozoic, Mount Isa Inlier, Queensland, Australia. In: Detailed Studies of the Mount Isa Inlier (edited by Stewart, A. J. & Blake, D.

H.) 243. Australian Geological Survey Organisation, Canberra, 75-110.

Nijman, W., van Lochem, J. H., Spliethoff, H. & Feijth, J. 1992b. Deformation model and sedimentation patterns of the Proterozoic of the Paroo Range, Mount Isa Inlier, Queensland, Australia, . In: Detailed Studies of the Mount Isa Inlier (edited by Stewart, A. J. & Blake, D. H.) Australian Geological Survey Organisation Bulletin 243, Canberra.

O'Dea, M. G., Lister, G., MacCready, T., Betts, P. G., Oliver, N. H. S., Pound, K. S., Huang, W. & Valenta, R. K. 1996. Geodynamic evolution of the Proterozoic Mount Isa terrain., in Burg, J.P., and Ford, M., eds., Orogeny through time. Geological Society Special Publication 121, 99-122.

O'Dea, M. G. & Lister, G. S. 1995. The role of ductility contrast and basement architecture in the structural evolution of the Crystal Creek Block, Mount Isa Inlier, NW Queensland, Australia. Journal of Structural Geology 17, 949-960.

O'Dea, M. G., Lister, G. S., Betts, P. G. & Pound, K. S. 1997a. A shortened intraplate rift system in the Proterozoic Mount Isa terrane, NW Queensland, Australia. Tectonics 16, 425-441.

O'Dea, M. G., Lister, G. S., Maccready, T., Betts, P. G., Oliver, N. H. S., Pound, K. S., Huang, W., Valenta, R. K., Oliver, N. H. S. & Valenta, R. K. 1997b. Geodynamic evolution of the Proterozoic Mount Isa terrain. Geological Society of London, Special Publications 121, 99-122.

Page, R. W., Jackson, M. J. & Krassay, A. A. 2000. Constraining sequence stratigraphy in North Australian basins; SHRIMP U-Pb zircon geochronology between Mt Isa and McArthur River. Australian Journal of Earth Sciences 47, 431-459.

Page, R. W. & Sweet, I. P. 1998. Geochronology of basin phases in the western Mt Isa Inlier, and correlation with the McArthur Basin. Australian Journal of Earth Sciences 45, 219-232.

Painter, M. G. M., Golding, S. D., Hannan, K. W. & Neudert, M. K. 1999. Sedimentologic, petrographic, and sulfur isotope constraints on fine-grained pyrite formation at Mount Isa Mine and environs, Northwest Queensland, Australia. Economic Geology and the Bulletin of the Society of Economic Geologists 94, 883-912.

Perkins, C., Heinrich, C. A. & Wyborn, L. A. I. 1999. (super 40) Ar/ (super 39) Ar geochronology of copper mineralization and regional alteration, Mount Isa, Australia. Economic Geology and the Bulletin of the Society of Economic Geologists 94, 23-36.

Perkins, W. G. 1984. Mount Isa silica dolomite and copper orebodies: The result of a syntectonic hydrothermal alteration system. Economic Geology 79, 601-637.

Perkins, W. G. 1990. Mount Isa copper orebodies. Geology of the mineral deposits of Australia and Papua New Guinea 14, 935-941.

Perkins, W. G. 1997. Mount Isa lead-zinc orebodies; replacement lodes in a zoned syndeformational copper-lead-zinc system? Ore Geology Reviews 12, 61-111.

Perkins, W. G. 1998. Timing of formation of Proterozoic stratiform fine-grained pyrite; post-diagenetic cleavage replacement at Mount Isa? Metallogeny of the McArthur River-Mount Isa-Cloncurry minerals province 93, 1153-1164.

Power, W. L., and T. E. Tullis. 1995. A review of the fractal character of natural fault surfaces with implications for friction and the evolution of fault zones. In: Fractals in The Earth Sciences (edited by Barton, P. L. a. C.). Plenum, New York, 85-105.

Power, W. L. & Durham, W. B. 1997. Topography of natural and artificial fractures in granitic rocks: Implications for studies of rock friction and fluid migration. International Journal of Rock Mechanics and Mining Sciences 34, 979-989.

Power, W. L. & Tullis, T. E. 1992. The Contact Between Opposing Fault Surfaces at Dixie Valley, Nevada, and Implications for Fault Mechanics. J. Geophys. Res. 97, 15425-15435.

Power, W. L., Tullis, T. E. & Weeks, J. D. 1988. Roughness and Wear During Brittle Faulting. J. Geophys. Res. 93, 15268-15278.

Power, W. L., and Tullis, T. E., 1991. Euclidean and Fractal Models for the Description of Rock Surface Roughness. Journal of Geophysical Research 96, 415-424.

Robertson, C. W. 1982. The role of pre-existing sulphides in copper-ore formation at Mount Isa, Queensland. BMR Journal of Australian Geology and Geophysics 7, 119-124.

Rowland, J. V. & Sibson, R. H. 2001. Extensional fault kinematics within the Taupo Volcanic Zone, New Zealand: Soft-linked segmentation of a continental rift system. New Zealand Journal of Geology and Geophysics 44, 271-283.

Sagy, A., Brodsky, E. E. & Axen, G. J. 2007. Evolution of fault-surface roughness with slip. Geology 35, 283-286.

Scott D.L., Rawlings D.J., Page R.W., Tarlowski C.Z., Idnurm M., Jackson M.J. & Southgate P.N. 2000. Basement framework and geodynamic evolution of the Palaeoproterozoic superbasins of north-central Australia: an integrated review of geochemical, geochronological, and geophysical data. Australian Journal of Earth Sciences 47, 341-380.

Shaw, T. 2005. 500 OB Scoping Study 2005: Geological Summary: Xstrata Copper Internal Paper.

Sibson, R. H. 1995. Selective fault reactivation during basin inversion: potential for fluid redistribution through fault-valve action. Geological Society of London, Special Publications 88, 3-19.

Smith, W. D. 1969. Penecontemporaneous faulting and its likely significance in relation to Mt Isa ore deposition. Special Publication - Geological Society of Australia 2, 225-235.

Solomon, P. J. 1965. Investigations into sulfide mineralization at Mount Isa, Queensland. Economic Geology and the Bulletin of the Society of Economic Geologists 60, 737-765.

Southgate P.N., Bradshaw B.E., Domagala J., Jackson M.J., Idnurm M., Krassay A.A., Page R.W., Sami T.T., Scott D.L., Lindsay J.F., McConachie B.A. & Tarlowski C.Z. 2000a. Chronostratigraphic basin framework for Palaeoproterozoic rocks (1730-1575 Ma) in northern Australia and implications for base-metal mineralisation. Australian Journal of Earth Sciences 47, 461-483.

Stewart, A. J. 1992. The role of thrusting in the structural development of the Mount Isa Mine and its relevance to exploration in the surrounding region; discussion. Economic Geology and the Bulletin of the Society of Economic Geologists 87, 1659-1664.

Suteanu, C. 2009. Fractals Dynamic Systems in Geoscience: Natural Hazards - Short Course. In: 5th International Conference on Fractals and Dynamic Systems in Geoscience, James Cook University.

Swager, C. P. 1983. Microstructural development of the silica-dolomite and copper mineralisation at Mount Isa, north-west Queensland, with speacial emphasis on the timing and mechanism of mineralisation, Ph.D. thesis, James Cook Univ.

Swager, C. P. 1985. Syndeformational carbonate-replacement model for the copper mineralization at Mount Isa, Northwest Queensland; a microstructural study. Economic Geology and the Bulletin of the Society of Economic Geologists 80, 107-125.

Swager, C. P., Perkins, W. G. & Knights, J. G. 1987. Stratabound phyllosilicate zones associated with syntectonic copper orebodies at Mt. Isa, Queensland. Australian Journal of Earth Sciences 34, 463-476.

Talwani, P. 1999. Fault geometry and earthquakes in continental interiors. Tectonophysics 305, 371-379.

Walsh, J. J. & Watterson, J. 1989. Displacement gradients on fault surfaces. Journal of Structural Geology 11, 307-316.

Waring, C. L., Heinrich, C. A. & Wall, V. J. 1998. Proterozoic metamorphic copper deposits. AGSO Journal of Australian Geology and Geophysics 17, 239-246.

White, N. J., Jackson, J. A. & McKenzie, D. P. 1986. The relationship between the geometry of normal faults and that of the sedimentary layers in their hanging walls. Journal of Structural Geology 8, 897-909.

Wilde, A. R., Jones, P. A., Gessner, K., Ailleres, L., Gregory, M. J. & Duncan, R. J. 2006. A Geochemical Process Model for the Mount Isa Copper Orebodies. Economic Geology 101, 1547-1567.

Winsor, C. N. 1983. Syntectonic vein and fibre growth associated with multiple slaty cleavage development in the Lake Moondarra area, Mount Isa, Australia. Tectonophysics 92, 195-210.

Preamble to paper 2

The previous paper (paper 1) analysed the meso- to macroscale (m-km) geometry of the Paroo Fault using techniques such as Gaussian curvature, spanned length roughness, slip and dilation tendency, and thickness analysis of the fault zone filling in order to understand the formation and development of the Paroo Fault. The results from this paper hint that the timing of the formation of the copper orebodies is perhaps not as described by previous authors. The next paper (paper 2) examines the geometry and mineralogy of the Paroo Fault Zone at the micro- to mesoscale (μm-m) using underground mapping, petrography and scanning electron microscope cathodoluminescence, to further understand the mode of formation of the fault zone filling and the development of the Paroo Fault. This paper demonstrates that the timing of formation of the copper orebodies is not as has been described by previous authors.

Paper 2 - The formation and development of the Paroo Fault and its relationship to the Mount Isa copper orebodies, NW Queensland

Ryan D. Long, Nicholas H. S. Oliver, Brian G. Rusk and Thomas G. Blenkinsop

1. Abstract

The Mount Isa copper orebodies lie adjacent to or perched above the Paroo Fault which juxtaposed the basement footwall rocks against a younger hangingwall sequence hosting the ores, before the first phase of contractional deformation of the Isan Orogeny. The copper orebodies and a silica-dolomite halo at Mount Isa formed before or early during the second contractional deformation event (east-west shortening; D_2). This was followed by the formation of the Paroo Fault Zone filling by repeated extraction of quartz from the Urquhart Shale directly above the fault and precipitation within the fault. This created zones of quartz enrichment and depletion at three scales within the Paroo Fault. Zoning between the quartz-poor Urquhart Shales and quartz-rich filling in the Paroo Fault occurs at 10 m scales. Zoning between quartz bands and graphitic alternations within the fault filling occurs at 0.5-60 cm scales. Graphitic

stylolite seams are separated by quartz at 0.2-10 mm scales. The 0.5-60 cm zoning of the quartz bands and graphite seams would have created a series of surfaces very favourable for movement (graphitic seams) between the harder quartz bands. Movement on the graphitic seams explains the lack of a conventional core and damage zone within the fault. A later (D_3) north northwest-south southeast phase of shortening has caused the Paroo Fault and Urquhart Shales to fold around and buttress against the copper orebodies. Chalcopyrite could have been remobilised by the last fluid flow during $D_{3,}$ creating the distribution described as syn-D_3 by previous authors.

Keywords

Mount Isa, copper deposit, scanning electron microscope cathodoluminescence, Paroo Fault, fault zoneation.

2. Introduction

The giant (>200 Mt at 2 % Cu; NW Bullock personal communication 2010) Mount Isa copper deposit lies within the Western Fold Belt of the Proterozoic Mount Isa Inlier (Fig. 16). The copper orebodies are located above the Paroo Fault, which has juxtaposed the Cromwell Metabasalt and Lena Quartzite of the Eastern Creek Volcanics (1710 ± 25 Ma; Gulson et al., 1983) against the Mount Isa Group (Age for Urquhart Shale formation is 1655 ± 4 Ma; Page et al., 2000). The timing of this juxtaposition relative to the copper mineralisation has remained a topic of considerable controversy, as has the timing of the intense silicification and dolomitisation which forms a halo surrounding the copper orebodies (Finlow-Bates and Stumpfl, 1979).

Further controversy at Mount Isa centres on the spatial relationship between the lead-zinc-silver orebodies, inferred by most researchers to have a syngenetic origin (Stanton, 1963; Finlow-Bates and Stumpfl, 1979) and the copper orebodies, which show many epigenetic features (Robertson, 1982; Perkins, 1984). The lead-zinc-silver orebodies overly the copper orebodies and are not contained within the silica-dolomite halo (Fig. 17; Finlow-Bates and Stumpfl, 1979).

Three main models have been proposed to explain the spatial relationship between the copper and the lead-zinc-silver orebodies. In the first model the lead-zinc-silver orebodies are syngenetic and copper orebodies are epigenetic (Robertson, 1982; Gulson et al., 1983; Swager, 1983; 1985; Perkins, 1984; Bell et al., 1988; Heinrich et al., 1995; Miller, 2007). In this model the early lead-zinc-silver mineralisation created favourable conditions for the subsequent epigenetic copper orebodies to form; such as a pre-existing sulphur source (Robertson, 1982), or a chemical anomaly generated by the diagenetic process associated with the early lead-zinc-silver orebodies (Heinrich et al., 1995). In the second model, both the lead-zinc-silver orebodies and copper orebodies are epigenetic. The lead-zinc-silver mineralisation formed by replacement along bedding in the upper limits of the deposit (distal from source) and the copper formed vein networks and breccia matrix closer to the Paroo Fault (Perkins, 1997; Davis, 2004). In the third model the copper-lead-zinc-silver orebodies are syngenetic. This model involves the remobilisation of copper during deformation of a syngenetic copper-lead-zinc-silver deposit (Stanton, 1963; Dunnet, 1976; Finlow-Bates and Stumpfl, 1979; McGoldrick and Keays, 1990).

The Paroo Fault lies directly below the copper and lead-zinc-silver orebodies at Mount Isa and has been considered a likely conduit for mineralising fluids which formed the orebodies (Robertson, 1982; Perkins, 1984; Andrew et al., 1989; Heinrich et al., 1989; 1993; 1995; Gessner et al., 2006; Kendrick et al., 2006; Kühn and Gessner, 2006; 2009; Kühn et al., 2006). Detailed analysis of the fault has not been undertaken previously, and its role has been largely assumed. This paper uses 10s of m to mm scales of observations to examine the distribution, orientation, textures and mineralogy of the Paroo Fault Zone filling in order to understand its development and its relationship to the copper orebodies and their silica-dolomite halo.

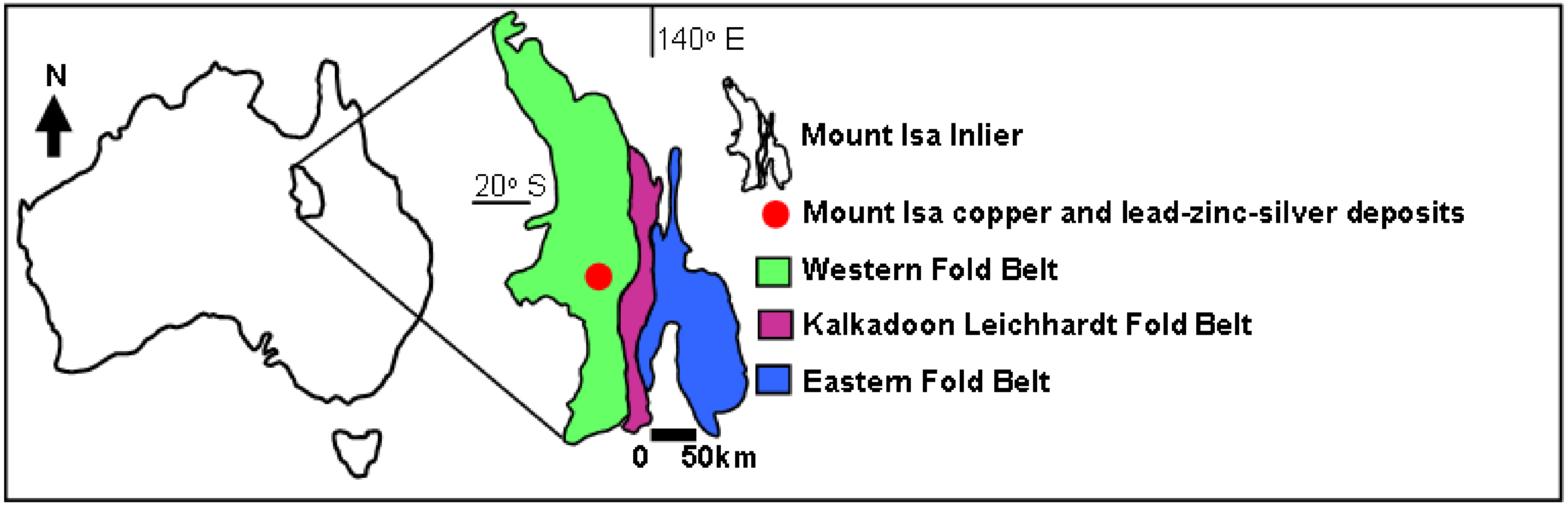

Fig. 16. Simplified tectonic map of the Mount Isa Inlier showing the Mount Isa copper and lead-zinc-silver deposit within the Western Fold Belt.

3. Geological setting

3.1. Regional Geology

The Western Fold Belt has developed as the result of a series of three stacked Superbasins on the Kalkadoon Leichhardt Block (Jackson et al., 2000; Scott et al., 2000; Southgate et al., 2000). The most recent of these are the Isa Superbasin (1670-1590 Ma Betts et al., 2006) and the Calvert Superbasin (1730-1670 Ma Betts et al., 2006), which contain the Lower MacNamara Group, Mount Isa Group, Surprise Creek Formation, Fiery Creek Volcanics and Bigie Formation, which were also defined as Cover Sequence 3 by Blake (1987). The Leichhardt Superbasin (1790-1730 Ma Betts et al., 2006) contains the Quilalar Formation, Myally Subgroup, Eastern Creek Volcanics and the Mount Guide Quartzite, which correspond to the Cover Sequence 2 (Blake, 1987). The Kalkadoon Leichhardt Block contains the Sulieman Gneiss, which corresponds to Cover Sequence 1 (Blake, 1987).

3.2. The Eastern Creek Volcanics

The Eastern Creek Volcanics forms the footwall to the copper mineralisation (Gulson et al., 1983; Hannan et al., 1993; Page et al., 2000; Fig. 17). The Lena Quartzite is the dominant rock type below all the copper orebodies. The Lena Quartzite has been described as metamorphosed felspathic arenites and is composed of quartz, albite, potassium feldspar, muscovite and chlorite with accessory tourmaline and zircon (Mathias and Clark, 1975). Directly below the Paroo Fault the quartzite has been extensively altered. In these areas the rock is now dominantly composed of quartz and carbonate with pervasive chlorite alteration and late pyrite. Sulphur isotopes in these pyrites (Andrew et al., 1989) suggest this alteration is related to the overlying copper orebodies (see discussion).

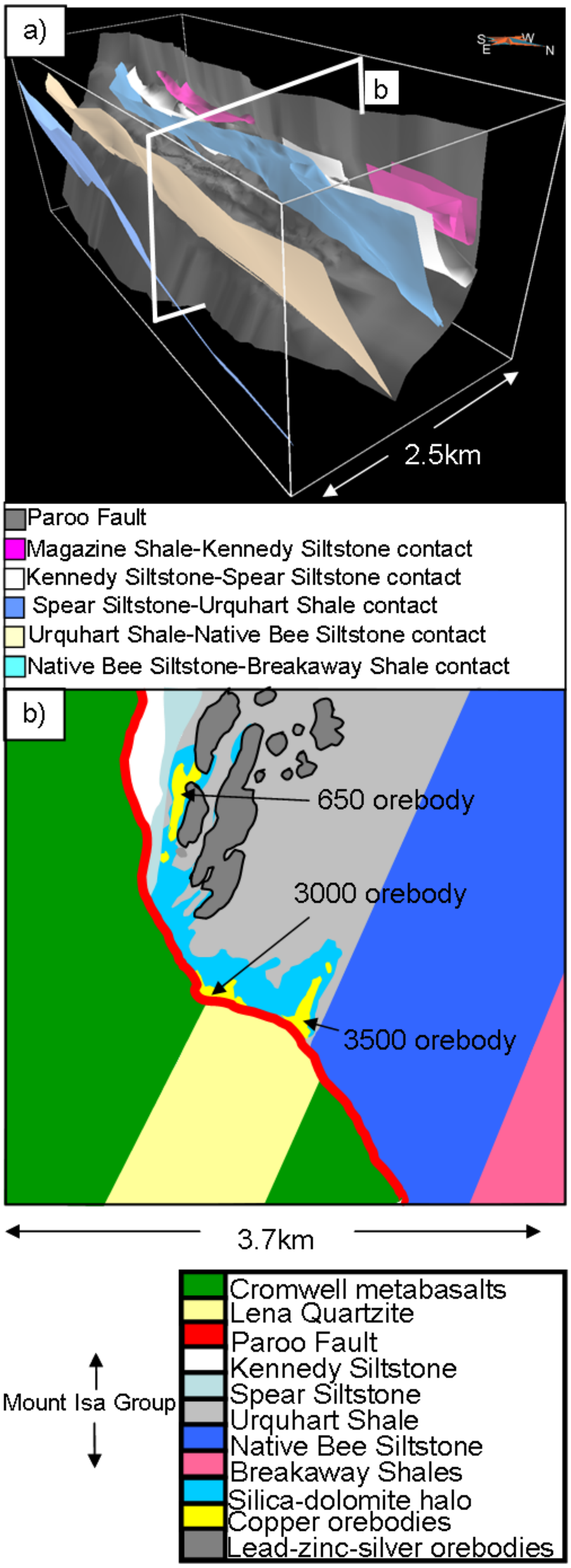

Fig. 17. a) The Mount Isa Group with the Paroo Fault dominantly dipping to the west apart from the Kennedy Siltstone and Magazine Shale which are folded openly in the

southern section and closed in the northern section; b) Simplified cross section of the Mount Isa copper orebodies and lead-zinc-silver orebodies from a northing of 6800 m. The Eastern Creek Volcanics (Cromwell Metabasalt and Lena Quartzite) have been juxtaposed against the Mount Isa Group by movement along the Paroo Fault, which was subsequently folded. Displayed are the perched non-stratiform 650 copper orebody, the non-stratiform 3000 copper orebody and the stratiform 3500 copper orebody. Surrounding the copper orebodies is the silica-dolomite halo.

3.3. Mount Isa Group

The Mount Isa Group generally dips and youngs to the west at steep to moderate angles (on average 60^{o}) apart from the youngest members of the group (the Kennedy Siltstone and Magazine Shale), which are in the core of a synform (Fig. 17). The stratigraphy of the Mount Isa Group is extensively described by Mathias and Clark (1975).

The Urquhart Shale formation (1655 ± 4 Ma; Page et al., 2000) of the Mount Isa Group which hosts the copper and lead-zinc-silver mineralisation at Mount Isa (Solomon, 1965; McDonald, 1970) is composed of three dominant rock types; barren tuffaceous carbonaceous dolomitic shale and siltstone, a pyritic and tuffaceous shale in which the lead-zinc-silver mineralisation is hosted, and the silica-dolomite halo which surrounds the copper mineralisation (Mathias and Clark, 1975).

The rocks which make up the silica-dolomite halo are classified into five basic types on the basis of their silica and dolomite content and degree of deformation (Mathias and Clark, 1975). The Dolomitic Recrystallised Shale, Irregularly Brecciated Recrystallised Shale and Crystalline Dolomite are dominantly found within the outer parts of the silica-dolomite halo (Scott, 1989). Recrystallised Shale consists of alternating bands of carbonaceous siliceous shales and pyritic shales with a matrix of fine grained dolomite. The Irregularly Brecciated Recrystallised Shale is composed of banded carbonaceous Siliceous Shale fragments with coarse crystalline dolomite in a matrix of quartz. Crystalline Dolomite is a medium to coarse grained dolomitic rock with no significant shale and minor interstitial quartz (Mathias and Clark, 1975).

The other two silica-dolomite rock types are Siliceous Shale and Fractured Siliceous Shale, which are more siliceous than the previous three rock types and are dominantly located closer to the Paroo Fault (see figures below). Siliceous Shale is a graphitic shale that has been silicified to various degrees; it contains well preserved bedding and limited copper mineralisation. The Fractured Siliceous Shale contains the majority of the copper mineralisation in various degrees of brecciation with a quartz matrix (Mathias and Clark, 1975).

3.4. Copper orebodies

The individual copper orebodies occur in two broad groups, stratiform and non-stratiform. These can be subdivided based on the position of the orebodies with respect to the Paroo Fault (Fig. 18). The 200 and 650 orebodies are non-stratiform and perched above the Paroo Fault. The hangingwall lens, footwall lens, 1100, S1900 and 3000 orebodies are non-stratiform and are adjacent to the Paroo Fault. The 500 orebody is stratiform and perched above the Paroo Fault and the N1900 and 3500 are also stratiform and are located adjacent to the Paroo Fault. We have examined these different orebody types in order to assess whether or not they formed at the same time and by the same processes. In particular the non-stratiform 3000 orebody and stratiform 3500 orebody were compared at exposure to thin section scale. The base of several other orebodies were also examined in transects across the underlying Paroo Fault (see below).

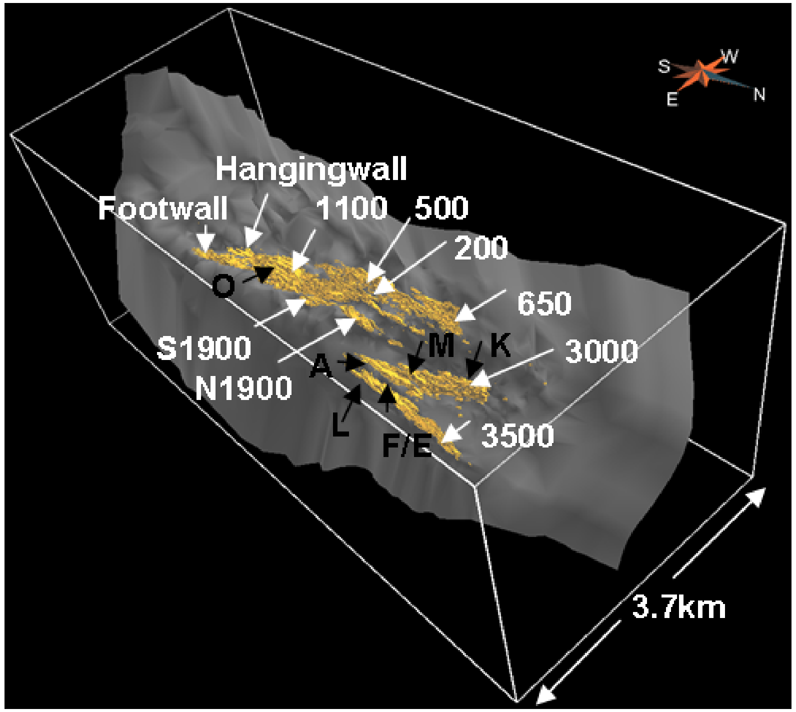

Fig. 18. The Paroo Fault (grey) and copper orebodies (2 % Cu; yellow) looking down to the southwest. The three-dimensional model of the Paroo Fault was created by the mine geologists (Xstrata Copper) in the mining software Minesight package using over 20,000 drill-holes and mapping from over 40 mine levels acquired over 85 years. The model was transferred to GoCAD for use here. The copper orebodies are labelled in white including; the perched stratabound and stratiform 500 orebody, the perched and non-stratiform 200 and 650 orebodies, the Paroo Fault adjacent stratiform N1900 and 3500 orebodies and non-stratiform Paroo Fault adjacent hangingwall lens, footwall lens, 1100 orebody S1900 and 3000 orebodies. The transects and sample locations are labelled in black.

3.5. Deformation history

The first phase of deformation (D_1) visible at the deposit scale, formed by north-south shortening which resulted in a penetrative slaty cleavage (S_1) at low angle to the bedding, which is visable north of the deposit in the lake Moondarra region (Bell, 1983; Winsor, 1983; 1986).

The second deformation event (D_2) was an east-west directed phase of shortening which resulted in the folding of the Paroo Fault into its sigmoidal shape and generated north-south folds within the Paroo Fault. North-south striking (axial surfaces) open folds were created in the Urquhart Shale together with a regional slaty cleavage which is sub-vertical and north-south striking.

The third deformation event (D_3) caused the Urquhart Shale to fold at the meter to hundred meter scales. The folds have a north northwest striking axial plane, with slaty to crenulation cleavage developed sub-parallel to these axial planes (Swager, 1985; Winsor, 1986). Previous research proposed that the copper orebodies formed during D_3, based largely on S_3 cleavages in clasts of breccia surrounded by a matrix of quartz and chalcopyrite that does not have S_3 cleavage (Swager, 1983; 1985; Perkins, 1984). Other supporting evidence for a D_3 formation of the copper orebodies includes; copper breccia veins with S_3 developed against their margins are crosscut by D_3 extension veins (Bell *et al.,* 1988), and the position of several orebodies within D_3 fold zones (Perkins, 1984; Bell *et al.,* 1988; Davis, 2004).

4. Methods

The Paroo Fault was examined at 16 underground locations. Detailed face maps of the contacts, cleavages, sulphide distribution, quartz distribution and folding were produced. High resolution digital photographs were taken of the Paroo Fault and stitched together to allow the mapping observations to be transferred on to the digital photographs. To ensure that the mapping was accurately transferred to the photographs, a 1 m by 1 m grid was spray painted along the drives for use as a scale prior to the mapping and photography.

In order to investigate the role of the Paroo Fault in the copper mineralisation, the geology of the fault was studied in transects from the basement to the overlying shales in six locations, chosen to give the best holistic view of the Paroo Fault from the limited access available. The transects were taken from the 1100 orebody, and within and near to the 3000 and 3500 orebodies (Table 3 and Fig. 17). Oriented samples were taken from the Lena Quartzite in the basement, across the fault zone filling and into the overlying Urquhart Shales and/or chalcopyrite mineralisation.

From the samples, three orthogonal thin sections were prepared to ensure the mineralogy and texture of the sample was observed accurately. Petrography was undertaken to understand the variations in mineralogy, textures and paragenesis across the fault zone filling. One 150 μm thick section was prepared from each sample for scanning electron microscope cathodoluminescence (SEM-CL) to compare with the optical microscopy.

Grey scale images of quartz and carbonate were collected from carbon-coated thick sections, using a SEM equipped with a Robinson CL detector and photomultiplier (spectral range 310-650 nm). Instrument operating conditions were set to an accelerating voltage of 20 kV and a beam current of ~10 nA (James Cook University Advanced Analytical Centre).

Location				
General	Mine drive	Location code	Sample	Sample Location
Outside 3000	27C 6934 XC	K	4	Top of Paroo Fault Zone filling
Outside 3000	27C 6934 XC	K	5	Lena Quartzite 3m from Paroo Fault Zone
Outside 3000	27C 6934 XC	K	7	Urquhart Shale
In 3000	27 Q635 DPT	M	1	Centre of Paroo Fault Zone filling
In 3000	28 Q635 DPT	M	4	Lena Quartzite 1.5m from Paroo Fault
In 3000	29 Q635 DPT	M	5	Urquhart Shale 0.5m above the Paroo Fault Zone
Between 3000 & 3500	29E 6448 XC	A	10	Lena Quartzite 4m from Paroo Fault
Between 3000 & 3500	29E 6448 XC	A	1	Base of Paroo Fault Zone filling
Between 3000 & 3500	29E 6448 XC	A	4	Centre of Paroo Fault Zone filling
Between 3000 & 3500	29E 6448 XC	A	14	Top of Paroo Fault Zone filling
Between 3000 & 3500	29E 6448 XC	A	7	Urquhart Shale
In 3500	29E 6570 XC	E	2	Urquhart Shale 10cm from Paroo Fault Zone
In 3500	30E 6515 XC	F	8	Lena Quartzite 17m from Paroo Fault
In 3500	30E 6515 XC	F	12	Top of Paroo Fault Zone filling
Outside 3500	30A X620 RPAC	L	1	Lena Quartzite 0.5m from Paroo Fault Zone
Outside 3500	30A X620 RPAC	L	2	Centre of Paroo Fault Zone filing
Outside 3500	30A X620 RPAC	L	3	Urquhart Shale 70cm from Paroo Fault Zone
In 1100	18B V39 SWXC	O	2	Centre of Paroo Fault Zone filling
In 1100	18B V39 SWXC	O	6	Lena Quartzite 20m from Paroo Fault Zone
In 1100	18B U413 DP1	O	7	Urquhart Shale

Table 3. Locations and sample numbers of samples taken in the transects across the Lena Quartzite, Paroo Fault Zone filling and Urquhart Shale.

5. Results

5.1. Macroscale geometry of the Paroo Fault

The Paroo Fault has a sigmoidal shape composed of a steeply west dipping to the south and east dipping to the north upper limb, a shallowly east dipping central section and lower limb that dips steeply to the east (Fig. 5). The copper orebodies are located adjacent to the shallowly east dipping section of the fault or perched above the central or upper section.

5.2. Mesoscale lithological patterning immediately around the Paroo Fault

The infill of the Paroo Fault is zoned from quartz-rich to quartz-poor rocks at three scales (Fig. 19). At meter scales away from the orebodies, there is a steeply west dipping (60-80^{o}) zone of quartz-poor (< 20 % silica) Urquhart Shale above the quartz-rich Paroo Fault Zone filling, immediately above which is quartz-rich (> 60 % silica), less altered Urquhart Shale (Fig. 19a). The quartz content was visually estimated by comparing samples taken from each of the areas. Locally, the quartz-poor zone is missing where chalcopyrite-rich ore abuts against the Paroo Fault (see below) but elsewhere this zone is typically between 3 m and 10 m thick. It is not clear whether the thickness of the fault zone filling relates directly to the area of quartz depletion in the Urquhart Shale. At the cm scale, within the Paroo Fault Zone filling, there are alternating bands of quartz-rich and quartz-poor material (Fig. 19b). The dark material is typically graphitic and highly sheared. At the mm to microscopic scales there are styolitic or sheared seams of graphitic material which commonly abruptly truncate quartz grains and grain boundaries (Fig. 19c).

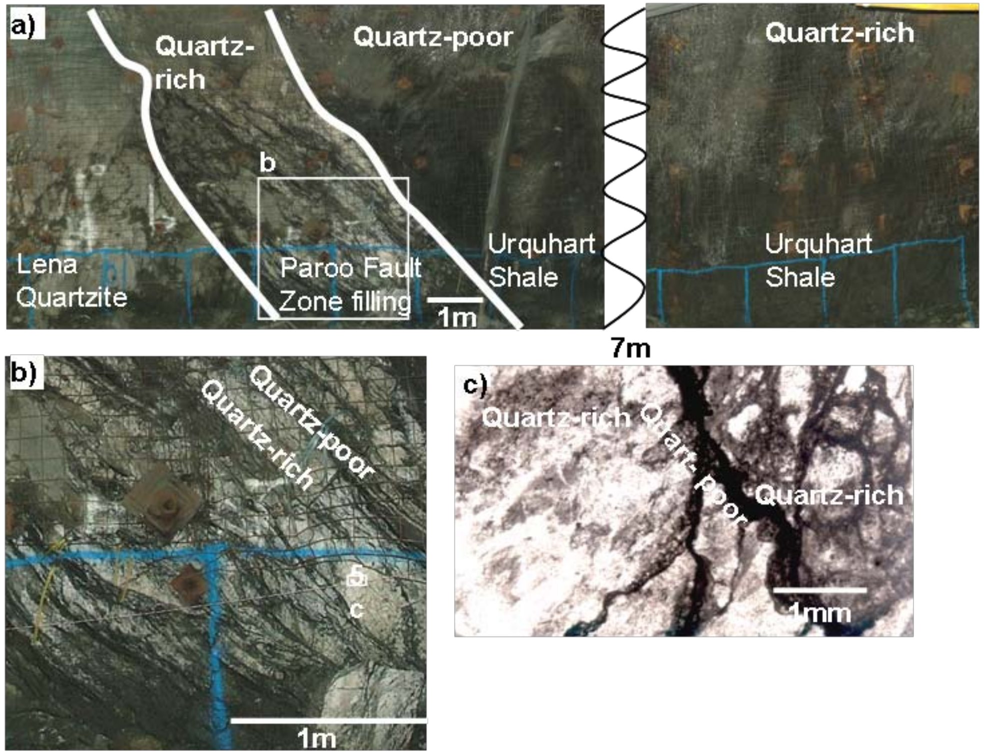

Fig. 19. Photographs and a photomicrograph showing the three scales of segregation of quartz and graphite; a) At the larger scales (>10 m) there is zoning between the quartz-poor Urquhart Shales and quartz-rich filling in the Paroo Fault Zone. Stitching pattern represents a separation distance of 7 m between the two photographs; b) At the intermediate scales (0.1-60 cm) there is zoning between the quartz bands and graphitic alternations within the fault fill; c) At the microscopic scales (0.2-10 mm) there is zoning between the graphitic stylolite seams and adjacent quartz crystals.

5.3. Mineralisation types within the copper orebodies

There are three main types of chalcopyrite mineralisation within the Mount Isa copper deposit; massive, crackle breccia and vein networks. The massive chalcopyrite is the highest grade (>7 % Cu) and occurs in the centre of the orebodies adjacent to the Paroo Fault (Figs. 20 and 21). The massive chalcopyrite can be weakly foliated (Fig. 22a). Bedding is rarely present within the clasts of Silicified Shale.

Chalcopyrite in crackle breccia (2.5-7 % Cu) occurs as the matrix to clasts of Silicified Shale (Fractured Siliceous Shale; Figs. 20, 21 and 22). It is located in the centre of the orebodies grading out from the massive chalcopyrite adjacent to the Paroo Fault towards the edges and tops of the orebodies. Bedding is commonly preserved within this type of ore in the 3500 orebody and rarely within the 3000 orebody.

The vein network mineralisation (0.5-2.5 % Cu) occurs at the extremities of the orebodies, particularly at the edges and more prevalently at the tops. Chalcopyrite occurs in quartz-carbonate veins within Silicified Shale and Recrystallised Dolomitic Shale (Figs. 20 and 21). Bedding is largely preserved within this ore type.

A fourth type of chalcopyrite mineralisation contained within partially Crystalline Dolomite is also defined here, though the scale of its distribution is unknown. Bedding-parallel chalcopyrite with S_2 cleavage cross-cutting it was observed at the edges of the 1100 orebody (Fig. 23). Within the copper orebodies bedding parallel chalcopyrite can be observed. This chalcopyrite has been folded and overprinted by axial planar cleavage in places, inferred to be S_2 on the basis of style, orientation and correlation with the detailed deformation chronology of Swager (1983). Chalcopyrite can also be found in a clast of silica-dolomite wrapped by S_2 cleavage and within the strain halo of the clast, suggesting that chalcopyrite formed before S_2 cleavage developed and was remobilised during D_2 deformation (Fig. 23).

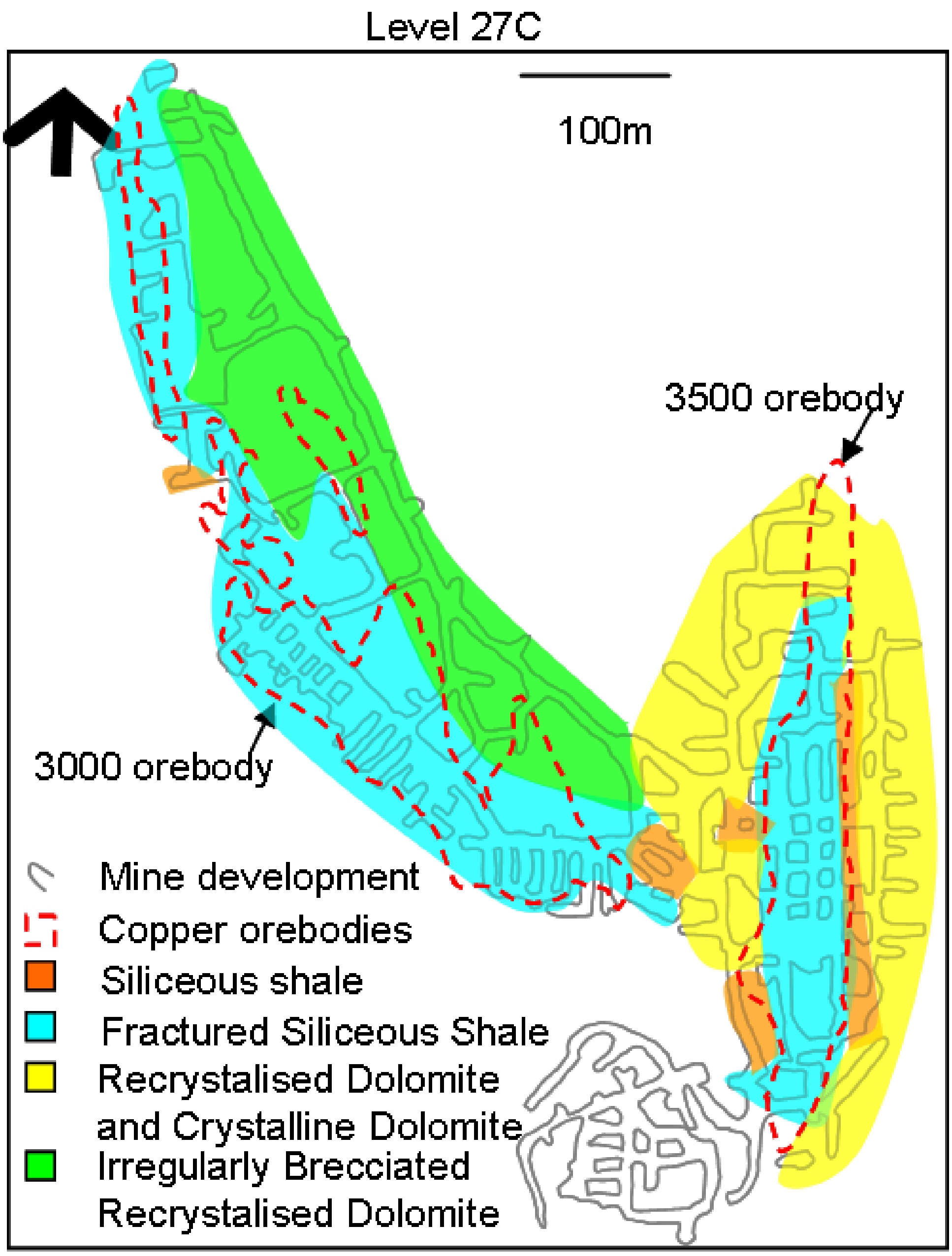

Fig. 20. Map of level 27C which shows the bottom of the 3000 and 3500 orebodies defined by a 2 % Cu cut-off grade and the distribution of the four major rock types. The rock types correlate with copper ore categories; the higher grade massive chalcopyrite and crackle breccias are contained within the Fractured Siliceous Shale and the lower grade vein networks are dominantly within the Silicified Shale and Recrystallised Dolomitic Shale.

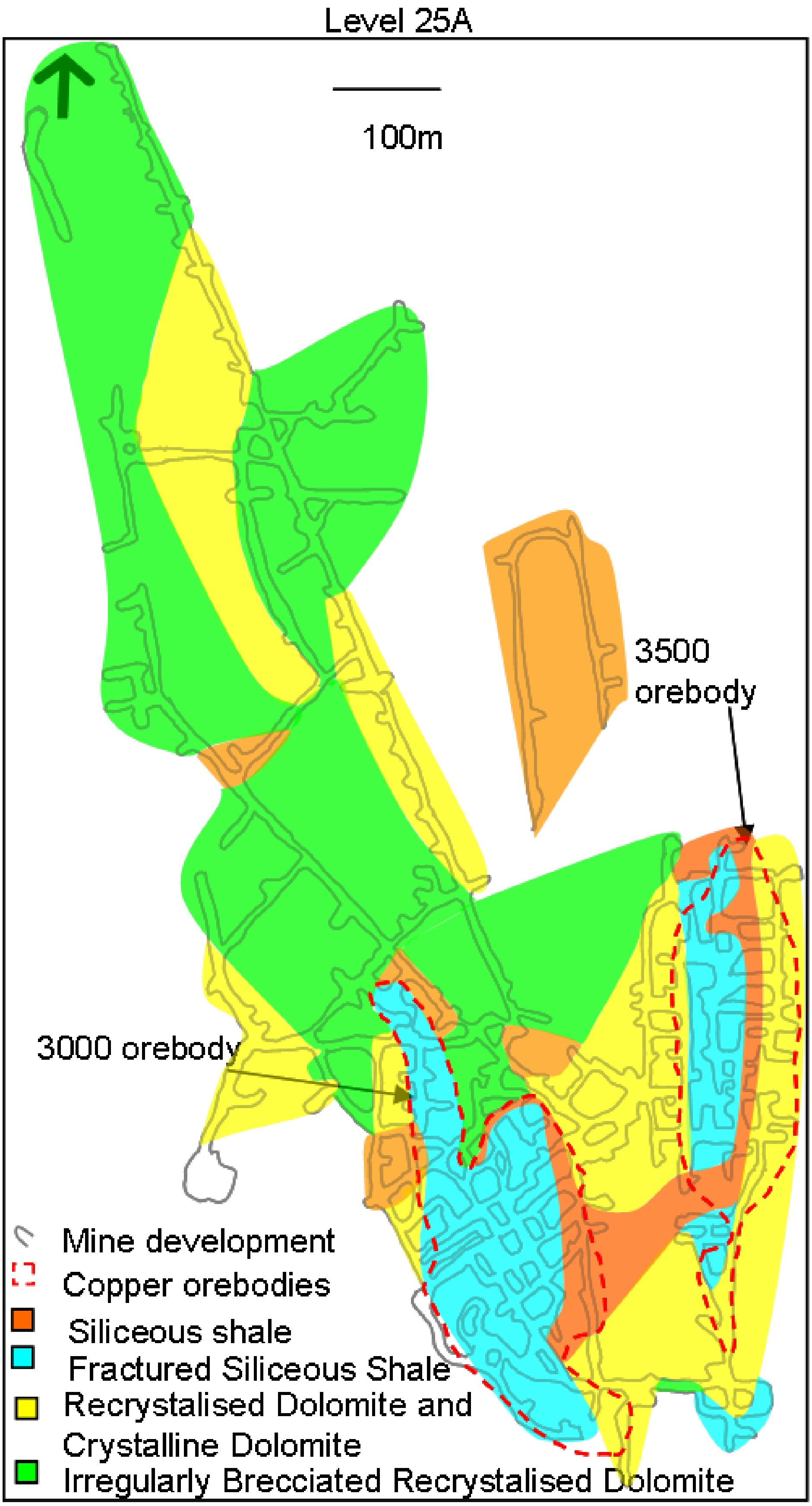

Fig. 21. Map of level 25A which shows the top of the 3000 and 3500 copper orebodies defined by a 2 % Cu cut-off grade and the distribution of the four major rock types. The

rock types correlate with copper ore categories; the higher grade massive chalcopyrite and crackle breccias are contained within the Fractured Siliceous Shale and the lower grade vein networks are dominantly within the Silicified Shale and Recrystallised Dolomitic Shale.

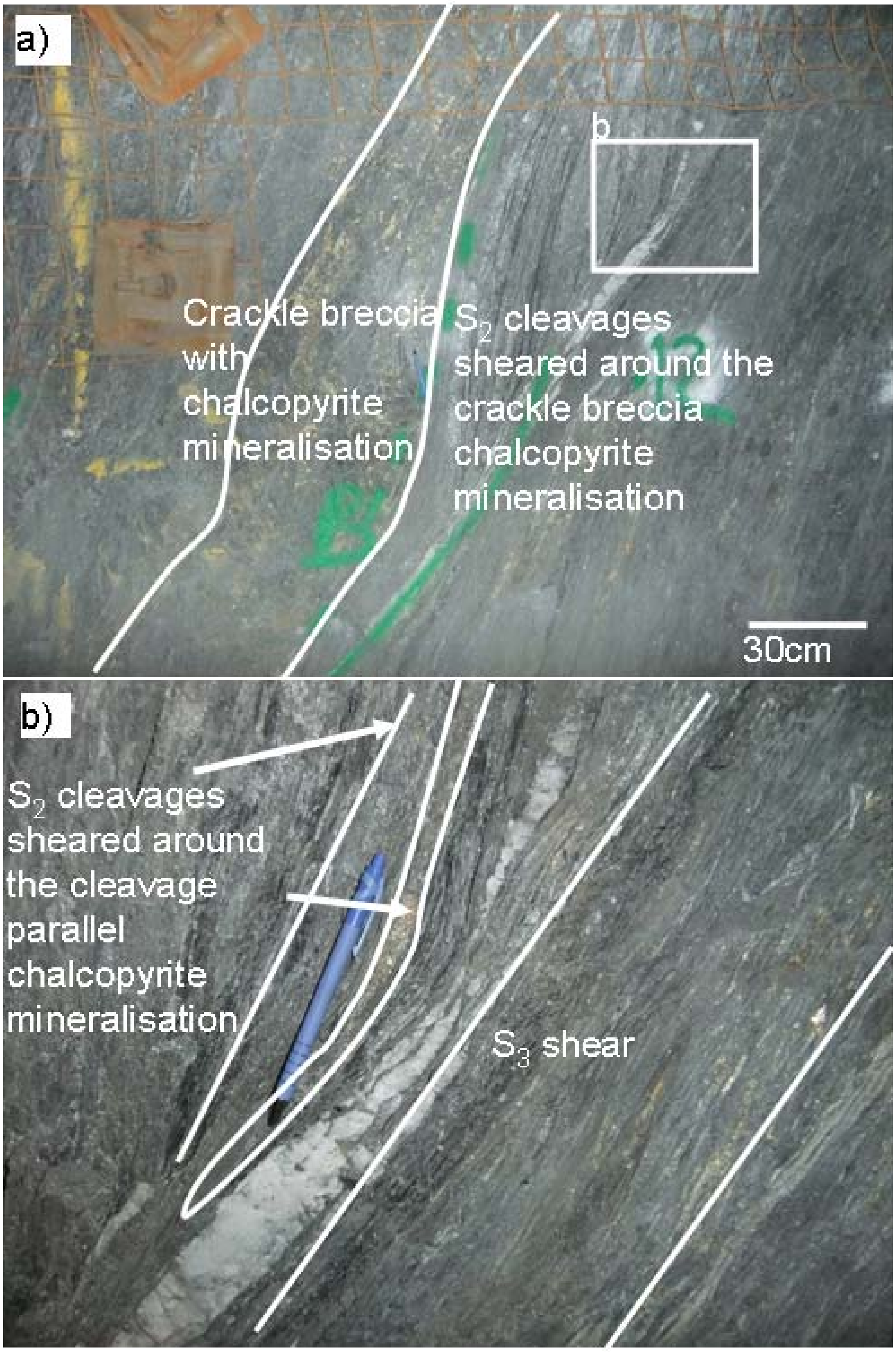

Fig. 22. a) Crackle breccias with sheared boundaries where S_2 cleavages are deformed around the chalcopyrite breccia by D_3 indicating pre-D_3 chalcopyrite; b) S_2 cleavage

parallel chalcopyrite mineralisation with S_2 cleavage deforming around it due to an S_3 shear, also indicating pre-D_3 chalcopyrite.

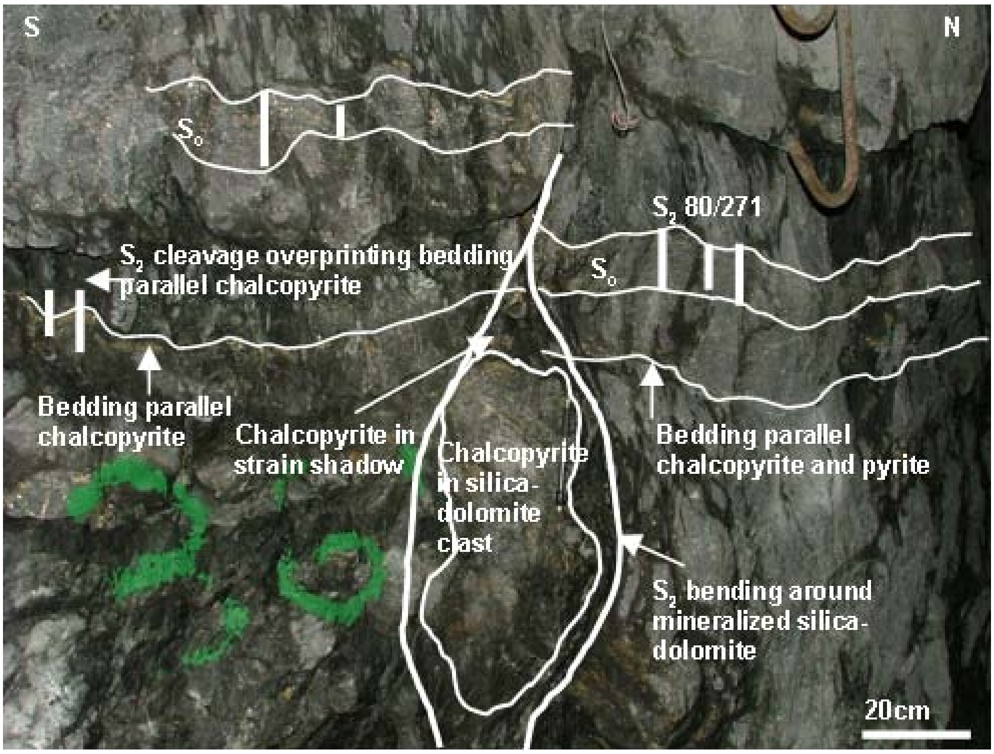

Fig. 23. Photograph of 15 level C52BP in the 1100 orebody where bedding parallel chalcopyrite is cross cut by S_2 cleavage and small D_2 folds. Chalcopyrite is also present within the silica-dolomite clast and strain halo surrounding it indicating there is pre-D_3 chalcopyrite within the 1100 orebody.

5.4. Mesoscale deformation features in the footwall

Cleavage observed in the Lena Quartzite in the areas analysed in this project is been termed S_3 on the basis of style, orientation and correlation with the detailed deformation chronology of Swager (1983; see below). Though S_2 cleavage has been reported in the basement by Perkins (1984) it was not recognised in this project. Folds have also been observed within the Lena Quartzite (Fig. 24).

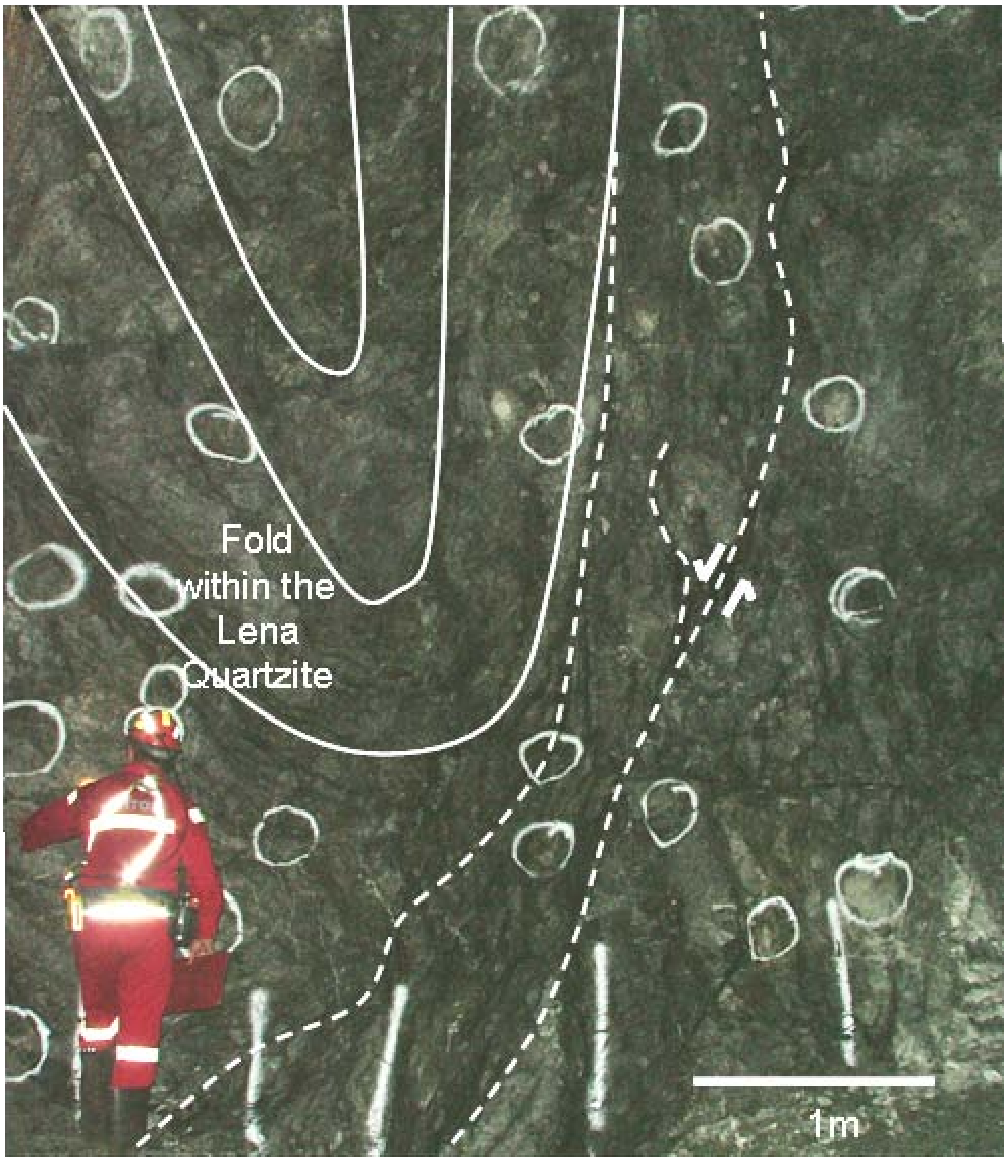

Fig. 24. Photograph from P68 RAR on level 32D, of a fold in the Lena Quartzite which has been offset by a normal fault demonstrating that the basement rocks have undergone both ductile and brittle deformation.

5.5. Mesoscale deformation features within the Paroo Fault

The Paroo Fault Zone filling was examined in the west dipping upper section, shallow east dipping central and lower east dipping sections for evidence that may define when and how the fault zone filling formed.

5.5.1 Upper steeply east dipping section

In the upper steeply east dipping section the fault zone filling is typically less than a meter thick and consists of up to nine alternating subparallel layers of quartz and graphitic material (Fig. 25a). The alternating layers are also subparallel to the edge of the Paroo Fault. The thickness of the graphitic material is consistently between 5 and 20 mm and the quartz filling is generally thicker and more variable, between 10 and 600 mm (Fig. 25b).

The quartz filling in the upper section of the fault forms rectangular blocks and the graphitic filling occurs along all the edges of the blocks (Figs. 25b and c). The fault zone filling is folded locally, with the deformation facilitated by shears along the graphitic seams, fractured phacoids and rare boudinaged folds (Figs. 25b and c). There is weak shearing in the graphitic seams around the quartz blocks. D_3 cleavage can be seen in both the footwall of the Paroo Fault (Lena Quartzite) and in the hangingwall (Urquhart Shales) but not within the fault zone filling. This was probably due to the contrast in strength of the quartz with the graphitic seams, with deformation accommodated by movement along the graphitic seams. The local folding and boudinage textures of the quartz indicate it shares the same ductile deformation history as the overlying and underlying rocks.

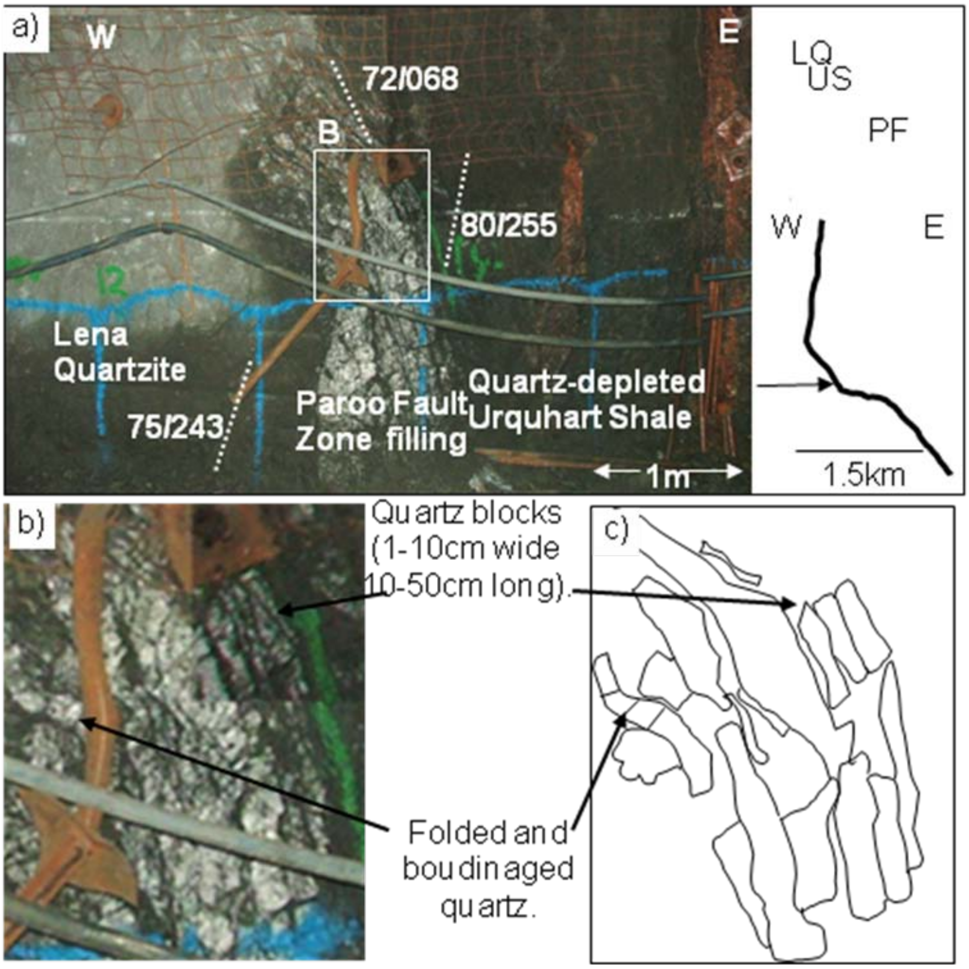

Fig. 25. a) Photograph of the steeply east dipping section of the Paroo Fault Zone on level 27C 6934XC west of the 3000 copper orebody at the northern end of the mine. S_3 cleavage can be seen in both the underlying Lena Quartzite and overlying quartz-depleted Urquhart Shale. The equal area lower hemisphere stereographic projection shows the orientation of Paroo Fault (PF) and S_3 cleavage in Urquhart Shales (US) and Lena Quartzite (LQ); b) enlarged photograph of the fault zone filling; c) outline showing the shape and size of the quartz blocks within the Paroo Fault Zone filling.

5.5.2 Shallow east dipping section

In the shallow section, the Paroo Fault Zone filling thickens between the east side of the non-stratiform copper orebodies and the west side of a D_2 antiformal fold hinge in the Paroo Fault. The fault zone filling can be over 25 m thick near the 1100 orebody but in general it is 1-3 m (Fig. 26a). The quartz-depleted Urquhart Shales which dip steeply towards the Paroo Fault show evidence of a late reverse movement that has deformed the S_3 cleavage (Fig. 26a). This indicates the quartz depletion occurred during or before D_3.

The quartz phacoids and graphite-rich bands within the fault zone filling are more numerous in the flatter section of the Paroo Fault, with up to 25 layers of each lithology (Fig. 26a). The alternating bands are also subparallel to the edge of the fault in this section. The thickness of the graphitic layers within the shallow east dipping section of the fault is largely uniform and generally thicker than the upper section of the Paroo Fault, between 5 and 100 mm. The thickness of the quartz phacoids is variable from 20 to 250 mm (Figs. 26b and c). The phacoids in this section of the Paroo Fault Zone filling are not rectangular like the upper section but have been sheared into elongate phacoids interpreted here as evidence of increased deformation in this section.

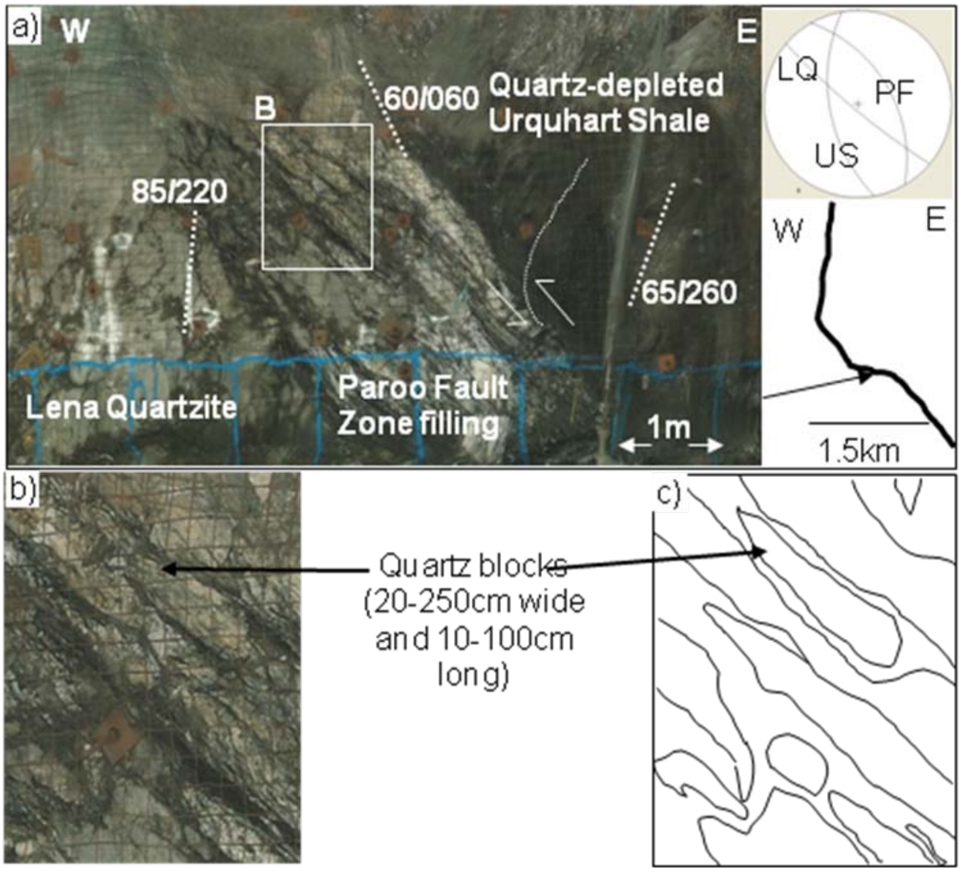

Fig. 26.a) Photograph of the shallowly easterly dipping section of the Paroo Fault Zone at level 29E 6448XC west of the 3500 copper orebody. S_3 cleavage can be seen in both the underlying Lena Quartzite and overlying quartz-depleted Urquhart Shale. The S_3 cleavage has been deformed by late reverse movement on the Paroo Fault. The equal area lower hemisphere stereographic projection shows the orientation of Paroo Fault (PF) and S_3 cleavage in Urquhart Shales (US) and Lena Quartzite (LQ); b) enlarged photograph of the fault zone filling; c) outline showing the shape and size of the clasts of quartz within the Paroo Fault Zone filling.

At the meter-scales, D_3 ductile deformation features appear to postdate the copper orebodies (Figs. 27 and 28). The north northwest trending folds in figs. 27 and 13 wrap around the western edges of the 3000 copper orebody indicating folding occurred after orebody formation. Within the Paroo Fault Zone filling the alternations of graphite and quartz are also folded indicating that the fault zone filling was formed prior to folding and was folded after the copper orebody was formed. Shear sense indicators in D_3 cleavages within the quartz-depleted Urquhart Shale demonstrate that minor reverse movement (east-west shortening) occurred after D_3. In these locations, unlike locations where unmineralised Urquhart Shale abuts the Paroo Fault, the Paroo Fault is directly adjacent to massive copper sulphide, and there is no zone of quartz-depleted carbonaceous material between the orebody and the fault.

Fig. 27. Photograph of the Paroo Fault Zone filling at level 29E 6570XC in the 3000 orebody displaying a antiformal fold with a north northwest orientated axial plane (D_3) in the Paroo Fault. The contact between the massive chalcopyrite (3000 orebody) and the fault is sharp and interfingering, indicating the fault has been buttressed against the copper orebody. The sheared graphite and quartz alternations within the filling are also folded demonstrating the fault zone filling was formed prior to folding and that the fault zone filling was folded after the copper orebody was formed. Shear sense indicators within the quartz depleted Urquhart Shale demonstrate reverse movement (shortening) was associated with the fold.

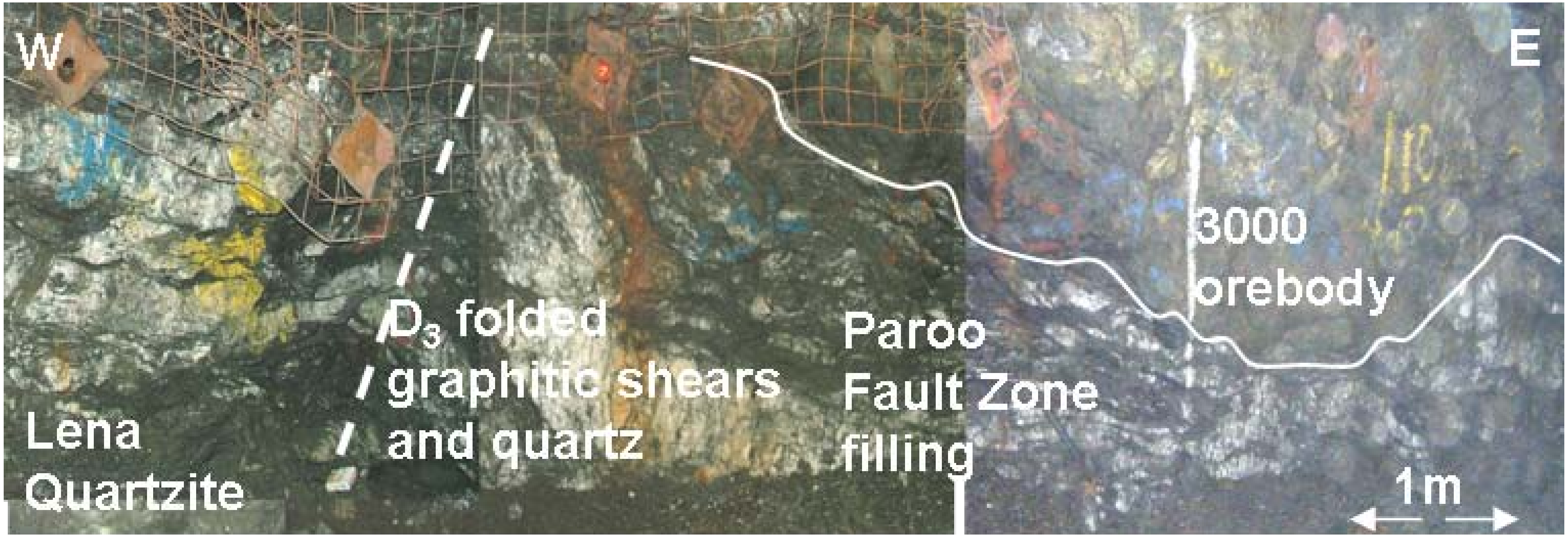

Fig. 28. Photograph of the Paroo Fault at 27 level Q635 DPT in the 3000 orebody displaying a antiformal folded fault zone with a north northwest striking axial plane (S_3). There is a sharp and interfingering contact between the massive chalcopyrite (3000 orebody) and the Paroo Fault Zone. The fault zone filling is folded in a D_3 orientation demonstrating that the fault zone filling was formed prior to folding. The copper orebodies would have formed prior to the D_3 deformation which folded the fault zone filling (see discussion).

5.5.3 Lower steeply east dipping section

In the lower section of the fault, the fault zone filling is substantially thinner (Fig. 29), varying from 10s of cm wide to zero. No carbonaceous alternations are present within the quartz fault zone filling. The Urquhart Shale directly above the Paroo Fault here is silicified and there is no zone of quartz-depletion (Fig. 29).

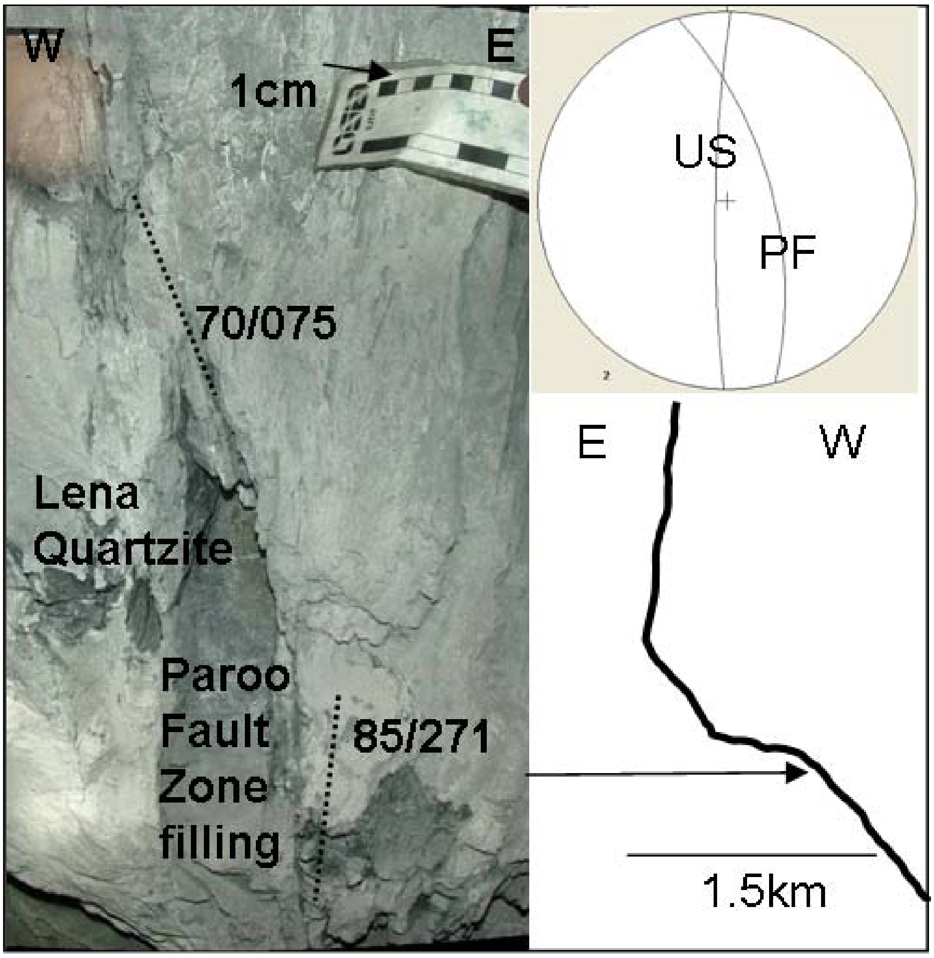

Fig. 29. Photograph of the lower steeply east dipping section of the Paroo Fault east of 3500 orebody in the northern end of the mine level 30A X620 RPAC. Only minor quartz filling can be found in this section of the fault. The equal area lower hemisphere

stereographic projection shows the orientation of Paroo Fault (PF), and S_3 cleavage in the Urquhart Shales (US).

5.6. Microscopic textures and deformation features of the Paroo Fault Zone

A detailed study of the changes in mineralogy and paragenesis was made in three parts of the fault zone (Fig. 30) termed here top, middle and bottom at the six locations described in Table 3 and Fig. 18.

Fig. 30. Photograph of the Paroo Fault Zone showing how the fault was divided up for sampling. The top of the fault zone is within 25 cm of the contact with the Urquhart Shale. Within this section there is an increased amount of shale fragments and carbonate. The bottom of the fault zone is generally within 25 cm of the basement rocks, the fault zone filling here contains a larger proportion of altered Lena Quartzite fragments. The middle section of the fault is defined as the filling between the top and bottom section of the fault zone.

5.6.1 Top of the Paroo Fault Zone

Carbonate is the dominant mineral in the filling at the top of the fault (50-80 %; Fig. 31b). Shale fragments are randomly distributed (5-10 %; Fig. 31a) and the amount of quartz varies (5-40 %) at the expense of carbonate and the graphitic material (10-3 %). Sulphides in small amounts are sometimes present (>0-5 %).

Coarse subhedral quartz crystals (100-2500 μm) contain many features indicative of post-crystallization deformation (Fig. 31c). Deformation features include multiple generations of transgranular fluid inclusion planes, undulose extinction, kink bands, inter-fingering and stylolitic grain boundaries and subgrains.

Coarse dolomite crystals (>1.2 cm; Fig. 31f) are subhedral and some of the smaller carbonate crystals have a bladed shape but are randomly orientated (Fig. 31d). The carbonates are cross-cut by veins of quartz that have associated pyrite and chalcopyrite (Figs. 31e and f). The pyrites have pressure fringes in the surrounding quartz indicating some post crystallization deformation (Fig. 31g). The preservation of the original bladed shape of the dolomite (Figs. 31c and d) suggests the carbonates grew late in the deformation history, or that strong partitioning of strain within the fault has occurred.

Although some strain has been clearly taken up by the quartz, most deformation was localized in the graphitic seams, which are strongly foliated and in places stylolitised (Fig. 31h). Associated with these seams are fine quartz grains (30-200 μm) which may have developed from fracturing of the larger grains or by the precipitation from another fluid during the shearing. The lack of secondary fluid inclusions, undulose extinction or subgrains indicate that the fine quartz formed towards the end of the overall ductile deformation history of the Paroo Fault Zone.

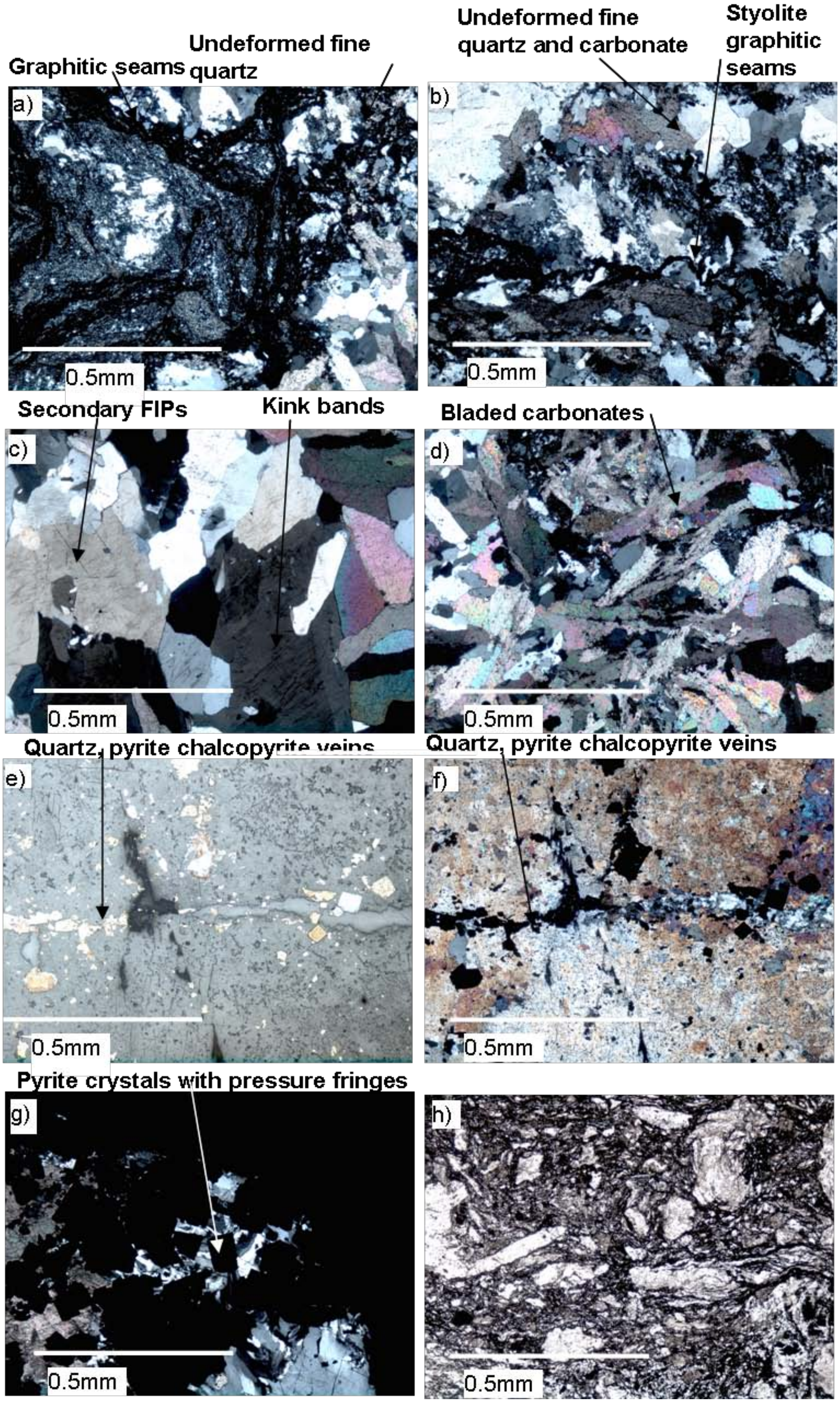

Fig. 31.Features of the top of the Paroo Fault Zone filling. a) Sample F12a cross polarized photomicrograph of the angular shale fragments associated with graphitic seams and undeformed fine quartz; b) Sample A14a cross polarized photomicrograph of undeformed fine quartz and carbonate associated with a styolitic graphitic seam; c)

Sample F12g cross polarized photomicrograph of the coarse subhedral quartz which has deformation textures including multiple transgranular fluid inclusion planes, undulose extinction, minor kink bands and serrated grain boundaries which van be seen to have formed subgrains in places; d) Sample F12a cross polarized photomicrograph of bladed carbonate crystals; e) Sample K4g reflective light photomicrograph of a quartz, pyrite and chalcopyrite veins cross cutting carbonate crystals; f) Sample K4g cross polarized photomicrograph of a quartz, pyrite and chalcopyrite veins cross cutting carbonate crystals; g) Sample K4e cross polarized photomicrograph of pyrite crystals with pressure fringes in the surrounding quartz; h) Sample F12d plane polarized light photomicrograph of the sheared nature of the polymictic fragments associated with the graphitic seams.

5.6.2 Centre of the Paroo Fault Zone

The filling in the center of the Paroo Fault Zone is dominated by quartz (60-98 %) with minor carbonate (0-40 %), graphitic seams (>2 %) and minor sulphides (0-2 %). The quartz is dominantly very coarse (0.3-7 mm) and subhedral suggesting growth into fluid filled cavities during periods of low differential stress.

Despite the overall grain shapes, there are abundant deformation indicators in the coarse quartz. These include undulose extinction, kink bands and serrated grain boundaries, subgrains, and abundant transgranular fluid inclusion planes (Figs. 32a and b). The graphitic seams which are deformed into stylolites (Fig. 32b) are rarer than at the top of the Paroo Fault Zone filling. Associated with the graphitic seams there are often fine quartz grains (20-300 μm; Fig. 32d). These strain free grains are similar to those in the upper part of the fault zone.

The carbonate crystals are coarse (0.02-6 mm) and contain deformation twins indicating deformation (Fig. 32c). Pyrite and chalcopyrite are present along carbonate and quartz grain boundaries and within the coarse quartz (Fig. 32d). Pyrite is also found within the graphitic seams (Fig. 32e). The coarser quartz surrounding the pyrites contains pressure fringes indicating post sulphide deformation. Late strain free quartz occurs as veins which form overgrowths on the host grains (Fig. 32f).

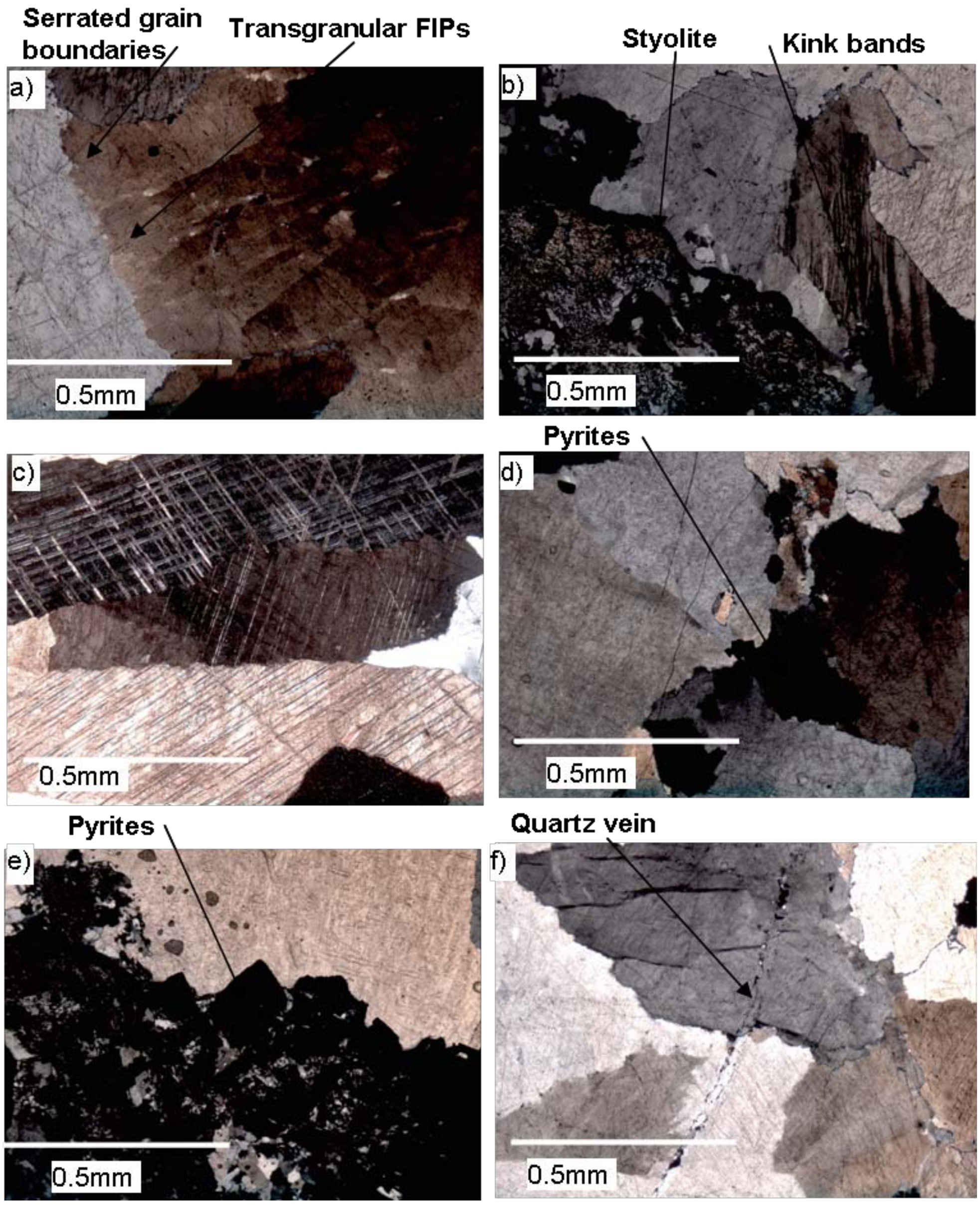

Fig. 32. Features of the centre of the Paroo Fault Zone filling. a) Sample M1g cross polarized photomicrograph of coarse quartz grains with undulose extinction, serrated grain boundaries and transgranular fluid inclusion planes; b) Sample M1g cross polarized photomicrograph of coarse quartz with kink bands adjacent to a graphitic and carbonate bearing stylolite seam; c) Sample L2d cross polarized photomicrograph of deformation twins within carbonate crystals; d) Sample M1e cross polarized photomicrograph of pyrite at the grain boundaries of coarse quartz grains; e) Sample A4a cross polarized photomicrograph of pyrite associated with a graphitic stylolite seam; f) Sample M1e cross polarized photomicrograph of a late quartz vein which contains few fluid inclusions and no deformation textures but where quartz grains takes on the orientation of the host grains.

5.6.3 Bottom of the Paroo Fault Zone

At the bottom of the Paroo Fault Zone filling is a breccia with a greater variety of clasts than the upper sections, containing large amounts of altered basement rocks as breccia fragments (30-40 %), graphitic seams (30-40 %), quartz (10-20 %), chlorite (0-10 %) and minor sulphides (<2 %; Figs. 33a and b).

The banded carbonate-graphite seams and angular clasts of altered basement rock are highly fractured and brecciated (Fig. 33b). There are some coarse quartz crystals (0.5-6 mm) which possess the same deformation features seen in the coarse quartz in the centre of the Paroo Fault Zone. Small largely-undeformed euhedral crystals of quartz (0.03-0.1 mm) are more prevalent than in the upper sections of the faults. They are associated with some of the graphitic seams (Fig. 33c).

Pyrite is dominantly found associated with the graphitic seams but is also present with chalcopyrite in the coarse quartz. Late veins of undeformed quartz cross cut and have been partially reoriented by movement on the graphitic seams. There is widespread chlorite alteration that appears to have occurred late in the paragenesis (Fig. 33a).

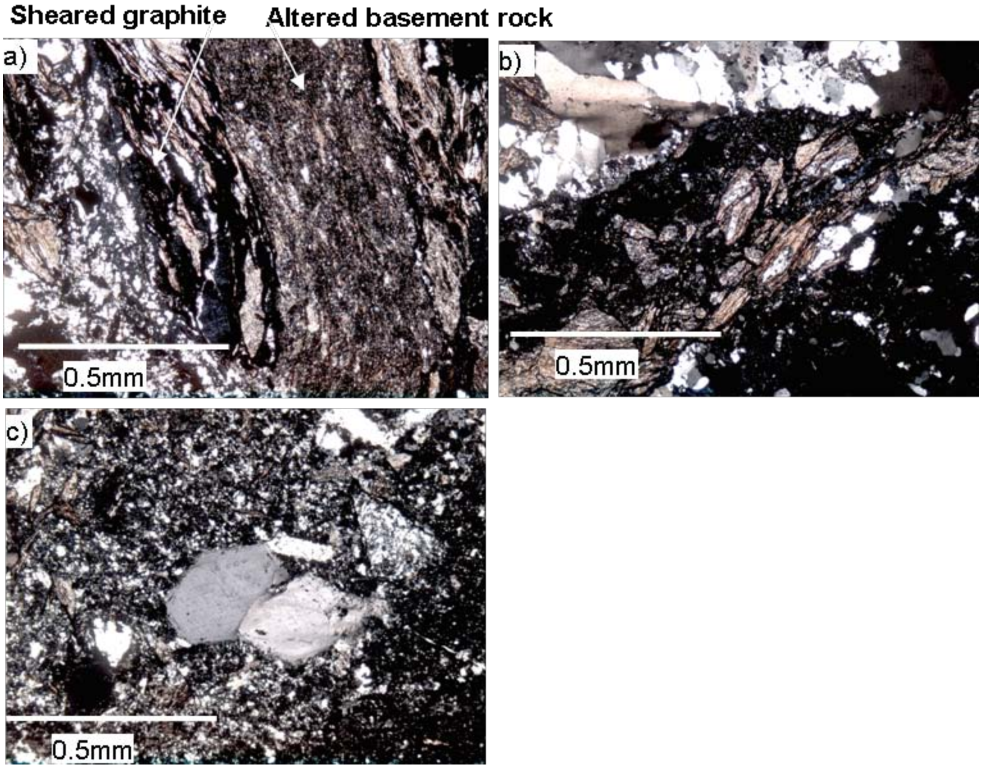

Fig. 33. Features of the bottom of the Paroo Fault Zone filling. a) Sample A1a cross polarized photomicrograph of altered basement rock, sheared graphite and chlorite; b) Sample A1d cross polarized photomicrograph showing the brecciated and polymictic nature of the fault fill at the base of the Paroo Fault; angular clasts of basement rock strain free quartz and sheared graphite can be observed; c) Sample A1d cross polarized photomicrograph of euhedral late strain free quartz grains within the fault filling.

5.7. Cathodoluminescence textures

In order to further understand the paragenesis of the fault zone filling and the quartz veins and replacement associated with the silica-dolomite alteration and basement alteration, SEM-CL imaging was undertaken on the Paroo Fault Zone filling, silica-dolomite halo and Lena Quartzite. These multiple generations of quartz and carbonate have not previously been described from the Mount Isa copper deposit.

5.7.1 Paroo Fault Zone filling

The earliest minerals identified in the Paroo Fault Zone filling are carbonates, the first of which (C_1) is a low luminescent carbonate. In places, it has been fractured, dissolved and replaced by moderately luminescent carbonate (C_2) which shows evidence of being deformed in the form of kinks and transgranular fluid inclusion planes.

This was followed by successive generations of quartz which form the coarse quartz crystals mentioned earlier. (Q_1) has a high luminescence and is present as clasts (10-500 μm) that have been partially replaced by and incorporated into Q_2 (Figs. 34a, e and g). Q_2 is moderately luminescent quartz consisting of angular remnant clasts (250-1500 μm; Figs. 34a, e and g). Q_3 occurs as veins and a low luminescent matrix surrounding and partially replacing the earlier generations, and is closely associated with chalcopyrite and pyrite (Figs. 34a, c, e and g). Late inclusion free veins which crosscut the coarse quartz grains are moderately luminescent quartz (Q_4; Fig. 34c). In the top of the fault Q_4 forms the small undeformed quartz grains, associated with the carbonaceous stylolite seams and carbonaceous seams. These cathodoluminescence textures do not appear to crosscut grain boundaries, but can crosscut subgrain boundaries.

After recrystallization of the coarse quartz there was at least one phase of deformation responsible for forming the prismatic sub-grains, kink bands, transgranular fluid inclusion planes, penetrating grain boundaries and bulging grain boundaries which incorporated all the generations of quartz. This deformation event is also responsible for creating the strain shadow in the quartz surrounding the pyrite crystals.

K4 - West of the 3000 orebody – top of the fault	C_1	C_2	Q_1	Q_2	Q_3, P, CP	Cl, G	Q_4
M1 - Below the 3000 orebody – centre of the fault				Q_2	Q_3, P, CP	Cl, G	
A1 - Between the 3000 and 3500 orebodies – base of the fault				Q_2	Q_3, P, CP	Cl, G	
A4 - Between the 3000 and 3500 orebodies – centre of the fault			Q_1	Q_2	Q_3, P, CP	Cl, G	
A14 - Between the 3000 and 3500 orebodies – top of the fault	C_1	C_2	Q_1	Q_2	Q_3, P, CP	Cl, G	Q_4
F12 - Below the 3500 orebody – top of the fault	C_1	C_2	Q_1	Q_2	Q_3	Cl, G	Q_4
L2 – East of 3500 orebody – centre of the fault	C_1	C_2	Q_1	Q_2	Q_3, P, CP	Cl, G	
O2 – Below 1100 orebody – centre of the fault			Q_1	Q_2	Q_3	Cl, G	Q_4

Table 4. Paragenetic chart of the samples from Table 3 and Fig. 18 showing the generations of quartz and carbonate from within the Paroo Fault Zone filling. Paragenesis was determined on the bases of cross cutting relationships and replacement textures.

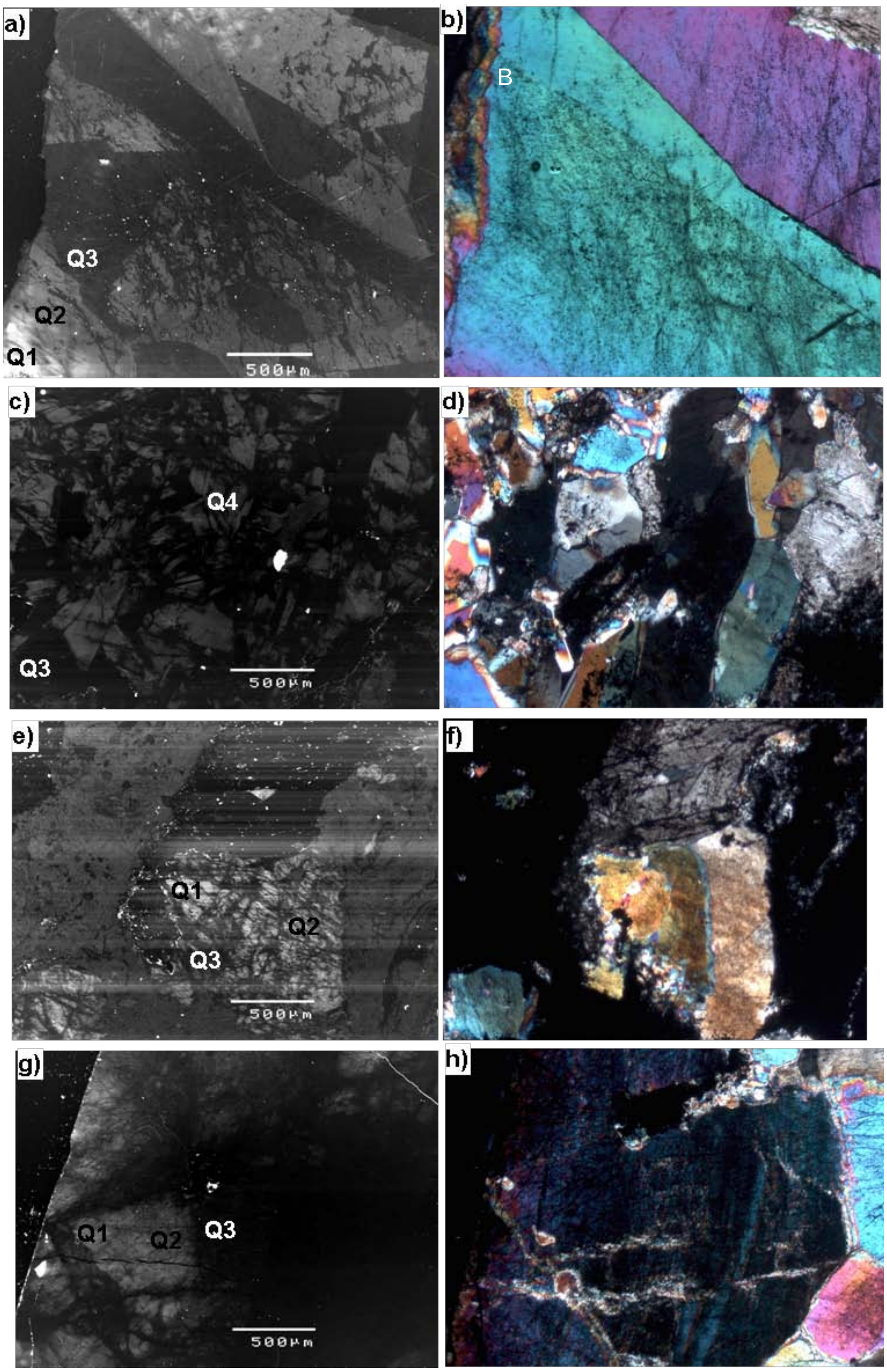

Fig. 34. SEM-CL images of the Paroo Fault Zone filling. a) Sample L2 SEM-CL photomicrograph of the coarse quartz from the center of the Paroo Fault Zone filling showing the relationship of the three successive quartz generations. Q_1 has a high luminosity and is surrounded and replaced by the moderately luminescent Q_2 which has in turn been partially replaced by and cross cut by the low luminescent Q_3; b) Sample L2 cross polar photomicrograph of the SEM-CL photomicrograph in 34a. The different

generations of quartz can be seen not to cross cut grain boundaries; c) Sample A14 SEM-CL cathodoluminescent photomicrograph of the fine quartz from the top of the Paroo Fault Zone filling showing the moderately luminescent quartz (Q_4) which forms the crystals; d) Sample A14 cross polar photomicrograph of the SEM-CL photomicrograph in 34c; e) Sample F12 SEM-CL photomicrograph of the coarse quartz from the top of the Paroo Fault Zone filling; f) Sample F12 cross polar photomicrograph of the SEM-CL photomicrograph in 34e; g) Sample A4 SEM-CL photomicrograph of the coarse quartz from the top of the Paroo Fault Zone filling; h) Sample A4 cross polar photomicrograph of the SEM-CL photomicrograph in 34g.

5.7.2 Urquhart Shale above the Paroo Fault Zone

The first formed carbonate (C_1) occurs as very fine (5-80 μm) clasts with a low luminosity (Fig. 35a). These carbonate grains are associated with small lenses (<200 μm) of high luminosity quartz (Q_1) in a matrix of moderately luminescent replacive quartz (Q_2; Fig. 35a). Coarse euhedral pyrite and chalcopyrite was dominantly formed post Q_2 (Fig. 35c). Chalcopyrite occurs as irregular blebs at the boundaries of Q_2 and Q_3 and in some cases within Q_3 (Fig. 35c). Q_3 occurs as cavity filling low luminescent veins partially replacing Q_2 veins and as strain halos around coarse euhedral pyrite (Figs. 35a and c). Deformed graphitic and chlorotic stylolites cross cut the Q_2 and Q_3 veins. Q_4 forms high luminescent thin veins (20 μm) that cross cut the earlier generations have been deformed (Figs. 35a and c).

K7 - West of the 3000 orebody	C_1			Q_2	Q_3, P, CP	Cl, G	
M5 - Below the 3000 orebody	C_1		Q_1	Q_2	Q_3, P, CP	Cl, G	
A7 - Between the 3000 and 3500 orebodies			Q_1	Q_2	Q_3, P, CP	Cl, G	Q_4
E2 - Below the 3500 orebody	C_1	C_2	Q_1	Q_2	Q_3, P, CP	Cl, G	
L3 – East of 3500 orebody	C_1	C_2		Q_2	Q_3, P, CP	Cl, G	
O7 – Below 1100 orebody		C_2	Q_1	Q_2	Q_3, P,		

Table 5. a paragenetic chart of the samples from Table 3 and Fig. 18 showing the generations of quartz and carbonate from within the Urquhart Shales directly above the Paroo Fault. Paragenesis was determined on the basis of cross cutting relationships and replacement textures.

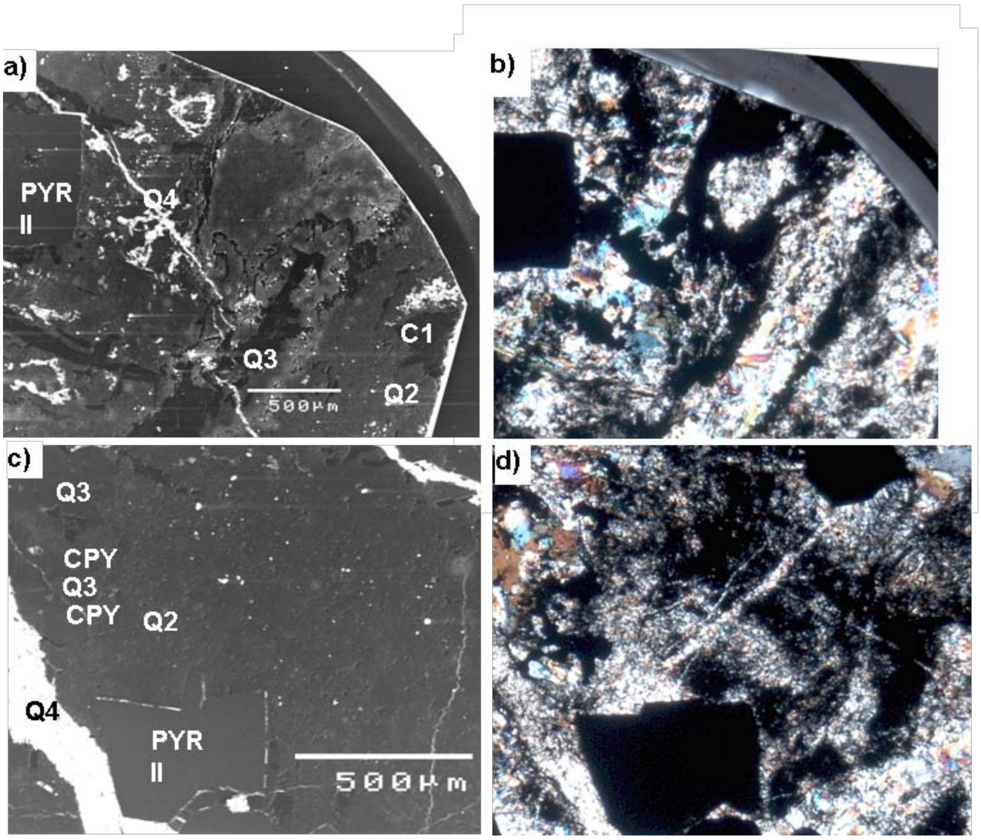

Fig. 35. SEM-CL images of the Urquhart Shale. a) Sample A7 SEM-CL photomicrograph of sample A7 (Urquhart Shale) showing the relationship of the early low luminescent C_1 and high luminescent Q_1. Surrounding this is moderately luminescent Q_2 which has been cut by veins of low luminescent Q_2. Pyrite II occurs adjacent to Q_2 and Q_3. Q_4 veins of high luminosity quartz cross cut the earlier generations and have been deformed by a late

deformation event; b) Sample A7 cross polar photomicrograph of the SEM-CL photomicrograph in 35a. The three early generations of quartz (Q_1, Q_2 and Q_3) can be seen not to cross cut grain boundaries. Q_4 veins do cross cut the grain boundaries and thus post date them; c) Sample A7 SEM-CL photomicrograph of sample A7 (Urquhart Shale) showing the relationship of the moderately luminescent Q_2 and low luminescent Q_3 to the chalcopyrite (CPY) and pyrite (PYR II) from the fractured siliceous shale; d) Sample A7 cross polar photomicrograph of the cathodoluminescent photomicrograph in 35c.

5.7.3 Lena Quartzite

C_1 has a high luminescence and forms subrounded clasts (10-100 μm) in the samples in the immediate vicinity of the Paroo Fault. In samples F8 and A10 which are less altered than the other samples, C_1 replaces detrital quartz grains and early pyrites. In the case of A10 where the C_1 has replaced the pyrite, it has itself been partially replaced by later chlorite alteration.

Q_1, a high luminescent quartz, occurs as angular clasts of variable sizes that replace pre-existing minerals (Fig. 36a). The moderately luminescent Q_2 forms veins (10 μm) which in most samples have been highly deformed (Fig. 36a)- However, in sample F8 which still has the original quartzite texture preserved, veins are undeformed.

Q_3 low luminescent quartz forms large veins (100 μm) which are generally undeformed and cross cut and offset Q_2 (Fig. 36a). Q_4 occurs as a network of thin (<10 μm) undeformed very low luminosity quartz veins which cross cut but do not offset Q_3 (Fig. 36a).

Q_5 is the last generation to affect the basement. It forms highly luminescent veins which are undeformed (50-100 μm), and also occurs as infill in extension fractures which have brecciated the rock (10 μm; Fig. 36a). Chlorite alteration occurs along fractures and grain boundaries and is spatially associated with late euhedral–subhedral pyrites.

K5 - West of the 3000 orebody		**Q_1**	**Q_2**	**Q_3, P,**	**Q_4**	**Q_5**	**Cl, G**
M4 - Below the 3000 orebody	**C_1**	**Q_1**	**Q_2**	**Q_3, P,**		**Q_5**	
A10 - Between the 3000 and 3500 orebodies	**C_1**	**Q_1**	**Q_2**	**Q_3, P,**			
F8 - Below the 3500 orebody	**C_1**	**Q_1**	**Q_2**	**Q_3, P,**		**Q_5**	**Cl, G**
L1 – East of 3500 orebody	**C_1**	**Q_1**	**Q_2**	**Q_3, P,**			
O6 – Below 1100 orebody	**C_1**	**Q_1**	**Q_2**	**Q_3, P,**		**Q_5**	

Table 6. a paragenetic chart of the samples from Table 3 and Fig. 18 showing the generations of quartz and carbonate from within the Lena Quartzite directly below the Paroo Fault. Paragenesis was determined on the bases of cross cutting relationships and replacement textures.

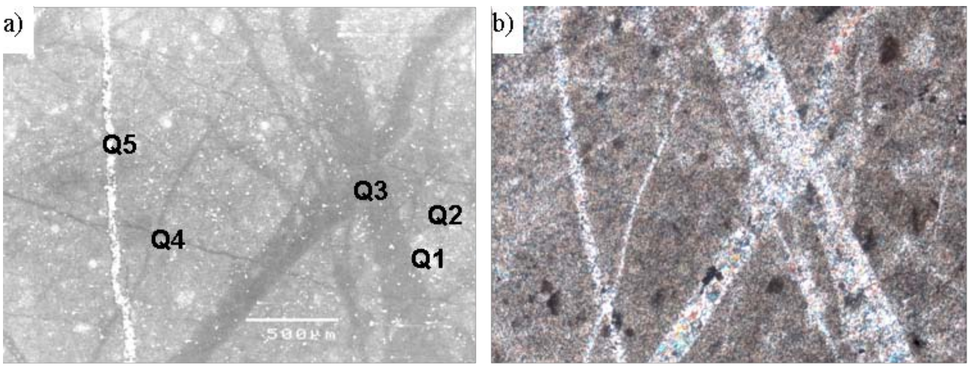

Fig. 36. SEM-CL images of Lena Quartzite. a) SEM-CL photomicrograph of sample K5 (Lena Quartzite) showing the early high luminosity Q_1 clasts within the moderately luminescent Q_2. This is cross cut by the thick low luminescent Q_3 veins which in turn is cross cut by the thin low luminosity Q_4 veins. Lastly the high luminescent Q_5 veins form; b) cross polar photomicrograph of the SEM-CL photomicrograph in 36a.

6. Discussion

6.1. Development of the Paroo Fault Zone filling

It is difficult to classify the Paroo Fault Zone in terms of the core and damage zones as defined by Caine et al. (1996). The fault zone displays distributed deformation along multiple slip surfaces of graphitic material between layers of quartz (Figs. 19, 25 and 26), instead of a fault core along which most of the displacement has occurred and associated damage zone. The explanation for this unusual fault structure lies in the mode of formation of the Paroo Fault Zone filling. The quartz from the filling could be derived, at least in part (extra silica may also have been introduced from an external source), from the quartz depleted area of shales above it, which is more than double its thickness (Fig. 19). The alternations within the Paroo Fault Zone filling are not related to crack seal mechanisms as they are not the correct scale (too big) and there are no characteristic sharp boundaries on both sides of the contacts (Cox and Etheridge, 1983). The alternations may be due to the repeated extraction of quartz from the Urquhart Shales and subsequent precipitation of quartz within the fault. This would leave behind a graphite-rich layer above the fault zone filling, part of which could become sheared into the fault zone during each successive extraction and precipitation event. The result of this is a fault zone filling consisting of alternations of quartz and graphite, where the majority of slip would take place on the graphitic seams preventing the development of a core and damage zone.

The formation of the fault zone filling must have occurred prior to the main phase of D_2 because Perkins (1984) described S_2 cleavage in the graphitic rich, quartz depleted Urquhart Shale. The consistent subparallel orientation of the alternations of graphitic material and quartz in the fault zone filling with the edge of the Paroo Fault, in the steeply dipping upper section (Fig. 7, 25) and the shallow east dipping section of the fault (Fig. 26) are further evidence of the timing of the fault zone filling's formation. The filling is likely to have formed prior to the folding of the fault during D_2 and D_3 to remain subparallel to the fault edge in two sections of the fault that have different orientations (Figs. 27b and c). The lack of shearing in the graphitic layers and lack of shear deformation affecting the quartz bands in the upper and lower section of the Paroo Fault indicate that the fault fill is less deformed when compared to middle flatter section.

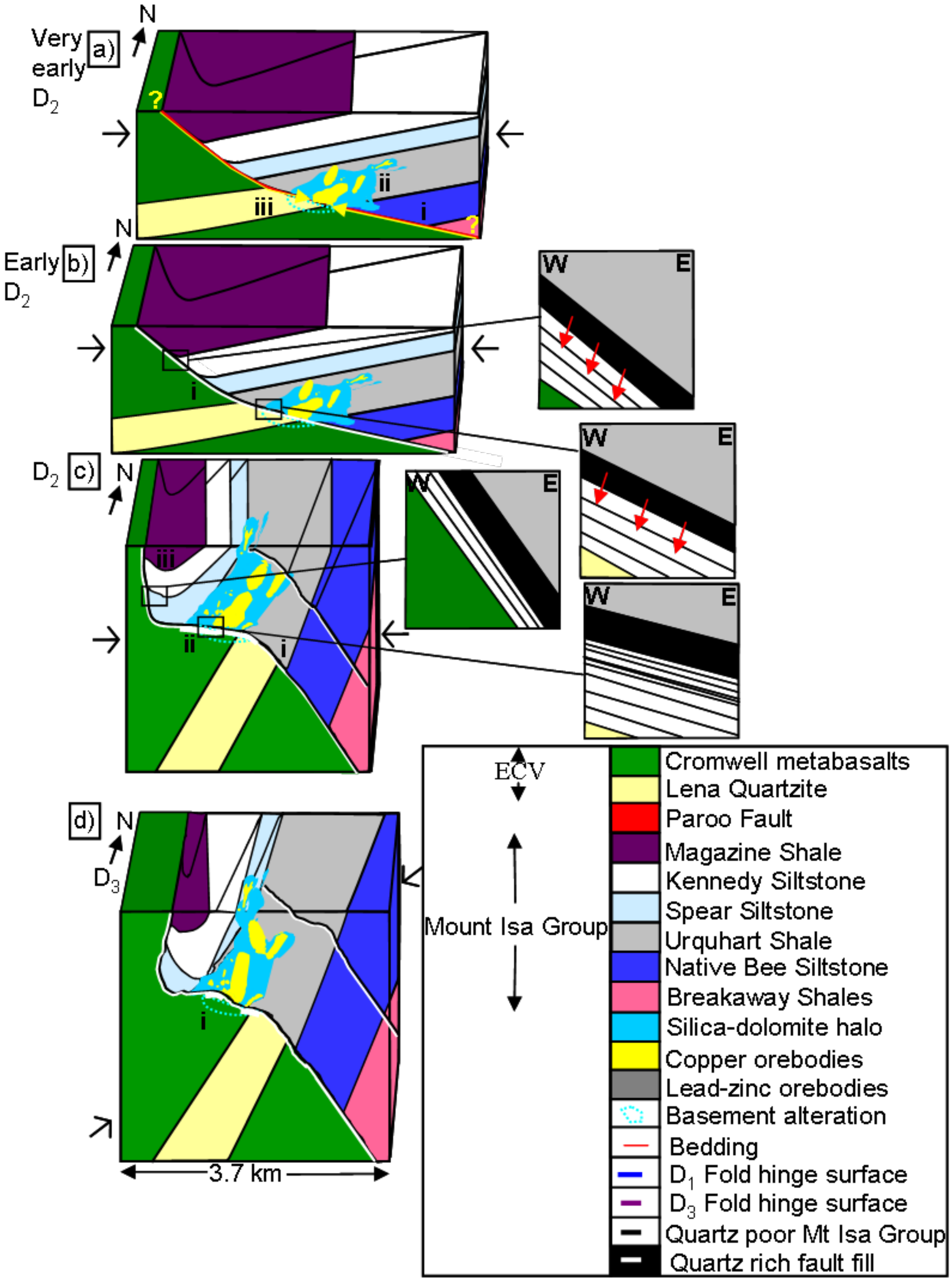

Fig. 37. Cartoon showing the evolution of the Paroo Fault and Mount Isa copper orebodies; ai) Copper bearing fluid/enter via the Paroo Fault from above and or below, aii) Forming the silica-dolomite halo and copper orebodies, aiii) the same fluids cause alteration in the basement rocks; bi) Quartz is removed from the quartz depleted zone directly above the Paroo Fault and is precipitated in stages within the fault, forming the quartz-graphite zoning at several scales; ci) The fault zone filling is forced out of the D_2 fold hinges, cii) into the area between the two fold hinges, ciii) The synsedimentary

folding exaggerated by D_2 deformation; di) Paroo Fault deforms against the copper orebodies and the fault zone filling is sheared into its present position.

If the quartz from the Paroo Fault was derived from the quartz-depleted Urquhart Shales, which were originally silicified during the formation of silica-dolomite halo, the quartz from the Paroo Fault Zone filling would have formed after the development of the silica-dolomite halo. SEM-CL textures from the fault cannot be compared with those from the silica-dolomite halo and Lena Quartzite as they have formed from different fluids. Based on their luminosity, quartz and carbonate generations can be correlated between the Lena Quartzite and Urquhart Shales (Table 7) indicating the two were probably adjacent prior to the introduction of the Paroo Fault Zone filling. The earliest formed quartz from the fault zone filling based on its luminosity could be related to late veins which cross cut the silica-dolomite halo and the Lena Quartzite. Early carbonate is dominantly found in the fault zone filling adjacent to the carbonaceous material enriched Urquhart Shale. This has been followed by four successive generations of quartz with each generation partially replacing its successor. The SEM-CL and petrography shows that most quartz in the fault zone filling was deformed. This is further evidence that the quartz was formed prior to at least one phase of deformation.

Urquhart shale	Lena Quartzite	Paroo Fault Zone filling	Luminosity
C_1	C_1		High
C_2			Low
Q_1	Q_1		High
Q_2	Q_2		Moderate
Q_3, P, CP	Q_3, P		Low
	Q_4		Low
Cl, G			N/A
		C_1	Low
		C_2	Moderate
Q_4	Q_5	Q_1	High
		Q_2	Moderate
		Q_3, P, CP	Low
		Cl, G	N/A
		Q_4	High

Table 7. Paragenetic summary of the different generations of quartz and carbonate from the Mount Isa copper deposit, which were correlated on the basis of their luminosity.

The paragenesis from this study supports the evidence of Perkins (1984) and Swager (1985) that silicification occurred after dolomite precipitation within the silica-dolomite halo. However, the dolomite formation was not a single event, but is the result of at least two generations of precipitation of carbonates, with different luminosities. There is no systemic relationship between the SEM-CL defined quartz generations in the Paroo Fault Zone filling quartz and the meso-scale zonation in the Paroo Fault. The successive replacive generations of quartz are present throughout the fault zone filling. This indicates that the process which formed the outcrop scale alternations of quartz and graphite are not related to the changes in the composition of the quartz generations. Graphite is paragenetically late in the Paroo Fault. However, the carbon isotopes (Heinrich et al., 1989) from Paroo Fault Zone graphite have a signal similar to that of the Urquhart Shale, and graphite is chemically inert in most low-medium temperature hydrothermal systems (Rumble et al., 1986). One way to form hydrothermal graphite is by mixing of methane and carbon dioxide; however this is a complex process and would have caused a spread in the carbon isotopic data (Craw, 2002). The graphite was likely concentrated in the base of the Urquhart Shale by removal of silica leaving behind residual graphite seams that recrystallised and acted as preferential shears during D_2 and $D_{3,}$ explaining its apparent young paragenesis.

6.2. Paragenesis of the Copper orebodies

Evidence of the fault zone filling forming after the copper orebodies comes from the sulphur isotope work of Andrew et al. (1989). The sulphides in the Urquhart Shales have a $\delta^{34}S$ range of 1.4-24 ‰ and the sulphides from the basement rocks away from the copper mineralisation have a range of 3-7 ‰. The sulphides from the basement rocks in the vicinity of the orebodies have higher $\delta^{34}S$ values (12.2-23.3 ‰), similar to that of the sulphides from the copper orebodies (8-25 ‰) indicating that at the time of orebody formation the two must have been juxtaposed. Both Andrew et al. (1989) and Heinrich et al. (1995) regarded the altered basement rocks (ECV) under the orebodies as part of the hydrothermal footprint of ore formation. The Paroo Fault Zone filling could not have been formed before this time as it is likely to have acted as a barrier to stop sulphur isotope exchange across the hangingwall and footwall (Figs. 22a and b).

After the fault zone filling was formed it may have acted as a barrier to any upward migrating fluid indicating the fault zone filling could have developed after the copper orebodies. There is only minor chalcopyrite preserved within the fault zone filling. If the fault zone filling was formed before the copper orebodies the mineralising fluid would have been reduced by the graphitic layers within the fault and would contain significant mineralisation; unless the method of ore formation involved a downward flowing ore bearing fluid during D_3. The fault zone filling may have acted as a barrier to downward fluid flow and caused the precipitation of the copper ore above the fault. If this was the case it would be expected that the highly graphitic quartz depleted shales adjacent to the Paroo Fault (formed prior to or early in D_2) would be extensively mineralised. Minor chalcopyrite mineralisation is found within these shales suggesting that the copper orebodies formed before the quartz depletion, i.e. before D_2 when the quartz-depleted shale developed and before S_2 cleavage.

The mesoscale observations (Figs. 12 and 13) demonstrate that the graphite and quartz alternations within the fault zone filling were folded by D_3 deformation. This Indicates that the chalcopyrite mineralisation had localised in a D_3 fold hinge, and the Paroo Fault Zone filling was not formed after the orebodies in D_3 as proposed by Swager (1983; 1985);

Perkins, (1984; 1990; 1997); Bell et al., (1988); Bell and Hickey, (1998); Davis, (2004); Miller, (2006). Another line of evidence for a pre-D_3 and probably pre or early D_2 origin for the copper orebodies is provided by bedding parallel bands of chalcopyrite and pyrite which have been folded by D_2 folds and possess S_2 cleavage (Fig. 23). Chalcopyrite is present within a silica-dolomite clast, surrounded by a D_2 fabric, and within the strain halo surrounding the clast, suggesting a pre-D_2 to early D_2 origin. Remobilisation and re-precipitation during D_3 could be responsible for forming the textures in chalcopyrite provided as evidence for the D_3 origin of the copper orebodies of previous authors (Swager, 1983, 1985; Perkins, 1984; Bell et al., 1988; Davis, 2004). Evidence from the SEM-CL study demonstrates that there have been multiple generations of fluids along the Paroo Fault that could have remobilised chalcopyrite during the subsequent deformation events.

The evidence presented here suggests copper introduction predates the Paroo Fault Zone filling, and that the latter predates most D_2 deformation. The question still remains whether the fault zone filling, silica-dolomite halo and copper orebodies formed during D_1 or very early during $D_{2.}$ D_2 is likely to have been a major dilational event on the Paroo Fault as it caused the sigmoidal shape to develop in the fault. Early on during this shortening the composition contrast between the contact of the Eastern Creek Volcanics and Urquhart Shales may have acted as a zone of weakness and a site favourable for dilation and influx of fluids during shearing on the Paroo Fault. Mathias and Clark (1975) suggest that the Paroo Fault Zone filling formed in the waning stages of copper ore genesis. The evidence presented here would also agree with this conclusion. However the timing of ore deposition proposed here is earlier than previous authors have suggested (Swager, 1983; 1985; Perkins, 1984; Bell et al., 1988; Bell and Hickey, 1998; Davis, 2004; Miller, 2006).

7. Conclusion

The work presented here supports the epigenetic model for the formation of the copper orebodies (Robertson, 1982; Gulson et al., 1983; Swager, 1983; 1985; Perkins, 1984; Bell et al., 1988; Heinrich et al., 1995; Miller, 2007), but has not examined the origin of the lead-zinc-silver orebodies. A new model for the timing of the copper orebodies and associated silica-dolomite halo formation is proposed based on sub-mm to 10's m scales observations. The copper orebodies were not formed during the east northeast-west southwest shortening event (D_3) as has been described by previous authors (Swager, 1983; 1985; Perkins, 1984; Bell *et al.,* 1988; Davis, 2004; Miller, 2007). The copper orebodies likely developed early during an east-west shortening event (D_2) although they could have formed during north-south shortening (D_1). Observations of several generations of quartz and dolomite from SEM-CL demonstrate that multiple episodic fluids have affected the copper orebodies, silica-dolomite halo and the Lena Quartzite. Subsequent to the formation of the copper orebodies and silica-dolomite halo, the Paroo Fault Zone filling formed by repeated dilation on the fault which created a cavity into which the quartz filling precipitated. The quartz filling is likely to have been derived from the overlying silica-poor Urquhart Shales, possibly with some externally derived silica (Fig. 37b). The 0.5-60 cm scale alternations of quartz and graphite explains why the Paroo Fault does not have the typical core and damage zones seen in most faults. The graphitic layers acted as a lubricant allowing deformation to occur on multiple surfaces. There appears to have been at least five fluids of contrasting compositions or five stages in the evolution of the chemistry of the fluid(s) which formed the Paroo Fault Zone filling. The earliest of these fluids has infiltrated the Lena Quartzite and silica-dolomite halo and formed veins. During the D_3 event the Paroo Fault became buttressed against the copper orebodies. This resulted in north northwest-south southeast folds within the Paroo Fault. The shales surrounding the copper orebodies were folded around the mineralisation into north northwest-south southeast folds with a folded S_2 cleavage that overprints the chalcopyrite mineralisation developed (Fig. 37d). Remobilisation of some of the copper mineralisation during D_3 could be responsible for forming the structures described by previous authors as evidence for a D_3 timing for copper orebodies formation. This model for the formation of the copper orebodies at Mount Isa creates fresh exploration potential in the Western Fold Belt of the Mount Isa Inlier. Faults folded during D_2 may contain significant copper mineralisation at depth.

7.1. References

Andrew AS, Heinrich CA, Wilkins RWT, Patterson DJ (1989) Sulfur isotope systematics of copper ore formation at Mount Isa, Australia. Economic Geology and the Bulletin of the Society of Economic Geologists 84:1614-1626

Bell TH (1983) Thrusting and duplex formation at Mount Isa. Nature 304:493-497

Bell TH, Hickey KA (1998) Multiple Deformations with Successive Subvertical and Subhorizontal Axial Planes in the Mount Isa Region: Their Impact on Geometric Development and Significance for Mineralization and Exploration. Economic Geology 93:1369-1389

Bell TH, Perkins WG, Swager CP (1988) Structural controls on development and localization of syntectonic copper mineralization at Mount Isa, Queensland. Economic Geology and the Bulletin of the Society of Economic Geologists 83:69-85

Caine JP, Evans JP, Forster CB (1996) Fault zone architecture and permeability structure. Geology 24; 1025-1028

Cox SF, Etheridge MA (1983) Crack-seal fibre growth mechanisms and their significance in the development of oriented layer silicate microstructures. Tectonophysics 92:147-170

Craw D (2002) Geochemistry of late metamorphic hydrothermal alteration and graphitisation of host rock, Macraes gold mine, Otago Schist, New Zealand. Chemical Geology 191:257-275

Davis TP (2004) Mine-scale structural controls on the Mount Isa Zn-Pb-Ag and Cu orebodies. Economic Geology and the Bulletin of the Society of Economic Geologists 99:543-559

Dunnet D (1976) Mt Isa; reconstruction of a faulted ore body. Philosophical Transactions of the Royal Society of London, Series A: Mathematical and Physical Sciences 283:333-344

Farquharson RB, Richards JR (1974) U-Th-Pb isotope systematics related to igneous rocks and ore Pb, Mount Isa, Queensland. Mineralium Deposita 9:339-356

Finlow-Bates T, Stumpfl EF (1979) The copper and lead-zinc-silver orebodies of Mt. Isa Mine, Queensland; products of one hydrothermal system. Annales de la Societe Geologique de Belgique 102:497-517

Gulson BL, Perkins WG, Mizon KJ (1983) Lead isotope studies bearing on the genesis of copper orebodies at Mount Isa, Queensland. Economic Geology and the Bulletin of the Society of Economic Geologists 78:1466-1504

Hannan KW, Golding SD, Herbert HK, Krouse HR (1993) Contrasting alteration assemblages in metabasites from Mount Isa, Queensland; implications for copper ore genesis. Economic Geology and the Bulletin of the Society of Economic Geologists 88:1135-1175

Heinrich CA, Andrew AS, Wilkins RWT, Patterson DJ (1989) A fluid inclusion and stable isotope study of synmetamorphic copper ore formation at Mount Isa, Australia. Economic Geology and the Bulletin of the Society of Economic Geologists 84:529-550

Heinrich CA, Bain JHC, Mernagh TP, Wyborn LAI, Andrew AS, Waring CL, (1995) Fluid and mass transfer during metabasalt alteration and copper mineralization at Mount Isa, Australia. Economic Geology and the Bulletin of the Society of Economic Geologists 90:705-730.

Mathias BV, Clark GJ (1975) Mount Isa copper and silver-lead-zinc orebodies; Isa and Hilton mines. Monograph Series - Australasian Institute of Mining and Metallurgy 5:351-371

McDonald JA (1970) Some effects of deformation on sulfide-rich layers in lead-zinc ore bodies, Mount Isa, Queensland. Economic Geology and the Bulletin of the Society of Economic Geologists 65:273-298

McGoldrick PJ, Keays RR (1990) Mount Isa copper and lead-zinc-silver ores; coincidence or cogenesis? Economic Geology and the Bulletin of the Society of Economic Geologists 85:641-650

Miller JM (2007) Structural controls on the Mt Isa Copper deposit, QLD. Project I7, Predictive Mineral Discovery CoOperative Research Centre

Oliver NHS, Valenta RK, Wall VJ (1990) The effect of heterogeneous stress and strain on metamorphic fluid flow, Mary Kathleen, Australia, and a model for large-scale fluid circulation. Journal of Metamorphic Geology 8:311-331

Page RW, Jackson MJ, Krassay AA (2000) Constraining sequence stratigraphy in North Australian basins; SHRIMP U-Pb zircon geochronology between Mt Isa and McArthur River. Australian Journal of Earth Sciences 47:431-459

Perkins WG (1984) Mount Isa silica dolomite and copper orebodies: The result of a syntectonic hydrothermal alteration system. Economic Geology 79:601 - 637

Perkins WG (1990) Mount Isa copper orebodies. Geology of the mineral deposits of Australia and Papua New Guinea 14:935-941

Perkins WG (1997) Mount Isa lead-zinc orebodies; replacement lodes in a zoned syndeformational copper-lead-zinc system? Ore Geology Reviews 12:61-111

Robertson CW (1982) The role of pre-existing sulphides in copper-ore formation at Mount Isa, Queensland. BMR Journal of Australian Geology and Geophysics 7:119-124

Rumble DIII, Duke EF, Hoering TL (1986) Hydrothermal graphite in New Hampshire: Evidence of carbon mobility during regional metamorphism. Geology 14:452-455

Scott KM (1989) Dolomite compositions as a guide to epigenetic copper mineralization, Mount Isa Inlier, NW Queensland. Mineralium Deposita 24:29-33

Sibson RH (1989) Earthquake faulting as a structural process. Journal of Structural Geology 11:1-14

Solomon PJ (1965) Investigations into sulfide mineralization at Mount Isa, Queensland. Economic Geology and the Bulletin of the Society of Economic Geologists 60:737-765

Stanton RL (1963) Elemental constitution of the Black Star orebodies, Mount Isa, Queensland, and its interpretation. Inst Min & Met , B , Tr, 672:69-124

Swager CP (1983) Microstructural development of the silica-dolomite and copper mineralisation at Mount Isa, north-west Queensland, with speacial emphasis on the timing and mechanism of mineralisation. Ph.D. thesis, James Cook Univ

Swager CP (1985) Syndeformational carbonate-replacement model for the copper mineralization at Mount Isa, Northwest Queensland; a microstructural study. Economic Geology and the Bulletin of the Society of Economic Geologists 80:107-125

Swager CP, Perkins WG, Knights JG (1987) Stratabound phyllosilicate zones associated with syntectonic copper orebodies at Mt. Isa, Queensland. Australian Journal of Earth Sciences 34:463-476

Winsor CN (1983) Syntectonic vein and fibre growth associated with multiple slaty cleavage development in the Lake Moondarra area, Mount Isa, Australia. Tectonophysics 92:195-210

Winsor C N (1986) Intermittent folding and faulting in the Lake Moondarra area, Mount Isa, Queensland. Australian Journal of Earth Sciences 33:7-42

Preamble to paper 3

The previous papers (papers 1 and 2) examined the geometry and mineralogy of the Paroo Fault at the micro- to macroscale (μm-km) to understand the formation and development of the Paroo Fault and the copper orebodies. This next paper (paper 3) examines the geometry of the Urquhart Shales at the meso- to macroscale (m-km) to provide further constraints on the formation and development of the copper orebodies. The paper also re-examines the evidence of previous authors timing for the formation of the copper orebodies in light of the new evidence presented in this thesis and re-interprets it. The result of this is a comprehensive model for the formation of the copper orebodies earlier than proposed by previous authors.

Paper 3 - The formation of the Mount Isa copper orebodies, NW Queensland - a new paragenesis based on macroscopic structural elements

Ryan D. Long, Thomas G. Blenkinsop and Nicholas H. S. Oliver

1. Abstract

The timing for the formation of the Mount Isa copper orebodies has been debated for over 85 years, with models for both a syngenetic and epigenetic formation proposed. Within the epigenetic model there is further disagreement for the timing of the orebodies. To resolve the controversy surrounding the formation of the copper orebodies, mapping of the deposit has been re-examined. Previously unrecognised early folds within the Urquhart Shales that have no control on the copper mineralisation and appear to predate it have been observed. These folds have variably orientated east-west hinge surfaces and were probably formed by north-south shortening (D_1). Subsequent folds which have north-south (D_2) and NNW-SSE (D_3) orientated hinge surfaces refold the D_1 folds. The D_3 folds also wrap around the non-stratiform copper orebodies, demonstrating that the D_3 folds developed after the formation of the copper orebodies. The geometric observations of the folds and their relationship to the copper orebodies suggest that the Mount Isa copper orebodies were formed after

the development of the D_1 folds and before the D_3 folds, during the east-west shortening event (D_2).

Keywords: Mount Isa copper deposit, re-examination, folding.

2. Introduction

Re-interpretation of existing data can be very important in geological research, especially where the original data-source is inaccessible. The re-examination of data such as maps (Lowell, 1968), structures (Miller *et al.,* 2001; Miller and Wilson, 2004) and geochemistry (Mote *et al.,* 2001) combined with collection and analysis of new data has lead to the discovery of numerous orebodies, and re-interpretation of the formation history of various mineral deposits (Page *et al.,* 2005; Brems *et al.,* 2009).

The Mount Isa copper orebodies have been examined for over 85 years yet a conclusive model for their formation has not yet been proposed. Models for both the syngenetic and epigenetic formation of the copper orebodies have been suggested with further disagreement for the timing of the epigenetic model. The current evidence for these models does not conclusively demonstrate the timing of the formation of the copper orebodies, and a detailed re-examination of the deposit is required.

This paper re-examines the existing dataset for the Mount Isa copper orebodies with the aim to improve the constraints on the origin of this world class deposit. A wealth of mapping data is available, including bedding, fault, fold and cleavage measurements, which were collected during the mining of the copper orebodies over the last 70 years. This mapping database represents an invaluable resource because most of the mapped areas are no longer accessible due to backfilling and shot-creeting. Recently mapped areas were not available to previous researchers allowing this paper to utilise the most comprehensive dataset in the history of the deposit. This work has lead to the development of an enhanced model for the timing of the formation of the copper orebodies and, in a detailed review of the previous models, re-interpretation of their evidence.

3. Review

3.1. Background geology

The Mount Isa copper deposit is located within the Western Fold Belt of the Mount Isa Inlier, northwest Queensland (Fig. 38), and was discovered in 1923, and mined since 1940. The deposit is estimated to have originally contained over 200 Mt at 2 % Cu and is one of the largest sediment hosted copper deposits in the world. The remaining measured resources of 48 Mt at 2.1 % Cu from the X41 Mine and 49 Mt at 3.2 % Cu from the Enterprise Mine (Xstrata Copper ore reserves and resources, 2009; Fig. 39) mean that Mount Isa remains an important deposit in the world copper market.

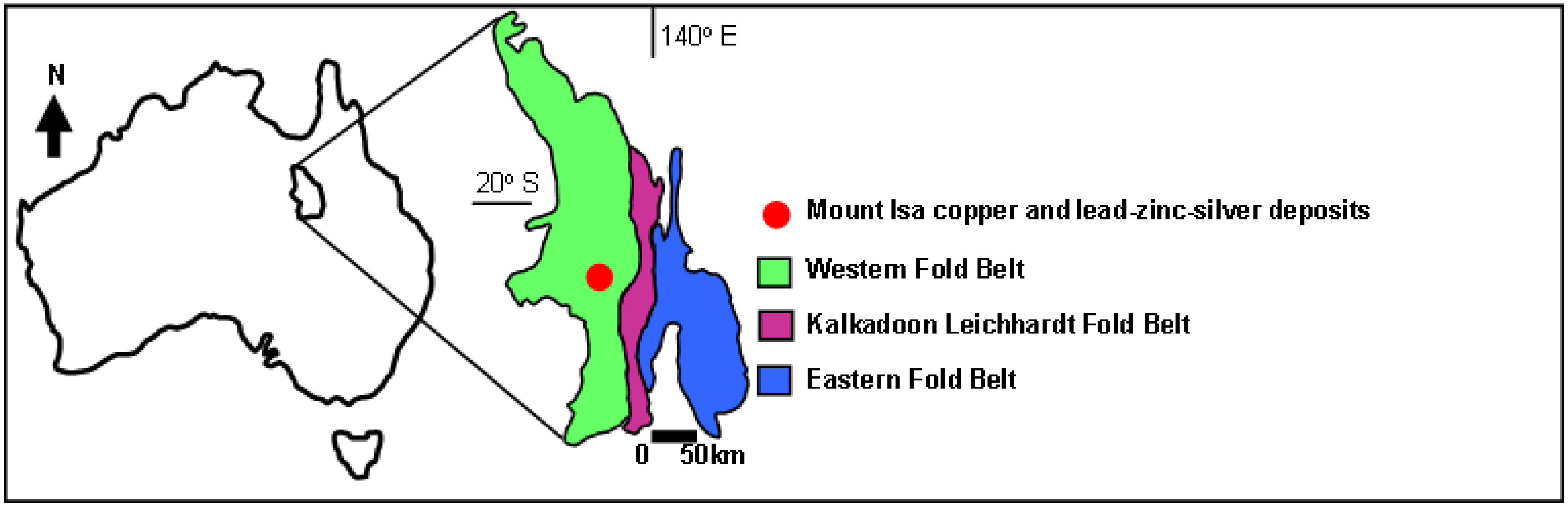

Fig. 38. Simplified tectonic map of the Mount Isa Inlier showing the Mount Isa copper and lead-zinc-silver deposit.

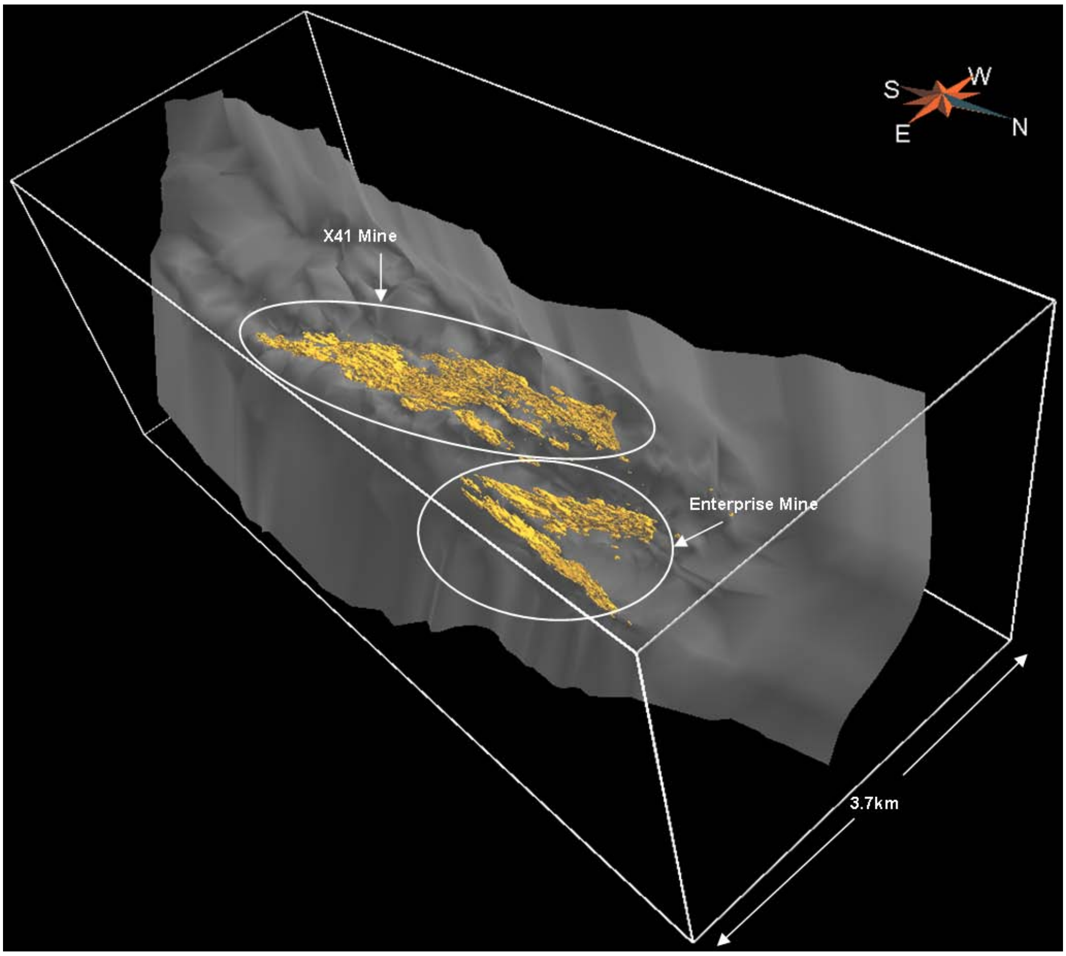

Fig. 39. The Paroo Fault (grey) with the copper orebodies labelled (yellow) showing the Enterprise and X41 Mines. The model is based on data collected by the mine geologists (MIM and Xstrata Copper) since drilling began in the 1930's.

The juxtaposition of the Mount Isa Group (including the copper hosting Urquhart Shale Formation, 1655 ± 4 Ma; Page *et al.,* 2000) against the underlying Eastern Creek Volcanics (1710 ± 25 Ma; Gulson *et al.,* 1983) occurred by normal movement on the Paroo Fault (Paper 1). The Mount Isa Group and the Eastern Creek Volcanics generally dips steeply to the west (Fig. 40A). The Mount Isa Group is locally folded and youngs to the west, with the Magazine Shale being the youngest member and the

Breakaway Shale the oldest. The stratigraphy of the Mount Isa Group is described in detail by Mathias and Clark (1975). The Urquhart Shale contains all the copper and lead-zinc-silver mineralisation within the Mount Isa Group (Solomon, 1965; McDonald, 1970). The lead-zinc-silver orebodies which are stratiform lie above the Paroo Fault outside the silica-dolomite halo that surrounds the copper orebodies (Finlow-Bates, 1979). The copper orebodies, which can be stratiform and non-stratiform, lie adjacent to the Paroo Fault or perched above it.

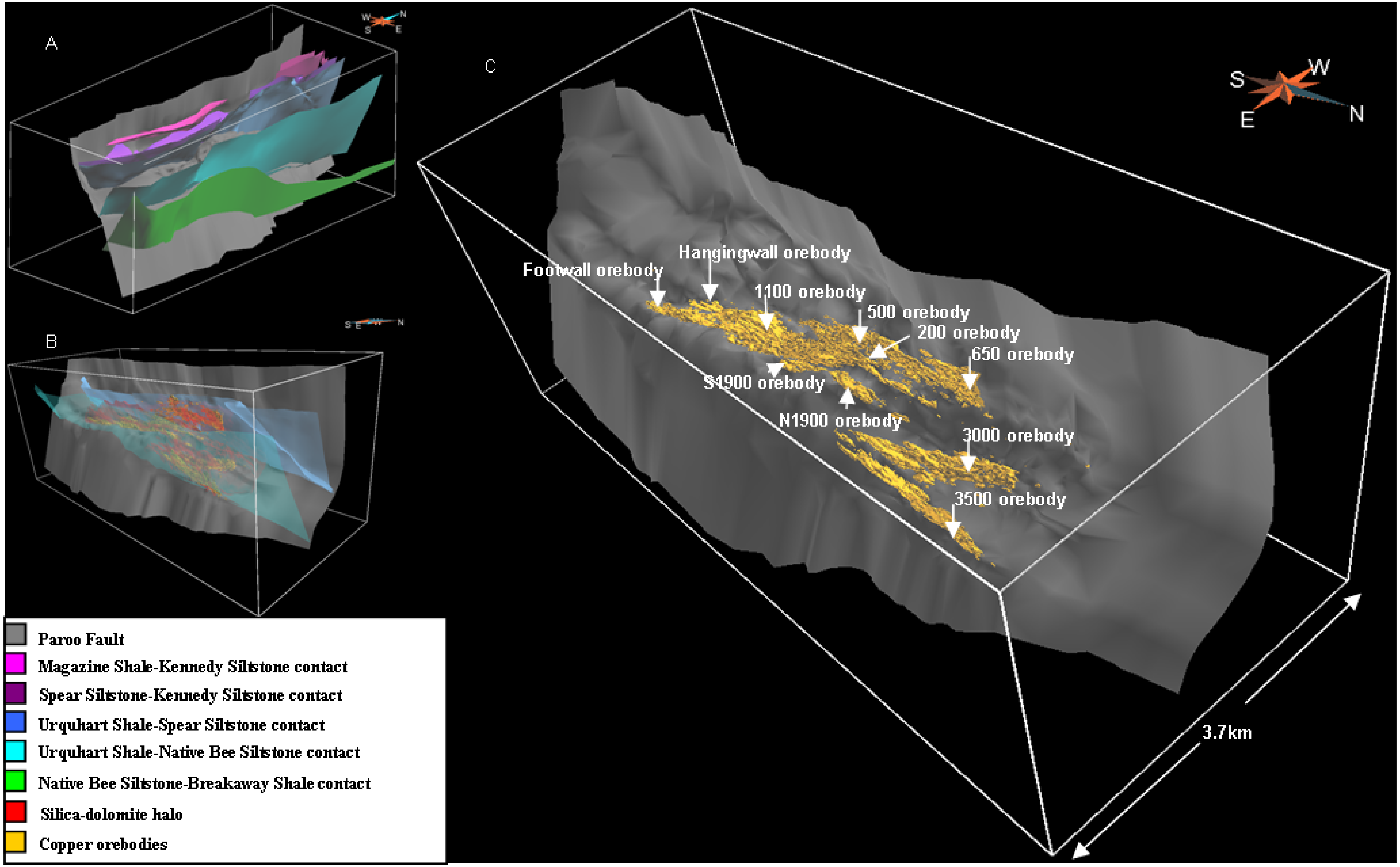

A
B
C
W
N
S
E
Footwall orebody
Hangingwall orebody
1100 orebody
500 orebody
200 orebody
650 orebody
S1900 orebody
N1900 orebody
3000 orebody
3500 orebody
3.7km
Paroo Fault
Magazine Shale-Kennedy Siltstone contact
Spear Siltstone-Kennedy Siltstone contact
Urquhart Shale-Spear Siltstone contact
Urquhart Shale-Native Bee Siltstone contact
Native Bee Siltstone-Breakaway Shale contact
Silica-dolomite halo
Copper orebodies

Fig. 40. The geology of the Mount Isa copper deposit; A) The Paroo Fault (grey) with the Mount Isa Group, B) The Paroo Fault (grey) with the stratigraphic boundaries of the Urquhart Shales (blue and turquoise) which contain the silica-dolomite halo (red) that surrounds the copper orebodies (yellow), C) The Paroo Fault (grey) with the copper orebodies labelled (yellow). The model is based on data collected by the mine geologists (MIM and Xstrata Copper) since drilling began in the 1930's.

3.2. Previous work on the deformation history of the Mount Isa Copper orebodies

The sequence of deformation events that have affected the Mount Isa copper and lead-zinc-silver deposits has been vigorously debated for over 50 years. Large folds (3 m – 50 m amplitudes) and small scale folds (amplitudes of 1 cm – 200 cm) within the Urquhart Shale around the lead-zinc-silver mineralisation were originally attributed to the development of a regional anticline (McDonald, 1970). An important aspect of this early work was the demonstration that the folding was not syn-sedimentary, based on crenulation cleavages, faults and fractures closely related to the folds, and changes in the structure and textures of the sulphides in proximity to the folds. However, Mathias and Clark (1975) recognised that the deformation history was more complex than McDonald's (1970) regional anticline event. Three episodes of faulting and shearing that affected both the Mount Isa Group and the underlying Eastern Creek Volcanics in the vicinity of the copper and lead-zinc-silver deposits were described (Mathias and Clark 1975). Mathias and Clark's (1975) early deformation event involved the development of north-south faults and shears which dominantly dip to the west, formed synchronously with the regional anticline. In the second event, sets of conjugate normal faults, dipping to the west and SW respectively, intersected the first structures. These were succeeded by a third episode of faulting forming reverse faults that dip to the NW.

Mathias and Clark's (1975) episodes of faulting fit with the series of deformation events described by Bell *et al.* (1988). Bell *et al.* (1988) described the Paroo Fault initiating as a thrust in a duplex during a north-south orientated shortening event (D_1). The fault was subsequently rotated during an east-west shortening event (D_2) in to its present orientation. A final phase of ENE-WSW shortening (D_3) deformed the deposit. Evidence for the north-south shortening event (D_1) comes from S_1 cleavages within the deposit as well as dolomitic extension veins (Swager, 1985). D_1 folds within the Mount Isa Group have been described north of the mine. These have east-west striking hinge surfaces with axial planar slaty cleavage (S_1; Winsor, 1983). Smaller scale west verging folds which have wavelengths of 1 to 200 mm within the lead-zinc-silver deposit were attributed to D_1 by Perkins (1997).

Following D_1, D_2 deformation created folds with north-south orientated hinge surfaces which re-folded the D_1 folds producing a weak slaty cleavage in the Lake Moondarra area north of Mount Isa (Winsor, 1983). Other D_2 structures observed within the deposit include; pervasive S_2 slaty cleavage in the dolomitic shales and the carbonaceous shales (Swager, 1985), dolomitic extension veins parallel to S_2 cleavage, and north-south faults (Fig. 41).

The third deformation event (D_3) formed folds with NNW-SSE orientated hinge surfaces with a weak S_3 slaty cleavage within the lead-zinc-silver orebodies (Swager, 1983). Other D_3 structures include the folds in the Urquhart Shale with NNW-SSE oriented hinge surfaces which surround the 650 copper orebody (Bell et al., 1988), 1100 copper orebody (Perkins, 1984) and the 3000 copper orebody (Davis, 2004). S_3 slaty cleavage in the dolomitic shales and S_3 crenulation cleavage in the carbonaceous shales and D_3 dolomitic and quartzitic extension veins parallel to S_3 are further evidence of D_3 deformation. NE-SW faults which offset the 3000 orebody (Fig. 3; Miller, 2007), the 650 orebody (Perkins, 1984) and the stratabound 3500 orebody (Fig. 41) are also likely to be D_3 structures, described as being reactivated during D_4 (Miller, 2007). D_4 folds described by Bell *et al.* (1988) and Miller (2007) occur locally, with weak NW-SE striking S_4 crenulation cleavage in the carbonaceous shales.

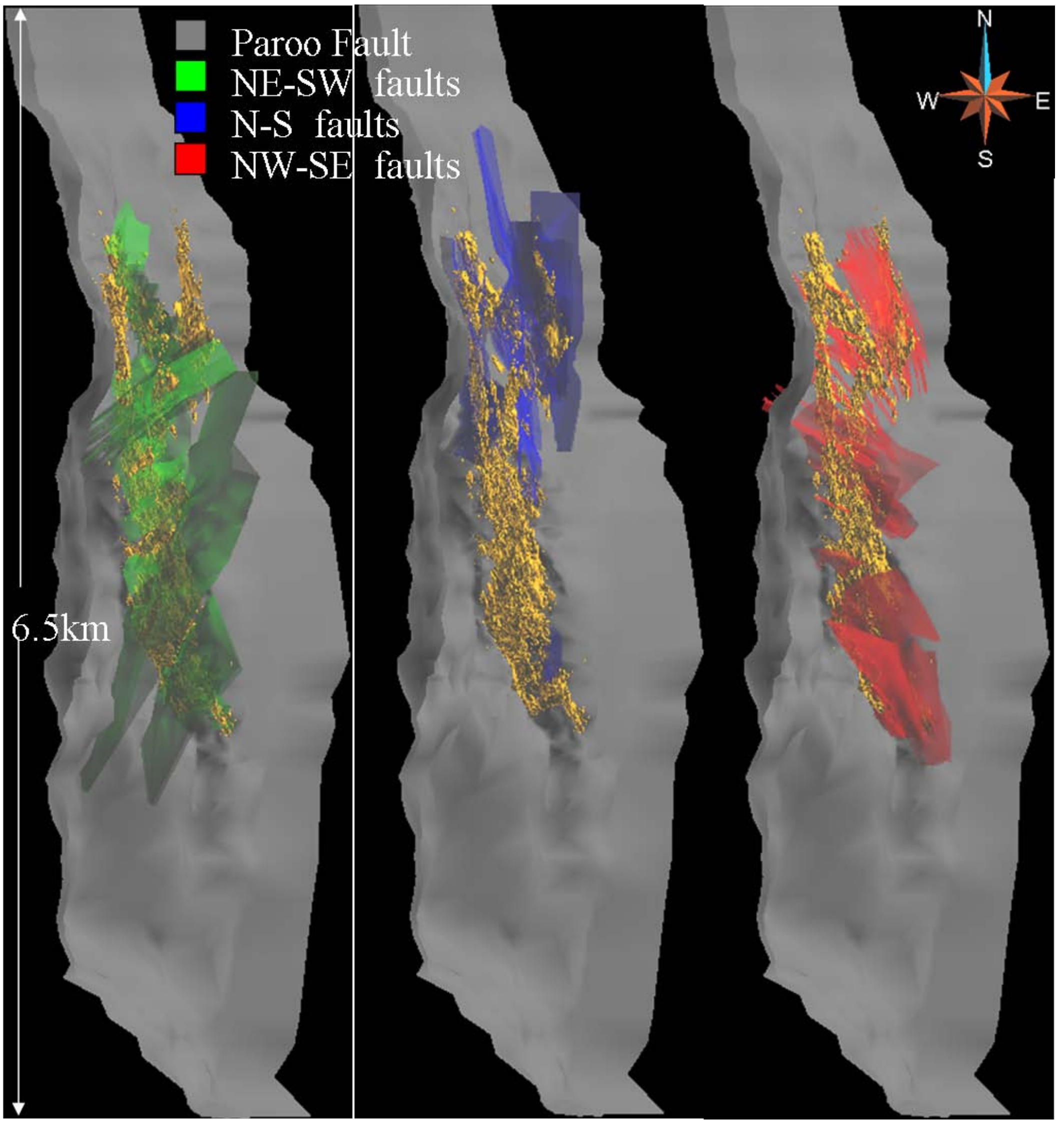

Fig. 41. The Paroo Fault displaying the three dominant orientations of faults in the Mount Isa copper deposit; northeast southwest (green), north-south (blue) and northwest-southeast (red). The model is based on data collected by the mine geologists (MIM and Xstrata Copper) since drilling began in the 1930's.

The thrust duplex model put forward by Bell *et al*. (1988) for explaining the formation of the Paroo Fault has been challenged by numerous authors (Connors *et al.,* 1992; Stewart, 1992; Nijman *et al.,* 1992a; b; Lister, 1993; O'Dea *et al.,* 1996; 1997a; Betts *et al.,* 1998; 2003; Betts, 1999; Betts and Lister, 2002; Gibson and Henson, 2005). An examination of locations of importance to the thrusting model found no evidence of the roof thrusts but revealed that the thrust imbricates are actually normal fault graben (Stewart, 1992). Many of the east-west thrust faults termed D_1 by Bell *et al.* (1988) crosscut D_2 folds and must therefore be younger (Stewart, 1992). Also some of the D_1 thrust faults described by Bell *et al.* (1988) dip towards the south not the north, which is incompatible with the thrust duplex model (Dunnet, 1976; Derrick, 1982; Stewart, 1992; Nijman *et al.,* 1992a; b; O'Dea and Lister, 1995; O'Dea *et al.,* 1997a). Many authors suggest that extension during the deposition of the Mount Isa Group provides an explanation for the formation of the early faults (Connors *et al.,* 1992; Stewart, 1992; Nijman *et al.,* 1992a; b; Lister, 1993; O'Dea *et al.,* 1996; 1997a; Betts *et al.,* 1998; 2003; Betts, 1999; Betts and Lister, 2002; Gibson and Henson, 2005) described as thrusts by Bell *et al.* (1988). Despite disagreeing with the thrust duplex model, Gibson and Henson (2005) describe a phase of early north-south thrusting that occurred after extension.

Working south of the Mount Isa deposits, MacCready (2006) determined that pre-D_1 north-south extension was responsible for juxtaposing the Mount Isa Group against the Eastern Creek Volcanics, followed by east directed thrusting. Following this north-south extension occurred, followed by a second period of thrusting. It is likely that MacCready's (2006) pre-D_1 north-south extension event is part of Mount Isa Rift Event described by O'Dea *et al.* (1997), Betts *et al.* (1998; 1999; 2006), Betts (2001) and Betts and Lister (2001). This rift event caused the reactivation of north-south growth faults, such as the Paroo Fault, and east-west cross faults as growth faults (Betts *et al.,* 1998; 2003; Betts and Lister, 2001) and would have been responsible for juxtaposing the Eastern Creek Volcanic against the Mount Isa Group (Paper 1).

Excluding the thrust duplex in favour of extensional normal faulting, the deformation sequence first proposed by Bell (1983), with minor early north-south shortening (D_1; Gibson and Henson, 2005), followed by east-west shortening (D_2) and ENE-WSE shortening (D_3; Swager, 1983; 1985; Perkins, 1984; 1997; Bell *et al.,* 1988; Davis, 2004; Miller, 2007) is used here.

3.3. Timing of the formation of the Mount Isa copper orebodies

There are three dominant models for the timing of the formation of the Mount Isa copper orebodies. The first model is that the copper orebodies formed during deposition of the Urquhart Shale and synchronous with the lead-zinc-silver orebodies (Stanton, 1963; Dunnet, 1976; Finlow-Bates and Stumpfl, 1979; McGoldrick and Keays, 1990). In the other two models the copper orebodies formation is epigenetic (Robertson, 1982; Gulson *et al.,* 1983). The second model proposed an early D_3 timing for copper mineralisation (Swager, 1983; 1985; Perkins, 1984; Bell *et al.,* 1988; Davis, 2004). In the third model the copper orebodies were formed during late D_3 (called late D_4 in Miller 2007 after Davis's 2004 deformation sequence).

3.3.1 Syngenetic formation of the Mount Isa copper orebodies

The proposed evidence for the syngenetic origin of the copper orebodies comes firstly from suggestive geochemical evidence, and secondly from permissive explanations of how an apparent epigenetic texture could form by syngenetic means. The direct evidence comes from two sources. The first is early statistical work on the element composition distributions between the lead-zinc-silver orebodies and the perched 500 and 650 copper orebodies. The overlap in the non-sulphide bulk chemistry and Al_2O_3 vs. CO_2 between the lead-zinc-silver and copper orebodies suggests that they represent sub-facies of a single basin deposit (Stanton, 1963). The second is the volatile and precious metal trace element concentrations, S/Se ratios and heavy sulphur isotope vales from the two deposits, which indicate the fluid would have been cool (<200 ^{o}C) and low in S for both the copper and the lead-zinc-silver ores, suggesting a common source (McGoldrick and Keays, 1990).

The first piece of permissive evidence for syngenetic copper, which comes from Dunnet (1976), was that the apparent epigenetic texture of the copper ores was due to extensive recrystallization by pore fluids associated with movements on the Mount Isa/Paroo Faults. The second piece of permissive evidence was described by Finlow-Bates and Stumpfl (1979) who interpreted the copper orebodies as representing the product of subsurface deposition from the same mineralising fluid that formed the lead-zinc-silver deposits. The authors point out that the silica-dolomite breccia contains rare copper mineralisation as replacement of small pyrite grains at the edges of the clasts, indicating that the brecciation occurred in proximity to the Paroo Fault prior to sulphide mineralisation. The copper sulphides were then deposited within the breccias and the lead-zinc-silver mineralisation was deposited exhalatively on the seafloor.

3.3.2 Epigenetic early D_3 deposition of the Mount Isa copper orebodies

Suggestive evidence for the early D_3 formation of the copper orebodies comes from Swager (1983; 1985), Perkins (1984) and Bell *et al.* (1988). Permissive evidence comes from Perkins (1984), Bell *et al.* (1988) and Davis (2004). The suggestive evidence for the D_3 age of copper mineralisation is largely based on S_3 cleavage observed in clasts of breccia surrounded by a quartz and chalcopyrite matrix with no cleavage (Swager, 1983; 1985; Perkins, 1984). Strain free polygonal quartz surrounding chalcopyrite in quartz-dolomite-chalcopyrite veins was used to infer the chalcopyrite has not been deformed and must have been formed in the last deformation event to affect the deposit (Swager, 1985). Swager (1985) also indicates that there is no evidence of remobilization within the quartz-dolomite-chalcopyrite veins because the inclusion free quartz has the same optical orientation as the inclusion rich zones. Copper breccia veins also show evidence of D_3 deformation including S_3 development against their margins and are crosscut by sub-horizontal extension veins formed during the later stages of D_3 (Bell *et al.,* 1988). Suggestive evidence for the epigenetic formation of the silica-dolomite halo comes from porphyroblasts of dolomite within the silica-dolomite halo, described by Swager (1983) to overprint S_2 cleavage indicating that the dolomite formed after D_2. The permissive evidence is centred on the position of the 650 copper orebody (Perkins, 1984), the 1100 and 1900 orebodies (Bell *et al.,* 1988) and 3000 (Davis, 2004) within D_3 fold zones. The permissive evidence for the development of the silica dolomite halo during D_3 is the NNW-SSE orientation of the halo (Bell *et al.,* 1988).

3.3.3 Epigenetic late D_3 deposition of the Mount Isa copper orebodies

Miller (2007) argues for a late D_3 age (termed D_4 in Miller, 2007) for the formation of the copper orebodies based on the orientation of extension veins associated with the copper orebodies and Paroo Fault. The intersection direction between the extension veins and bedding (slip surfaces) pitches steeply to the south on the west-dipping bedding surfaces and the hangingwall transport direction is top to the SE consistent with late D_3 deformation.

3.4. The geometry of the Mount Isa Group

The Mount Isa Group generally dips 65-70 ^{o} towards the west, apart from the Kennedy Siltstone and Magazine Shale that have been locally folded in the vicinity of the Paroo Fault. This folding is open in the southern end of the deposit and becomes tighter in the northern area of the deposit (Fig. 40A). Within the Urquhart Shales there are several other types of fold discussed later.

3.5. Rock types of the silica-dolomite halo

The silica-dolomite halo (Fig. 40B) generally has a more siliceous core grading out into more dolomite rich areas. There are five dominant rock types within the silica-dolomite halo that vary in terms of silicification, dolomitisation, brecciation and recrystallization (Mathias and Clark, 1975). Recrystallised Shale is composed of alternating bands of carbonaceous siliceous shales and pyritic shales in a matrix of fine dolomite. Crystalline Dolomite is dominantly dolomite of a medium to coarse grain size with little or no shale. Minor interstitial quartz can be present. The Irregularly Brecciated Recrystallised Shale is composed of Recrystallised Shale fragments with coarse crystalline dolomite in a matrix of dolomite and quartz (Mathias and Clark, 1975). Siliceous Shale is a black carbonaceous chert, with well preserved bedding and limited copper mineralisation, which has undergone various degrees of sillification. The Fractured Siliceous Shale is poorly bedded silicified shale in a quartz sulphide matrix. It is the dominant host to the copper mineralisation and has undergone various degrees of brecciation (Mathias and Clark, 1975).

3.6. The geometry of the Mount Isa copper orebodies

Both the copper and lead-zinc-silver orebodies at Mount Isa are stratabound within the Urquhart Shale (Solomon, 1965; McDonald, 1970). The copper orebodies are surrounded by a NNW trending silica-dolomite halo (Fig. 40B), which has a core of more siliceous material surrounded by dolomitic rocks (Finlow-Bates and Stumpfl, 1979).

The Mount Isa copper deposit consists of ten large orebodies (Figs. 40 and 41), three of which are stratiform (500, northern 1900 and 3500) and seven are non-stratiform (hangingwall lens, footwall lens 200, 650, 1100, southern 1900 and 3000). Some of these orebodies are perched (200, 500 and 650) above the Paroo Fault while others lie directly above it (hangingwall lens, footwall lens, 1100, southern & northern 1900, 3000 and 3500; Fig. 42). Smaller orebodies such as the 400 and 700 are not discussed here.

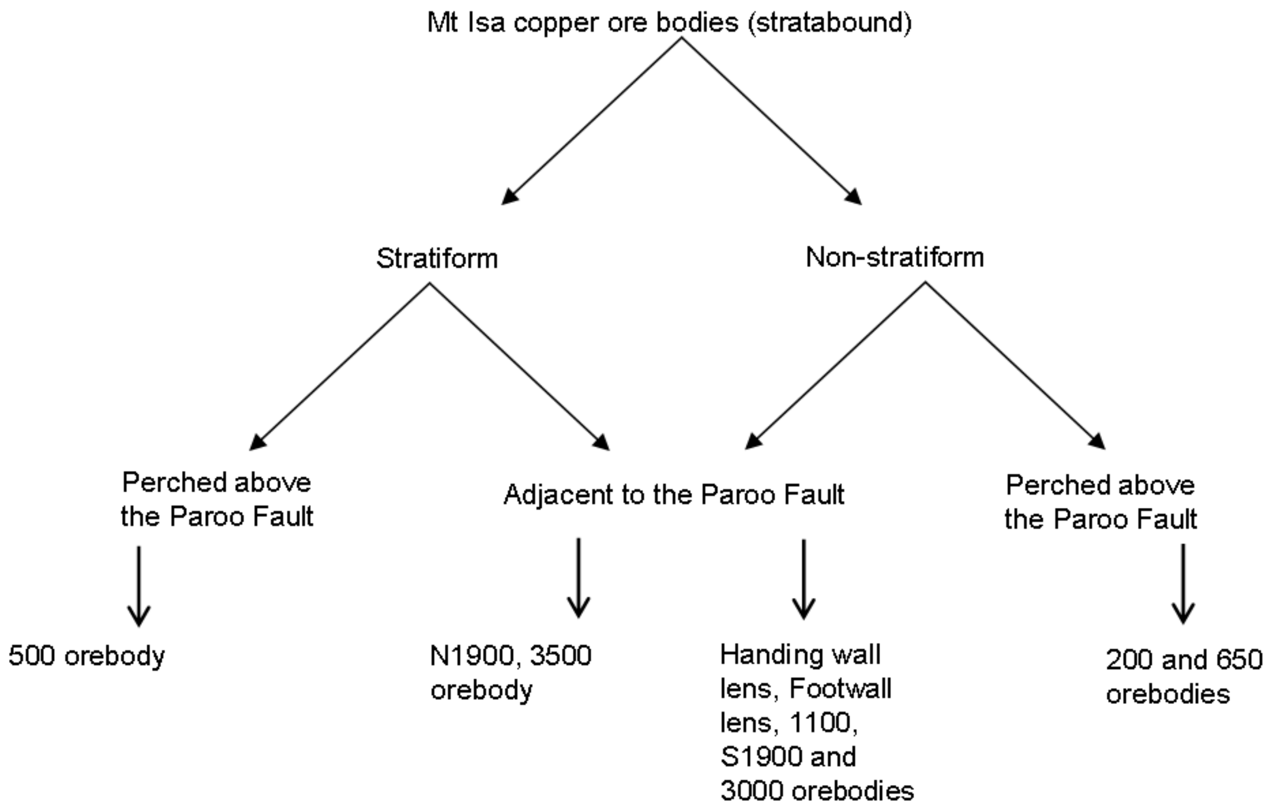

Fig. 42. Diagram summarising the different types of copper orebody at Mount Isa. Orebodies can be stratiform or non-stratiform and are also located adjacent to the Paroo Fault or perched above it

.

The 200 copper orebody (Fig. 40) has a strike length of 300 m and a maximum width of 50 m and is contained within Recrystallised Shale. The 200 orebody lies within the same lobe of silica dolomite that includes the 1100 orebodies. It abuts against the lead-zinc-silver orebodies and bedding within it does not appear to be folded (Davis, 2004).

The 500 copper orebody (Fig. 40) has a strike length of 1300 m and a maximum width of 230 m. It is located between two lead-zinc-silver orebodies in large tongues of silica-dolomite that have sharp contacts with the surrounding shales (Mathias and Clark, 1975). The main host rocks for the chalcopyrite mineralisation are Crystalline Dolomite, Irregularly Brecciated Recrystallised Shale and Recrystallised Shale (Mathias and Clark, 1975).

The 650 copper orebody (Fig. 40) has a strike length of 320 m and a maximum width of 30 m and is located just northwest of the 500 copper orebody in a similar geological setting. Both orebodies have grades of 2.3 % Cu. The copper mineralisation is hosted in Recrystallised Shale and Irregularly Brecciated Recrystallised Shale (Robertson, 1982 and Perkins, 1984). Nodular euhedral coarse grained pyrite and subhedral pyrrhotite are found in both the 500 and 650 copper orebodies (Mathias and Clark, 1975).

The 1100 copper orebody (Fig. 40) has a strike length of 2330 m and a maximum width of 530 m. The high grade (1.7 % Cu) core is contained within fractured siliceous shale that has gradationally contact becomes more dolomitic towards the outer edge. Bands of fine grained pyrite (I) can be found inter-fingering the silica-dolomite. The footwall of the copper orebody has a large amount of coarse pyrite (II) within the graphitic shale but the high grade ore zones contain little coarse pyrite (II; Robertson, 1982). The copper orebody lies within a NNW-SSE synforms.

The northern 1900 copper orebody (Fig. 40) has a strike length of 440 m and a maximum width of 80 m and lies within a D_2 antiform and D_2 syncline. The southern section is 470 m long and 160 m wide (maximum) and lies within a D_2 synform. The southern 1900 copper orebody has similar characteristics to the 1100 orebody with Fractured Siliceous Shales that grade into Irregularly Brecciated Recrystallised Shales with Recrystallised Shale at the extremities whereas the northern section is more fault controlled. Both have grades of about 1.6 % Cu (Mathias and Clark, 1975).

The hangingwall lens copper orebody (Fig. 40) has a strike length of 700 m and a maximum width of 260 m. There is little to no pyrrhotite is found within the copper orebody. The footwall orebody has a strike length of 430 m and a width of 140 m. It is higher grade (6 % Cu) than the 1100 copper orebody and contains little fine grained pyrite (I). Course grained pyrite (II) occurs in the quartz depleted shales directly above the Paroo Fault.

The 3000 copper orebody (Fig. 40) has a strike length of 1200 m, a maximum width of 290 m and a grade of 2 % Cu. It consists of a chalcopyrite and silica-breccia core surrounded by a halo of Siliceous Shales and Recrystallised Shales with lesser Irregularly Brecciated Recrystallised Shale. In the hanging wall of the orebody there are pyritic shale layers and an increase in the fine grained pyrite (I) occurs in the southern footwall edge of the copper orebody (Shaw, 2005).

The 3500 copper orebody (Fig. 40) has a strike of 1340 m, a maximum width of 260 m and a grade of 2 % Cu. The copper orebody is located on the hinge of a D_2 fold in the Paroo Fault and has a taller, thinner shape than the other copper orebodies located on the basement contact. The copper orebody contains large amounts of remnant bedding compared to the other copper orebodies, implying it is less deformed. It is dominantly contained within the Fractured Siliceous Shale.

4. Methods

The mine mapping data base has been compiled by the mine geologists (Xstrata Copper) over 85 years. The database contains information on the orientation of bedding, cleavages, joints, folds and faults. 40 mine levels were examined and 7 were chosen (2 within the X41 Mine and 5 within the Enterprise Mine; Fig. 39) for further detailed analysis based on size and position with respect to the copper orebodies (levels with larger exposure of in the copper orebodies were preferentially selected).

The geology for these levels was examined on 1:1250 scale maps. Bedding orientations were interpreted across the drives. In some areas, such as level 29E, the degree of complexity demanded 1:300 scale maps. The four maps which showed the most detailed fold relationships were then chosen for presentation in this publication. The maps presented here are simplifications of the original maps; not all the bedding interpretations and orientations could be added to the figures due to the huge number of measurements. Instead regularly spaced orientations were chosen to represent the overall trend in bedding orientations. The copper orebodies described here are defined by a 2 % Cu grade shell.

5. Results

5.1. Level 27C RL 2055m

This is the deepest of the mine levels presented; it is within the Enterprise Mine and the 3000 and 3500 copper orebodies (Fig. 43). There are two dominant set of folds are observed within this level. The apparent first generation folds have east-west striking hinge surfaces that plunge to the north and the NW. These folds have 10’s m - 100’s m amplitudes but characteristically have open to gentle inter-limb angles (80^{o} - 170^{o}). These folds do not appear to have any direct relationship to the formation of the copper orebodies and occur within them. Smaller amplitude folds with similar orientations possibly formed at the same time and are concentrated within the stratiform 3500 orebody which has relict bedding preserved, and to the east of it. The non-stratiform 3000 orebody has less preserved bedding and folds are not observed within it possibly due to the higher degrees of brecciation of the host rocks.

The apparent second generation of folds have NNW-SSE hinge surfaces and plunge to the NNW. These folds have smaller amplitude (10’s m) and smaller inter-limb angle than the folds with east-west hinge surfaces ($<80^{o}$). They are not observed within the copper orebodies but occur in between them, dominantly on the eastern margin of the 3000 copper orebody. They have been observed to re-fold the large amplitude folds with east-west hinge surfaces and possibly wrap around the copper orebodies.

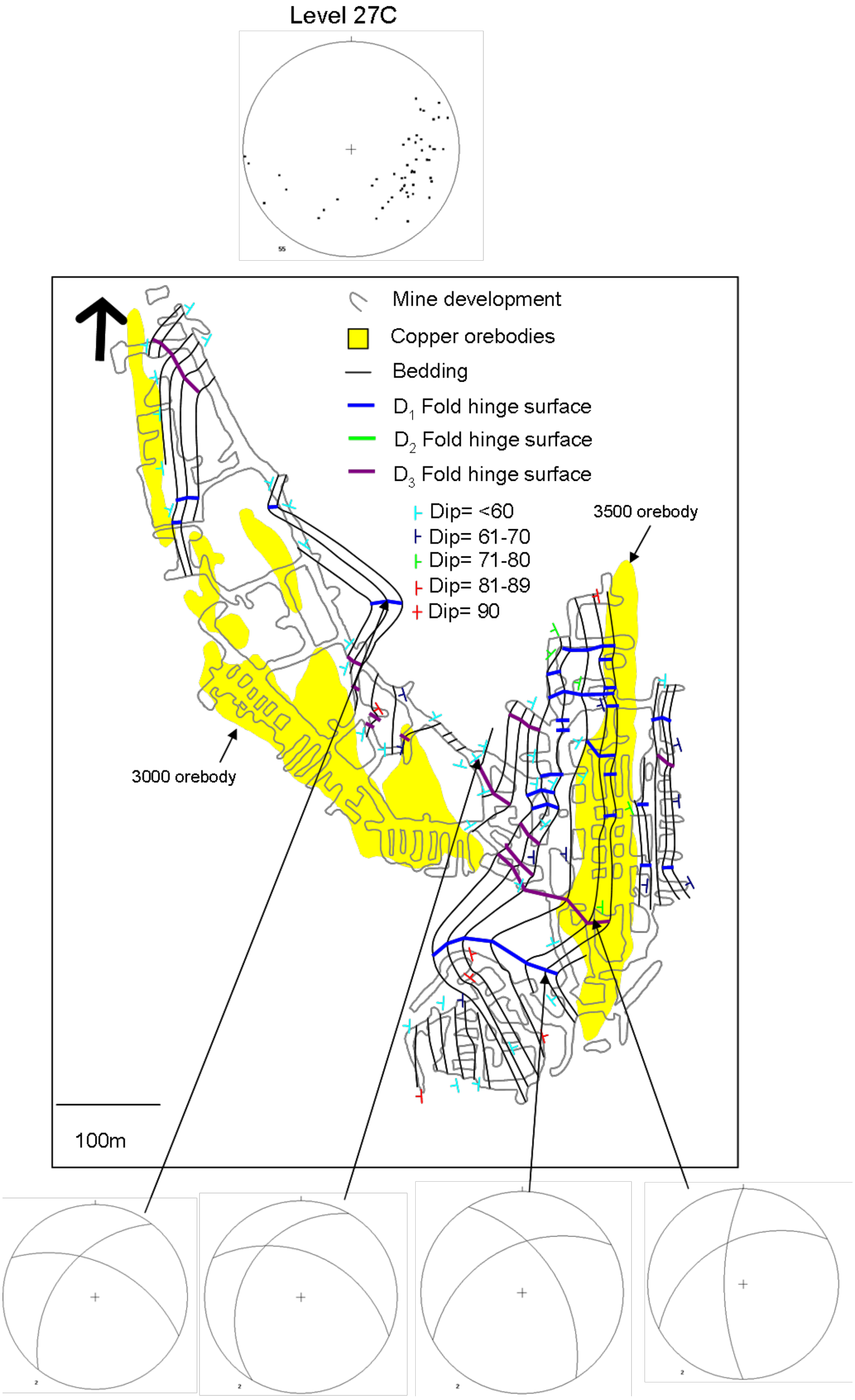

Fig. 43. Simplified geological map of mine level 27C (RL 2055m) based on the mapping done by Xstrata copper mine geologists. The 3000 and 3500 copper orebodies are show in yellow, the drives are shown as grey outlines. Bedding is shown in black lines. D_1

(west to east striking hinges) folds are observed and can be seen to predate D_3 (north northwest-south southeast striking hinges). The D_3 folds can be seen wrapping around the copper orebodies. The steroplot at the top of the figure shows the poles to planes for all the bedding orientations on this level. The lower steroplots show the orientation of two folds limbs (bedding) as planes, fold hinges are inferred at the intersection of the great circles.

5.2. Level 26B RL 2100 m

This level is also within the Enterprise Mine and contains the 3000 and 3500 copper orebodies. In this level the same two generations of folds which can be seen in the previous level (Fig. 44) are recognised. The folds with east-west hinge surfaces plunge towards the west and the folds with NNW-SSE hinge surfaces plunge towards the NW. Some smaller amplitude folds with east-west hinge surfaces are observed to the east of the 3000 copper orebody and within the 3500 orebody.

The folds with NNW-SSE hinge surfaces are not observed to refold the folds with east-west hinge surfaces on this level, but appear to wrap around the copper orebodies. In the southern end of the 3000 copper orebodies there is a small v-shaped gap in the copper orebody (labelled iin Fig. 44). A fold with a NNW-SSE hinge surfaces is formed in this gap.

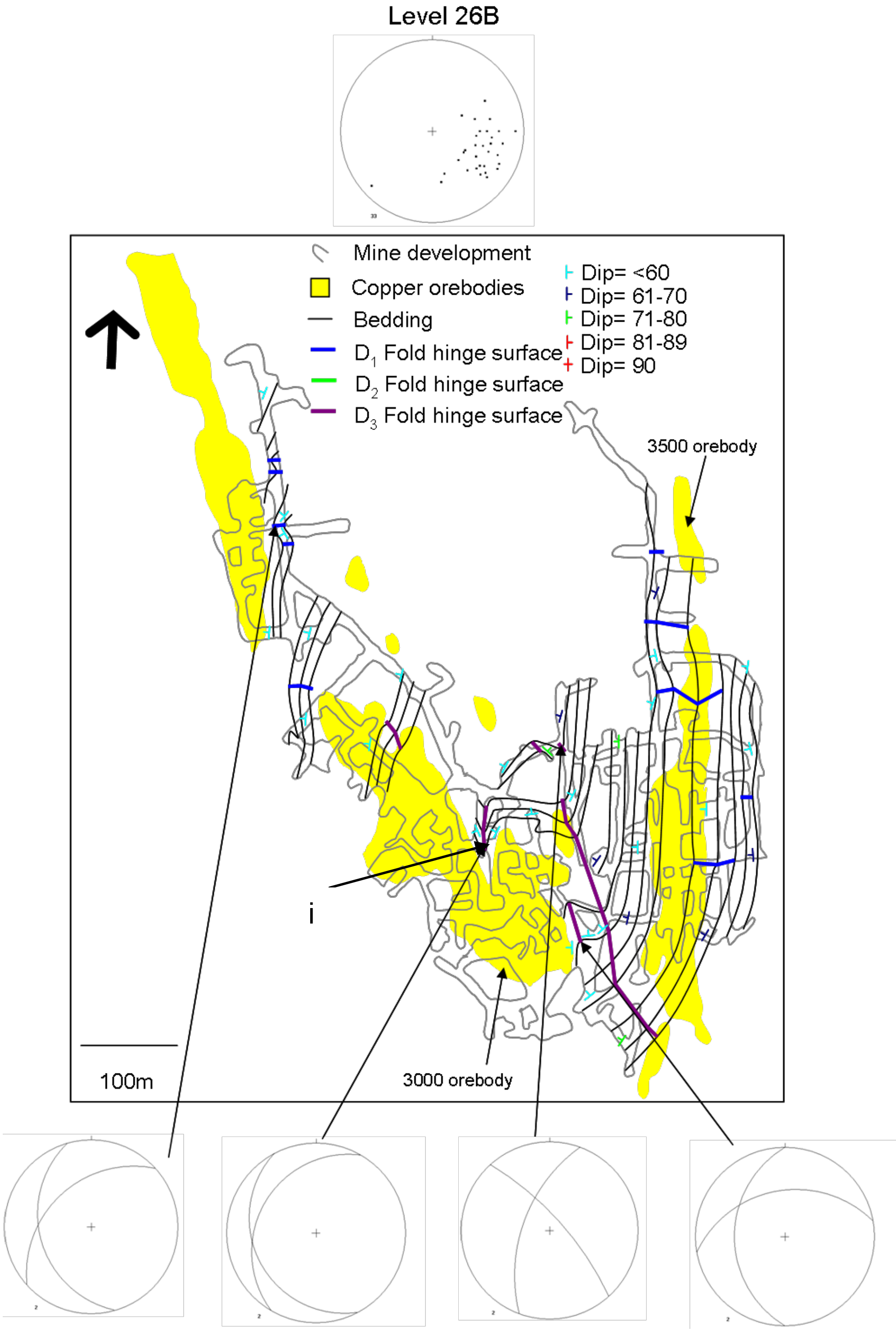

Fig. 44. Simplified geological map of mine level 26B (RL 2100 m) based on the mapping done by Xstrata copper mine geologists. The 3000 and 3500 copper orebodies are show in yellow, the drives are shown as grey outlines. Bedding is shown in black lines and is well preserved within the 3500 orebody. The D_3 folds can be seen wrapping around the copper orebodies. The steroplot at the top of the figure shows the poles to planes for all the bedding orientations on this level. The lower steroplots show the orientation of two

folds limbs (bedding) as planes, fold hinges are inferred at the intersection of the great circles.

5.3. Level 25A RL 2160 m

This level is also within the Enterprise Mine. It lies at the top of the 3000 and 3500 orebodies (Fig. 45). This is one of the largest levels within the mine and contains more information than the two previous levels. Two areas have been enlarged so that the detailed fold relationships can be observed (Fig. 46). Three orientations of fold hinge surfaces are observed within this level; east-west, NNW-SSE and north-south. The folds with east-west hinge surfaces plunge towards the northwest and northeast, the folds with NNW-SSE hinge surfaces plunge towards the NW and the folds with north-south hinge surfaces plunge towards the south.

The smaller amplitude folds with east-west hinge surfaces are, as with the previous two levels, located within the 3500 copper orebody. Unlike the previous two levels no larger amplitude folds with east-west hinge surfaces are observed between the copper orebodies. The larger amplitude folds with east-west hinge surfaces are observed to the west and NW of the 3000 copper orebody. These folds appear to have been re-folded, enlarged in Fig. 46. The folds with NNW-SSE hinge surfaces are located between, and to the northwest, of the copper orebodies where they appear to re-fold the folds with east-west hinge surfaces. The folds with NNW-SSE hinge surfaces again appear to wrap around the copper orebodies, in some cases mimicking the shape of the 3000 copper orebody (Fig. 45). The third group of folds based on hinge surfaces orientations (north-south) can only be observed in two locations, one of which is enlarged (Fig. 46). Based on the location, orientation and rarity of these folds it is not clear as whether they represent a different generation of fold or are just the result of the interaction between the two other fold generations and the copper orebodies.

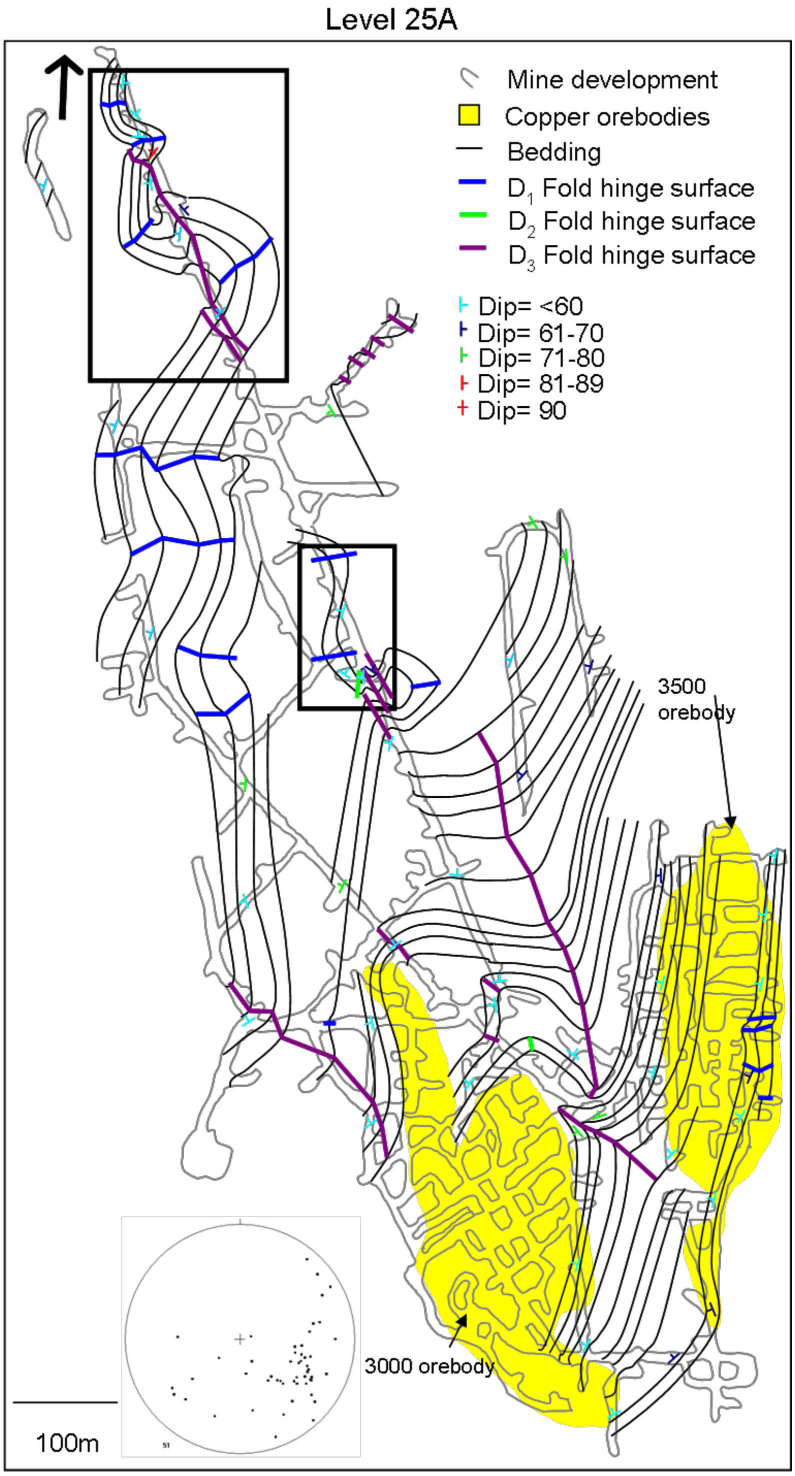

Fig. 45. Simplified geological map of mine level 25A (RL 2160 m) based on the mapping done by Xstrata copper mine geologists. The 3000 and 3500 copper orebodies are show in yellow, the drives are shown as grey outlines. Bedding is shown in black lines. D_1 (west to east orientated hinges) folds are observed and can be seen to predate D_3 (north northwest-south southeast orientated hinges). Some D_3 folds wrap around the copper

orebodies and refold the D_1 folds. The steroplot at the botttom of the figure shows the poles to planes for all the bedding orientations on this level.

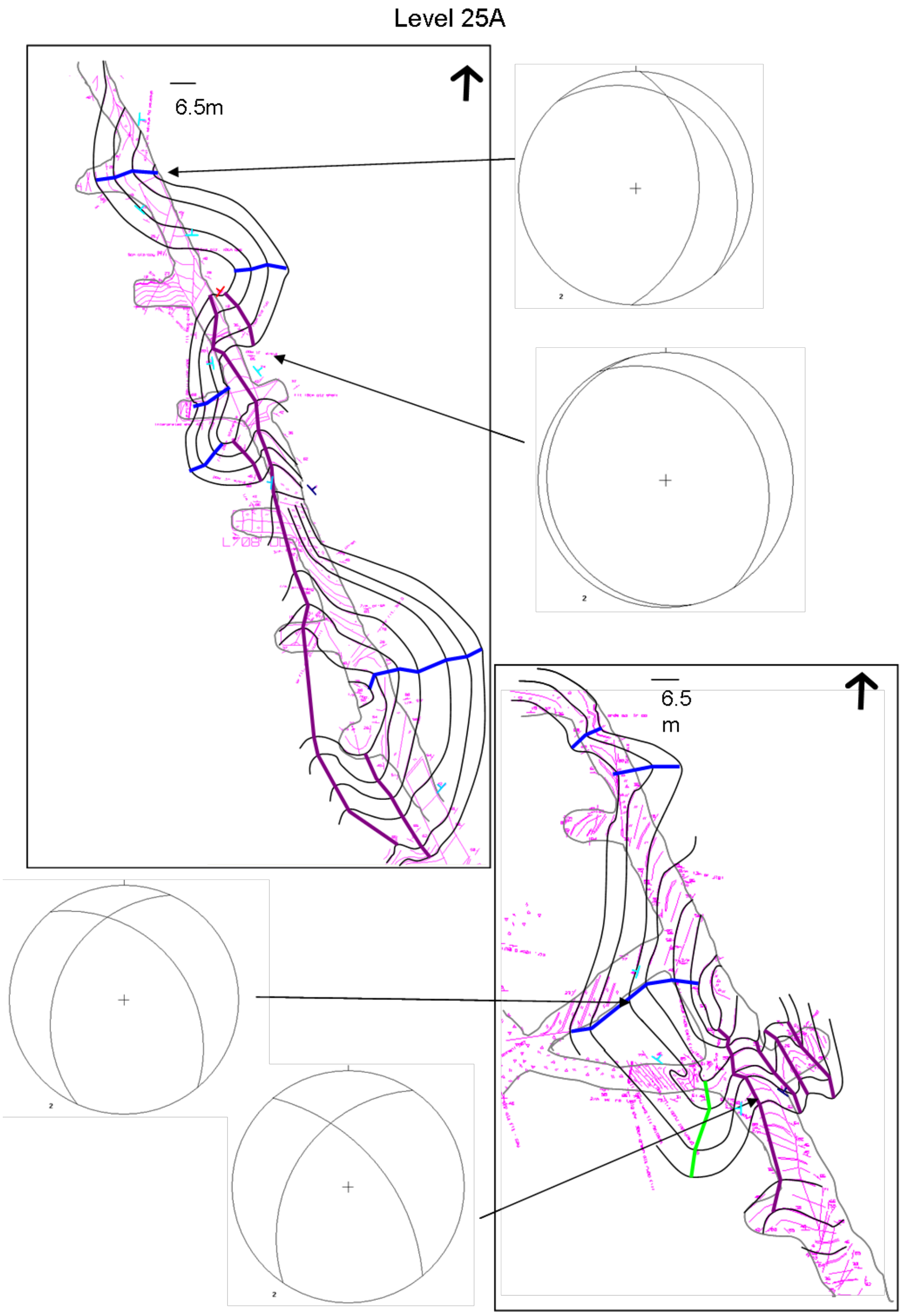

Fig. 46. Detail of simplified geological map of mine level 25A (RL 2160 m; Fig. 45) drives are shown as grey outlines. The mapping is shown in purple and the bedding is shown in black lines. D_1 (west to east orientated hinges) folds are observed and are folded by D_3

(north northwest-south southeast orientated hinges) folds. A) is located to the north of Fig. 45; B) is located to the south of Fig. 45. The four steroplots show the orientation of two folds limbs (bedding) as planes, fold hinges are inferred at the intersection of the great circles.

5.4. Level 17D RL 2649 m

This level is within the X41 Mine and contains the northern end of the 1100 copper orebody (Fig. 47). Within this copper orebody only one small amplitude fold with an east-west hinge surfaces is observed on this level. Larger amplitude folds with east-west hinge surfaces are located to the east and west of the 1100 copper orebody. The folds with east-west hinge surfaces appear to have been re-folded by folds with NNW-SSE hinge surfaces which appear to wrap around the 1100 copper orebody. Folds with NNW-SSE hinge surfaces are west plunging. In the NE section of the level a single fold with a north-south orientated hinge is observed plunging to the west.

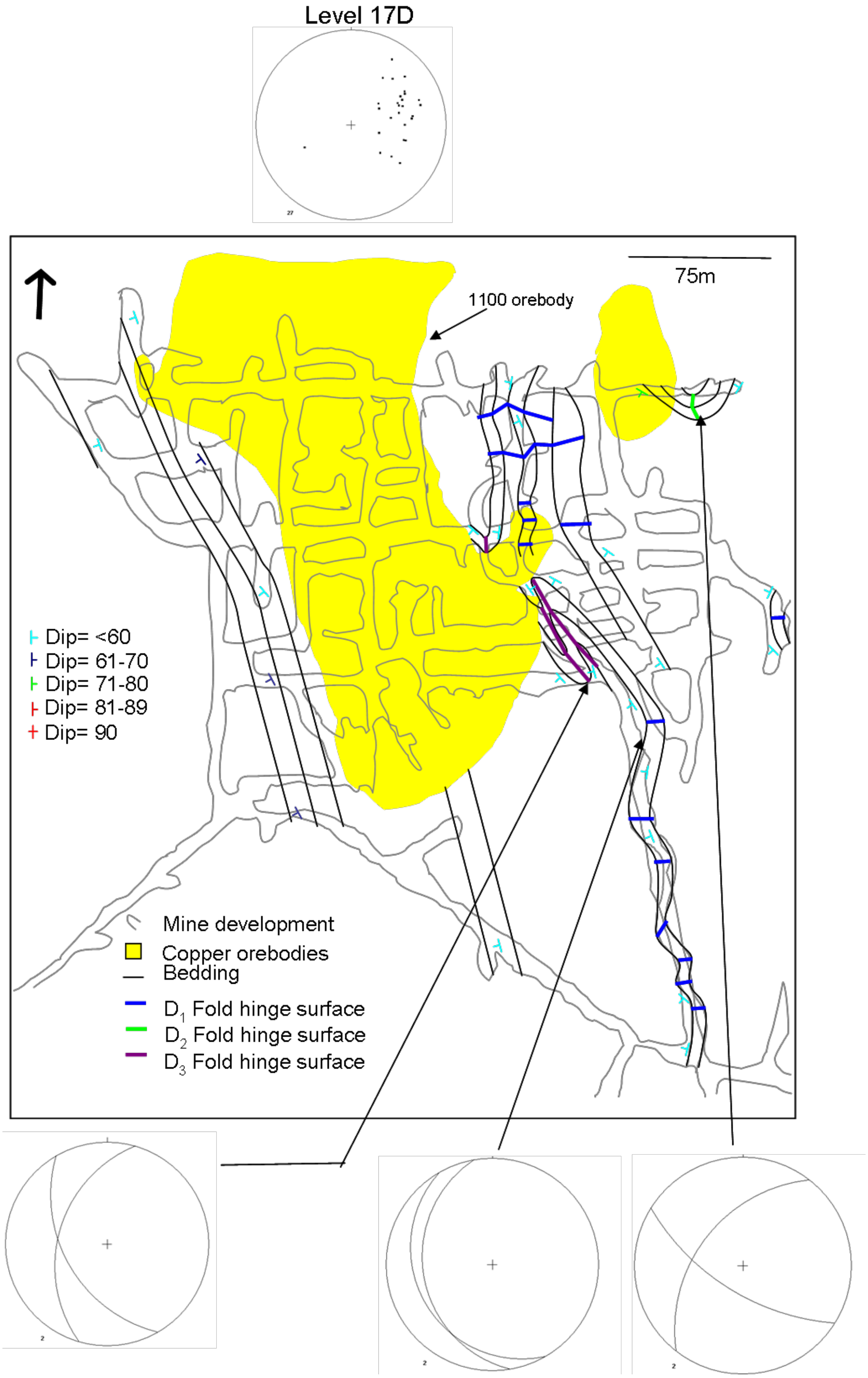

Fig. 47. Simplified geological map of mine level 17D (RL 2649 m) based on the mapping done by Xstrata copper mine geologists. The 1100 copper orebody is show in yellow, the drives are shown as grey outlines. Bedding is shown in black lines. D_1 (west to east

orientated hinges) folds are folded by D_3 (north northwest-south southeast orientated hinges) folds.

6. Discussion

The discussion is presented in two parts; the first is a discussion of the results from the re-examination of the mapping database. The second part examines the observations of previous authors and re-interprets their significance in light of the new results presented here.

6.1. D_2 formation of the Mount Isa copper orebodies

Despite there being obvious differences in the copper orebodies geometries, the copper orebodies have largely been considered to have formed in a single deformation event (D_3) with the variation in geometries reflecting formation mechanisms (Stanton, 1963; Dunnet, 1976; Finlow-Bates and Stumpfl, 1979; Robertson, 1982; Gulson *et al.,* 1983; Swager, 1983; 1985; Perkins, 1984; Bell *et al.,* 1988; McGoldrick and Keays, 1990; Davis, 2004; Miller, 2007). This paper proposes that the stratiform and the non-stratiform copper orebodies are synchronous but have undergone different degrees of deformation subsequent to their formation resulting in their contrasting orientations. Based on the macroscale orientation of the Urquhart Shales relative to the copper orebodies a new timing for copper mineralisation during D_2 is proposed. The suggestive evidence from geometrical features is more difficult to re-interpret to suit another model for the timing of copper orebody formation, the evidence that of previous authors.

The variable orientation of the folds with east-west orientated hinge surfaces is consistent with re-orientation during later deformation, possibly suggesting they would have formed early, perhaps during D_1. Their presence within the 3500 and 1100 copper orebodies and outside the copper orebodies may suggest that they formed prior to copper mineralisation but had no control on the copper distribution. The apparent refolding of the D_1 folds by the folds with NNW-SSE hinge surfaces indicates that the folds with NNW-SSE hinge surfaces formed after the D_1 folds. The folds with NNW-SSE hinge surfaces have an orientation consistent with the observations of Swager (1983) perhaps suggesting they formed in D_3. These folds appear to wrap around the copper orebodies and could indicate that the copper mineralisation formed before D_3. It is unclear whether the few folds with north-south hinge surfaces were formed during $D_{2,}$ which produced the folds with north-south hinge surfaces in the Paroo Fault, or whether they represent local distortion of D_3 folds by the copper orebodies.

D_1 folds have not previously been recognised from the copper deposit or the lead-zinc silver deposits at this scale. Perkins (1997) recognized very small (1-200 mm) folds within the lead-zinc-silver deposits he classified as $D_{1,}$ but based on their orientation, these are more likely to be D_2 folds. The D_1 folds appear to have no relationship with the copper orebodies. If the copper orebodies formed during D_1, some relationship with D_1 folds would be expected. If the D_1 folds formed after copper mineralisation, they might wrap around the copper orebodies as the D_3 folds do. The D_1 folds could have formed prior to copper mineralisation. D_3 folds appear to wrap around the edges of the 3000 and 1100 copper orebodies and would therefore postdate it (Figs. 43, 44, 45, 46, 47 48E). In the 3500 copper orebody the bedding is north-south and has not been obviously deformed by D_2 or D_3 folds. The 3500 copper orebody is stratiform and has a north-south orientation unlike the non-stratiform 3000 and 1100 copper orebodies. This could possibly indicate that the non-stratiform copper orebodies have undergone remobilisation and possibly re-orientation of D_2 folds where as the stratiform copper orebodies have not (Figs. 48C and D).

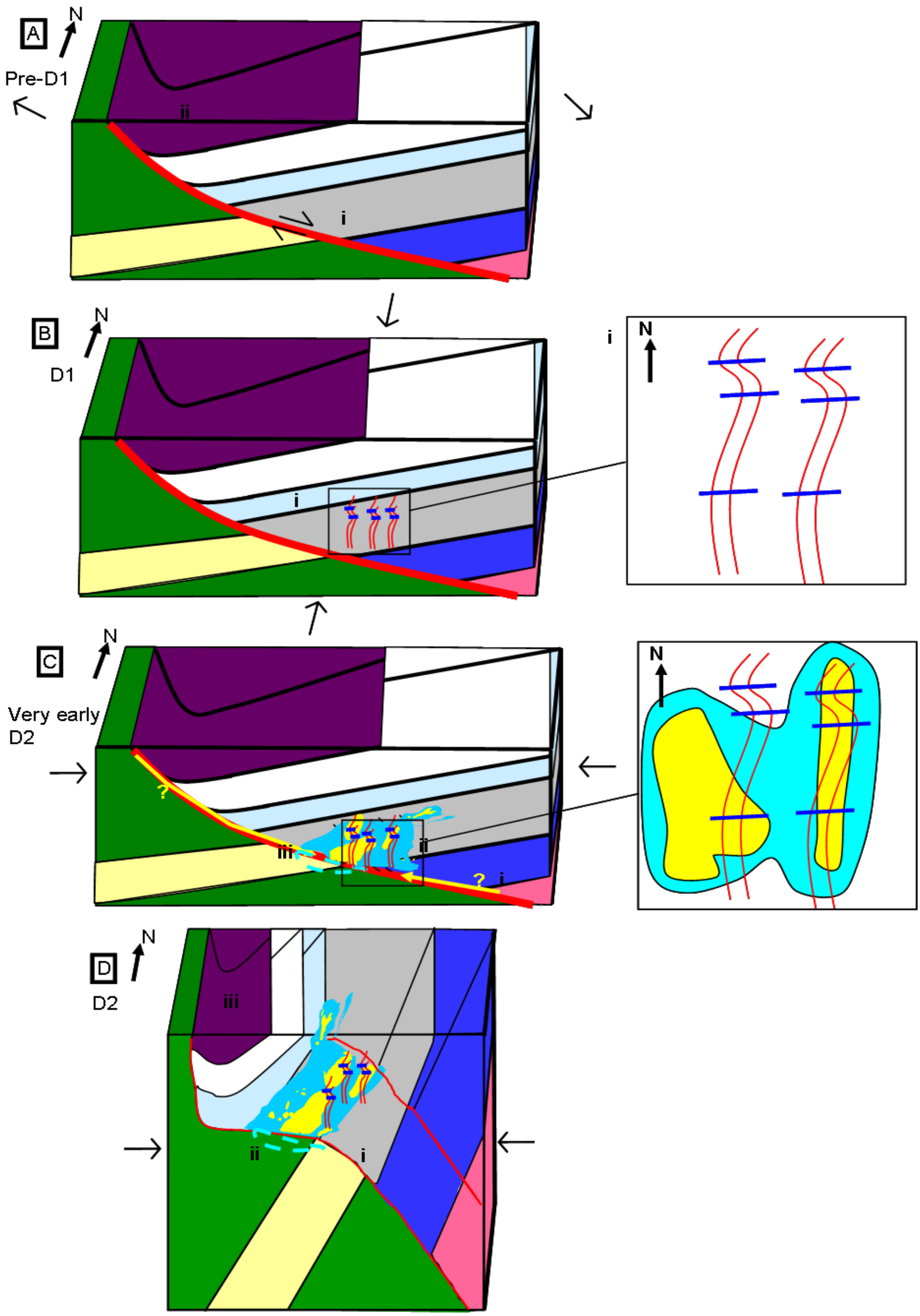
A
N
Pre-D1
ii
i
B
N
D1
i
i
N
C
N
Very early
D2
?
iii
ii
?
i
N
D
N
D2
iii
ii
i

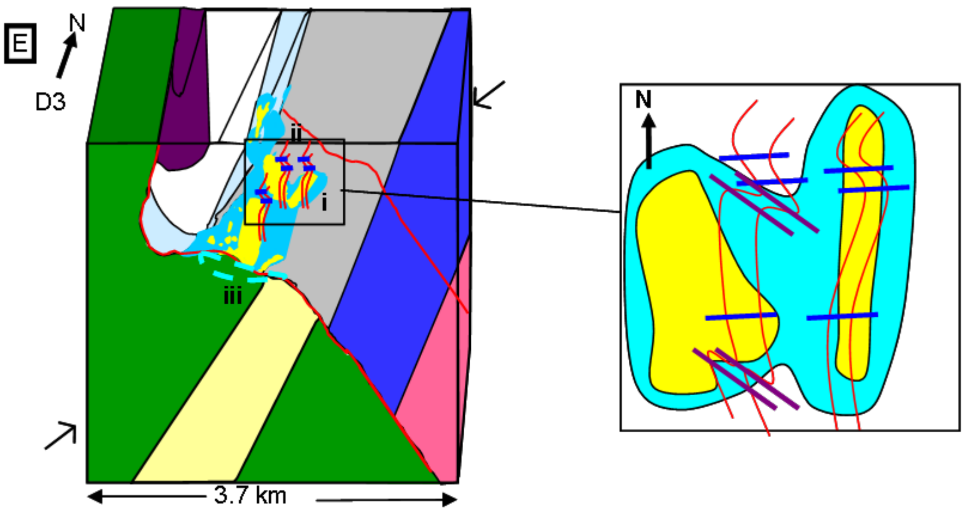

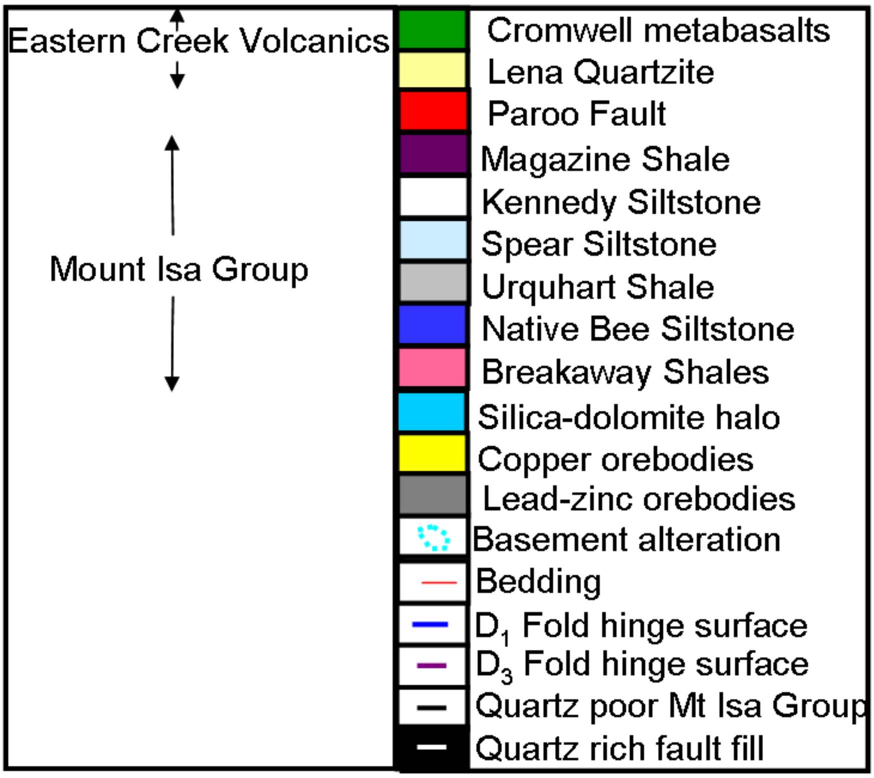

Fig. 48. Cartoon showing the evolution of the Paroo Fault and Mount Isa copper orebodies; Ai) Pre-D_1 normal movement on a listric graben fault, Aii) during the deposition of the Magazine Shales and Kennedy Siltstone; Bi) north-south shortening causes the east-west striking folds in the Urquhart Shales; Ci) Copper bearing fluid/enter via the Paroo Fault from above and or below, Cii) Forming the silica-dolomite halo and copper orebodies, Ciii) the same fluids cause alteration in the basement rocks; Di) The synsedimentary folds tightened by D_2 deformation; Ei) D_3 folds deform D_1 folds, Eii) D_3

folds wrap around the copper orebodies, Eiii) Paroo fault deforms against the copper orebodies and the fault fill is sheared into its present position.

The geometric evidence presented here is insightful but requires that the observations of previous authors be analysed and reinterpreted for a conclusive model for the D_2 formation of the copper orebodies to be generated.

6.2. Syngenetic deposition of the Mount Isa copper orebodies

Stanton (1963) uses the similarity in the element composition distributions between the lead-zinc-silver orebodies and the perched 500 and 650 copper orebodies. This work does not involve any of the copper orebodies found adjacent to the Paroo Fault, due to limited exposure at the time and interpretations about all of the copper orebodies cannot be drawn from his study. It is possible that the perched 500 and 650 copper orebodies have a different formation mechanism to the copper orebodies that lie adjacent to the Paroo Fault that may involve the replacement of pre-existing sulphides. This could result in similar element composition distributions variations between the perched copper orebodies and the lead-zinc-silver orebodies.

McGoldrick and Keays (1990) compared the 1100 copper orebody to the lead-zinc-silver orebodies and argued that this fluid would have to have been cool (<200 ^{o}C) and low in S for both the copper and the lead-zinc-silver ore-bearing fluids implying that the two deposits had the same source. Compared to large quantity of evidence in the form of sulphur isotopes provided by Andrew *et al.* (1989) and Heinrich *et al.* (1989), fluid inclusion systematics provided by Heinrich and Cousens (1989), Heinrich *et al.* (1989; 1993) and Kendrick *et al.* (2006), and the alteration assemblages within the Eastern Creek Volcanics (Heinrich *et al.*, 1989; 1993; 1995), which demonstrate that multiple fluids were involved in the formation of the copper orebodies, McGoldrick and Keays (1990) evidence is insubstantial. The heavy sulphur isotope vales from the lead-zinc-silver and copper deposits are interpreted to indicate a common source for the lead-zinc-silver and copper deposits (McGoldrick and Keays, 1990). However this does not indicate a common source for the two deposits, but only that the sources produced similar sulphur isotope values in the orebodies. McGoldrick and Keays's (1990) also state that there is a lack of obvious conduits for hydrothermal fluid to form the copper orebodies; but the Paroo Fault is an obvious conduit for fluids. The permissive arguments that try to explain the apparent epigenetic texture of the copper orebodies create complex explanations when the simple explanation that the copper orebodies are epigenetic is the logical conclusion.

6.3. Early D_3 formation of the Mount Isa copper orebodies

The dominant evidence for D_3 copper mineralisation was provided by Swager (1983; 1985) and Perkins (1984). S_3 cleavage in clasts within the breccia and the absence of S_3 cleavage within silica-chalcopyrite matrix is described as evidence of D_3 copper mineralisation. The main problem with this interpretation is that the evidence does not preclude that the chalcopyrite was formed earlier and re-mobilized by a further stage of brecciation (D_3). Another line of evidence used by Swager (1985) to support an early D_3 formation of the copper orebodies is that the strain free polygonal quartz surrounding the chalcopyrite indicates that the chalcopyrite has not been deformed. Swager (1985) states that re-crystalisation of chalcopyrite bearing veins has not occurred because there is a similar optical orientations in inclusion free zones in dolomite and quartz prisms surrounding inclusion rich grains. Cathodoluminescence presented in Paper 2 has demonstrated that this is not the case and that these veins contain multiple generations of quartz which could have formed strain free quartz within the veins after D_3 even if the veins were formed earlier.

The S_3 cleavage development against the margins of copper bearing breccias and the crosscutting subhorizontal extension veins which formed during D_3 (Bell *et al.,* 1988) is equally indicative of a pre-D_3 origin of the copper orebodies as it is of a D_3 origin. The NNW-SSE orientation of the silica-dolomite halo which matches the proposed shortening direction for the D_3 event was proposed by Bell *et al.* (1988) to be evidence of its D_3 formation. However the silica-dolomite halo could simply have formed during D_2 and been deformed into its current orientation during D_3. The maps generated here demonstrate that contrary to the evidence of Perkins (1984), Bell *et al.* (1988) and Davis (2004), the 1100, 3000 and 3500 copper orebodies are not contained within D_3 folds in the Urquhart Shale. Rather the D_3 folds wrap around the copper orebodies. During the course of their work Perkins (1984); Swager (1985) had limited exposures available to them and were restricted to outcrops of the 1100 copper orebody. In the course of this study the 1100, 3000 and 3500 copper orebodies were all examined. The mechanisms of copper formation during D_3 have been extensively described by Heinrich *et al.* (1989; 1993; 1995). The new pre to early D_2 timing for the formation of the copper orebodies would still be compatible with the mechanism of copper formation proposed by Heinrich *et al.* (1989; 1993; 1995).

6.4. Late D_3 formation of the Mount Isa copper orebodies

There is a potential problem with the evidence used for late D_3 ages for copper formation (Miller, 2007). The Paroo Fault has been shown by Paper 1 to have been re-activated multiple times and therefore σ_2 is not necessarily within the plane of the Paroo Fault. An extensional fracture on the Paroo Fault could form at angles between 0^o and 90^o with the maximum resolved shear stress (Blenkinsop, 2008). It is likely that these extension veins represent localized D_3 re-mobilization of pre-existing copper.

7. Conclusion

The increase in exposure created by recent mining at Mt isa copper mine has provided a larger data base than was available to previous authors. Through the detailed examination of the mapping data a new timing for the formation of copper mineralisation has been established. Early macroscopic folds with east-west hinge surfaces (D_1) that predate the copper mineralisation have been described for the first time within the copper deposit. Folds with NNW-SSE hinge surfaces (D_3) have re-folded the D_1 folds in the vicinity of the copper orebodies. The D_3 folds wrap around the copper orebodies providing a clear indication that the copper orebodies formed before D_3 folding. The copper orebodies must have developed between D_1 and D_3 and probably during D_2. Therefore other faults within the Western Fold Belt folded during D_2 may contain significant copper mineralisation. The observations of D_3 folds wrapping around the copper orebodies can not easily be explained by a D_3 timing for copper ore genesis. The evidence provided by previous authors for the D_3 to late D_3 timing for the copper orebodies can be explained by the re-mobilisation of a pre-existing copper orebody. This model resolves the long-established controversy surrounding the timing of the formation Mount Isa copper deposit and demonstrates that the re-examination of evidence can be critical in geological research.

8. Acknowledgements

Thanks to Xstrata Copper for providing logistical support partly funded through the Xstrata Community Partnership Program, North Queensland. We thank the entire mine and exploration geology staff for all their help.

9. References

Andrew, A. S., Heinrich, C. A., Wilkins, R. W. T. & Patterson, D. J. 1989. Sulfur isotope systematics of copper ore formation at Mount Isa, Australia. Economic Geology and the Bulletin of the Society of Economic Geologists, **84**, 1614-1626.

Bell, T. H. 1983. Thrusting and duplex formation at Mount Isa. Nature, **304**, 493-497.

Bell, T. H. & Hickey, K. A. 1998. Multiple Deformations with Successive Subvertical and Subhorizontal Axial Planes in the Mount Isa Region: Their Impact on Geometric Development and Significance for Mineralization and Exploration. Economic Geology, **93**, 1369-1389.

Bell, T. H., Perkins, W. G. & Swager, C. P. 1988. Structural controls on development and localization of syntectonic copper mineralization at Mount Isa, Queensland. Economic Geology and the Bulletin of the Society of Economic Geologists, **83**, 69-85.

. Betts, P. G., 2001, Three-dimensional structure along the inverted Palaeoproterozoic Fiery Creek fault system, Mount Isa Terrane, Australia: Journal of Structural Geology, **23**, p. 1953-1969.

Betts, P. G. 1999. Palaeoproterozoic mid-basin inversion in the northern Mt. Isa terrane, Queensland. Australian Journal of Earth Sciences, **46**, 735-748.

Betts, P. G., Giles, D. & Lister, G. S. 2003. Tectonic environment of shale-hosted massive sulfide Pb-Zn-Ag deposits of Proterozoic northeastern Australia. Economic Geology and the Bulletin of the Society of Economic Geologists, **98**, 557-576.

Betts, P. G., Giles, D., Mark, G., Lister, G. S., Goleby, B. R., and Aillères, L., 2006, Synthesis of the proterozoic evolution of the Mt Isa Inlier: Australian Journal of Earth Sciences, **53**, 187-211.

Betts, P. G., and Lister, G. S., 2001, Comparison of the 'strike-slip' versus the 'episodic rift -sag' models for the origin of the Isa Superbasin: Australian Journal of Earth Sciences, **48**, 265-280.

Betts, P. G. & Lister, G. S. 2002. Geodynamically indicated targetting strategy for shale-hosted massive sulfide Pb-Zn-Ag mineralisation in the Western Fold Belt, Mt Isa terrane. Australian Journal of Earth Sciences, **49**, 985-1010.

Betts, P. G., Lister, G. S. & O'Dea, M. G. 1998. Asymmetric extension of the middle Proterozoic lithosphere, Mount Isa Terrane, Queensland, Australia. Tectonophysics, **296**, 293-316.

Betts, P. G., Lister, G. S., and Pound, K. S., 1999, Architecture of a Palaeoproterozoic rift system; evidence from the Fiery Creek Dome region, Mt. Isa Terrane: Australian Journal of Earth Sciences, **46**, 533-554.

Blanchard, R. & Hall, G. 1937. Mount Isa [Queensland] ore deposition. Economic Geology and the Bulletin of the Society of Economic Geologists, **32**, 1042-1057.

Blenkinsop, T. G. 2008. Relationships between faults, extension fractures and veins, and stress. Journal of Structural Geology, **30**, 622-632.

Brems, D., Muchez, P., Sikazwe, O. & Mukumba, W. 2009. Metallogenesis of the Nkana copper-cobalt South Orebody, Zambia. Journal of African Earth Sciences, **55**, 185-196.

Connors, K. A., Proffett, J. M., Lister, G. S., Scott, R. J., Oliver, N. H. S. & Young, D. J. 1992. Geology of the Mount Novit Ranges, southwest of Mt Isa mine. In: Detailed Studies of the Mt Isa Inlier (edited by Stewart, A. J. & Blake, D. H.). Australian Geological Survey Organisation, Canberra, **243**, 137-160.

Davis, T. P. 2004. Mine-scale structural controls on the Mount Isa Zn-Pb-Ag and Cu orebodies. Economic Geology and the Bulletin of the Society of Economic Geologists, **99**, 543-559.

Derrick, G. M. 1982. A Proterozoic rift zone at Mount Isa, Queensland, and implications for mineralisation. BMR Journal of Australian Geology and Geophysics, **7**, 81-92.

Dunnet, D. 1976. Mt Isa; reconstruction of a faulted ore body. Philosophical Transactions of the Royal Society of London, Series A: Mathematical and Physical Sciences, **283**, 333-344.

Farquharson, R. B. & Richards, J. R. 1974. U-Th-Pb isotope systematics related to igneous rocks and ore Pb, Mount Isa, Queensland. Mineralium Deposita, **9**, 339-356.

Finlow-Bates, T. 1979. Cyclicity in the lead-zinc-silver-bearing sediments at Mount Isa mine, Queensland, Australia, and rates of sulfide accumulation. Economic Geology and the Bulletin of the Society of Economic Geologists, **74**, 1408-1419.

Finlow-Bates, T. 1980. Cyclicity in the lead-zinc-silver-bearing sediments at Mount Isa Mine, Queensland, Australia, and rates of sulfide accumulation; reply. Economic Geology and the Bulletin of the Society of Economic Geologists, **75**, 8.

Finlow-Bates, T. & Stumpfl, E. F. 1979. The copper and lead-zinc-silver orebodies of Mt. Isa Mine, Queensland; products of one hydrothermal system. Annales de la Societe Geologique de Belgique, **102**, 497-517.

Gessner, K. 2009. Coupled Models of Brittle-plastic Deformation and Fluid Flow: Approaches, Methods, and Application to Mesoproterozoic Mineralisation at Mount Isa, Australia. Surveys in Geophysics, **30**, 211-232.

Gessner, K., Jones, P. A., Wilde, A. R. & Kühn, M. 2006. Significance of strain localization and fracturing in relation to hydrothermal mineralization at Mount Isa, Australia. Journal of Geochemical Exploration, **89**, 129-132.

Gibson, G. M. & Henson, P. A. 2005. Chapter 6: Post-depositional deformation in the Western Succession. In: Project I1: 3D Basin Architecture & Mineral Systems in the Mt Isa Western Succession (edited by Gibson, G. M. & Hitchman, A. P.). Predictive Mineral Discovery Cooperative Research Centre, Canberra, 147 - 176.

Gulson, B. L., Perkins, W. G. & Mizon, K. J. 1983. Lead isotope studies bearing on the genesis of copper orebodies at Mount Isa, Queensland. Economic

Geology and the Bulletin of the Society of Economic Geologists, **78**, 1466-1504.

Hannan, K. W., Golding, S. D., Herbert, H. K. & Krouse, H. R. 1993. Contrasting alteration assemblages in metabasites from Mount Isa, Queensland; implications for copper ore genesis. Economic Geology and the Bulletin of the Society of Economic Geologists, **88**, 1135-1175.

Heinrich, C. A., Andrew, A. S., Wilkins, R. W. T. & Patterson, D. J. 1989. A fluid inclusion and stable isotope study of synmetamorphic copper ore formation at Mount Isa, Australia. Economic Geology and the Bulletin of the Society of Economic Geologists, **84**, 529-550.

Heinrich, C. A., Bain, J. H. C., Mernagh, T. P., Wyborn, L. A. I., Andrew, A. S., and Waring, C. L., 1995, Fluid and mass transfer during metabasalt alteration and copper mineralization at Mount Isa, Australia. Economic Geology and the Bulletin of the Society of Economic Geologists, **90**, 705-730.

Heinrich, C. A., Bain, J. H. C., Fardy, J. J. & Waring, C. L. 1993. Br/Cl geochemistry of hydrothermal brines associated with Proterozoic metasediment-hosted copper mineralization at Mount Isa, northern Australia. Geochimica et Cosmochimica Acta, **57**, 2991-3000.

Heinrich, C. A. & Cousens, D. R. 1989. Semi-quantitative electron microprobe analysis of fluid inclusion salts from the Mount Isa copper deposit (Queensland, Australia). Geochimica et Cosmochimica Acta, **53**, 21-28.

Kendrick, M. A., Duncan, R. & Phillips, D. 2006. Noble gas and halogen constraints on mineralizing fluids of metamorphic versus surficial origin: Mt Isa, Australia. Chemical Geology, **235**, 325-351.

Kühn, M., Dobert, F. & Gessner, K. 2006. Numerical investigation of the effect of heterogeneous permeability distributions on free convection in the hydrothermal system at Mount Isa, Australia. Earth and Planetary Science Letters, **244**, 655-671.

Kühn, M. & Gessner, K. 2006. Reactive transport model of silicification at the Mount Isa copper deposit, Australia. Journal of Geochemical Exploration, **89**, 195-198.

Kühn, M. & Gessner, K. 2009. Testing Hypotheses for the Mount Isa Copper Mineralisation with Numerical Simulations. Surveys in Geophysics, **30**, 253-268.

Lister, G. S. 1993. The role of thrusting in the structural development of the Mount Isa Mine and its relevance to exploration in the surrounding region; discussion. Economic Geology and the Bulletin of the Society of Economic Geologists, **88**, 479.

Love, L. G. & Zimmerman, D. O. 1961. Bedded pyrite and micro-organisms from the Mount Isa shale. Economic Geology and the Bulletin of the Society of Economic Geologists, **56**, 873-896.

Lowell, J. D. 1968. Geology of the Kalamazoo orebody, San Manuel District, Arizona. Economic Geology, **63**, 645-654.

MacCready, T. 2006. Structural evolution of the southern Mt Isa Valley. Australian Journal of Earth Sciences, **53**, 27-40.

Mathias, B. V. & Clark, G. J. 1975. Mount Isa copper and silver-lead-zinc orebodies; Isa and Hilton mines. Monograph Series - Australasian Institute of Mining and Metallurgy, **5**, 351-371.

McDonald, J. A. 1970. Some effects of deformation on sulfide-rich layers in lead-zinc ore bodies, Mount Isa, Queensland. Economic Geology and the Bulletin of the Society of Economic Geologists, **65**, 273-298.

McDonald, J. A. & Williams, N. 1980. Cyclicity in the lead-zinc-silver-bearing sediments at Mount Isa Mine, Queensland, Australia, and rates of sulfide accumulation; discussion. Economic Geology and the Bulletin of the Society of Economic Geologists, **75**, 8.

McGoldrick, P. J. & Keays, R. R. 1990. Mount Isa copper and lead-zinc-silver ores; coincidence or cogenesis? Economic Geology and the Bulletin of the Society of Economic Geologists, **85**, 641-650.

Miller, J. M. 2007. Structural controls on the Mt Isa Copper deposit, QLD. In: Project I7. Predictive Mineral Discovery CoOperative Research Centre.

Miller, J. M., Dugdale, L. J. & Wilson, C. J. L. 2001. Variable hangingwall palaeotransport during Silurian and Devonian thrusting in the western Lachlan Fold Belt: missing gold lodes, synchronous Melbourne Trough sedimentation and Grampians Group fold interference. Australian Journal of Earth Sciences: An International Geoscience Journal of the Geological Society of Australia, **48**, 901 - 909.

Miller, J. M. & Wilson, C. J. L. 2004. Structural analysis of faults related to a heterogeneous stress history: reconstruction of a dismembered gold deposit, Stawell, western Lachlan Fold Belt, Australia. Journal of Structural Geology, **26**, 1231-1256.

Mote, T. I., Brimhall, G. H., Tidy-Finch, E., Muller, G. & Carrasco, P. 2001. Application of Mass-Balance Modeling of Sources, Pathways, and Sinks of Supergene Enrichment to Exploration and Discovery of the Quebrada

Turquesa Exotic Copper Orebody, El Salvador District, Chile. Economic Geology, **96**, 367-386.

Nijman, W., Mijnlieff, H. F. & Schalkwijk, G. 1992a. The Hero Fan Delta (Lower Mount Isa Group) and its structural control: deformation in the Hero/Western Fault Zone and Paroo Range compared, Proterozoic, Mount Isa Inlier, Queensland, Australia. In: Detailed Studies of the Mount Isa Inlier (edited by Stewart, A. J. & Blake, D. H.). Australian Geological Survey Organisation, Canberra, **243**, 75-110.

Nijman, W., van Lochem, J. H., Spliethoff, H. & Feijth, J. 1992b. Deformation model and sedimentation patterns of the Proterozoic of the Paroo Range, Mount Isa Inlier, Queensland, Australia. In: Detailed Studies of the Mount Isa Inlier (edited by Stewart, A. J. & Blake, D. H.) Australian Geological Survey Organisation Bulletin **243.**

O'Dea, M. G., Lister, G., MacCready, T., Betts, P. G., Oliver, N. H. S., Pound, K. S., Huang, W. & Valenta, R. K. 1996. Geodynamic evolution of the Proterozoic Mount Isa terrain. Orogeny through time, **121**, 99-122.

O'Dea, M. G., Lister, G. S., Betts, P. G. & Pound, K. S. 1997. A shortened intraplate rift system in the Proterozoic Mount Isa terrane, NW Queensland, Australia. Tectonics, **16**, 425-441

Page, R. W., Jackson, M. J. & Krassay, A. A. 2000. Constraining sequence stratigraphy in North Australian basins; SHRIMP U-Pb zircon geochronology between Mt Isa and McArthur River. Australian Journal of Earth Sciences, **47**, 431-459.

Page, R. W., Stevens, B. P. J. & Gibson, G. M. 2005. Geochronology of the Sequence Hosting the Broken Hill Pb-Zn-Ag Orebody, Australia. Economic Geology, **100**, 633-661.

Perkins, W. G. 1984. Mount Isa silica dolomite and copper orebodies: The result of a syntectonic hydrothermal alteration system. Economic Geology, **79**, 601 - 637.

Perkins, W. G. 1997. Mount Isa lead-zinc orebodies; replacement lodes in a zoned syndeformational copper-lead-zinc system? Ore Geology Reviews, **12**, 61-111.

Robertson, C. W. 1982. The role of pre-existing sulphides in copper-ore formation at Mount Isa, Queensland. BMR Journal of Australian Geology and Geophysics, **7**, 119-124.

Scott, K. M. 1989. Dolomite compositions as a guide to epigenetic copper mineralization, Mount Isa Inlier, NW Queensland. Mineralium Deposita, **24**, 29-33.

Shaw, T. 2005. 500 OB Scoping Study 2005: Geological Summary: Xstrata Copper Internal Paper.

Solomon, P. J. 1965. Investigations into sulfide mineralization at Mount Isa, Queensland. Economic Geology and the Bulletin of the Society of Economic Geologists, **60**, 737-765.

Stanton, R. L. 1963. Elemental constitution of the Black Star orebodies, Mount Isa, Queensland, and its interpretation. Inst Min & Met , B , Tr, **672**, 69-124.

Stewart, A. J. 1992. The role of thrusting in the structural development of the Mount Isa Mine and its relevance to exploration in the surrounding region; discussion. Economic Geology and the Bulletin of the Society of Economic Geologists, **87**, 1659-1664.

Swager, C. P. 1983. Microstructural development of the silica-dolomite and copper mineralisation at Mount Isa, north-west Queensland, with speacial emphasis on the timing and mechanism of mineralisation, Ph.D. thesis, James Cook Univ.

Swager, C. P. 1985. Syndeformational carbonate-replacement model for the copper mineralization at Mount Isa, Northwest Queensland; a microstructural study. Economic Geology and the Bulletin of the Society of Economic Geologists, **80**, 107-125.

Waring, C. L., Heinrich, C. A. & Wall, V. J. 1998. Proterozoic metamorphic copper deposits. AGSO Journal of Australian Geology and Geophysics, **17**, 239-246.

Wilde, A. R., Jones, P. A., Gessner, K., Ailleres, L., Gregory, M. J. & Duncan, R. J. 2006. A Geochemical Process Model for the Mount Isa Copper Orebodies. Economic Geology, **101**, 1547-1567.

Winsor, C. N. 1983. Syntectonic vein and fibre growth associated with multiple slaty cleavage development in the Lake Moondarra area, Mount Isa, Australia. Tectonophysics, **92**, 195-210.

Preamble to paper 4

The previous papers (papers 1, 2 and 3) have concentrated of the structural evidence for the formation of the Paroo Fault and the copper orebodies and their associated silica-dolomite halo. This paper (paper 4) examines the composition of the fluid sources for the Paroo Fault, copper orebodies and silica-dolomite halo using halogen systematics. The halogen dataset includes data collected as part of this project as well as that of previous authors. The dataset is re-interpreted in light of new timing constraints provided by the previous papers (papers 1, 2 and 3) to create a new model of the fluid flow history of the Mount Isa copper deposit.

Paper 4 - The Mount Isa Copper orebodies - insights from fluid inclusion halogens

Ryan D. Long, Nicholas H. S. Oliver, Poul Emsbo, Brian G. Rusk and Thomas G. Blenkinsop

1.1. Abstract

This study compares the halogen systematics of fluid inclusions from the Mount Isa copper orebodies, silica-dolomite halo, basement and Paroo Fault Zone filling. The Br, Cl and Na ratios demonstrate that the copper orebodies, silica-dolomite halo and Paroo Fault Zone filling were formed from fluid that derived its salinity from a bittern brine. The similarity between the halogen ratios from the basement and the copper orebodies demonstrates that the alteration in the basement is related to the copper mineralising fluids. The decrease in the Br/Cl, Na/Cl and Na/Br ratios from quartz to dolomite, chalcopyrite and pyrite indicates an evolution in the composition of the bittern brine. From this a paragenesis of quartz and dolomite followed by chalcopyrite and pyrite can be established. Ca enrichment in some fluid inclusions relative to modern seawater probably indicates the fluids passed through Ca-rich rocks such as the Eastern Creek Volcanics and/or dolomitic rocks of the Mount Isa Group.

Keywords; Halogens, Mount Isa Copper deposit

2. Introduction

Understanding the role of the fluids involved in the formation of ore deposits has a great impact on exploration programs. Basinal brines have been demonstrated to be important sources of chemical agents involved in some mineralisation processes (Kesler et al., 1995; 1996; 2007; Chetty and Frimmel, 2000; Wilkinson, 2001; Grandia et al., 2003; Gilg et al., 2006; Huizenga et al., 2006; Vandeginste et al., 2007; Johnson et al., 2009). Other mineralizing fluids may gain salinity from crystallizing igneous rocks or interaction with evaporites.

The halogen (Na, Cl and Br) systematics of fluid inclusions can be used as geochemical tracers to identify the source of brine salinity in ore deposits because the halogen content of fluids are not readily affected by water-rock interactions (Kesler et al., 1995; 1996; 2007; Chetty and Frimmel, 2000; Wilkinson, 2001; Grandia et al., 2003; Gilg et al., 2006; Huizenga et al., 2006; Vandeginste et al., 2007; Johnson et al., 2009).

At Mount Isa there has been a large amount of research to understand the genesis of the deposit from a geochemical perspective (Love and Zimmerman, 1961; Stanton, 1963; Solomon, 1965; McDonald, 1970; Finlow-Bates and Stumpfl, 1979; Gulson et al., 1983; Swager et al., 1987; Andrew et al., 1989; Heinrich and Cousens, 1989; Heinrich et al., 1989; 1993; 1995; Scott, 1989; McGoldrick and Keays, 1990; Hannan et al., 1993; Kendrick et al., 2006; Wilde et al., 2006). Its formation is still debated and in a series of recent papers a new timing and mechanism for the formation of the Mount Isa copper orebodies has been proposed (Papers 1, 2 and 3). In this investigation we examine the fluids involved in the formation of the copper deposits and alteration of the silica-dolomite halo and basement rocks. The halogen contents of minerals from the Mount Isa copper deposit were analyzed in order to understand the source of the brine salinity which formed the deposits.

This paper summarizes the previous work done on the mineralizing fluid compositions from Mount Isa, and adds new data to the existing datasets for orebody quartz and carbonate halogens. Halogen systematics of sulphides from the copper deposit have been measured for the first time. New samples of quartz and carbonate from locations not considered by earlier workers have been included, particularly the Paroo Fault Zone and basement rocks. Detailed fluid inclusion petrography is beyond the scope of this current contribution, and awaits further investigation, along with laser ablation inductively coupled plasma mass spectrometry (**LA**-**ICP-MS**) of selected inclusions. Here, the work focuses on the now well established technique of bulk crush-leaching of fluid inclusions and analysis of the halogen ratios derived.

3. Geological setting

The Mount Isa Inlier is a world class base metal province (Fig. 49). The SEDEX lead-zinc deposits within the Inlier form two types. The first, McArthur-type (including Mount Isa lead-zinc-silver deposit) precipitated from oxidised brines evolved from sedimentary basins dominated by carbonates, evaporites, and haematitic sandstone and shales during the Paleoproterozoic. The other lead-zinc SEDEX deposit type is the Selwyn type deposit, which precipitated from reduced brine sourced from reduced siliclastic and shale basins during the Palaeozoic (Cooke et al., 2000). The copper-gold deposits within the Inlier also formed during the Proterozoic (Davidson and Large, 1998), but are mostly epigenetic and strongly structurally controlled, with both basinal and magmatic-hydrothermal fluid characteristics (Williams et al., 2005; Kendrick et al., 2007).

At Mount Isa, the copper orebodies which have an epigenetic texture are spatially associated with overlying lead-zinc-silver orebodies that have syngenetic texture (Finlow-Bates, 1979). The copper orebodies and lead-zinc-silver orebodies are broadly stratabound within the Urquhart Shale Formation of the Mount Isa Group (Solomon, 1965; McDonald, 1970). The Mount Isa Group (Urquhart Shale formation 1655 ± 4 Ma; Page et al., 2000) has been juxtaposed against the Lena Quartzite and Cromwell Metabasalt of the Eastern Creek Volcanics (1710 ± 25 Ma; Gulson et al., 1983) by normal movement on a rift fault (Fig. 50) during the deposition of the Kennedy Siltstone and Magazine Shale (Paper 1).

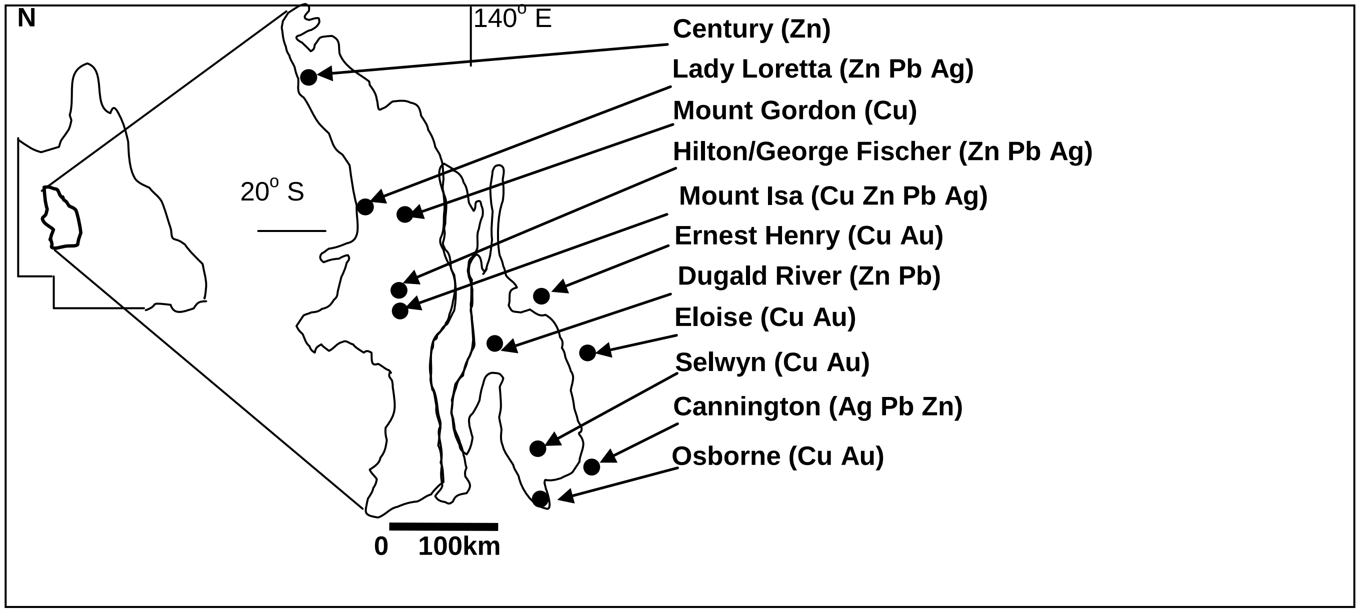

Fig. 49. Simplified tectonic map of the Mount Isa Inlier showing the copper and lead-zinc deposits contained within the region.

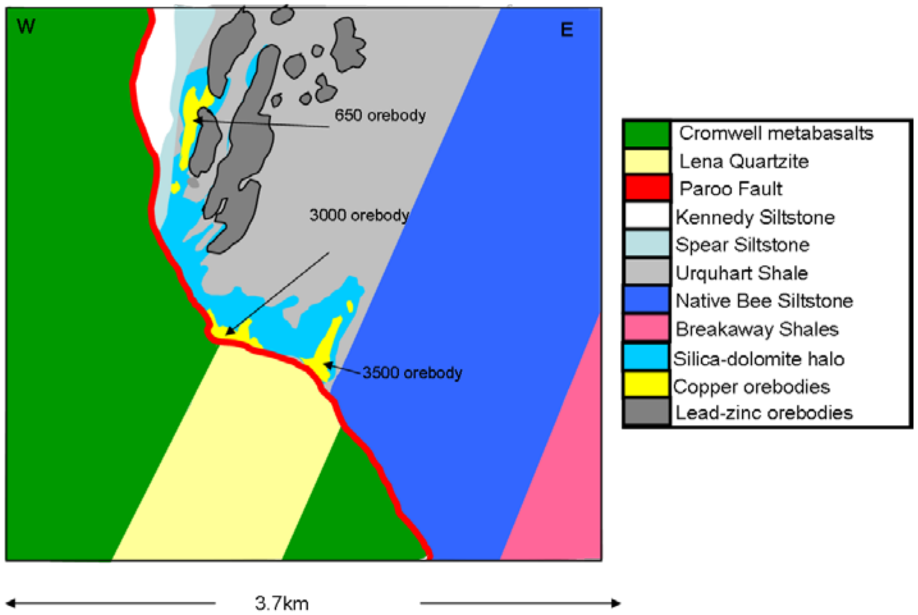

Fig. 50. Simplified cross section of the Mount Isa copper orebodies (yellow) and lead-zinc-silver orebodies (grey) at a northing of 7706800 m. The Eastern Creek Volcanics (Cromwell Metabasalt and Lena Quartzite) have been juxtaposed against the Mount Isa Group by movement along the Paroo Fault (red), which was subsequently folded. Displayed are the perched non-stratiform 650 copper orebody, the non-stratiform 3000 copper orebody and the stratiform 3500 copper orebody. Surrounding the copper orebodies is the silica-dolomite halo (blue).

The copper orebodies and associated silica-dolomite alteration halo were formed early during the east-west shortening event by the influx of multiple generations of fluids (Paper 2). After the development of the copper orebodies the Paroo Fault was filled with alternating quartz and graphite rich layers by repeated extraction and precipitation of quartz from the overlying Urquhart Shales (Paper 2). The Paroo Fault folded during copper mineralisation in a phase of east-west shortening (D_2) and a phase of east southeast-west northwest shortening (D_3; Papers 1 and 2).

The relationship between the lead-zinc-silver orebodies which have a syngenetic texture and the copper orebodies that have an epigenetic texture has been a topic of considerable debate in the literature. There are three explanations for this unusual relationship. Firstly, syngenetic lead-zinc-silver may have provided favorable structural and/or geochemical conditions for epigenetic copper to develop (Robertson, 1982; Gulson et al., 1983; Swager, 1983; 1985; Perkins, 1984; 1990; Bell et al., 1988; Andrew et al., 1989; Heinrich and Cousens, 1989; Heinrich et al., 1989; 1993; 1995; Bell and Hickey, 1998; Waring et al., 1998; Davis, 2004; Kendrick et al., 2006; Miller, 2007), for example, by replacement of earlier lead-zinc-silver sulfides. In another model both the copper and the lead-zinc-silver orebodies are considered epigenetic, with the lead-zinc-silver mineralisation replacing bedding, resulting in an apparent syngenetic texture (Perkins, 1997; Davis, 2004). The final model considers syntectonic remobilization of copper from a syngenetic zoned copper-lead-zinc-silver deposit, to produce the epigenetic texture of the copper orebodies (Solomon, 1965; Smith, 1969; Mathias and Clark, 1975; Finlow-Bates and Stumpfl, 1979; McGoldrick and Keays, 1990).

The copper orebodies have two morphologies - stratiform such as the 500, N1900 and 3500 orebodies, and non-stratiform including 200, 650, 1100, S1900 and 3000 orebodies (Fig. 51). These orebodies can be further subdivided on the basis of whether they lie adjacent to the Paroo Fault of perched hundreds of meters above it (Paper 2). Paper 3 proposed that the difference in shape between the stratiform and non-stratiform copper orebodies was due to the east southeast-west northwest shortening event (D_3) which deformed some of the copper orebodies (non-stratiform) and not others (stratiform). The reason why some of the orebodies are perched above the fault and others are perched remains largely unanswered. Halogen systematics of fluid inclusions from chalcopyrite, pyrite and quartz from the orebodies are presented here in an attempt to understand the spatial and conflicting textural relationships.

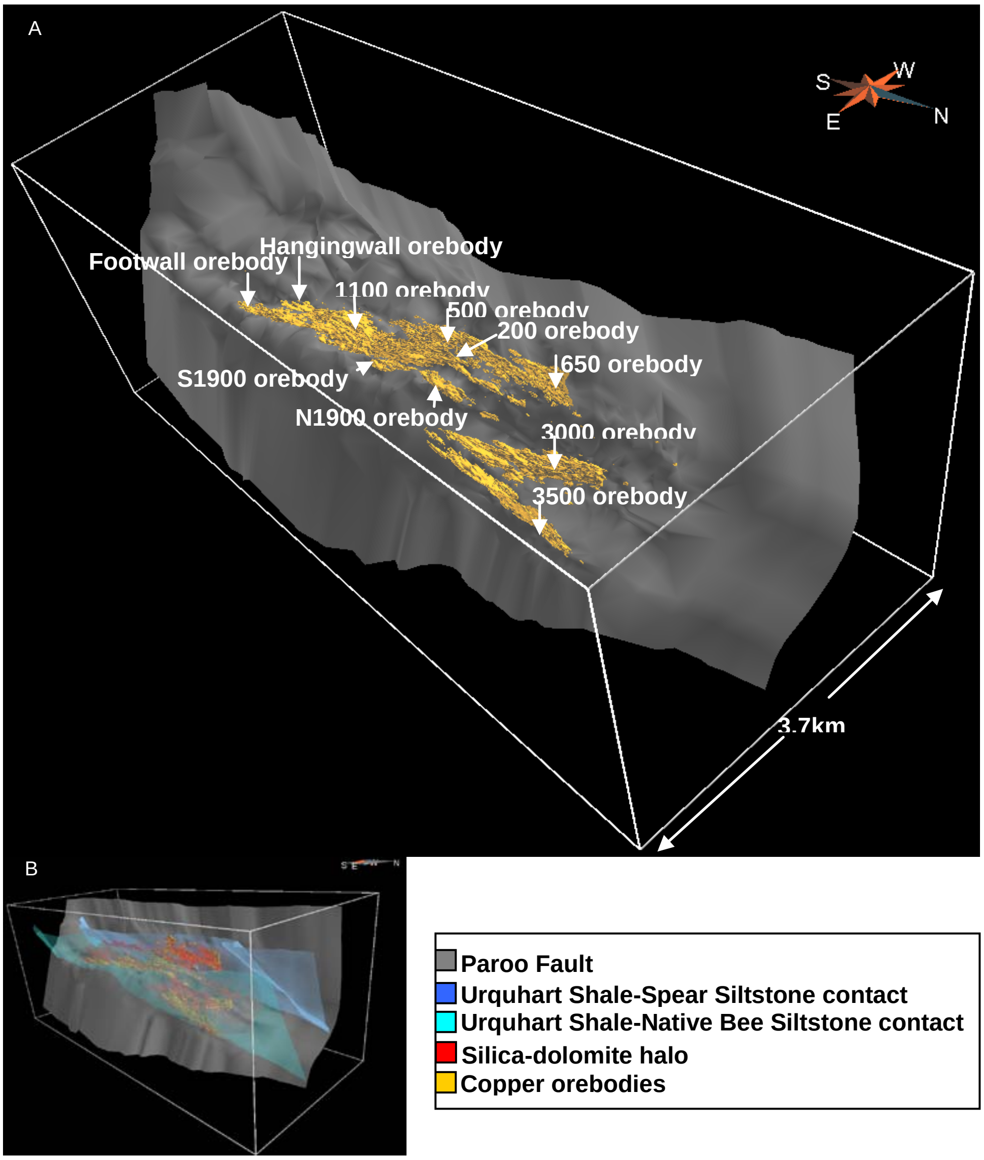

Fig. 51. A) The Paroo Fault (grey) with the copper orebodies labeled (yellow); B) The Paroo Fault (grey) with the stratigraphic boundaries of the Urquhart Shales (blue and turquoise) which contain the silica-dolomite halo (red) that surrounds the copper orebodies (yellow).

4. Previous work

4.1. Fluid inclusions from the Mount Isa copper deposit

The fluid inclusions from the Mount Isa copper deposit have been extensively described (Heinrich et al., 1989; Kendrick et al., 2006). Within the dolomite breccia there are two groups of inclusions. The first are $CaCl_2$ rich two phase liquid-vapour inclusions (Group 1) which have a melting temperature of -20 to -30 ^{o}C, homogenization temperature of 250 ^{o}C and salinities ~20-26 wt.% NaCl-$CaCl_2$. The second group (Group 2) are CO_2 rich two phase liquid-vapour inclusions with a melting temperature between 0 to -4^{o}C, homogenization temperature of 250 ^{o}C and a salinity less than ~6.5 wt.% NaCl eq. Within quartz veins from the silica-dolomite the inclusions are NaCl rich two phase liquid-vapour inclusions (Group 3) with a melting temperature of -5 to -17 ^{o}C, homogenization temperature of 140-220 ^{o}C and a salinity of 8-29 wt.% NaCl eq. (Heinrich et al., 1989; Kendrick et al., 2006) Samples of quartz from the Paroo Fault Zone filling also contain primary inclusions similar to Group 3 inclusions and inclusions with lower salinities 8 to <1 wt.% NaCl eq. (Kendrick et al., 2006). A fourth group of inclusions (Group 4) was described by Heinrich et al., (1989) but not recognized by Kendrick et al., (2006). These are calcic low temperature secondary inclusions occurring along fluid inclusion planes, and post dating all stages of mineralisation.

4.2. Fluids and fluid pathways during the formation of the Mount Isa copper deposit

The K-feldspar-siderite-ankerite alteration surrounding the syngenetic lead-zinc-silver mineralisation at Mount Isa has been suggested to have localised the formation of a prograde metamorphic network of carbonate veins (Waring et al., 1998). This vein network may have provided a pathway for the retrograde metamorphic fluids forming the epigenetic copper orebodies. Halogen geochemistry from fluid inclusions from the Mount Isa copper orebodies has shown that there were two prograde carbonate-bearing fluids involved in the formation of the dolomitic alteration (Heinrich et al., 1989; Kendrick et al., 2006). One of the fluids was a CaCl-rich brine with a high salinity (~25 wt %), which was thought to be derived from the altered Eastern Creek Volcanics. The other CO_2 rich fluid had a low salinity, representing metamorphic fluid within the Urquhart Shale. The subsequent retrograde fluids which formed the siliceous alteration that overprints the dolomitic alteration was NaCl rich, and varied from high (10-20 wt %) to low salinity (4-9 wt %). The carbon, oxygen and hydrogen isotope values indicate the fluid originated as an oxidised evolved basin brine or an evaporite-derived by metamorphic fluid (Waring et al., 1998; Heinrich and Cousens, 1989; Heinrich et al., 1989). Noble gas ratios used together with halogen geochemistry (Kendrick et al., 2006) demonstrate that surface-derived bittern brine mixed with a deeply-derived metamorphic fluid, forming the silica-dolomite halo and the copper mineralisation.

Sulphur isotopes from the copper ores and pyrites within the Urquhart Shale indicate that the shale provided a major sulphur component to the copper ores. A variable component of the copper orebodies sulphur was derived from a ^{34}S-enriched source by a retrograde fluid which also contained the copper (Andrew et al., 1989). This ^{34}S-enriched source could have been seawater sulphate, sulphur leached under oxidized conditions, or most likely was a brine that interacted with sulphate bearing evaporites.

McGoldrick and Keays (1990) used the S/Se ratios of the copper and lead-zinc-silver ores to propose that there was no magmatic sulphur within the copper or lead-zinc-silver orebodies, and that the Eastern Creek Volcanics did not provide any sulphur to the copper ores. The S/Se ratios indicate a likely sedimentary brine source supporting the idea of an evaporite derived metamorphic fluid. These authors propose a common origin for the different ore types, based partly on this evidence.

Br/Cl ratios of saline fluid inclusions from late quartz-dolomite-chalcopyrite breccias were compared with similar inclusions of from regionally metasomatised Eastern Creek Volcanics (Heinrich et al., 1993). The inclusions had identical Br/Cl ratios indicating the Eastern Creek Volcanics could be a source of the copper in the Mount Isa copper orebodies. The high Br/Cl ratios suggest the fluids originated as a basin brine, but must have been available during the retrograde metamorphism. In contrast, Hannan et al. (1993) examined regional copper abundances in the Eastern Creek Volcanics and indicated that copper mobility was limited to strata-parallel redistribution in zones close to high fluid flow. This suggested to these authors that the Eastern Creek Volcanics could not be the source of the copper in the Mount Isa copper ores. However, kilometer-scale fracture zones that have associated carbonate-Fe oxide alteration which cut all penetrative foliations in the Eastern Creek Volcanics were interpreted as representing the conduits in which an oxidized, sulphate bearing brine leached copper from the Eastern Creek Volcanics (Heinrich et al., 1995). The large hydrothermal anhydrite body north of the copper orebodies is further evidence for the influx of an oxidized brine being involved in the formation of the copper orebodies (Wilde et al., 2006), although the copper source is not clearly resolved by this observation.

The oxidized, sulphate and copper bearing brine was focused in to the reduced Urquhart Shale, in which early prograde carbonate veins had created pathways for the retrograde fluid to form the copper orebodies, according to the model of Warning et al. (1998). The low ^{13}C and high ^{34}S alteration in the Eastern Creek Volcanics directly below the copper orebodies would also have formed from this fluid reacting with the basement (Andrew et al., 1989; Heinrich et al., 1995). Based on noble gas and halogen ratios of fluid inclusions, it has also been suggested that after silica-dolomite and copper development, a late surficial fluid which flowed along regional faults may have flowed through the Paroo Fault, terminating mineralisation (Kendrick et al., 2006). Another formation method for the Paroo Fault fill was proposed in Paper 2. They suggest that the fault fill was formed from repeated extraction from the Urquhart Shales directly above the fault and precipitation of quartz in to the Paroo Fault Zone.

5. Sample locations

The samples analysed in this project come from the 650, Hangingwall Lens, Footwall Lens, 3000, 3500 orebodies (Fig. 51), the Paroo Fault Zone filling and the Lena Quartzite. This widespread distribution of the samples is broader than previously analysed in the literature, and includes new analyses of sulphides from the copper orebodies which allows improved characterisation of the copper orebodies and associated rocks. Brief descriptions of the samples and their locations are found in Table 8.

Sample number	Mine location	General Location	Mineral analysed	Macroscale assemblage
650	DH 200306312 256.8m	650 orebody	Pyrite	Vein (dolomite, chalcopyrite, pyrite with minor quartz) within a Dolomitic Recryst
1900	Level 18B T52 BP	1900 orebody	Chalcopyrite	Massive chalcopyrite, pyrite and minor pyrrhoitite and host altered shale
FW	Level 17 X36SE DR	Footwall Lens orebody	Pyrite	Chalcopyrite and pyrite breccia in Fractures Siliceous Shale
HW Lens	Level 18B T38 SDR	Hangingwall Lens orebody	Pyrite	Vien network in dolomitic breccia (chalcopyrite, pyrite and quartz)
3000	Level 20C N58S W	3000 orebody	Chalcopyrite	Copper breccia (chalcopyrite, pyrite and pyrrhotite minor quartz)
M-5	Level 27 Q635 DPT	3000 Orebody	Chalcopyrite	Copper breccia (quartz, dolomite, chalcopyrite with minor pyrite, pyrrhotite chlorite and graphite)
02 02 02	Level 27 6396 XC	3000 orebody	Chalcopyrite	Copper breccia
03 01 05	Level 27C P63N DRV	3000 orebody	Chalcopyrite	Copper breccia
03 01 01	Level 27C P63N DRV	3000 orebody	Chalcopyrite	Late chalcopyrite vein cross cutting breccia (contains carbonate/quartz contamination)
03 01 06	Level 27C P63N DRV	3000 Orebody	Chalcopyrite	Copper breccia
03 05 03	Level 29E U636 CO	3500 orebody	Pyrite	Copper breccia
03 03 04	Level 30E V70 FRAC	3500 orebody	Pyrite	Extension vein associated with quartz
01 02 12	Level 29E U69 CO	3500 orebody	Quartz	Copper breccia
01 02 08	Level 29E U69 CO	3500 Orebody	Chalcopyrite	Copper breccia
03 01 06	Level 27C P63N DRV	3500 Orebody	Dolomite	Copper breccia
03 05 01	Level 29E U636 CO	3500 Orebody	Chalcopyrite	Copper breccia
01 02 01	Level 29E U69 CO	Basement	Pyrite	
K-5	Level 27C 6934 XC	Basement	Quartz	Vein containing (quartz and pyrite with minor chlorite)
M-4	Level 27 Q635 DPT	Basement	Dolomite	Vein containing (dolomite, quartz and pyrite)
F-8	Level 29E 6515 XC	Basement	Quartz	Vein containing (dolomite, quartz and pyrite with minor chlorite)
L-1	Level 30A X620 RPAC	Basement	Quartz	Vein containing (quartz and dolomite)
O-6	Level 18B V39 SWXC	Basement	Quartz	Vein containing (quartz, dolomite and pyrite)
F5	Level 29E 6515 XC	Basement	Quartz	Disseminated chalcopyrite and pyrite in metamorphosed Lena Quartzite
A10	Level 29E 6448 XC	Basement	Quartz	Disseminated chalcopyrite and pyrite in metamorphosed Lena Quartzite
A23	Level 29E 6448 XC	Paroo Fault	Quartz	Disseminated chalcopyrite, pyrite and galena in quartz fault fill
K4	Level 27C 6934 XC	Paroo Fault	Quartz	Tope of the Paroo Fault fill (carbonate and quartz with minor chalcopyrite and pyrite)
M-1	Level 27 Q635 DPT	Paroo Fault	Quartz	Center of the Paroo Fault fill (quartz with minor pyrite, chalcopyrite, chlorte and graphite)
F-12	Level 29E 6515 XC	Paroo Fault	Quartz	Top of the Paroo Fault fill (quartz and dolomite with minor chlorite and graphite)
L-2	Level 30A X620 RPAC	Paroo Fault	Dolomite	Center of the Paroo Fault fill (quartz and dolomite with minor pyrite, chalcopyrite, chlorte and graphite)
O-2	Level 18B V39 SWXC	Paroo Fault	Quartz	Center of the Paroo Fault fill (quartz with minor chlorte and graphite)

Table 8 The location and assemblages of the samples used in this report.

6. Methodology

11 samples of chalcopyrite and 6 samples of pyrite were analyzed from the following settings; the 3000 orebody (7), 3500 orebody (5), 1900 orebody (1), Footwall Lens orebody (1), Hangingwall Lens orebody (1), 650 orebody (1), and Lena Quartzite (1). 10 samples of quartz were also analyzed from the Paroo Fault Zone filling (5) and veins within the Lena Quartzite (5). 3 samples of dolomite were analysed from the Paroo Fault Zone filling (1), Lena Quartzite (1) and the 3500 orebody. These samples were removed using an air chisel to chip off a large amount of material. Using a microscope, pure samples of the individual minerals (Table 8) were selected and used for analysis.

Halogens were analyzed by bulk crush-leach ion chromatography at the USGS in Denver, Colorado. Approximately 500 mg of fluid inclusion-hosting mineral is crushed in a vacuum, and a spiked solution is injected into the crushed quartz chamber where it mixes with the inclusion fluids before being passed through chromatography columns. The volume of fluid released from this method is far higher than for individual destructive or non-destructive techniques (e.g. LA-ICPMS or PIXE) allowing far greater precision and accuracy in determining the fluid composition.

The analytical ease of the method is compromised by the fact that all fluid inclusions, of all generations, are analysed simultaneously, so that all fluid entrapment paragenetic stages are captured. None-the-less, the method is widely applied despite its inherent limitations, especially where other techniques can be used to identify different paragenetic stages. This technique analyses not only the halogens, Cl and Br, but also quantifies with reference to 1 molar Cl, both cations and other anions including Na, K, Mg, Ca, Sr, F, acetate, PO4, CO3, SO4.

7. Results

The Br/Cl ratio for chalcopyrite (0.004-0.015 wt), pyrite (0.004-0.013 wt), dolomite (0.004-0.009 wt) and quartz (0.004-0.007 wt) presented here are similar to those values quartz and dolomite collected by Kendrick et al. (2006; 0.003-0.011 wt) and to some extent are similar to the results from assemblages collected by Heinrich et al. (1993; 0.008-0.16 wt; Fig. 52). The sulphides have a slightly larger range of values compared to the quartz and dolomite values.

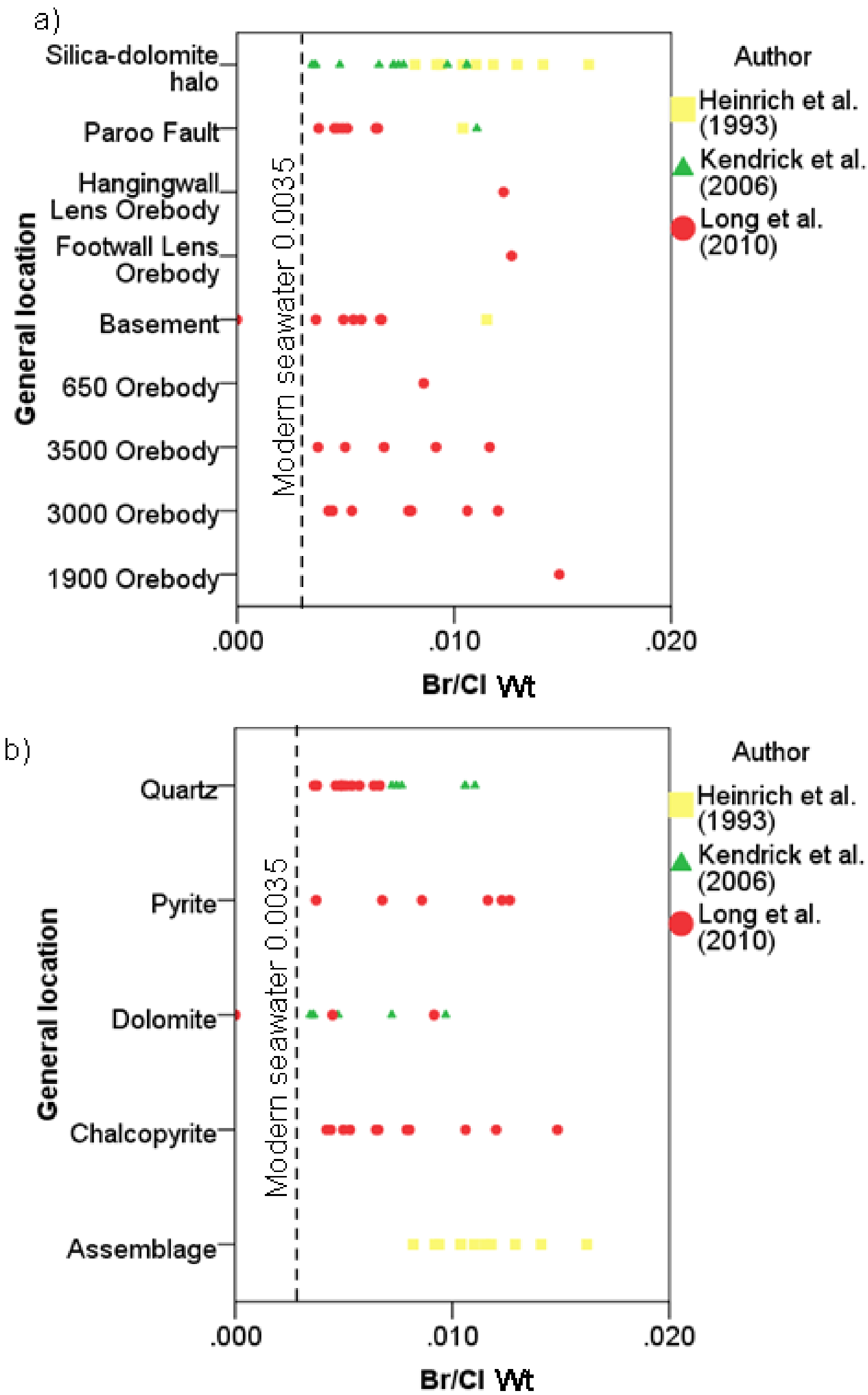

Fig. 52. Comparison between halogen systematics collected here and the work of Heinrich et al. (1993) and Kendrick et al. (2006); a) classifies the halogen systematics by general location; b) classifies the halogen systematics by minerals analyzed.

Measured molar Cl/Br ratios range between 151 and 604 and the Na/Cl ratios are between 0.48 and 0.84 for the copper orebodies (Fig. 53), indicating that cations besides Na comprise between about 10 and 30 weight % of the fluid compositions. The bulk of the charge balance is made up by Ca and K. The Paroo Fault Zone filling has a less variable range in Cl/Br ratios (between 347 and 598) than the copper orebodies and the Na/Cl ratios are between 0.55 and 0.89 again indicating that cations besides Na comprise between about 10 and 30 weight % of the fluid compositions. The veins within the basement show molar Cl/Br ratios between 338 and 620 and Na/Cl ratios between 0.51 and 0.88, again indicating that cations besides Na comprise between about 10 and 30 % of the fluid compositions. Some of the samples have undergone some Na-loss while those to the right have undergone Na-enrichment, relative to modern seawater.

The copper orebodies, Paroo Fault Zone filling and basement veins all plot close to the seawater evaporation trajectory (SET) indicating that the fluids from which the minerals were formed probably had a bittern brine halogen source (Figs. 53, 54, 55, 56). All the data is located between the seawater field the $MgSO_4$ field, dominantly above the halite field (Figs. 53, 54, 55, 56). The Ca/Cl ratios (Fig. 55), between 0.02 and 0.53 for minerals from all locations, show a large Ca enrichment relative to evaporated seawater. The minerals from all locations also show strong Mg depletion relative to evaporated seawater (Fig. 56).

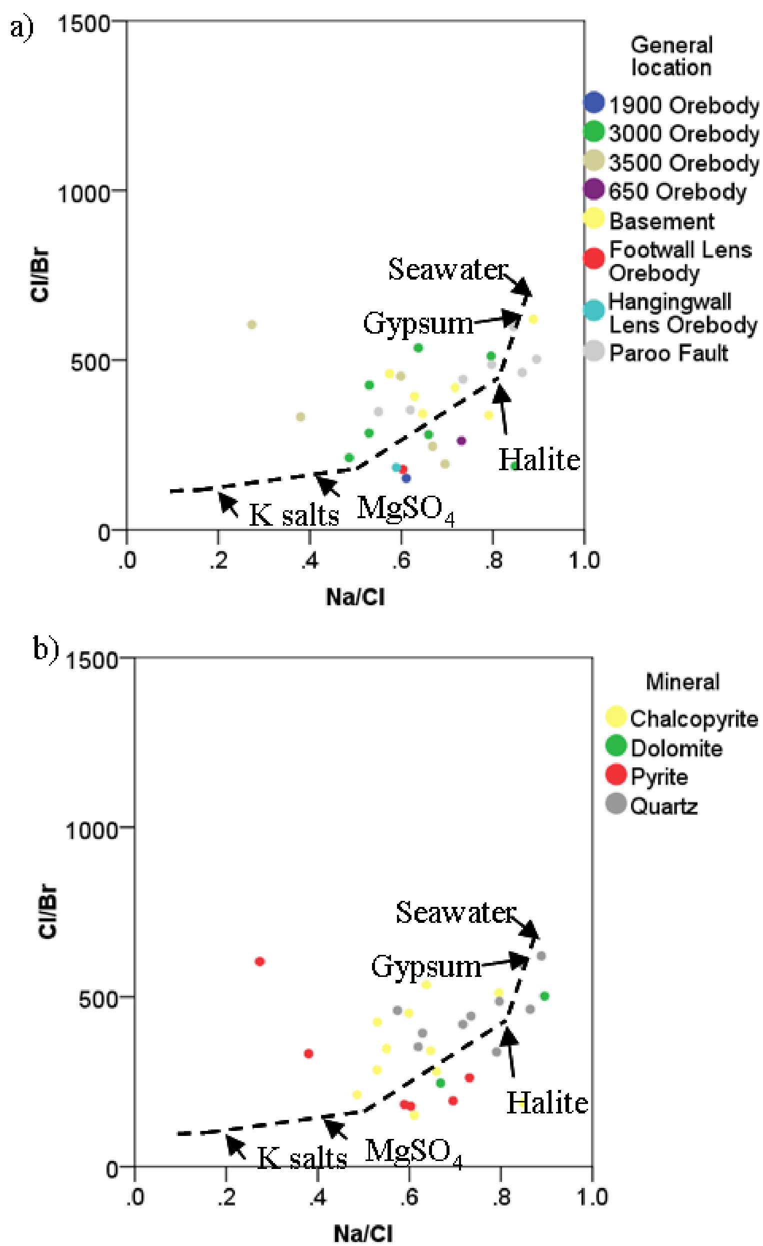

Fig. 53. Halogen discrimination diagrams; a) Cl/Br vs. Na/Cl plot showing the general location of the samples. The dashed line shows the seawater evaporation trajectory (SET). The samples plotting to the left of the SET represent fluids produced by evaporated seawater which have undergone some Na-loss while those to the right have undergone Na-enrichment; b) Cl/Br vs. Na/Cl plot showing the minerals analyzed.

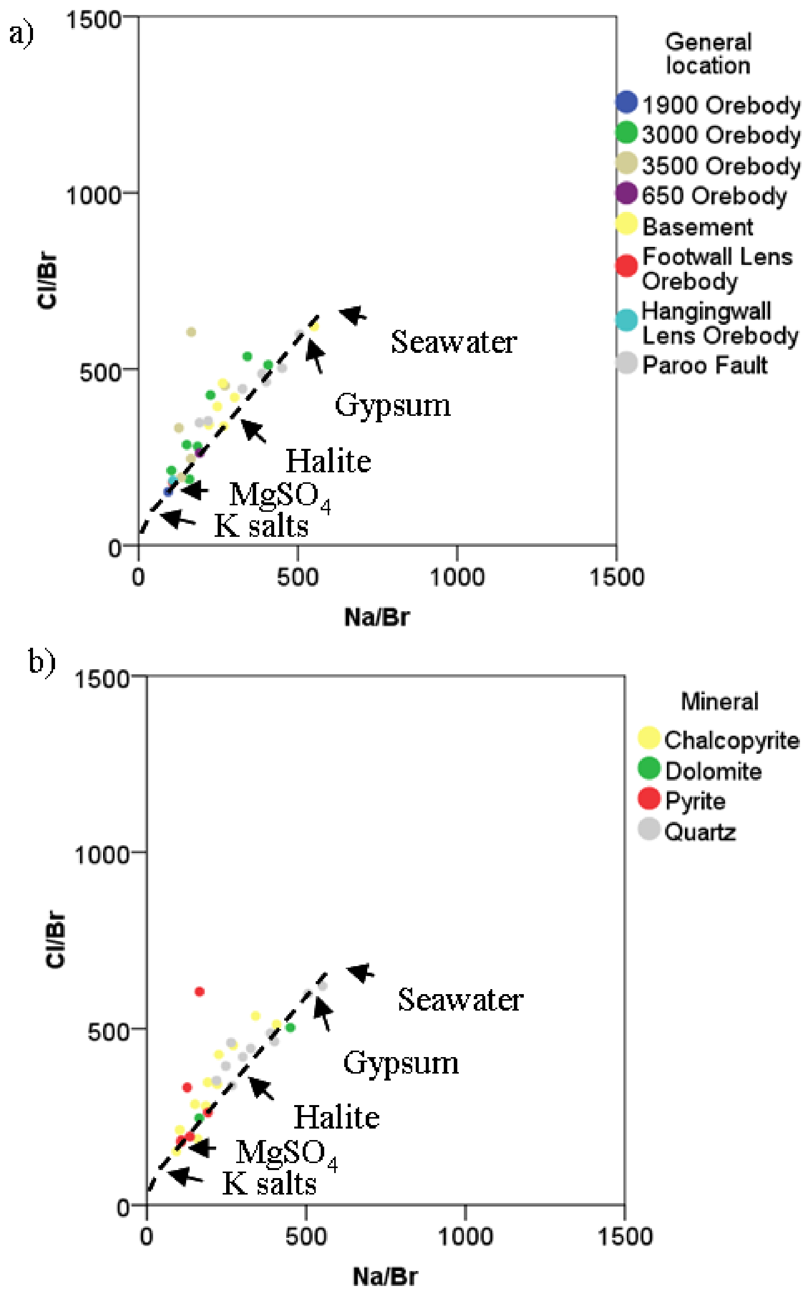

Fig. 54. Halogen discrimination diagrams A) Cl/Br vs. Na/Br plot showing the general location of the samples. The dashed line shows the SET. The arrows point to the first visible appearance of evaporite minerals during the evaporative evolution of seawater. All copper orebodies plot along the SET, indicating that they have a bittern brine origin. Two samples of pyrite from the 3500 orebody plot slightly off the SET indicating some kind of Cl enrichment and Na depletion relative to modern seawater; B) Cl/Br vs. Na/Br plot showing the minerals analysed.

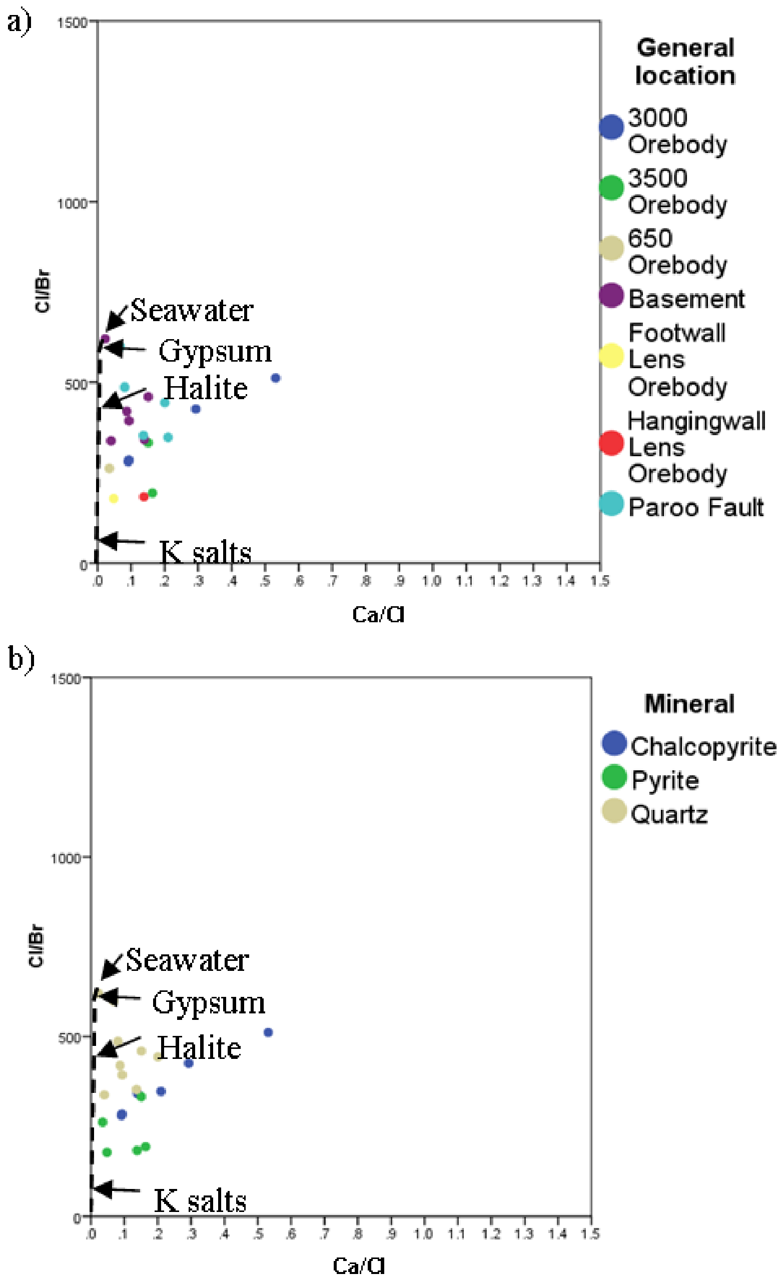

Fig. 55. Halogen discrimination diagrams from this study, SET shown as dashed line; A) Cl/Br vs. Ca/Cl plot showing the general location of the samples. All samples show Ca enrichment over evaporated seawater, probably related to dolomitisation associated with the silica-dolomite halo; B) Cl/Br vs. Ca/Cl plot showing the minerals analyzed. Quartz, pyrite and chalcopyrite appear to occur in different fields.

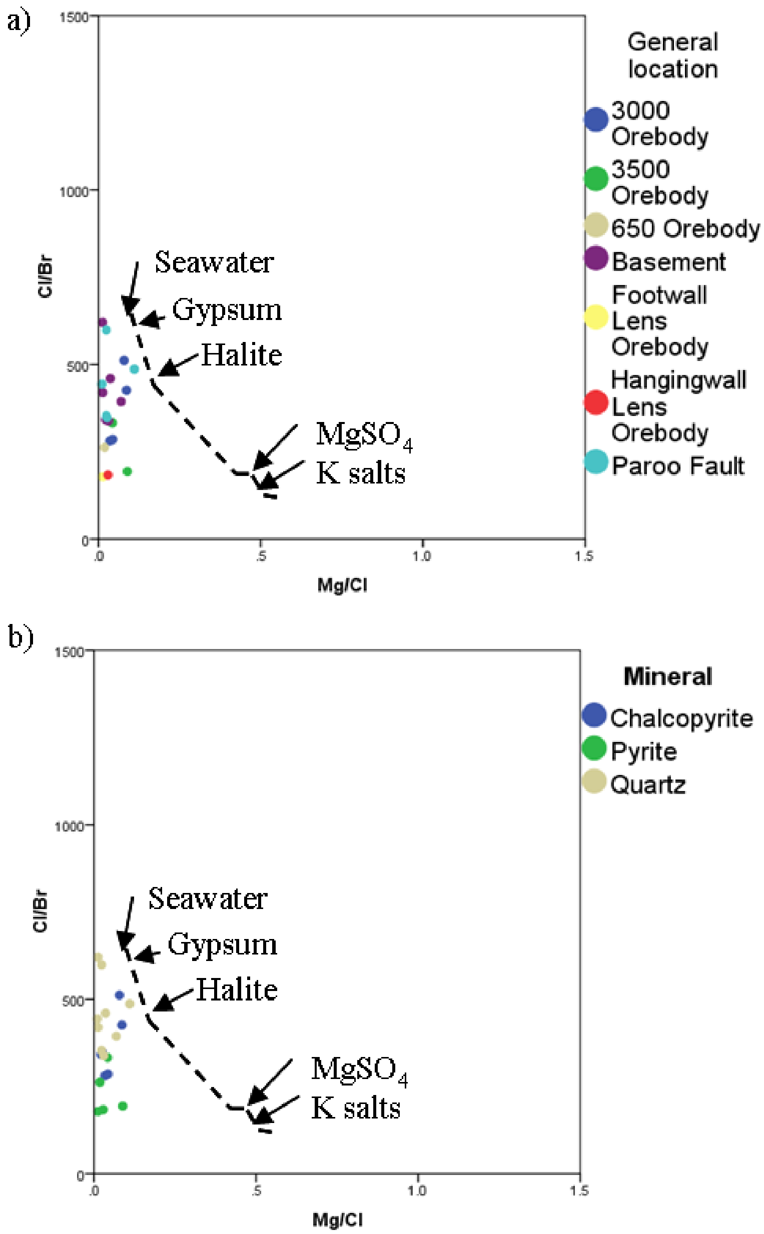

Fig. 56. Halogen discrimination diagrams from this study, SET shown as dashed line; A) Cl/Br vs. Mg/Cl plot showing the general location of the samples. Quartz and pyrites show strong Mg depletion from evaporated seawater, interpreted to be due to dolomitisation; B) Cl/Br vs. Mg/Cl plot showing the minerals analyzed. The chalcopyrites have a mixed Mg/Cl ratio indicating Mg enrichment and depletion and the dolomites are enriched in Mg.

8. Discussion

The sulphide, quartz and dolomite values for Cl/Br vs. Na/Cl, Cl/Br vs. Na/Br, Cl/Br vs. Ca/Cl and Cl/Br vs. Mg/Cl all plot in the SET indicating an inherited marine brine source for the halogens within the copper deposit, the Paroo Fault Zone filling and the basement veins. They also imply that this fluid interacted with all of these rocks, because there is no clear distinction in the specific ratios between the Urquhart Shales hosting the main copper orebodies, the Paroo Fault, and the footwall rocks. However, in all the plots quartz occurs towards the top of the SET with chalcopyrite and pyrite towards the bottom. This could represent a progressively evaporating surface fluid that was tapped at different times, moved downwards, and precipitated these (non evaporative) minerals in a sequence. The similarities in the halogen systematics for the basement samples and the copper orebody samples is further evidence to support the work of Andrew et al. (1989) and Heinrich et al. (1995) who demonstrated that the altered Eastern Creek Volcanics below the copper orebodies was part of the hydrothermal footprint of ore formation. The pattern of Ca enrichment (Fig. 55) and Mg depletion (Fig. 56) noted above could indicate that these fluids exchanged cations with previously seafloor-altered metabasalts which can show depleted Mg and enriched Ca in some parts of their alteration systems (Seyfried and Bischoff, 1979). However, the effect on the fluid compositions of multiple precipitation (and possible dissolution) stages of dolomite, is not understood at this stage.

This data supports the evidence of Kendrick et al. (2006) that the copper orebodies and silica-dolomite halo was formed due to the mixing of a bittern brine and metamorphic fluid. Interestingly, however, it is more likely to mix metamorphic fluids with basinal fluids early in the metamorphic cycle (e.g. Oliver et al., 2006). One problem with models for late- or post-Isan Orogeny copper genesis is that a source for bittern brines is less obvious than in the early metamorphic stages when residual basinal fluids may have occupied pore space. This problem was addressed in part by Wilde et al. (2006) who proposed a young source for bittern brines, in a post-metamorphic ore genesis scenario, but that is not well supported by recent structural studies (Papers 1, 2 and 3).

Most of the samples do not lie on the SET and this may represent the mixing of halite saturated brine with a Cl-poor fluid (Connolly et al., 1990; Vandeginste et al., 2007) or more likely may represent the difference in ancient seawater composition compared to modern seawater as demonstrated by Kesler et al. (2007).

Heinrich et al. (1993) and Kendrick (2006) suggested a post D_3 timing for the formation of the copper orebodies and had difficulty to find a bittern brine source that was not metamorphosed. The new timing for copper mineralisation presented in Papers 1, 2 and 3 does not need an exotic brine source, as the fluid can be contained within the Urquhart Shale. Further the data presented here is closer to seawater indicating the fluid is possibly not as evolved as described by Heinrich et al. (1993). The broader spread of data shown by the recent studies also suggests more than one fluid may have contributed. Normal metamorphic fluids cannot explain the high Br/Cl ratio obtained by Heinrich et al. (1993); however the lower ratios presented here for the Paroo Fault Zoneand Basement veins can possibly be explained by a normal metamorphic fluid.

9. Conclusions

The halogen systematics presented in this paper demonstrate that the copper orebodies, silica-dolomite halo, basement footwall alteration and Paroo Fault Zone filling formed from fluid that gained its salinity from a bittern brine. This demonstrates that the alteration in the basement is related to the copper mineralising fluids. Further possible evidence of the basement's role in the mineralisation process is the Ca enrichment in the fluid inclusions relative to modern seawater which suggests the mineralising fluids passed through Ca-rich rocks such as the Eastern Creek Volcanics, which have been proposed as a source for the copper mineralisation by several authors. There was an evolution in the halogen composition of the bittern brine between quartz and dolomite formation, and chalcopyrite and pyrite formation, possibly caused by a) progressive evaporation of the brine source and similarly progressive migration of such fluids downwards into the ore genesis location, b) the degree of fluid/rock interaction changing with time, or c) a different intrinsic capacity of each mineral to trap fluids or variable salinity. The new timing for copper mineralisation means that an exotic source for the mineralising fluid is no longer needed and the bittern brine may have originated within the Mount Isa Group.

10. References

Andrew, A. S., Heinrich, C. A., Wilkins, R. W. T., and Patterson, D. J., 1989. Sulfur isotope systematics of copper ore formation at Mount Isa, Australia: Economic Geology and the Bulletin of the Society of Economic Geologists. 84, 1614-1626.

Bell, T. H., 1991. The Role of thrusting in the Structural Development of the Mount Isa Mine and its Relevance to Exploration in the Surrounding Region: Economic Geology. 86, 1602-1625.

Bell, T. H., and Hickey, K. A., 1998. Multiple Deformations with Successive Subvertical and Subhorizontal Axial Planes in the Mount Isa Region: Their Impact on Geometric Development and Significance for Mineralization and Exploration: Economic Geology. 93, 1369-1389.

Bell, T. H., Perkins, W. G., and Swager, C. P., 1988. Structural controls on development and localization of syntectonic copper mineralization at Mount Isa, Queensland: Economic Geology and the Bulletin of the Society of Economic Geologists. 83, 69-85.

Blanchard, R., and Hall, G., 1937. Mount Isa [Queensland] ore deposition: Economic Geology and the Bulletin of the Society of Economic Geologists. 32, 1042-1057.

Carr, G., 2010. Giant Pb-Zn ores revealed by their Pb Isotopes, 13th Quadrennial IAGOD Symposium 2010 'GIANT ORE DEPOSITS DOWN-UNDER' Adelaide, Australia

Chetty, D., and Frimmel, H. E., 2000. The role of evaporites in the genesis of base metal sulphide mineralisation in the Northern Platform of the Pan-African Damara Belt, Namibia: geochemical and fluid inclusion evidence from carbonate wall rock alteration: Mineralium Deposita. 35, 364-376.

Connolly, .A., Walter, .M., Baadsgaard,H., and. Longstaffe, F.J. 1990 Origin and evolution of formation waters, Alberta Basin, Western Canada Sedimentary Basin. I. Chemistry. *Appl. Geochem.,* 5, 375–395

Cooke, D. R., Bull, S. W., Large, R. R., and McGoldrick, P. J. 2000 The Importance of Oxidized Brines for the Formation of Australian Proterozoic Stratiform Sediment-Hosted Pb-Zn (Sedex) Deposits; Economic Geology, 95, 1-18.

Davidson, G. J., and Large, R. R. 1998. Proterozoic copper-gold deposits: Journal of Australian Geology and Geophysics, 17, 105-113.

Davis, T. P., 2004. Mine-scale structural controls on the Mount Isa Zn-Pb-Ag and Cu orebodies: Economic Geology and the Bulletin of the Society of Economic Geologists, 99, 543-559.

Dunnet, D., 1976. Mt Isa; reconstruction of a faulted ore body: Philosophical Transactions of the Royal Society of London, Series A: Mathematical and Physical Sciences. 283, 333-344.

Farquharson, R. B., and Richards, J. R., 1974. U-Th-Pb isotope systematics related to igneous rocks and ore Pb, Mount Isa, Queensland: Mineralium Deposita. 9, 339-356.

Finlow-Bates, T., and Stumpfl, E. F., 1979. The copper and lead-zinc-silver orebodies of Mt. Isa Mine, Queensland; products of one hydrothermal system: Annales de la Societe Geologique de Belgique. 102, 497-517.

Gessner, K., 2009. Coupled Models of Brittle-plastic Deformation and Fluid Flow: Approaches, Methods, and Application to Mesoproterozoic Mineralisation at Mount Isa, Australia: Surveys in Geophysics. 30, 211-232.

Gessner, K., Jones, P. A., Wilde, A. R., and Kühn, M., 2006. Significance of strain localization and fracturing in relation to hydrothermal mineralization at Mount Isa, Australia: Journal of Geochemical Exploration. 89, 129-132.

Gilg, H., Boni, M., Balassone, G., Allen, C., Banks, D., and Moore, F., 2006. Marble-hosted sulfide ores in the Angouran Zn-(Pb–Ag) deposit, NW Iran: interaction of sedimentary brines with a metamorphic core complex: Mineralium Deposita. 41, 1-16.

Grandia, F., Canals, A., Cardellach, E., Banks, D. A., and Perona, J., 2003. Origin of Ore-Forming Brines in Sediment-Hosted Zn-Pb Deposits of the Basque-Cantabrian Basin, Northern Spain: Economic Geology. 98, 1397-1411.

Gulson, B. L., Perkins, W. G., and Mizon, K. J., 1983. Lead isotope studies bearing on the genesis of copper orebodies at Mount Isa, Queensland: Economic Geology and the Bulletin of the Society of Economic Geologists. 78, 1466-1504.

Hannan, K. W., Golding, S. D., Herbert, H. K., and Krouse, H. R., 1993. Contrasting alteration assemblages in metabasites from Mount Isa, Queensland; implications for copper ore genesis: Economic Geology and the Bulletin of the Society of Economic Geologists. 88, 1135-1175.

Heinrich, C. A., Andrew, A. S., Wilkins, R. W. T., and Patterson, D. J., 1989. A fluid inclusion and stable isotope study of synmetamorphic copper ore formation at Mount Isa, Australia: Economic Geology and the Bulletin of the Society of Economic Geologists. 84, 529-550.

Heinrich, C. A., Bain, J. H. C., Mernagh, T. P., Wyborn, L. A. I., Andrew, A. S., and Waring, C. L., 1995. Fluid and mass transfer during metabasalt alteration and copper mineralization at Mount Isa, Australia. Economic Geology and the Bulletin of the Society of Economic Geologists. 90, 705-730.

Heinrich, C. A., Bain, J. H. C., Fardy, J. J., and Waring, C. L., 1993. Br/Cl geochemistry of hydrothermal brines associated with Proterozoic metasediment-hosted copper mineralization at Mount Isa, northern Australia: Geochimica et Cosmochimica Acta. 57, 2991-3000.

Heinrich, C. A., and Cousens, D. R., 1989. Semi-quantitative electron microprobe analysis of fluid inclusion salts from the Mount Isa copper deposit (Queensland, Australia): Geochimica et Cosmochimica Acta. 53, 21-28.

Huizenga, J.-M., Gutzmer, J., Banks, D., and Greyling, L., 2006. The Paleoproterozoic carbonate-hosted Pering Zn–Pb deposit, South Africa. II: fluid inclusion, fluid chemistry and stable isotope constraints: Mineralium Deposita. 40, 686-706.

Johnson, A., Shelton, K., Gregg, J., Somerville, I., Wright, W., and Nagy, Z., 2009. Regional studies of dolomites and their included fluids: recognizing multiple chemically distinct fluids during the complex diagenetic history of Lower Carboniferous (Mississippian) rocks of the Irish Zn-Pb ore field: Mineralogy and Petrology. 96, 1-18.

Kendrick, M. A., Duncan, R., and Phillips, D., 2006. Noble gas and halogen constraints on mineralizing fluids of metamorphic versus surficial origin: Mt Isa, Australia: Chemical Geology. 235, 325-351.

Kendrick, M. A., Mark, G., and Phillips, D., 2007. Mid-crustal fluid mixing in a Proterozoic Fe oxide Cu Au deposit, Ernest Henry, Australia: Evidence from Ar, Kr, Xe, Cl, Br, and I; in Earth and Planetary Science Letters. 256, 328-343.

Kesler, S. E., Appold, M. S., Martini, A. M., Walter, L. M., Huston, T. J., and Richard Kyle, J., 1995. Na-Cl-Br systematics of mineralizing brines in Mississippi Valley-type deposits: Geology. 23. 641-644.

Kesler, S. E., Martini, A. M., Appold, M. S., Walter, L. M., huston, T. J., and furman, F. C., 1996. Na-Cl-Br systematics of fluid inclusions from Mississippi Valley-type deposits, Appalachian Basin: Constraints on solute origin and migration paths: Geochimica et Cosmochimica Acta. 60, 225-233.

Kesler, S. E., Reich, M., and Jean, M., 2007. Geochemistry of fluid inclusion brines from Earth's oldest Mississippi Valley-type (MVT) deposits, Transvaal Supergroup, South Africa: Chemical Geology. 237, 274-288.

Kühn, M., Dobert, F., and Gessner, K., 2006. Numerical investigation of the effect of heterogeneous permeability distributions on free convection in the hydrothermal system at Mount Isa, Australia: Earth and Planetary Science Letters. 244, 655-671.

Kühn, M., and Gessner, K., 2006. Reactive transport model of silicification at the Mount Isa copper deposit, Australia: Journal of Geochemical Exploration. 89, 195-198.

Kühn, M., and Gessner, K., 2009. Testing Hypotheses for the Mount Isa Copper Mineralisation with Numerical Simulations: Surveys in Geophysics. 30, 253-268.

Love, L. G., and Zimmerman, D. O., 1961, Bedded pyrite and micro-organisms from the Mount Isa shale: Economic Geology and the Bulletin of the Society of Economic Geologists. 56, 873-896.

Mathias, B. V., and Clark, G. J., 1975. Mount Isa copper and silver-lead-zinc orebodies; Isa and Hilton mines: Monograph Series - Australasian Institute of Mining and Metallurgy. 5, 351-371.

McDonald, J. A., 1970. Some effects of deformation on sulfide-rich layers in lead-zinc ore bodies, Mount Isa, Queensland: Economic Geology and the Bulletin of the Society of Economic Geologists. 65, 273-298.

McDonald, J. A., and Williams, N., 1980. Cyclicity in the lead-zinc-silver-bearing sediments at Mount Isa Mine, Queensland, Australia, and rates of sulfide accumulation; discussion: Economic Geology and the Bulletin of the Society of Economic Geologists. 75, 1239-1241.

McGoldrick, P. J., and Keays, R. R., 1990. Mount Isa copper and lead-zinc-silver ores; coincidence or cogenesis?: Economic Geology and the Bulletin of the Society of Economic Geologists. 85, 641-650.

Miller, J. M., 2007. Structural controls on the Mt Isa Copper deposit, QLD, Project I7, Predictive Mineral Discovery CoOperative Research Centre.

Oliver, N. H. S., McLellan, J. G., Hobbs, B. E., Cleverley, J. S., Ord, A. & Feltrin, L. 2006 Numerical Models of Extensional Deformation, Heat Transfer, and Fluid Flows across Basement-Cover Interfaces during Basin-Related Mineralization. Economic Geology, 101, 1 – 31.

Page, R. W., Jackson, M. J., and Krassay, A. A., 2000. Constraining sequence stratigraphy in North Australian basins; SHRIMP U-Pb zircon geochronology between Mt Isa and McArthur River: Australian Journal of Earth Sciences. 47, 431-459.

Perkins, W. G., 1984. Mount Isa silica dolomite and copper orebodies: The result of a syntectonic hydrothermal alteration system: Economic Geology. 79, 601 - 637.

Perkins, W. G., 1990. Mount Isa copper orebodies: Geology of the mineral deposits of Australia and Papua New Guinea. 14, 935-941.

Perkins, W. G., 1997, Mount Isa lead-zinc orebodies; replacement lodes in a zoned syndeformational copper-lead-zinc system?: Ore Geology Reviews. 12, 61-111.

Robertson, C. W., 1982. The role of pre-existing sulphides in copper-ore formation at Mount Isa, Queensland: BMR Journal of Australian Geology and Geophysics. 7, 119-124.

Scott, K. M., 1989. Dolomite compositions as a guide to epigenetic copper mineralization, Mount Isa Inlier, NW Queensland: Mineralium Deposita. 24, 29-33.

Seyfried Jr, W. E., and Bischoff, J. L., 1979. Low temperature basalt alteration by sea water: an experimental study at 70°C and 150°C: Geochimica et Cosmochimica Acta, 43, 1937-1947.

Smith, W. D., 1969. Penecontemporaneous faulting and its likely significance in relation to Mt Isa ore deposition: Special Publication - Geological Society of Australia. 2, 225-235.

Solomon, P. J., 1965. Investigations into sulfide mineralization at Mount Isa, Queensland: Economic Geology and the Bulletin of the Society of Economic Geologists. 60, 737-765.

Stanton, R. L., 1963. Elemental constitution of the Black Star orebodies, Mount Isa, Queensland, and its interpretation: Inst Min & Met , B. 672, 69-124.

Swager, C. P., 1983. Microstructural development of the silica-dolomite and copper mineralisation at Mount Isa, north-west Queensland, with speacial emphasis on the timing and mechanism of mineralisation, Ph.D. thesis, James Cook Univ.

Swager, C. P., 1985. Syndeformational carbonate-replacement model for the copper mineralization at Mount Isa, Northwest Queensland; a microstructural study: Economic Geology and the Bulletin of the Society of Economic Geologists. 80, 107-125.

Swager, C. P., Perkins, W. G., and Knights, J. G., 1987. Stratabound phyllosilicate zones associated with syntectonic copper orebodies at Mt. Isa, Queensland: Australian Journal of Earth Sciences. 34, 463-476.

Vandeginste, V., Swennen, R., Gleeson, S., Ellam, R., Osadetz, K., and Roure, F., 2007. Geochemical constraints on the origin of the Kicking Horse and Monarch Mississippi Valley-type lead-zinc ore deposits, southeast British Columbia, Canada: Mineralium Deposita. 42, 913-935.

Waring, C. L., Heinrich, C. A., and Wall, V. J., 1998. Proterozoic metamorphic copper deposits: AGSO Journal of Australian Geology and Geophysics. 17, 239-246.

Wilde, A. R., Jones, P. A., Gessner, K., Ailleres, L., Gregory, M. J., and Duncan, R. J., 2006. A Geochemical Process Model for the Mount Isa Copper Orebodies: Economic Geology. 101, 1547-1567.

Wilkinson, J. J., 2001. Fluid inclusions in hydrothermal ore deposits: Lithos. 55, 229-272.

Williams, P. J., Barton, M. D., Johnson, D. A., Fontbote, L., De Haller, A., Mark, G., Oliver, N. H. S., and Marschik, R. 2005 Iron Oxide Copper-Gold Deposits: Geology, Space-Time Distribution, and Possible Modes of Origin. In: Hedenquist JW, Thompson JFH, Goldfarb RJ, and Richards JP (Eds) Economic Geology 100th Anniversary Volume 1905-2005. Society of Economic Geologists Inc, Colorado. 371-405.

Synopsis

When and how did the Eastern Creek Volcanics become juxtaposed against the Mount Isa Group?

Four models have been put forward to explain the juxtaposition of the Eastern Creek Volcanics against the Mount Isa Group. The model of MacCready (2006) requires three faults which would have a similar orientation to the Satellite-Biotite Fault, Native Bee Fault and the Clone Fault to explain the sigmoidal geometry and juxtaposition. There is no evidence of three such structures from the drill-holes or mine mapping database. Dunnet's (1976) "spoon fault" model was argued against by Bell et al. (1988) on the basis that the sigmoidal shape of the Paroo Fault could not be formed by this method without later complex interfering folds. Work examining the locations of importance to Bell's (1988) thrust duplex model for the formation of the Paroo Fault has shown there is no evidence of the roof thrusts in these areas and demonstrated that the thrust imbricates are actually normal faults (Stewart, 1992). Bell's (1988) model only manages to place younger rocks on old during thrusting by using a very complex geometrical argument. A much simpler alternative is a simple reactivated normal fault put forward by Betts and Lister (2002) and Betts et al. (2003). In this model the Paroo Fault developed during the Leichhardt Rift as a normal fault bounding a half graben and was reactivated during the late stages of the Mount Isa Rift Event.

The first reactivation occurred as a second stage of normal movement on the fault, propagating upwards into sediments which previously lay above the submerged rift margin, and juxtaposing Eastern Creek Volcanics against the Urquhart Shale. This sequence of events is firstly required to explain the abrupt juxtaposition of finely bedded carbonaceous shales (e.g. Urquhart Shale), with no observed thickness change approaching the fault, against the basement rocks, with the shales being at a very high angle to the fault. Secondly, the presence of hangingwall synforms in the Magazine Shale and the Kennedy Siltstone is tentatively proposed to be a consequence of compaction (with subsequent tightening during later Orogeny) during the burial of the uppermost formations of the Mount Isa Group, above the Urquhart Shale.

What was the sequence of deformation events that affected the host rocks and Paroo Fault?

After the initial normal-sense reactivation of the Paroo Fault, there was a phase of north-south shortening (D_1) that has apparently not affected the Paroo Fault, but caused the formation of north-south orientated folds that have 100 -10 m scale amplitudes. The open to gentle folds (80^o-170^o) were recognised from the reinterpretation of mine mapping (Paper 3). These folds have not been documented before at mine scales. The east-west folds were followed by a period of east-west shortening (D_2) that has caused the macroscale bends in the Paroo Fault as well as two pairs of north-south orientated synforms and antiforms with amplitudes between 200-300 m, shown by the Gaussian curvature analysis (Paper 1). North-south folds have also been observed from the reinterpretation of the mine mapping (Paper 3) within the Urquhart Shale. However it is not clear whether these folds formed in D_2 or resulted from variable folding during a subsequent event (e.g. D_3). ENE-WSW shortening (D_3) has caused two of NNW-trending synform antiform pairs in the Paroo Fault (recognised from the Gaussian curvature analysis), which have amplitudes of 100-300 m, which appear to interfere with the north-south orientated folds (D_2) of the Paroo Fault (Paper 1). These folds have been observed at the outcrop scale to wrap around the copper orebodies (Paper 2). NNW trending folds have also been recognised within the Urquhart Shale from the reinterpretation of the mine mapping (Paper 3). These have smaller amplitudes (>10 m) and open inter-limb angles and can be seen to interfere with the east-west faults (D_1) and appear to wrap around the copper orebodies.

When and how did the Paroo Fault fill with alternations of quartz and graphite form?

The subparallel orientation of the alternations within the Paroo Fault filling, relative to the fault, in both the steeply and shallowly dipping portions of the fault may indicate that the fault zone filling developed prior to folding in D_2 (Paper 2). This may have been very early in D_2 or in D_1. The thickness analysis has shown that the fault zone filling is thicker west of the large D_2 antiform hinge and the east of the copper orebodies due to deformation and shearing during D_2 and D_3 (Paper 1). The fault zone filling may have developed from repeated cycles of extraction of quartz from the silica-depleted Urquhart Shale and precipitation of quartz within the fault (Paper 2). This may explain why the Paroo Fault does not have a core or associated damage zone. Because the Fault could have been infilled with quartz during its formation, and SEM-CL has shown that multiple generations of quartz and dolomite were precipitated and remobilized during subsequent deformation (Paper 2), the fault appears to have healed repeatedly during each successive deformation stage. The silica depletion also may have occurred after ore genesis (otherwise ore fluids would have favoured the particularly graphite-rich rocks for precipitation) but before at least one of the ductile deformation fabrics, as a crenulation cleavage (S_2/S_3?) is commonly observed in the very graphite rich rocks.

When and how did the copper orebodies and associated alteration form and what deformation events have affected them?

The macroscale (m-km) observations of the Paroo Fault geometric model appear to indicate that the NNW trending folds within the Paroo Fault appear to deviate around the copper orebodies (Paper 1). Exposure scale (cm-m) observations demonstrate that the Paroo Fault fill in these NNW folds has been buttressed against the copper orebodies (Paper 2). This indicates that the copper orebodies formed prior to the shortening event (D_3) that formed the NNW trending folds. The timing of the fault zone filling relative to ore genesis is also constrained by observations of common sulphur isotope reservoirs between ore and the altered footwall (Andrews et al., 1989), supported here by strong overlap in the Br/Cl ratios of halogens contained in ore chalcopyrite and chalcopyrite hosted in altered footwall rocks (Paper 4). This may indicate that the basement rocks were altered by the same fluid that formed the copper orebodies, and this interaction must have occurred before the Paroo Fault was sealed by quartz and graphite (Paper 2). Further support for a pre-D_3 timing for orebody formation comes from the reinterpretation of the mine mapping in which the NNW trending folds recognised within the Urquhart Shale are apparently folded around, or buttressed against, around the copper orebodies (Paper 3). This is a different timing to that suggested by previous authors (Swager, 1983; 1985; Perkins, 1984; Bell et al., 1988; Davis 2004). The main evidence for D_3 copper mineralisation was provided by Swager (1983; 1985) and Perkins (1984) as S_3 cleavage in clasts within the breccia and the absence of S_3 cleavage within silica-chalcopyrite matrix. A problem with this evidence is it does not preclude earlier precipitation of chalcopyrite followed by a further stage of brecciation (D_3) which remobilized the chalcopyrite. Dilation tendency results have shown that during D_3 sites favorable for remobilization will be created below the non-stratiform copper orebodies (Paper 1) and above NNW trending folds within the Paroo Fault. This remobilization during D_3 can explain why D_3 cleavage in clasts within the copper ore breccia has been observed by previous authors.

Based on all the above evidence, it appears the original introduction of ore was before the Paroo Fault sealed, and thus before its folding by D_2, but after the formation of D_1 E-W folds in the Urquhart Shale. Subsequent D_3 deformation may have created dilation at the crest of the D_2 and D_3 folds in the Paroo, causing large scale remobilization of the earlier ore into new structural locations. This new timing for the formation of the copper orebodies has a significant impact on the interpretation of the halogen data collected here and that collected by previous workers (Heinrich et al., 1989; Kendrick et al., 2006). The bittern brine source of the fluids which formed the copper orebodies does not need to be exotic as argued by Heinrich et al. (1989) who required a high Br fluid source to have been derived from evolved evaporitic sediments that travelled downwards into the core of the orogenic belt late during the deformation history. Firstly, an early orogenic timing for ore genesis would have allowed the preservation of evolved basinal brines in the host sequences, thus making it easier to attain high Br/Cl ratios in the ores, rather than appealing to the difficult scenario of halogens derivation from an unidentified source. The Br/Cl ratios determined in this study and by Kendrick et al. (2006) range down to much lower values than recorded by Heinrich et al. (1993), down to as low as modern seawater (Paper 4). Thus, a mixing of low Br/Cl, probably high CO_2 early metamorphic fluids, with descending intrabasinal brines, may have provided favourable conditions for ore genesis.

The localisation of the copper orebodies within the Urquhart Shale during D_1 or early D_2 is not well constrained geometrically because of the subsequent deformation history. However, it was most likely to be due to a chemical and/or rheological anomaly generated by the sedimentary diagentic process associated with the early lead-zinc-silver orebodies (Heinrich et al., 1995). An untested possibility is that an early fault bend, or perhaps the anomalous mechanical properties of the early Pb-Zn-Ag orebodies, focussed fluid into the copper depositional sites, and also triggered an amplification of subsequent folds, and favourable conditions for strong remobilisation, during the Isan Orogeny.

Future work

Further halogens systematics on the lead-zinc-silver orebodies needs to be done to conclusively demonstrate that the copper orebodies are not genetically related to these orebodies. Copper and sulphur isotopes undertaken by LA-ICPMS will help to define the source of the copper at Mount Isa. An examination of the shape of the Paroo Fault north of the Mount Isa copper deposit at George Fisher mine may make a useful comparison for understanding the localisation of the copper mineralisation as there is no copper, only syngentic lead-zinc-silver mineralisation, in this mine. The spanned length analysis can be applied to a variety of geological structures instead of the more commonly used divider method for roughness studies.

Exploration Implications

Pre-existing faults that have been folded during D_2 may contain D_2 fold bends above which there is significant chalcopyrite mineralisation. These folded faults can be identified by looking for faults with orientations favourable for folding during D_2 (dominantly north-south striking faults) in rocks that were deposited before D_2. At the mine-scale there is an area of the Paroo Fault south of the copper orebodies, that has been demonstrated to have a high (>0.8) dilation tendency (Fig. 13). As the two other areas of the Paroo fault with a high dilation tendency have significant copper mineralisation directly above them, this is a target for future exploration dilling.

References:

Adshead-Bell, N. S. 1998. Evolution of the Starra and Selwyn high-strain zones, Eastern fold belt, Mount Isa Inlier; implications for Au-Cu mineralization. Economic Geology 93, 1450-1462.

Andrés, M., Tatiana, G., Jonas, K., Diana, M., Mauricio, P., Luis Ignacio, Q., German, R. & Manfred, R. S. 2009. The role of inherited extensional fault segmentation and linkage in contractional orogenesis: a reconstruction of Lower Cretaceous inverted rift basins in the Eastern Cordillera of Colombia. Basin Research 21, 111-137.

Andrew, A. S., Heinrich, C. A., Wilkins, R. W. T. & Patterson, D. J. 1989. Sulfur isotope systematics of copper ore formation at Mount Isa, Australia. Economic Geology and the Bulletin of the Society of Economic Geologists 84, 1614-1626.

Aviles, C. A., and Scholz, C. H., 1987. Fractal Analysis Applied to Characteristic Segments of the San Andreas Fault. Journal of Geophysical Research 92, 331-344.

Bell, T. H. 1983. Thrusting and duplex formation at Mount Isa. Nature 304, 493-497.

Bell, T. H., 1991. The Role of thrusting in the Structural Development of the Mount Isa Mine and its Relevance to Exploration in the Surrounding Region: Economic Geology. 86, 1602-1625.

Bell, T. H. & Hickey, K. A. 1998. Multiple Deformations with Successive Subvertical and Subhorizontal Axial Planes in the Mount Isa Region: Their Impact on Geometric Development and Significance for Mineralization and Exploration. Economic Geology 93, 1369-1389.

Bell, T. H., Perkins, W. G. & Swager, C. P. 1988. Structural controls on development and localization of syntectonic copper mineralization at Mount Isa, Queensland. Economic Geology and the Bulletin of the Society of Economic Geologists 83, 69-85.

Betts, P. G., 2001, Three-dimensional structure along the inverted Palaeoproterozoic Fiery Creek fault system, Mount Isa Terrane, Australia. Journal of Structural Geology 23, 1953-1969.

Betts, P. G. 1999. Palaeoproterozoic mid-basin inversion in the northern Mt. Isa terrane, Queensland. Australian Journal of Earth Sciences 46, 735-748.

Betts, P. G., Giles, D. & Lister, G. S. 2003. Tectonic environment of shale-hosted massive sulfide Pb-Zn-Ag deposits of Proterozoic northeastern Australia. Economic Geology and the Bulletin of the Society of Economic Geologists 98, 557-576.

Betts, P. G., Giles, D., Mark, G., Lister, G. S., Goleby, B. R., and Aillères, L., 2006, Synthesis of the proterozoic evolution of the Mt Isa Inlier. Australian Journal of Earth Sciences 53, 187-211.

Betts, P. G., and Lister, G. S., 2001, Comparison of the 'strike-slip' versus the 'episodic rift -sag' models for the origin of the Isa Superbasin. Australian Journal of Earth Sciences 48, 265-280.

Betts, P. G. & Lister, G. S. 2002. Geodynamically indicated targetting strategy for shale-hosted massive sulfide Pb-Zn-Ag mineralisation in the Western Fold Belt, Mt Isa terrane. Australian Journal of Earth Sciences 49, 985-1010.

Betts, P. G., Lister, G. S. & O'Dea, M. G. 1998. Asymmetric extension of the middle Proterozoic lithosphere, Mount Isa Terrane, Queensland, Australia. Tectonophysics 296, 293-316.

Betts, P. G., Lister, G. S., and Pound, K. S., 1999, Architecture of a Palaeoproterozoic rift system; evidence from the Fiery Creek Dome region, Mt. Isa Terrane. Australian Journal of Earth Sciences 46, 533-554.

Blanchard, R. & Hall, G. 1937. Mount Isa [Queensland] ore deposition. Economic Geology and the Bulletin of the Society of Economic Geologists, 32, 1042-1057.

Blenkinsop, T. G. 2008. Relationships between faults, extension fractures and veins, and stress. Journal of Structural Geology, 30, 622-632.

Brems, D., Muchez, P., Sikazwe, O. & Mukumba, W. 2009. Metallogenesis of the Nkana copper-cobalt South Orebody, Zambia. Journal of African Earth Sciences, 55, 185-196.

BMR. 1978. Mount Isa 1:100 000 Geological Series, Sheet 6756 (edited by Australia, G.).

Butler, R. W. H. 1989. The influence of pre-existing basin structure on thrust system evolution in the Western Alps. Geological Society of London, Special Publications 44, 105-122.

Caine, J. P., Evans, J. P. & Forster, C. B. 1996. Fault zone architecture and permeability structure. Geology 24, 1025-1028.

Candela, T., Renard, F., Bouchon, M., Brouste, A., Marsan, D., Schmittbuhl, J. & Voisin, C. 2009. Characterization of Fault Roughness at Various Scales: Implications of Three-Dimensional High Resolution Topography Measurements. Pure and Applied Geophysics 166, 1817-1851.

Carr, G., 2010. Giant Pb-Zn ores revealed by their Pb Isotopes, 13th Quadrennial IAGOD Symposium 2010 'GIANT ORE DEPOSITS DOWN-UNDER' Adelaide, Australia.

Chetty, D., and Frimmel, H. E., 2000. The role of evaporites in the genesis of base metal sulphide mineralisation in the Northern Platform of the Pan-African Damara Belt, Namibia: geochemical and fluid inclusion evidence from carbonate wall rock alteration: Mineralium Deposita. 35, 364-376.

Childs, C., Manzocchi, T., Walsh, J. J., Bonson, C. G., Nicol, A. & Schöpfer, M. P. J. 2009. A geometric model of fault zone and fault rock thickness variations. Journal of Structural Geology 31, 117-127.

Childs, C., Nicol, A., Walsh, J. J. & Watterson, J. 2003. The growth and propagation of synsedimentary faults. Journal of Structural Geology 25, 633-648.

Connolly, .A., Walter, .M., Baadsgaard,H., and. Longstaffe, F.J. 1990 Origin and evolution of formation waters, Alberta Basin, Western Canada Sedimentary Basin. I. Chemistry. *Appl. Geochem.,* 5, 375–395.

Connors, K. 1992. Hunter Resources Limited EPM 8315: Structural Controls on MIneralization in the Gunpowder Area. Etheridge & Henley Geoscience Consultants, 37.

Connors, K. A. & Lister, G. S. 1995. Polyphase deformation in the western Mount Isa Inlier, Australia; episodic or continuous deformation? Journal of Structural Geology 17, 305-328.

Connors, K. A., Proffett, J. M., Lister, G. S., Scott, R. J., Oliver, N. H. S. & Young, D. J. 1992. Geology of the Mount Novit Ranges, southwest of Mt Isa mine. In: Detailed Studies of the Mt Isa Inlier (edited by Stewart, A. J. & Blake, D. H.) 243. Australian Geological Survey Organisation, Canberra, 137-160.

Cooke, D. R., Bull, S. W., Large, R. R., and McGoldrick, P. J. 2000 The Importance of Oxidized Brines for the Formation of Australian Proterozoic Stratiform Sediment-Hosted Pb-Zn (Sedex) Deposits; Economic Geology, 95, 1-18.

Cox, S. F. & Etheridge, M. A. 1983. Crack-seal fibre growth mechanisms and their significance in the development of oriented layer silicate microstructures. Tectonophysics 92, 147-170.

Craw, D. 2002. Geochemistry of late metamorphic hydrothermal alteration and graphitisation of host rock, Macraes gold mine, Otago Schist, New Zealand. Chemical Geology 191, 257-275.

Davidson, G. J., and Large, R. R. 1998. Proterozoic copper-gold deposits: Journal of Australian Geology and Geophysics, 17, 105-113.

Davis, T. P. 2004. Mine-scale structural controls on the Mount Isa Zn-Pb-Ag and Cu orebodies. Economic Geology and the Bulletin of the Society of Economic Geologists 99, 543-559.

Derrick, G. M. 1982. A Proterozoic rift zone at Mount Isa, Queensland, and implications for mineralisation. BMR Journal of Australian Geology and Geophysics 7, 81-92.

Dunnet, D. 1976. Mt Isa; reconstruction of a faulted ore body. Philosophical Transactions of the Royal Society of London, Series A: Mathematical and Physical Sciences 283, 333-344.

Farquharson, R. B. & Richards, J. R. 1974. U-Th-Pb isotope systematics related to igneous rocks and ore Pb, Mount Isa, Queensland. Mineralium Deposita 9, 339-356.

Fernández-Martínez, J. L. & Lisle, R. J. 2009. GenLab: A MATLAB®-based program for structural analysis of folds mapped by GPS or seismic methods. Computers & Geosciences 35, 317-326.

Ferrill, D. A., Winterle, J., Wittmeyer, G., Sims, D., Colton, S., Armstrong, A., and Morris, A.P. 1999. Stressed Rock strains groundwater at yucca Mountain, Nevada. GSA Today 9, 1-8.

Finlow-Bates, T. 1979. Cyclicity in the lead-zinc-silver-bearing sediments at Mount Isa mine, Queensland, Australia, and rates of sulfide accumulation. Economic Geology and the Bulletin of the Society of Economic Geologists, 74, 1408-1419.

Finlow-Bates, T. 1980. Cyclicity in the lead-zinc-silver-bearing sediments at Mount Isa Mine, Queensland, Australia, and rates of sulfide accumulation; reply. Economic Geology and the Bulletin of the Society of Economic Geologists, 75, 8.

Finlow-Bates, T. & Stumpfl, E. F. 1979. The copper and lead-zinc-silver orebodies of Mt. Isa Mine, Queensland; products of one hydrothermal system. Annales de la Societe Geologique de Belgique 102, 497-517.

Gessner, K. 2009. Coupled Models of Brittle-plastic Deformation and Fluid Flow: Approaches, Methods, and Application to Mesoproterozoic Mineralisation at Mount Isa, Australia. Surveys in Geophysics 30, 211-232.

Gessner, K., Jones, P. A., Wilde, A. R. & Kühn, M.2006. Significance of strain localization and fracturing in relation to hydrothermal mineralization at Mount Isa, Australia. Journal of Geochemical Exploration 89, 129-132.

Ghisetti, F. C. & Sibson, R. H. 2006. Accommodation of shorteningal inversion in north-western South Island (New Zealand): Old faults versus new? Journal of Structural Geology 28, 1994-2010.

Giaccio, B., Galadini, F., Sposato, A., Messina, P., Moro, M., Zreda, M., Cittadini, A., Salvi, S. & Todero, A. 2003. Image processing and roughness analysis of exposed bedrock fault planes as a tool for paleoseismological analysis: results from the Campo Felice fault (central Apennines, Italy). Geomorphology 49, 281-301.

Gibson, G. M. & Henson, P. A. 2005. Chapter 6: Post-depositional deformation in the Western Succession. In: Project I1: 3D Basin Architecture & Mineral Systems in the Mt Isa Western Succession (edited by Gibson, G. M. & Hitchman, A. P.). Predictive Mineral Discovery Cooperative Research Centre, Canberra, 147-176.

Gilg, H., Boni, M., Balassone, G., Allen, C., Banks, D., and Moore, F., 2006. Marble-hosted sulfide ores in the Angouran Zn-(Pb–Ag) deposit, NW Iran:

interaction of sedimentary brines with a metamorphic core complex: Mineralium Deposita. 41, 1-16.

Grandia, F., Canals, A., Cardellach, E., Banks, D. A., and Perona, J., 2003. Origin of Ore-Forming Brines in Sediment-Hosted Zn-Pb Deposits of the Basque-Cantabrian Basin, Northern Spain: Economic Geology. 98, 1397-1411.

Gray, D. R. & Gregory, R. T. 2003. Fault geometry as evidence for inversion of a former rift basin in the Eastern Lachlan Orogen. Australian Journal of Earth Sciences: An International Geoscience Journal of the Geological Society of Australia 50, 513 - 523.

Gulson, B. L., Perkins, W. G. & Mizon, K. J. 1983. Lead isotope studies bearing on the genesis of copper orebodies at Mount Isa, Queensland. Economic Geology and the Bulletin of the Society of Economic Geologists 78, 1466-1504.

Hannan, K. W., Golding, S. D., Herbert, H. K. & Krouse, H. R. 1993. Contrasting alteration assemblages in metabasites from Mount Isa, Queensland; implications for copper ore genesis. Economic Geology and the Bulletin of the Society of Economic Geologists 88, 1135-1175.

Hayward, A. B. & Graham, R. H. 1989. Some geometrical characteristics of inversion. Geological Society London, Special Publications 44, 17-39.

Heinrich, C. A., Andrew, A. S., Wilkins, R. W. T. & Patterson, D. J. 1989. A fluid inclusion and stable isotope study of synmetamorphic copper ore formation at Mount Isa, Australia. Economic Geology and the Bulletin of the Society of Economic Geologists 84, 529-550.

Heinrich, C. A., Bain, J. H. C., Mernagh, T. P., Wyborn, L. A. I., Andrew, A. S., and Waring, C. L., 1995, Fluid and mass transfer during metabasalt alteration and copper mineralization at Mount Isa, Australia. Economic Geology and the Bulletin of the Society of Economic Geologists 90, 705-730.

Heinrich, C. A., Bain, J. H. C., Fardy, J. J. & Waring, C. L. 1993. Br/Cl geochemistry of hydrothermal brines associated with Proterozoic metasediment-hosted copper mineralization at Mount Isa, northern Australia. Geochimica et Cosmochimica Acta 57, 2991-3000.

Heinrich, C. A. & Cousens, D. R. 1989. Semi-quantitative electron microprobe analysis of fluid inclusion salts from the Mount Isa copper deposit (Queensland, Australia). Geochimica et Cosmochimica Acta 53, 21-28.

Holdsworth, R. E., Stewart, M., Imber, J. & Strachan, R. A. 2001. The structure and rheological evolution of reactivated continental fault zones: a review and case study. Geological Society of London, Special Publications 184, 115-137.

Huizenga, J.-M., Gutzmer, J., Banks, D., and Greyling, L., 2006. The Paleoproterozoic carbonate-hosted Pering Zn–Pb deposit, South Africa. II:

fluid inclusion, fluid chemistry and stable isotope constraints: Mineralium Deposita. 40, 686-706.

Jackson, J. & McKenzie, D. 1999. A hectare of fresh striations on the Arkitsa Fault, central Greece. Journal of Structural Geology 21, 1-6.

Jackson M.J., Scott D.L. & Rawlings D.J. 2000. Stratigraphic framework for the Leichhardt and Calvert Superbasins: review and correlations of the pre-1700 Ma successions between Mt Isa and McArthur River. Australian Journal of Earth Sciences 47, 381-403.

Johnson, A., Shelton, K., Gregg, J., Somerville, I., Wright, W., and Nagy, Z., 2009. Regional studies of dolomites and their included fluids: recognizing multiple chemically distinct fluids during the complex diagenetic history of Lower Carboniferous (Mississippian) rocks of the Irish Zn-Pb ore field: Mineralogy and Petrology. 96, 1-18.

Kelly, P. G., Peacock, D. C. P., Sanderson, D. J. & McGurk, A. C. 1999. Selective reverse-reactivation of normal faults, and deformation around reverse-reactivated faults in the Mesozoic of the Somerset coast. Journal of Structural Geology 21, 493-509.

Kendrick, M. A., Duncan, R. & Phillips, D. 2006. Noble gas and halogen constraints on mineralizing fluids of metamorphic versus surficial origin: Mt Isa, Australia. Chemical Geology 235, 325-351.

Kendrick, M. A., Mark, G., and Phillips, D., 2007. Mid-crustal fluid mixing in a Proterozoic Fe oxide Cu Au deposit, Ernest Henry, Australia: Evidence from Ar, Kr, Xe, Cl, Br, and I; in Earth and Planetary Science Letters. 256, 328-343.

Kesler, S. E., Appold, M. S., Martini, A. M., Walter, L. M., Huston, T. J., and Richard Kyle, J., 1995. Na-Cl-Br systematics of mineralizing brines in Mississippi Valley-type deposits: Geology. 23. 641-644.

Kesler, S. E., Martini, A. M., Appold, M. S., Walter, L. M., huston, T. J., and furman, F. C., 1996. Na-Cl-Br systematics of fluid inclusions from Mississippi Valley-type deposits, Appalachian Basin: Constraints on solute origin and migration paths: Geochimica et Cosmochimica Acta. 60, 225-233.

Kesler, S. E., Reich, M., and Jean, M., 2007. Geochemistry of fluid inclusion brines from Earth's oldest Mississippi Valley-type (MVT) deposits, Transvaal Supergroup, South Africa: Chemical Geology. 237, 274-288.

Keys, D. (2009) Mechanical localization of copper deposits in the Mt Isa Inlier, North Queensland , Ph.D. thesis, James Cook Univ.

Kondo, H., Awata, Y., Emre, O., Dogan, A., Ozalp, S., Tokay, F., Yildirim, C., Yoshioka, T. & Okumura, K. 2005. Slip Distribution, Fault Geometry, and Fault Segmentation of the 1944 Bolu-Gerede Earthquake Rupture, North Anatolian Fault, Turkey. Bulletin of the Seismological Society of America 95, 1234-1249.

Kühn, M., Dobert, F. & Gessner, K. 2006. Numerical investigation of the effect of heterogeneous permeability distributions on free convection in the hydrothermal system at Mount Isa, Australia. Earth and Planetary Science Letters 244, 655-671.

Kühn, M. & Gessner, K. 2006. Reactive transport model of silicification at the Mount Isa copper deposit, Australia. Journal of Geochemical Exploration 89, 195-198.

Kühn, M. & Gessner, K. 2009. Testing Hypotheses for the Mount Isa Copper Mineralisation with Numerical Simulations. Surveys in Geophysics 30, 253-268.

Lisle, R. J., Fernandez Martinez, J. L., Bobillo-Ares, N., Menendez, O., Aller, J. & Bastida, F. 2006. FOLD PROFILER: A MATLAB—based program for fold shape classification. Computers & Geosciences 32, 102–108.

Lisle, R. J. & Srivastava, D. C. 2004. Test of the frictional reactivation theory for faults and validity of fault-slip analysis. Geology 32, 569-572.

Lister, G. S. 1993. The role of thrusting in the structural development of the Mount Isa Mine and its relevance to exploration in the surrounding region; discussion. Economic Geology and the Bulletin of the Society of Economic Geologists 88, 479.

Lister G.S., O'Dea M.G. & Somaia I. 1999. A tale of two synclines: rifting, inversion and transpressional popouts at Lake Julius, northwestern Mt Isa terrane, Queensland. Australian Journal of Earth Sciences 46, 233-250.

Loosveld, R. & Schreurs, G. 1987. Discovery of thrust klippen, northwest of Mary Kathleen, Mt. Isa Inlier, Australia. Australian Journal of Earth Sciences 34, 387-402.

Love, L. G. & Zimmerman, D. O. 1961. Bedded pyrite and micro-organisms from the Mount Isa shale. Economic Geology and the Bulletin of the Society of Economic Geologists, 56, 873-896.

Lowell, J. D. 1968. Geology of the Kalamazoo orebody, San Manuel District, Arizona. Economic Geology**, 63,** 645-654.

MacCready, T. 2006. Structural evolution of the southern Mt Isa Valley. Australian Journal of Earth Sciences 53, 27-40.

Mathias, B. V. & Clark, G. J. 1975. Mount Isa copper and silver-lead-zinc orebodies; Isa and Hilton mines. Monograph Series - Australasian Institute of Mining and Metallurgy no. 5, 351-371.

Mazzoli, R. W. H. B. a. S. 2006. Styles of continental contraction: A review and introduction. Geological Society of America Special Papers 414, 1-10.

McDonald, J. A. 1970. Some effects of deformation on sulfide-rich layers in lead-zinc ore bodies, Mount Isa, Queensland. Economic Geology and the Bulletin of the Society of Economic Geologists 65, 273-298.

McDonald, J. A. & Williams, N. 1980. Cyclicity in the lead-zinc-silver-bearing sediments at Mount Isa Mine, Queensland, Australia, and rates of sulfide accumulation; discussion. Economic Geology and the Bulletin of the Society of Economic Geologists, 75, 8.

McGoldrick, P. J. & Keays, R. R. 1990. Mount Isa copper and lead-zinc-silver ores; coincidence or cogenesis? Economic Geology and the Bulletin of the Society of Economic Geologists 85, 641-650.

Miller, J. M. 2007. Structural controls on the Mt Isa Copper deposit, QLD. In: Project I7. Predictive Mineral Discovery CoOperative Research Centre, 70.

Miller, J. M., Dugdale, L. J. & Wilson, C. J. L. 2001. Variable hangingwall palaeotransport during Silurian and Devonian thrusting in the western Lachlan Fold Belt: missing gold lodes, synchronous Melbourne Trough sedimentation and Grampians Group fold interference. Australian Journal of Earth Sciences: An International Geoscience Journal of the Geological Society of Australia, 48, 901 - 909.

Miller, J. M. & Wilson, C. J. L. 2004. Structural analysis of faults related to a heterogeneous stress history: reconstruction of a dismembered gold deposit, Stawell, western Lachlan Fold Belt, Australia. Journal of Structural Geology, 26, 1231-1256.

Moeck, I., Kwiatek, G. & Zimmermann, G. 2009. Slip tendency analysis, fault reactivation potential and induced seismicity in a deep geothermal reservoir. Journal of Structural Geology 31, 1174-1182.

Morris, A., Ferrill, D. A. & Henderson, D. B. 1996. Slip-tendency analysis and fault reactivation. Geology 24, 275-278.

Mote, T. I., Brimhall, G. H., Tidy-Finch, E., Muller, G. & Carrasco, P. 2001. Application of Mass-Balance Modeling of Sources, Pathways, and Sinks of Supergene Enrichment to Exploration and Discovery of the Quebrada Turquesa Exotic Copper Orebody, El Salvador District, Chile. Economic Geology, 96, 367-386.

Mynatt, I., Bergbauer, S. & Pollard, D. D. 2007. Using diffrential geometry to describe 3-D folds. Journal of Structural Geology 29, 1256-1266.

Nemcok, M., Moore, J. N., Allis, R. & McCulloch, J. 2004. Fracture development within a stratovolcano: the Karaha-Telaga Bodas geothermal field, Java volcanic arc. Geological Society of London, Special Publications 231, 223-242.

Nijman, W., Mijnlieff, H. F. & Schalkwijk, G. 1992a. The Hero Fan Delta (Lower Mount Isa Group) and its structural control: deformation in the Hero/Western Fault Zone and Paroo Range compared, Proterozoic, Mount Isa Inlier, Queensland, Australia. In: Detailed Studies of the Mount Isa Inlier (edited by Stewart, A. J. & Blake, D. H.) 243. Australian Geological Survey Organisation, Canberra, 75-110.

Nijman, W., van Lochem, J. H., Spliethoff, H. & Feijth, J. 1992b. Deformation model and sedimentation patterns of the Proterozoic of the Paroo Range, Mount Isa Inlier, Queensland, Australia, . In: Detailed Studies of the Mount Isa Inlier (edited by Stewart, A. J. & Blake, D. H.) Australian Geological Survey Organisation Bulletin 243, Canberra.

O'Dea, M. G., Lister, G., MacCready, T., Betts, P. G., Oliver, N. H. S., Pound, K. S., Huang, W. & Valenta, R. K. 1996. Geodynamic evolution of the Proterozoic Mount Isa terrain., in Burg, J.P., and Ford, M., eds., Orogeny through time. Geological Society Special Publication 121, 99-122.

O'Dea, M. G. & Lister, G. S. 1995. The role of ductility contrast and basement architecture in the structural evolution of the Crystal Creek Block, Mount Isa Inlier, NW Queensland, Australia. Journal of Structural Geology 17, 949-960.

O'Dea, M. G., Lister, G. S., Betts, P. G. & Pound, K. S. 1997a. A shortened intraplate rift system in the Proterozoic Mount Isa terrane, NW Queensland, Australia. Tectonics 16, 425-441.

O'Dea, M. G., Lister, G. S., Maccready, T., Betts, P. G., Oliver, N. H. S., Pound, K. S., Huang, W., Valenta, R. K., Oliver, N. H. S. & Valenta, R. K. 1997b. Geodynamic evolution of the Proterozoic Mount Isa terrain. Geological Society of London, Special Publications 121, 99-122.

Oliver, N. H. S., McLellan, J. G., Hobbs, B. E., Cleverley, J. S., Ord, A. & Feltrin, L. 2006 Numerical Models of Extensional Deformation, Heat Transfer, and Fluid Flows across Basement-Cover Interfaces during Basin-Related Mineralization. Economic Geology, 101, 1 – 31.

Oliver, N. H. S., Valenta, R. K. & Wall, V. J. 1990. The effect of heterogeneous stress and strain on metamorphic fluid flow, Mary Kathleen, Australia, and a model for large-scale fluid circulation. Journal of Metamorphic Geology 8, 311-331.

Page, R. W., Jackson, M. J. & Krassay, A. A. 2000. Constraining sequence stratigraphy in North Australian basins; SHRIMP U-Pb zircon geochronology between Mt Isa and McArthur River. Australian Journal of Earth Sciences 47, 431-459.

Page, R. W., Stevens, B. P. J. & Gibson, G. M. 2005. Geochronology of the Sequence Hosting the Broken Hill Pb-Zn-Ag Orebody, Australia. Economic Geology, 100, 633-661.

Page, R. W. & Sweet, I. P. 1998. Geochronology of basin phases in the western Mt Isa Inlier, and correlation with the McArthur Basin. Australian Journal of Earth Sciences 45, 219-232.

Painter, M. G. M., Golding, S. D., Hannan, K. W. & Neudert, M. K. 1999. Sedimentologic, petrographic, and sulfur isotope constraints on fine-grained pyrite formation at Mount Isa Mine and environs, Northwest

Queensland, Australia. Economic Geology and the Bulletin of the Society of Economic Geologists 94, 883-912.

Perkins, C., Heinrich, C. A. & Wyborn, L. A. I. 1999. (super 40) Ar/ (super 39) Ar geochronology of copper mineralization and regional alteration, Mount Isa, Australia. Economic Geology and the Bulletin of the Society of Economic Geologists 94, 23-36.

Perkins, W. G. 1984. Mount Isa silica dolomite and copper orebodies: The result of a syntectonic hydrothermal alteration system. Economic Geology 79, 601-637.

Perkins, W. G. 1990. Mount Isa copper orebodies. Geology of the mineral deposits of Australia and Papua New Guinea 14, 935-941.

Perkins, W. G. 1997. Mount Isa lead-zinc orebodies; replacement lodes in a zoned syndeformational copper-lead-zinc system? Ore Geology Reviews 12, 61-111.

Perkins, W. G. 1998. Timing of formation of Proterozoic stratiform fine-grained pyrite; post-diagenetic cleavage replacement at Mount Isa? Metallogeny of the McArthur River-Mount Isa-Cloncurry minerals province 93, 1153-1164.

Power, W. L., and T. E. Tullis. 1995. A review of the fractal character of natural fault surfaces with implications for friction and the evolution of fault zones. In: Fractals in The Earth Sciences (edited by Barton, P. L. a. C.). Plenum, New York, 85-105.

Power, W. L. & Durham, W. B. 1997. Topography of natural and artificial fractures in granitic rocks: Implications for studies of rock friction and fluid migration. International Journal of Rock Mechanics and Mining Sciences 34, 979-989.

Power, W. L. & Tullis, T. E. 1992. The Contact Between Opposing Fault Surfaces at Dixie Valley, Nevada, and Implications for Fault Mechanics. J. Geophys. Res. 97, 15425-15435.

Power, W. L., Tullis, T. E. & Weeks, J. D. 1988. Roughness and Wear During Brittle Faulting. J. Geophys. Res. 93, 15268-15278.

Power, W. L., and Tullis, T. E., 1991. Euclidean and Fractal Models for the Description of Rock Surface Roughness. Journal of Geophysical Research 96, 415-424.

Robertson, C. W. 1982. The role of pre-existing sulphides in copper-ore formation at Mount Isa, Queensland. BMR Journal of Australian Geology and Geophysics 7, 119-124.

Rowland, J. V. & Sibson, R. H. 2001. Extensional fault kinematics within the Taupo Volcanic Zone, New Zealand: Soft-linked segmentation of a continental rift system. New Zealand Journal of Geology and Geophysics 44, 271-283.

Rumble, D. III, Duke, E. F. & Hoering, T. L. 1986. Hydrothermal graphite in New Hampshire: Evidence of carbon mobility during regional metamorphism. Geology 14, 452-455.

Sagy, A., Brodsky, E. E. & Axen, G. J. 2007. Evolution of fault-surface roughness with slip. Geology 35, 283-286.

Scott D.L., Rawlings D.J., Page R.W., Tarlowski C.Z., Idnurm M., Jackson M.J. & Southgate P.N. 2000. Basement framework and geodynamic evolution of the Palaeoproterozoic superbasins of north-central Australia: an integrated review of geochemical, geochronological, and geophysical data. Australian Journal of Earth Sciences 47, 341-380.

Scott, K. M. 1989. Dolomite compositions as a guide to epigenetic copper mineralization, Mount Isa Inlier, NW Queensland. Mineralium Deposita 24, 29-33.

Seyfried Jr, W. E., and Bischoff, J. L., 1979. Low temperature basalt alteration by sea water: an experimental study at 70°C and 150°C: Geochimica et Cosmochimica Acta, 43, 1937-1947.

Sibson, R. H. 1989. Earthquake faulting as a structural process. Journal of Structural Geology 11, 1-14.

Shaw, T. 2005. 500 OB Scoping Study 2005: Geological Summary: Xstrata Copper Internal Paper.

Sibson, R. H. 1995. Selective fault reactivation during basin inversion: potential for fluid redistribution through fault-valve action. Geological Society of London, Special Publications 88, 3-19.

Smith, W. D. 1969. Penecontemporaneous faulting and its likely significance in relation to Mt Isa ore deposition. Special Publication - Geological Society of Australia 2, 225-235.

Solomon, P. J. 1965. Investigations into sulfide mineralization at Mount Isa, Queensland. Economic Geology and the Bulletin of the Society of Economic Geologists 60, 737-765.

Southgate P.N., Bradshaw B.E., Domagala J., Jackson M.J., Idnurm M., Krassay A.A., Page R.W., Sami T.T., Scott D.L., Lindsay J.F., McConachie B.A. & Tarlowski C.Z. 2000a. Chronostratigraphic basin framework for Palaeoproterozoic rocks (1730-1575 Ma) in northern Australia and implications for base-metal mineralisation. Australian Journal of Earth Sciences 47, 461-483.

Stanton, R. L. 1963. Elemental constitution of the Black Star orebodies, Mount Isa, Queensland, and its interpretation. Inst Min & Met , B , Tr, 672, 69-124.

Stewart, A. J. 1992. The role of thrusting in the structural development of the Mount Isa Mine and its relevance to exploration in the surrounding region;

discussion. Economic Geology and the Bulletin of the Society of Economic Geologists 87, 1659-1664.

Suteanu, C. 2009. Fractals Dynamic Systems in Geoscience: Natural Hazards - Short Course. In: 5th International Conference on Fractals and Dynamic Systems in Geoscience, James Cook University.

Swager, C. P. 1983. Microstructural development of the silica-dolomite and copper mineralisation at Mount Isa, north-west Queensland, with speacial emphasis on the timing and mechanism of mineralisation, Ph.D. thesis, James Cook Univ.

Swager, C. P. 1985. Syndeformational carbonate-replacement model for the copper mineralization at Mount Isa, Northwest Queensland; a microstructural study. Economic Geology and the Bulletin of the Society of Economic Geologists 80, 107-125.

Swager, C. P., Perkins, W. G. & Knights, J. G. 1987. Stratabound phyllosilicate zones associated with syntectonic copper orebodies at Mt. Isa, Queensland. Australian Journal of Earth Sciences 34, 463-476.

Talwani, P. 1999. Fault geometry and earthquakes in continental interiors. Tectonophysics 305, 371-379.

Vandeginste, V., Swennen, R., Gleeson, S., Ellam, R., Osadetz, K., and Roure, F., 2007. Geochemical constraints on the origin of the Kicking Horse and Monarch Mississippi Valley-type lead-zinc ore deposits, southeast British Columbia, Canada: Mineralium Deposita. 42, 913-935.

Walsh, J. J. & Watterson, J. 1989. Displacement gradients on fault surfaces. Journal of Structural Geology 11, 307-316.

Waring, C. L., Heinrich, C. A. & Wall, V. J. 1998. Proterozoic metamorphic copper deposits. AGSO Journal of Australian Geology and Geophysics 17, 239-246.

White, N. J., Jackson, J. A. & McKenzie, D. P. 1986. The relationship between the geometry of normal faults and that of the sedimentary layers in their hanging walls. Journal of Structural Geology 8, 897-909.

Wilde, A. R., Jones, P. A., Gessner, K., Ailleres, L., Gregory, M. J. & Duncan, R. J. 2006. A Geochemical Process Model for the Mount Isa Copper Orebodies. Economic Geology 101, 1547-1567.

Wilkinson, J. J., 2001. Fluid inclusions in hydrothermal ore deposits: Lithos. 55, 229-272.

Williams, P. J., Barton, M. D., Johnson, D. A., Fontbote, L., De Haller, A., Mark, G., Oliver, N. H. S., and Marschik, R. 2005 Iron Oxide Copper-Gold Deposits: Geology, Space-Time Distribution, and Possible Modes of Origin. In: Hedenquist JW, Thompson JFH, Goldfarb RJ, and Richards JP (Eds) Economic Geology 100th Anniversary Volume 1905-2005. Society of Economic Geologists Inc, Colorado. 371-405.

Winsor, C. N. 1983. Syntectonic vein and fibre growth associated with multiple slaty cleavage development in the Lake Moondarra area, Mount Isa, Australia. Tectonophysics 92, 195-210.

Winsor, C. N. 1986. Intermittent folding and faulting in the Lake Moondarra area, Mount Isa, Queensland. Australian Journal of Earth Sciences 33, 7-42.

Appendix 1 – sample locations

Sample number	Mine location	General Location	Mineral analysed	Macroscale assemblage
3000	Level 20C N58S W	3000 orebody	Chalcopyrite	Copper breccia (chalcopyrite, pyrite and pyrrhotite minor quartz)
02 02 02	Level 27 6396 XC	3000 orebody	Chalcopyrite	Copper breccia
03 05 01	Level 29E U636 CO	3500 Orebody	Chalcopyrite	Copper breccia
03 01 06	Level 27C P63N DRV	3000 Orebody	Chalcopyrite	Copper breccia
01 02 01	Level 29E U69 CO	Basement	Chalcopyrite	Extension vein associated with quartz
M-1	Level 27 Q635 DPT	Paroo Fault	Chalcopyrite	Center of the Paroo Fault fill (quartz with minor pyrite, chalcopyrite, chlorte and graphite)
01 02 12	Level 29E U69 CO	3500 orebody	Pyrite	Copper breccia
03 03 04	Level 30E V70 FRAC	3500 orebody	Pyrite	Extension vein associated with quartz
650	DH 200306312 256.8m	650 orebody	Pyrite	Vein (dolomite, chalcopyrite, pyrite with minor quartz) within a Dolomitic Recryst
FW	Level 17 X36SE DR	Footwall Lens orebody	Pyrite	Chalcopyrite and pyrite breccia in Fractures Siliceous Shale
HW Lens	Level 18B T38 SDR	Hangingwall Lens orebody	Pyrite	Vien network in dolomitic breccia (chalcopyrite, pyrite and quartz)
F-8	Level 29E 6515 XC	Basement	Quartz	Vein containing (dolomite, quartz and pyrite with minor chlorite)
K-5	Level 27C 6934 XC	Basement	Quartz	Vein containing (quartz and pyrite with minor chlorite)
O-6	Level 18B V39 SWXC	Basement	Quartz	Vein containing (quartz, dolomite and pyrite)
L-1	Level 30A X620 RPAC	Basement	Quartz	Vein containing (quartz and dolomite)
M-4	Level 27 Q635 DPT	Basement	Quartz	Vein containing (dolomite, quartz and pyrite)
M-1	Level 27 Q635 DPT	Paroo Fault	Quartz	Center of the Paroo Fault fill (quartz with minor pyrite, chalcopyrite, chlorte and graphite)
O-2	Level 18B V39 SWXC	Paroo Fault	Quartz	Center of the Paroo Fault fill (quartz with minor chlorte and graphite)
F-12	Level 29E 6515 XC	Paroo Fault	Quartz	Top of the Paroo Fault fill (quartz and dolomite with minor chlorite and graphite)
K4	Level 27C 6934 XC	Paroo Fault	Quartz	Tope of the Paroo Fault fill (carbonate and quartz with minor chalcopyrite and pyrite)
M-5	Level 27 Q635 DPT	3000 Orebody	Chalcopyrite	Copper breccia (quartz, dolomite, chalcopyrite with minor pyrite, pyrrhotite chlorite and graphite)
03 01 05	Level 27C P63N DRV	3000 orebody	Chalcopyrite	Copper breccia
03 01 01	Level 27C P63N DRV	3000 orebody	Chalcopyrite	Late chalcopyrite vein cross cutting breccia (contains carbonate/quartz contamination)
03 05 03	Level 29E U636 CO	3500 orebody	Pyrite	Copper breccia
01 02 08	Level 29E U69 CO	3500 Orebody	Chalcopyrite	Copper breccia
03 01 06	Level 27C P63N DRV	3500 Orebody	Dolomite	Copper breccia
F5	Level 29E 6515 XC	Basement	Quartz	Disseminated chalcopyrite and pyrite in metamorphosed Lena Quartzite
A10	Level 29E 6448 XC	Basement	Quartz	Disseminated chalcopyrite and pyrite in metamorphosed Lena Quartzite
A23	Level 29E 6448 XC	Paroo Fault	Quartz	Disseminated chalcopyrite, pyrite and galena in quartz fault fill
L-2	Level 30A X620 RPAC	Paroo Fault	Dolomite	Center of the Paroo Fault fill (quartz and dolomite with minor pyrite, chalcopyrite, chlorte and graphite)

Appendix 2 – Halogen results

TABLES OF RAW DATA HAVE BEEN REMOVED